

University of Alberta

A Structural and Functional Investigation of Calnexin and its Unique
Cytoplasmic Domain

by

Allison Kraus

A thesis submitted to the Faculty of Graduate Studies and Research
in partial fulfillment of the requirements for the degree of

Doctor of Philosophy

Department of Biochemistry

©Allison Kraus

Fall 2011

Edmonton, Alberta

Permission is hereby granted to the University of Alberta Libraries to reproduce single copies of this thesis and to lend or sell such copies for private, scholarly or scientific research purposes only. Where the thesis is converted to, or otherwise made available in digital form, the University of Alberta will advise potential users of the thesis of these terms.

The author reserves all other publication and other rights in association with the copyright in the thesis and, except as herein before provided, neither the thesis nor any substantial portion thereof may be printed or otherwise reproduced in any material form whatsoever without the author's prior written permission.

Everything is theoretically impossible, until it is done. One could write a history of science in reverse by assembling the solemn pronouncements of highest authority about what could not be done and could never happen.

- Robert Heinlein

Abstract

Calnexin is a ubiquitously expressed endoplasmic reticulum chaperone that in conjunction with the similar endoplasmic reticulum chaperone calreticulin and protein disulfide isomerase ERp57, is responsible for protein folding and quality control in the secretory pathway. We generated a calnexin-deficient mouse model to use a loss-of function approach to study the role of calnexin. Calnexin-deficient mice are 30-50% smaller than their wild-type littermates and demonstrate neurological abnormalities characterized by gait disturbance, ataxia and a rolling walk. Neuron number, growth and function were unimpaired in the absence of calnexin. However, electron micrograph analysis indicates decompacted, disorganized myelin sheaths. Nerve conduction velocities were correspondingly reduced in sensory and motor neurons. The role of calnexin in myelination is a major discovery that provides a novel candidate gene for myelin disease and the resulting pathologies. Our work highlights a previously unidentified substrate specificity of a ubiquitous chaperone, showcasing the importance of specific chaperones and negating the notion that quality control is a redundant process. Investigation of the role calnexin plays in myelin formation and maintenance will help us understand myelin biology and the aberrant processes that result in dysmyelination and disease. Calnexin is composed of distinct functional and structural domains including an N-terminal globular and extended arm P-domain (N+P domain) that forms the protein folding module, a transmembrane domain, and a long C-terminal

cytoplasmic tail. The N+P domain of calnexin are reminiscent of another quality control chaperone, calreticulin, and calnexin and calreticulin are known to share folding substrates. However, the transmembrane domain and cytoplasmic tail of calnexin are unique and as calnexin plays a non-redundant role in myelin and myelin protein quality control, the C-tail could confer calnexin's specificity for membrane myelin proteins. To study the function of the C-tail, we employed techniques to look at the structure and biophysical characteristics as well as protein-protein interactions of the calnexin C-tail. A yeast-2-hybrid screen with the C-tail as bait identified UBC9, a SUMOylation E2 ligase, as a protein that interacts with the C-tail. Further biochemical studies reveal that the C-tail interacts with components of the SUMOylation machinery including UBC9, and can be SUMOylated *in vivo*. SUMOylation is a novel post-translational modification of the C-tail. Understanding the role of calnexin and its unique cytoplasmic tail will provide mechanistic insight into the function of a critical quality control chaperone, including understanding the specific role it plays in myelination.

Acknowledgements

There is a very long list of people who have contributed to my time spent as a PhD student, have challenged me to grow and learn and to whom I will be forever grateful. Marek, you have been an amazing source of support and an unparalleled mentor in science, wine and life. Thank you for your guidance and your encouragement. To all the members of the Michalak lab, present and former, you have taught me many things about science and life and I have truly enjoyed the experiences and laughs we have shared.

Thank you to my collaborators, who have been great teachers and sources for help. To my supervisory committee, thank you for your mentorship, the numerous letters of recommendation and all your help throughout my degree.

I am grateful to my friends and fellow graduate students for all of their support. To the members of The Muffins and the Biochemical Disasters, you have been a great outlet, source of inspiration, and I am thankful for the great times I have had as part of the team. Delaine, thank you for being my go-to person in times of frustration, celebration, or just because. To all of my friends, thank you for all of your positive encouragement.

To all my family, thank you for the pep talks, the care packages, the dinners and your unfaltering love and support. Mom, you have been my encouragement to follow what I love to do. Britt, you have always helped me strive for more and kept my perspective grounded. Kirsty, you have always been there to talk to, to encourage and remind me what is really important in life. Dad, you have helped me to challenge myself. Jack and Iris and Elaine, you have been my family from the moment I moved to Edmonton and have unquestioningly offered to help whenever needed.

Nate, you have been my driving force, my reins, and my voice of reason. You are my best friend and my greatest source of support. You truly have earned a honorary doctorate in the years I earned my own.

A PhD is not something achieved alone and to all those who helped me along the way, thank you.

Table of Contents

CHAPTER ONE - GENERAL INTRODUCTION	1
THE ENDOPLASMIC RETICULUM, A MULTIFUNCTIONAL ORGANELLE.....	2
<i>Morphology of the Endoplasmic Reticulum</i>	<i>2</i>
<i>The Endoplasmic Reticulum and Ca²⁺ Signaling.....</i>	<i>3</i>
<i>Protein folding, Quality Control and the N-glycan code.....</i>	<i>5</i>
<i>ER-associated Degradation (ERAD).....</i>	<i>11</i>
<i>ER Stress and the Unfolded Protein Response.....</i>	<i>16</i>
CALNEXIN.....	18
<i>A Component of Quality Control.....</i>	<i>18</i>
<i>Calnexin Structure.....</i>	<i>19</i>
CALNEXIN'S UNIQUE CYTOPLASMIC TAIL.....	24
<i>Phosphorylation of Calnexin.....</i>	<i>26</i>
<i>Other C-tail Post-translational Modifications.....</i>	<i>29</i>
SUMOYLATION.....	29
<i>Modification by SUMO.....</i>	<i>29</i>
<i>Function of SUMOylation.....</i>	<i>34</i>
QUALITY CONTROL AND MYELINATION.....	36
<i>Myelin.....</i>	<i>36</i>
<i>ER Protein Quality Control and Myelination.....</i>	<i>42</i>
<i>ER Stress in Dysmyelination.....</i>	<i>47</i>
<i>The Role of ER Ca²⁺ Stores in Myelin.....</i>	<i>50</i>
OBJECTIVES.....	52
HYPOTHESIS.....	52
REFERENCES.....	53
CHAPTER TWO - CALNEXIN DEFICIENCY IN A MOUSE MODEL	69
INTRODUCTION.....	70
MATERIALS AND METHODS.....	71
<i>Generation of Calnexin-deficient Mice.....</i>	<i>71</i>
<i>Genotype Analysis of Calnexin-deficient Mice.....</i>	<i>71</i>
<i>E. coli Expression and Purification of Calnexin Domains.....</i>	<i>73</i>

<i>Western Blot Analysis</i>	74
<i>Electrophysiology Measurements</i>	75
<i>Multifiber Motor and Sensory Conduction</i>	75
<i>Histological and Electron Microscopy Analyses</i>	76
<i>Flow Cytometry</i>	78
<i>Miscellaneous Procedures</i>	79
RESULTS	80
<i>Calnexin-deficient Mice</i>	80
<i>Calnexin-deficient Mice Display an Altered Phenotype Characterized by Gait Disturbance</i>	84
<i>Absence of Calnexin Results in Impaired Nerve Conduction Velocity</i>	86
<i>Dysmyelination in the Calnexin-deficient Mouse</i>	89
<i>Expression Profile of Calnexin-deficient Spinal Cord</i>	101
DISCUSSION	103
<i>Calnexin Deficiency Results in a Dysmyelinating Peripheral Neuropathy</i>	106
REFERENCES.....	108

CHAPTER THREE - STRUCTURAL ANALYSIS OF THE CALNEXIN CYTOPLASMIC

TAIL	111
INTRODUCTION	112
MATERIALS AND METHODS.....	113
<i>Expression and Purification of Recombinant Calnexin C-tail</i>	113
<i>Circular Dichroism Spectroscopy</i>	115
<i>Ruthenium Red</i>	115
<i>NMR spectroscopy</i>	116
RESULTS	117
<i>Calnexin C-tail Associates as a Homo-dimer</i>	119
<i>Circular Dichroism Analysis of the C-tail</i>	123
<i>Ruthenium Red Indicates the C-tail can Bind Ca²⁺</i>	125
<i>NMR Spectroscopy of the C-tail in Apo and Ca²⁺-bound States</i>	127
DISCUSSION	129
REFERENCES.....	132

CHAPTER FOUR - CALNEXIN FORMS COMPLEXES WITH COMPONENTS OF THE SUMOYLATION MACHINERY AND IS SUMOYLATED <i>IN VIVO</i>	134
INTRODUCTION	135
MATERIAL AND METHODS.....	138
<i>Yeast-2-Hybrid</i>	138
<i>Expression and Purification of Recombinant Calnexin Domains, UBC9 and in vitro SUMOylation</i>	139
<i>Plasmids and Mutagenesis</i>	140
<i>NMR Spectroscopy</i>	141
<i>Cell Lines, Cell Culture, Transfection and RNAi</i>	141
<i>Isolation of Microsomal Membranes</i>	142
<i>Immunoprecipitation and Western Blot Analysis</i>	143
<i>Cellular Fractionation</i>	144
<i>Miscellaneous</i>	145
RESULTS	146
<i>Components of the SUMOylation Machinery Interact with the Calnexin C-tail</i> ..	146
<i>UBC9 Expression in the Absence of Calnexin</i>	151
<i>The Calnexin C-tail Binds UBC9 in a Ca²⁺-Independent Manner</i>	156
<i>Association of UBC9 with the ER Membrane</i>	158
<i>The Calnexin C-tail is SUMOylated in vitro</i>	162
<i>Calnexin is SUMOylated in vivo</i>	164
<i>RanBPM and the C-tail</i>	166
DISCUSSION	169
<i>UBC9 and the Calnexin C-tail</i>	169
<i>Functional Implications of Calnexin SUMOylation</i>	172
REFERENCES.....	174
CHAPTER FIVE – DISCUSSION AND FUTURE DIRECTIONS	178
CALNEXIN PLAYS A CRITICAL AND NON-REDUNDANT ROLE IN NEURONAL SYSTEMS.....	180
<i>Calnexin and Myelination</i>	181
<i>Determining Folding Substrate Specificity: Calnexin versus Calreticulin</i>	182
<i>Calnexin as the Prototype Chaperone</i>	183
THE UNIQUE CALNEXIN C-TAIL.....	186
<i>Structural and Biophysical Characteristics</i>	187

<i>Protein-binding Partners</i>	188
THE MULTI-FACETED MOLECULAR CHAPERONE.....	191
REFERENCES.....	192
APPENDIX I - EXPRESSION OF FULL-LENGTH AND TRUNCATED CALNEXIN ON THE CALNEXIN-DEFICIENT MOUSE BACKGROUND	195
APPENDIX II - CALNEXIN AND METABOLISM	209
REFERENCES.....	216
APPENDIX III - PTP1B AND CALNEXIN	217
REFERENCES.....	221

List of Figures

Figure 1.1. The multifunctional ER.....	7
Figure 1.2. The N-glycan code.....	9
Figure 1.3. ER-associated degradation of terminally misfolded proteins.	15
Figure 1.4. Calnexin is composed of distinct functional and structural domains.	21
Figure 1.5. Amino acid sequence alignment of the calnexin C-tail in mammalian species.	25
Figure 1.6. The SUMOylation pathway.....	32
Figure 1.7. The compact myelin sheath.....	38
Figure 1.8. Quality control of myelin proteins.....	43
Figure 1.9. ER stress and misfolded myelin proteins.....	49
Figure 2.1. Generation of the calnexin-deficient mouse.....	83
Figure 2.2. Calnexin-deficient mice are smaller than their wild-type littermates and demonstrate a neurological disorder.	85
Figure 2.3. Calnexin in neuronal tissue.....	87
Figure 2.4. Neuronal function is not impaired but nerve conduction velocity is reduced in the absence of calnexin.....	90
Figure 2.5. Dysmyelination in the spinal cord.....	91
Figure 2.6. Dysmyelination in the sciatic nerve.....	93
Figure 2.7. Dysmyelination in the brain of calnexin-deficient mice.....	96
Figure 2.8. Histological analysis of calnexin-deficient tissues.....	98
Figure 2.9. Calnexin deficiency does not affect the immune system.	100
Figure 2.10. Decreased RNA expression levels of myelin proteins.	102
Figure 3.1. The calnexin C-tail is composed of multi-functional regions.....	118
Figure 3.2. The purified calnexin C-tail migrates as two species according to molecular weight.	121
Figure 3.3. Sedimentation-equilibrium analysis of the calnexin cytoplasmic tail (CNXC).	122

Figure 3.4. Circular dichroism analysis of the C-tail.	124
Figure 3.5. Ruthenium Red stain indicates the C-tail can bind Ca ²⁺	126
Figure 3.6. NMR spectroscopy of [¹⁵ N] C-tail indicates Ca ²⁺ binding.....	128
Figure 4.1. The calnexin cytoplasmic tail.....	147
Figure 4.2. UBC9 co-immunoprecipitates with calnexin.....	148
Figure 4.3. The cellular distribution of UBC9.....	150
Figure 4.4. UBC9 expression levels in the calnexin-deficient mouse are similar to wild-type.....	152
Figure 4.5. Depletion of components of the SUMOylation machinery has no impact on calnexin expression levels.	154
Figure 4.6. The global SUMOylation pattern is unchanged in the absence of calnexin.....	155
Figure 4.7. A 2D ¹ H- ¹⁵ N HSQC NMR spectra of the C-tail of calnexin before and after the addition of UBC9.	157
Figure 4.8. UBC9 has a bimodal cellular distribution.....	159
Figure 4.9. UBC9 associates with ER membranes.....	161
Figure 4.10. Calnexin is SUMOylated <i>in vitro</i> at K ⁵⁰⁶	163
Figure 4.11. Calnexin is SUMOylated <i>in vivo</i>	165
Figure 4.12. Cellular distribution of RanBPM.....	167
Figure 4.13. The C-tail binds UBC9 and can be SUMOylated.....	168
Figure AI.1. Schematic representation of the calnexin constructs used for transgenic mouse generation.....	198
Figure AI.2. The full-length and truncated calnexin proteins both localize to an ER-like structure.....	199
Figure AI.3. Genotyping strategy for the transgenic mouse lines.	200
Figure AI.4. Breeding strategy to generate the transgene on the calnexin- deficient background	202
Figure AI.5. RNA expression of the transgene in a comprehensive range of tissues.....	203
Figure AI.6. Reactivity of calnexin antibodies.....	204

Figure AI.7. Full-length calnexin is expressed in a comprehensive range of tissues.....	205
Figure AI.8. Truncated calnexin expression in mouse tissue.....	206
Figure AI.9. Transgenic mouse expressing full-length and truncated calnexin on a calnexin-deficient background gain weight similarly to wild-type animals.....	208
Figure AII.1. Calnexin-deficient mice have less fat than their wild-type counterparts.....	211
Figure AII.2. Hypothalamic malonyl CoA levels are elevated in calnexin-deficient mice.....	213
Figure AIII.1. Calnexin and PTP1B form complexes.....	220

List of Abbreviations

aa	amino acid
AAT	α 1-antitrypsin
AMPA	α -amino-3-hydroxy-methyl-4-isoxazole propionic acid
ATF6	activating transcription factor 6
Azc	L-azetidine 2-carboxylic acid
BiP	binding immunoglobulin protein
Ca ²⁺	calcium
CHOP	CCAAT/enhancer-binding protein (C/EBP) homologous protein
CICR	Ca ²⁺ -induced Ca ²⁺ release
CMAP	compound muscle action potential
CMT	Charcot-Marie-Tooth
CNP	2',3'-cyclic nucleotide 3'-phosphodiesterase
CNS	central nervous system
CNX	calnexin
CRAC	cholesterol recognition/interaction amino acid consensus
DLPFC	dorsolateral prefrontal cortex
DRP1	dynamin related protein 1
DSS	Dejerine-Sottas Syndrome
EDEM	ER degradation enhancing alpha-mannosidase-like protein
eIF2 α	eukaryotic translation initiation factor-alpha

ER	endoplasmic reticulum
ERAD	ER associated degradation
ERK-1	extracellular regulated kinase 1
Gfap	glial fibrillary acidic protein
GRP94	glucose-regulated protein 94
Her3	human epidermal growth factor receptor 3
HMGR	HMG-CoA reductase
IFN- γ	interferon- γ
InsP ₃ R	inositol 1,4,5-trisphosphate receptor
IRE1	inositol-requiring kinase 1
MAG	myelin-associated glycoprotein
MAL	myelin and lymphocyte protein
MAM	mitochondria associated ER membrane
MHC I	major histocompatibility complex class I
MOG	myelin oligodendrocyte glycoprotein
MS	Multiple Sclerosis
NDSM	negatively charged amino acid-dependent SUMOylation motif
NeuN	Neuronal Nuclei
NMDA	<i>N</i> -methyl-D-aspartate
NPC	Niemann Pick type C
Npl4	nuclear protein localization 4
OST	oligosaccharyltransferase
P0	myelin protein zero

PACS-2	phosphofurin acidic cluster sorting protein 2
PDI	protein disulfide isomerase
PDSM	phosphorylation-depepdent SUMOylation motif
PERK	double-stranded RNA-activated protein (PKR)-like endoplasmic reticulum kinase
PLP	proteolipid protein
PMD	Pelizaeus-Merzbacher disease
PMP22	peripheral myelin protein 22
PNS	peripheral nervous system
PPI	peptidyl-prolyl <i>cis-trans</i> isomerase
PSA-NCAM	polysialylated-neural cell adhesion molecule
PTP1B	protein tyrosine phosphatase 1B
RER	rough endoplasmic reticulum
RyR	ryanodine receptor
S1P	site-1 protease
S2P	site-2 protease
SAE	SUMO activating enzyme
SENP	Sentrin/SUMO-specific protease
SER	smooth endoplasmic reticulum
SERCA	sarcoplasmic/endoplasmic reticulum Ca ²⁺ ATPase
SIM/SBM	SUMO-interaction/binding motif
SLI	Schmidt-Lanterman incisures
SNAP	sensory nerve action potential

SQS	squalene synthase
SRP	signal recognition particle
SUMO	small ubiquitin-like modifier
TCR	T-cell receptor
Tr	Trembler
Tr-J	Trembler-J
UBC9	ubiquitin-conjugating enzyme 9
Ubx2	ubiquitin regulatory X 2
Ufd1	ubiquitin fusion-degradation 1
UGGT	UDP-glucose:glycoprotein transferase
Ulp	ubiquitin-like protein-specific protease
UPR	Unfolded Protein Response
VIMP	Vcp-interacting membrane protein
VWM	Vanishing White Matter disease
XBP1	X-box binding protein 1

CHAPTER ONE

GENERAL INTRODUCTION

A portion of this chapter has been accepted for publication. Kraus, A. and M. Michalak. *Endoplasmic reticulum quality control and dysmyelination*. Biomolecular Concepts. 2011.

The Endoplasmic Reticulum, a Multifunctional Organelle

Morphology of the Endoplasmic Reticulum

The endoplasmic reticulum (ER) is the largest component of the endomembrane system with its membrane accounting for approximately half of all cellular membranes [1]. It is organized into distinct domains including the nuclear envelope, sheet-like cisternae, and a polygonal array of tubules connected by three-way junctions [2]. This extensive membranous network has a common luminal space representing 10% of the total cell volume with ER membranes extending throughout a cell [1]. In the nervous system, the ER is even found in axons and the distal tips of neurites, a huge span considering the axonal tip can be upwards of several feet from its cell body in long human neurons [3]. Using electron microscopy, ER morphology was originally classified into two distinct domains: the rough (RER) and smooth (SER) membrane domains. The RER is identifiable by the presence of membrane bound ribosomes and is the site of the biosynthesis of membrane proteins, protein folding, modification and quality control. The SER is identified simply by the absence of membrane bound ribosomes. In neurons, the RER is found predominantly in the cell body and it is the SER that extends into the axons and distal tips of neurites. Morphologically, the RER corresponds to the sheet-like cisternae and the SER to the vesicular-tubular structures [4]. The nuclear membrane provides a third morphologically distinct region of the ER. The outer nuclear membrane is indistinguishable from the rough ER in terms

of protein markers and the inner membrane consists of a unique protein composition and contains the nuclear pores [5]. ER membranes have also been observed in close apposition to 5-20% of the total mitochondrial network, a proximity that provides a physical basis for Ca^{2+} signaling between the two organelles [6]. The ER and its diverse morphological domains support the unique and numerous cellular functions that take place in the ER and contribute to the dynamic role the ER plays in the cell.

The Endoplasmic Reticulum and Ca^{2+} Signaling

The ER provides the cellular compartment for lipid protein synthesis, protein folding and quality control, Ca^{2+} storage, and is involved in signal transduction processes such as the Unfolded Protein Response (UPR). The ER is responsible for the storage of the majority of intracellular Ca^{2+} and this high Ca^{2+} concentration is required for protein folding and glycoprotein processing [7, 8]. ER Ca^{2+} stores affect virtually every cellular function including protein folding and synthesis, muscle contraction and relaxation, embryogenesis and subsequent development, cell differentiation and proliferation, transcription factor activation, secretion, gene expression, learning and memory, membrane excitability, energy metabolism, cell cycle progression, and apoptosis [9]. ER Ca^{2+} homeostasis is maintained by balancing Ca^{2+} release from the ER by the inositol 1,4,5-trisphosphate receptor (InsP_3R) and ryanodine receptor (RyR) [5,6] with replenishment of the stores by sarcoplasmic/endoplasmic reticulum Ca^{2+} -ATPase (SERCA) [9]. The total Ca^{2+} concentration in the ER is in excess of 2 mM but the ER

employs a number of Ca^{2+} binding/buffering proteins to keep free ER Ca^{2+} in concentration ranges of 50 to 500 μM [10-12]. Calreticulin, glucose-regulated protein 94 (GRP94), and BiP are the most abundant Ca^{2+} buffering proteins found in the lumen of the ER. These proteins bind Ca^{2+} with high capacity at their highly acidic C-terminal domains [13-19]. The link between ER Ca^{2+} and protein sorting, the secretory pathway, and ER morphology was made when it was observed that ER resident proteins normally retained in the ER, including BiP, calreticulin, and PDI, are secreted when ER stores are depleted of Ca^{2+} in 3T3 and primary murine fibroblastoid LB1 and Cj8 cell lines [20]. Concurrently with the increased secretion of ER resident proteins, Ca^{2+} depletion of the stores results in changes in ER morphology and the ER becomes more vesicular or tubulovesicular as compared to the perinuclear cisternae arrangement in control cells [20]. The interdependence of ER morphology and Ca^{2+} again emerges when we consider mitochondrial associated membranes (MAMs) and the close proximity of mitochondria and ER membranes. This close apposition is known to facilitate the rapid uptake of Ca^{2+} into mitochondria from Ca^{2+} microdomains created by release of Ca^{2+} from InsP_3R [6]. Tethering of mitochondrial and ER membranes determines ER morphology as the ER becomes fragmented in the absence of mitofusin-2. Further, loss of mitofusin-2 tethering results in slower Ca^{2+} uptake during InsP_3 -mediated Ca^{2+} signaling [21]. Disruption of MAMs is induced with the siRNA depletion of PACS-2 and inhibits ER Ca^{2+} release and the onset of apoptosis. Interestingly, PACS-2 is known to mediate the subcellular

localization of calnexin depending on its phosphorylation status and sort it primarily to MAMs [22].

Protein folding, Quality Control and the N-glycan code

Protein folding is an essential process for every cell and is assisted by cellular chaperones. Protein folding quality control employs molecular chaperones that bind to nascent polypeptides and aid their folding and assembly processes while preventing unfolded protein aggregation. There are a number of chaperones dedicated to specific folding related functions including the classical chaperones (BiP, GRP94), lectin chaperones (calnexin and calreticulin), redox enzymes (PDI, ERp57), proline isomerases, and sugar processing enzymes (Glucosidase I and II, ER Mannosidase I and II, UGGT) [23]. These chaperones and other folding enzymes provide a way to ensure only properly folded and assembled proteins are trafficked from the ER and proteins that cannot be properly folded are targeted to the ER associated degradation pathway. Protein folding in the ER begins when a nascent polypeptide is translocated into the ER lumen, a process that takes place both co- and post-translationally (Figure 1.1). Co-translational translocation, the dominant mechanism in mammals, is where nascent polypeptides are targeted to the ER by a ribonucleoprotein complex consisting of the signal recognition particle (SRP) and its ER membrane surface SRP-receptor (SR) [24]. SRP binds to the signal sequence of nascent proteins emerging from the ribosome [25] and arrests protein translation until the ribosome, nascent

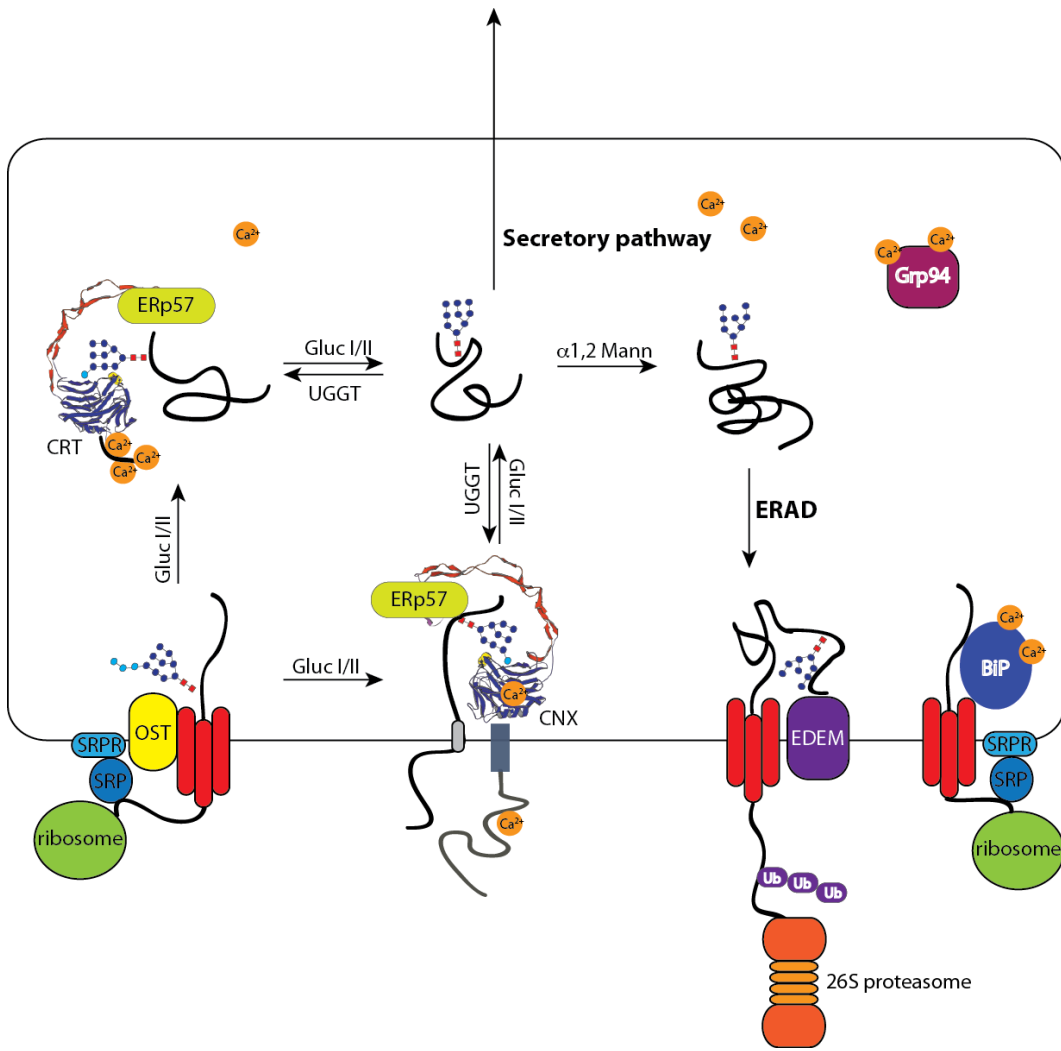


Figure 1.1. The multifunctional ER.

ER resident chaperones aid the folding of nascent polypeptides translocated into the ER lumen. Newly translated proteins containing a signal sequence are recognized by the signal recognition particle (SRP) and targeted to the ER, where SRP binds to its receptor, bringing the translating protein and the ribosome as a complex to the Sec61 translocon at the ER membrane. Polypeptides are inserted through the heterotrimeric Sec61 complex. The transmembrane complex oligosaccharide transferase (OST) transfers a pre-assembled two N-acetylglucosamine, nine mannose, three terminal glucose ($\text{Glc}_3\text{Man}_9\text{GlcNAc}_2$) core oligosaccharide en bloc to N-X-S/T (where X is any amino acid except Pro) N-glycosylation sites. The $\text{Glc}_3\text{Man}_9\text{GlcNAc}_2$ oligosaccharide is trimmed sequentially by Glucosidase I and II to a mono-glucosylated form ($\text{Glc}_1\text{Man}_9\text{GlcNAc}_2$). This mono-glucosylated form is recognized by the lectin chaperones calreticulin (CRT) and calnexin (CNX). Calreticulin and calnexin are highly similar with calreticulin being a soluble protein and calnexin membrane anchored. Both CRT and CNX bind ER oxidoreductase ERp57 at the tip of their P-domain to aid folding of proteins requiring disulfide bonds. Glucosidase II removes the terminal glucose from the oligosaccharide, leaving $\text{Man}_9\text{GlcNAc}_2$. If the protein has achieved its proper conformation it exits the ER to be trafficked through the secretory pathway. Unfolded proteins are inserted back into the CNX/CRT cycle when UGGT re-glucosylates the substrate. Proteins unable to achieve their appropriate structure (e.g. proteins containing mutations) are extracted from the calnexin cycle, and the carbohydrate on the unfolded substrate subjected to sequential cleavage of terminal mannose residues by α 1,2 Mannosidase, preventing re-glucosylation by UGGT. This allows recognition by EDEM that transports the protein to the retrotranslocon where the unfolded protein is translocated across the ER membrane, ubiquitinated and targeted to the proteasome for destruction.

polypeptide, and SRP reach the ER localized SRP-receptor. Signal sequences for ER targeting are remarkably diverse with only one unifying property: a hydrophobic core with an uninterrupted stretch of at least six non-hydrophilic residues [26]. An early comparative sequence analysis showed that while there is a lack of significant homology, signal sequences are typically 20-30 amino acid residues consisting of a basic “N domain”, a 7-13 amino acid residue hydrophobic “H domain” and a slightly polar “C domain” [27]. The diversity of signal sequences provides an opportunity to embed substrate-specific information for additional control of protein biogenesis [28]. Post-translational translocation has also been documented in mammalian species [29] where polypeptides less than 75 amino acid residues are transported to the ER with the help of Hsp70 and Hsp40 chaperone families. Once the peptides reach the ER membrane, they are translocated into the lumen through the heterotrimeric Sec61 translocon. Resident ER luminal proteins assist in this translocation, including BiP, an HSP70 protein chaperone involved in maintaining the permeability barrier by selectively sealing the luminal end of the translocon pore [30, 31]. Once nascent proteins have entered the ER lumen, they are bound by protein chaperones that assist in their folding and assembly. Proteins without a consensus N-glycosylation site early in their amino acid sequence associate with BiP and Erdj proteins [32]. PDI and peptidyl-prolyl cis-trans isomerases (PPI) catalyze protein folding through the formation and isomerization of the

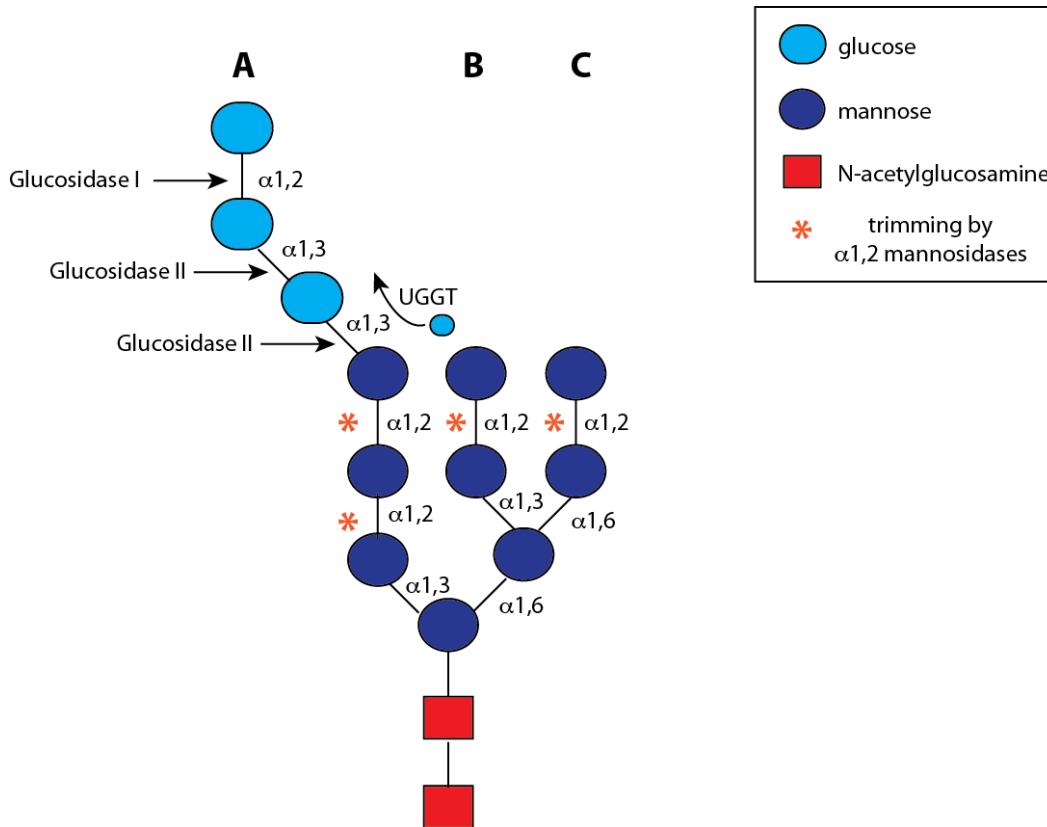


Figure 1.2. The N-glycan code.

The N-linked core oligosaccharide structure is depicted (figure modified from [33]). A, B, and C denote the branch. The glucose moieties are trimmed sequentially by Glucosidase I and II and the mono-glucosylated form ($\text{Glc}_1\text{Man}_9\text{GlcNAc}_2$) allows interaction with the ER lectin chaperones calreticulin (CRT) and calnexin (CNX). Trimming of the terminal glucose by Glucosidase II is reversed by the re-addition of a glucose residue by UDP-glucose:glycoprotein transferase (UGGT). The glycan can be trimmed by ER $\alpha 1,2$ mannosidases, terminally extracting the protein from the calnexin cycle to target it for ER-associated degradation (ERAD).

disulfide bond, often a rate-limiting step in protein folding [34, 35]. Members of the protein disulfide isomerase (PDI) family aid protein folding by forming (oxidizing), breaking (reducing), and re-arranging (isomerization) of disulfide bonds. PPIs, also called rotamases, catalyze the slow isomerization of cis/trans prolyl peptide bonds necessary for proteins to obtain their native conformation [36]. Polypeptides containing a consensus site can be N-glycosylated. The most prominent modification of secretory proteins in eukaryotic cells, N-glycosylation is initiated at the ER membrane where two N-acetylglucosamine and nine mannoses with three terminal glucoses (Glc₃Man₉GlcNAc₂) are assembled and transferred as a core oligosaccharide onto asparagine residues of the consensus site (Asn-X-Ser/Thr, where X is any amino acid except Pro) of a nascent polypeptide [33]. Assembly of the oligosaccharide is anchored by the lipid carrier dolichylpyrophosphate (Dol-PP) and is initiated on the cytoplasmic side of the ER as a lipid-linked intermediate. A series of glycosyl transferases assemble a mannose₅-N-acetylglucosamine₂ oligosaccharide (Man₅GlcNAc₂-PP-Dol) that is translocated across the ER membrane by a flippase (Rft1 in yeast) [37]. Assembly is completed in the ER lumen where glucosyl transferases use dolichylphosphomannose and dolichylphosphoglucose as substrates. Oligosaccharyltransferase (OST) is an eight-subunit protein complex that catalyzes the addition of the oligosaccharide onto N-glycosylation consensus sites. OST is associated with the translocon complex and adds the oligosaccharide when the consensus site is only 12-14 residues into the ER

lumen [38]. The three terminal glucoses are trimmed by glucosidase I and II, and reglucosylation takes place by UDP-glucose:glycoprotein transferase (UGGT). Calnexin and calreticulin bind the glucose α -1,3 mannose glycosidic bond on high mannose containing asparagine-linked oligosaccharides in a Ca^{2+} -dependent manner [39], beginning a protein folding quality control cycle known as the calnexin cycle. The disulfide isomerase ERp57 is recruited by calnexin and calreticulin to assist with protein folding. UGGT can discriminate between folded and unfolded proteins [96], ensuring that only unfolded proteins are re-glucosylated. A terminal mannose can be trimmed by ER mannosidases. As monoglucosylated oligosaccharides ($\text{Glc}_1\text{Man}_9\text{GlcNAc}_2$) interact with calreticulin and calnexin, the deglucosylation–glucosylation cycle ensures that unfolded proteins remain bound to molecular chaperones until they are properly folded [39]. The calnexin–calreticulin, deglucosylation–glucosylation cycle ensures the folding and quality control of nascent glycoproteins; however, when proteins remain unfolded or are damaged, they undergo ER-associated degradation (ERAD). ERAD ensures that misfolded and damaged proteins are degraded, as well as that normal proteins maintain turnover rates.

ER-associated Degradation (ERAD)

Proteins are targeted for ERAD when they persist in an unfolded/misfolded conformation over time. Glycosylated polypeptides can undergo one or more cycles of release and re-association as part of the calnexin cycle until they achieve the appropriate folding conformation [40].

UGGT keeps substrates in the calnexin cycle by adding back a glucose to replace the glucose trimmed by glucosidase II. To avoid futile cycling, UGGT only recognizes near native or pseudo native conformers and ignores extensively misfolded polypeptides [41]. When a substrate persistently fails to attain its native structure, ER-resident exo-mannosidases progressively remove terminal α 1,2 mannose residues, which reduces the ability of UGGT to re-glucosylate the substrate [42]. Mannose trimming generates the N-glycan degradation signal which is a terminal α 1,6-linked mannose generated by processing of the C-branch by Htm1p, the yeast orthologue of EDEM [43]. This degradation signal recruits ERAD lectins containing mannose 6-phosphate receptor homology domains (MRH) such as OS-9 and XTP3-transactivated gene B (XTP3-B) [44]. Trimming of mannose residues is obligatory for ERAD substrates and pharmacologic inhibition of α 1,2 mannosidases prevents glycoprotein degradation [45-49]. Mannose trimming is essential for association with the ER lectin XTP3-B, substrate accumulation in the ERAD staging ground and delivery to E3 ubiquitin ligases [50]. Misfolded proteins and their ERAD chaperones are targeted to ERAD complexes that contain a retrotranslocation membrane channel for movement of the substrate to the cytoplasm for proteasomal degradation. The identity of the ERAD retrotranslocation channel has been controversial for some time and several candidates have been proposed including Sec61 and Derlin 1 [51]. Sec61, a major component of the translocation channel importing polypeptides into the ER [52, 53], is thought to be involved in

retrotranslocation. This is supported by evidence indicating Sec61p depletion or blockage with stalled nascent chain-ribosome complexes prevents the export of the A1 subunit of cholera toxin and amyloid beta-peptide from the ER lumen [54, 55]. However, the crystal structure of the archaeal homologue of Sec61, SecY, indicates the limiting diameter of the pore to be a mere 3 Å and it is not understood how a preprotein segment in extended conformation at approximately 12 Å passes through the pore, or how the pore would accommodate the 30 Å extended oligosaccharides attached to even fully unfolded polypeptides [56-58]. Derlin-1 was first identified as a required component of ERAD when deletion of the yeast homologue Der1p abolished degradation of ERAD substrate proteins [59]. There are three members of the Derlin family in mammalian cells: Derlin-1, -2 and -3. Derlin-1 is essential for the degradation of class I MHC molecules and expression of a Derlin-1 dominant negative construct impedes this destruction [60]. Derlin-1 is known to associate in a complex with the cytosolic ATPase p97 and Vcp-interacting membrane protein (VIMP) and treatment with DTT to induce misfolded protein exit from the ER demonstrates an accumulation of newly synthesized proteins with VIMP [61]. Further, blocking Derlin-1 expression induced the unfolded protein response, consistent with the accumulation of misfolded proteins [61]. Derlin-2 and -3 are also known to associate with p97 and EDEM and overexpression of Derlin-2 or -3 accelerated the degradation of misfolded glycoproteins and conversely, their knockdown blocked degradation [62].

Further evidence for Derlin proteins as the elusive retrotranslocon versus Sec61 include the observation that real-time translocation of non-glycosylated pro- α factor from mammalian microsomes is blocked by Derlin-1 antibodies but is unaffected by Sec61 antibodies [63].

While the identity of the retrotranslocon remains contentious, what is known is that once proteins are extracted from the ER to the cytosol, they are degraded by the 26S proteasome. Protein dislocation from the ER requires substrate polyubiquitination and is coordinated by cytosolic ubiquitin binding chaperones such as the hexameric AAA-ATPase complex Cdc48/p97 that aids translocation and presents substrates to the proteasome [64-66]. Cofactors that interact with the complex are involved in binding the ubiquitylated polypeptide and include Ufd1 and Npl4. The Cdc48/p97-Ufd1-Npl4 is recruited to the ER membrane through Ubx2 (the yeast homolog of erasin), a transmembrane ERAD cofactor known to bind ubiquitinated substrates and dedicated E3 ligases [67, 68]. It has been proposed that ERAD substrates are ubiquitinated as they emerge on the cytosolic face, a modification that might prevent translocation back into the ER lumen [69], and the ubiquitinated substrate recognized by Cdc48/p97-Ufd1-Npl4 for extraction [70].

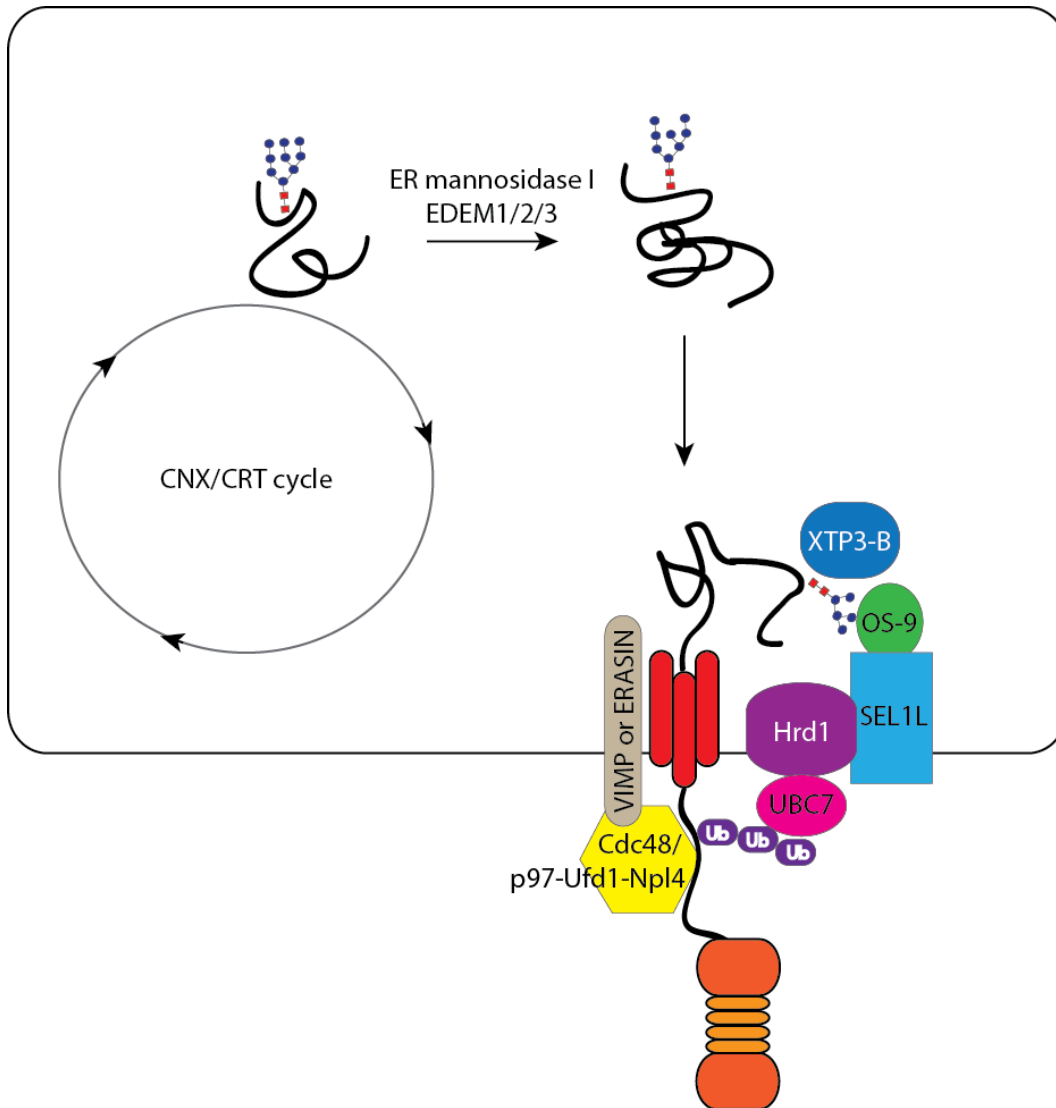


Figure 1.3. ER-associated degradation of terminally misfolded proteins.

Misfolded glycoproteins are extracted from the calnexin cycle when $\alpha 1,2$ ER mannosidases remove terminal $\alpha 1,2$ mannose residues, preventing reassociation of the glycan with UGGT. ER-associated degradation (ERAD) lectins with mannose 6-phosphate receptor homology (MRH) domains, such as XTP3-B and OS-9 recognize the $\text{Man}_{5-6}\text{GlcNAc}_2$ glycan and target the misfolded glycoprotein to ERAD complexes. These complexes consist of a retrotranslocation pore (Derlin-1 or Sec61), the membrane the Hrd1-SEL1L ubiquitin ligase complex, an E2 ubiquitin conjugating enzyme such as UBC7, and the hexameric AAA-ATPase complex Cdc48/p97-Ufd1-Npl4 to aid translocation through the pore, Cdc48/p97-Ufd1-Npl4 is recruited to ER membranes through Vcp-interacting membrane protein (VIMP) or erasin.

ER Stress and the Unfolded Protein Response

Protein translation at the ER needs to meet cellular requirements while still maintaining quality control of the proteins that exit the ER. During episodes of cell stress or insult, protein folding in the ER may be perturbed and in an effort to restore homeostasis, a pathway known as the UPR is activated [71]. UPR employs three ER transmembrane sensors, pancreatic ER kinase (PERK), inositol-requiring kinase 1 (IRE1), and activating transcription factor 6 (ATF6), to coordinate a cellular response to an increased protein load. Activation of PERK leads to the phosphorylation of eukaryotic translation initiation factor- α (eIF2 α) and a subsequent attenuation of general translation while concomitantly up-regulating the translation of proteins involved in amino acid metabolism, protein secretion, and the antioxidant response. Activation of IRE1 and ATF6 leads to the transcription of genes encoding components that increase ER folding capacity, protein export, and degradation [71]. Sustained or overwhelmed UPR leads to ER Ca²⁺ release, apoptosis and cell death [72]. BiP is a critical component of UPR induction. BiP is known to associate with unfolded proteins in the ER lumen through recognition of exposed hydrophobic regions and maintain proteins in a folding-competent state [73]. BiP binds to the three UPR sensors and is competitively titrated away by the presence of unfolded proteins. With the accumulation of misfolded proteins in the ER and ER stress, BiP binds to unfolded proteins and releases ATF6 to translocate to the Golgi, where it is cleaved in its luminal domain by site 1 protease and in

its N-terminal membrane anchored half by site 2 protease [74]. This releases the cytosolic bZIP domain of ATF6 to translocate to the nucleus and activate transcription of ERAD components and chaperones, including BiP, to deal with the protein load. Calreticulin is also involved in a glycosylation-dependent retention of ATF6 in the ER [75]. During ER stress conditions, completely glycosylated ATF6 is rapidly degraded by the proteasome and newly synthesized ATF6 is underglycosylated to overcome its interaction with calreticulin [75, 76]. BiP binds to the luminal domains of both IRE1 and PERK in an inactive state and accumulation of unfolded proteins in the ER competitively titrates BiP away to allow the activation of IRE1 and PERK [77]. Without BiP binding, IRE1 undergoes dimerization, autophosphorylation and subsequent activation of its endoribonuclease (RNase) domain [78, 79]. Activated RNase activity leads to the splicing of XBP-1, which introduces an alternative C terminus with increased transcription activation potential [80, 81]. IRE1 activation and XBP-1 mRNA splicing leads to the transcriptional up-regulation of chaperones such as BiP and GRP94 and components of ERAD such as EDEM and UBC7. The ER luminal domains of IRE1 and PERK are functionally interchangeable [82] and upon BiP dissociation, similar to IRE1, PERK undergoes dimerization and autophosphorylation. PERK activation leads to the phosphorylation of eIF2 α and an inhibition of general translation [83]. By utilizing these three transmembrane sensors, the ER is able to coordinate a response to protein load to stop general translation, up-regulate necessary components of

protein folding and to remove accumulating misfolded proteins from the ER in an effort to restore protein homeostasis.

Calnexin

A Component of Quality Control

Calnexin is a Type I integral membrane protein resident in the ER. Established as a bona fide molecular chaperone, calnexin binds monoglycosylated nascent polypeptides translated through the ER to assist in their folding and to ensure only properly folded and assembled proteins exit the ER.

Calnexin was discovered two decades ago by two independent groups. The Williams group identified an 88-kD protein associated with newly synthesized major histocompatibility complex class I (MHC I) molecules [84]. Within months, the Bergeron group isolated a 90-kDa integral membrane phosphoprotein of the ER in a complex with the phosphoglycoprotein SSR α . The 90-kDa protein had a high degree of amino acid sequence identity to calreticulin, and it was subsequently dubbed calnexin [85]. Shortly thereafter, the p88 molecular chaperone was identified to be the aforementioned calnexin [86]. Since then, calnexin has been shown to be an important lectin molecular chaperone critical for protein folding quality control [87].

As lectin chaperones, calnexin and calreticulin bind monoglycosylated polypeptides in the ER. However, calnexin and calreticulin are

also known to act as chaperones for non-glycosylated substrates [39]. A recent 1.55 Å resolution structure of the calreticulin N-domain identified a peptide-binding site formed by an interaction of the N-terminal extension with the edge of the lectin site [88]. Although the peptide binding domain of calnexin has not been characterized, the soluble ER luminal domain of calnexin can suppress the aggregation of non-glycosylated firefly luciferase [89]. Further studies with this assay demonstrate the globular domain binds hydrophobic peptides with micromolar affinity and while the arm does not directly bind substrates, it enhances the aggregation suppression of firefly luciferase, presumably by steric constraint of large polypeptide chains [90].

Calnexin Structure

Calnexin is composed of distinct functional and structural domains. As an integral membrane protein, it spans into two very distinct molecular environments with an ER luminal folding module, a transmembrane domain, and a cytoplasmic tail (Figure 1.4). Following removal of its signal sequence, human calnexin is 572 amino acid residues in length (571 amino acids in mouse and rat, 573 amino acid residues in dog) with the majority of the protein residing in the ER lumen (amino acids 1-463). Calnexin makes a single pass through the ER membrane with amino acid residues 484-573 residing in the cytoplasm. Calnexin is highly conserved across species with 92% percent identity as determined by amino acid sequence alignment using ClustalW2 multiple sequence alignment.

Calnexin can be divided functionally into several domains: the ER luminal domain, the transmembrane domain, and the C-tail. A crystal structure of the ER luminal region of calnexin has been solved and indicates the presence of two distinct domains with different functional capabilities: a compact globular domain (designated the N-domain) and a long arm stretching 140 Å from the globular domain [91]. The compact globular domain (amino acid residues 61-262 and 415-458) is composed of a β sandwich of two antiparallel β sheets. There are two disulfide bonds, one in the globular domain (Cys¹⁶¹-Cys¹⁹⁵) and one in the arm (Cys³⁶¹-Cys³⁶⁷). The putative carbohydrate binding site was modeled within the concave β sheet of the globular domain and Ca²⁺ is thought to bind in the convex β sheet of the globular domain. The arm is composed of proline-rich tandem sequence repeats, a region which has been termed the P-domain. Two different proline-rich sequence motifs (denoted 1 & 2) are repeated four times each within the amino acid residues 277-410 in the linear pattern 11112222. The P-domain forms a large hairpin arm where each copy of motif 1 interacts with the adjacent motif 2. Together, the structural data indicates that the mono-glucosylated high mannose oligosaccharide binds the luminal domain, and the flexible P-domain can wrap around folding substrates or interact with other proteins of the folding machinery, such its known interaction with ERp57 [91, 92].

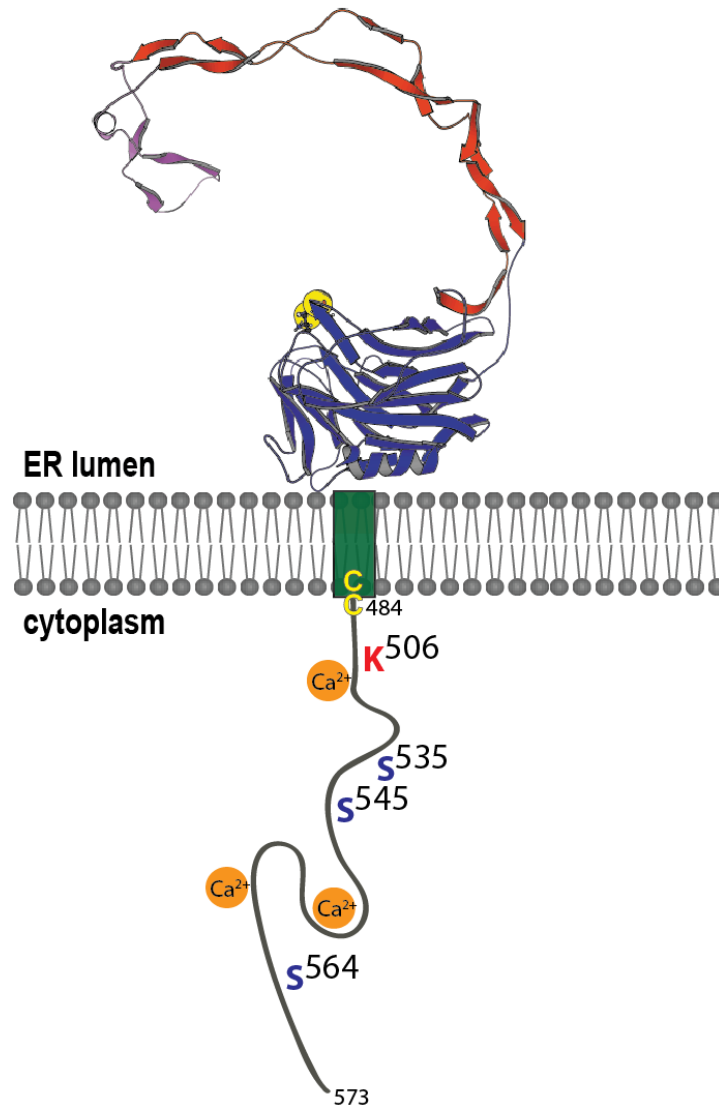


Figure 1.4. Calnexin is composed of distinct functional and structural domains.

Calnexin is composed out of distinct structural domains including a globular domain (N-domain) shown in blue and an extended arm (P-domain) shown in red in the ER lumen, a transmembrane domain shown in green and a cytoplasmic domain in black. The N-domain binds mono-glucosylated substrates and ERp57 binds to the tip of the flexible P-domain to assist with folding. Sites of cytoplasmic tail post-translational modification are marked with the *Canis familiaris* calnexin numbering as follows: juxtamembrane cysteine residues (C) that can be palmitoylated are marked in yellow,, the modifiable lysine for SUMO addition (Chapter 4) is marked in red (K⁵⁰⁶) and phosphorylatable serine amino acid residues (S) are indicated in blue.

Calnexin and calreticulin share remarkable amino acid sequence and structural similarities. The structure of calreticulin has been modeled based on the crystal structure of calnexin and the NMR structure of calreticulin's P domain [93, 94] and it demonstrates that the luminal domain of calnexin and calreticulin share significant structural homology. A recent X-ray structure of calreticulin's N-domain shows calreticulin and calnexin share common folds and despite differences in most of the surface-exposed side chains two patches of residues are highly conserved [88]. The first patch corresponds functionally to the lectin-binding domain demonstrating the carbohydrate binding domain is highly conserved between calreticulin and calnexin [88]. Considering the structural and lectin site binding similarities, it is not surprising that calnexin and calreticulin share many folding substrates and it is ER membrane proximity that contributes to the distinct substrate specificities of either chaperone [95]. Soluble calnexin (N+P-domain) expressed in L cells (mouse fibroblasts) shows a similar substrate specificity to calreticulin. Conversely, when calreticulin is membrane-anchored with the transmembrane domain of calnexin, the substrate specificity is similar to that of calnexin [96]. It is possible that calnexin function could be partitioned according to a specific molecular domain (i.e. luminal domain versus cytosolic tail). The structural homology of calnexin's luminal domain and calreticulin makes the transmembrane domain and cytoplasmic tail of calnexin a unique defining feature.

Previous studies in yeast provide us with some insights into the function of the calnexin C-tail. The calnexin homologue in *Saccharomyces cerevisiae*, Cne1p, is 24% identical and 31% similar at the amino acid level to mammalian calnexin [97]. Cne1p is an integral membrane protein, however, it does not bind Ca^{2+} and the predicted Cne1p sequence terminates directly after the transmembrane domain with only one amino acid predicted to be cytosolically exposed [97]. Cne1p is not essential in *S. cerevisiae* as yeast strains with a deletion of the CNE1 gene were viable and grew at normal rates and only small effects were noted on the quality control and secretion of select glycoproteins [97]. In contrast, the *Schizosaccharomyces pombe* calnexin homologue, Cnx1, is essential for viability [98]. Cnx1 is 38% identical to canine calnexin but only 22% identical to *S. cerevisiae* Cne1p. Cnx1 is a Ca^{2+} -binding integral membrane glycoprotein with a cytoplasmic domain [98]. *S. pombe* lethality due to *cnx1+* deletion could be rescued with the luminal domain of Cnx1. However, later studies in *S. pombe* revealed that a truncated Cnx1 protein, called mini-Cnx1p and consisting of only the last 123 amino acid residues including 52 amino acids of the luminal domain, the 23 amino acid transmembrane domain and the 48 amino acid cytoplasmic tail, could also rescue viability [99]. This was attributed to the ability of BiP to form a complex with the 52 amino acid of the luminal domain and postulated that this 52 amino acid portion of the luminal domain was the essential component for the rescue of *cnx1+* deletion *S. pombe*. The equivalent 52 amino acids in *Yarrowia lipolytica* was shown to interact with the β subunit

of the Sec61 translocon. The transmembrane domain and cytoplasmic tail would anchor this essential part of calnexin in the appropriate membrane proximal position for this interaction and interaction with nascent polypeptide substrates and it is interesting that this portion, and not the chaperone domain of calnexin, is sufficient for viability in *S. pombe*.

While studies in yeast provide some clues as to the importance of the C-tail, limited studies have addressed the molecular characteristics of the calnexin C-tail in mammalian systems. To date, only a handful of C-tail interacting proteins have been identified and a few studies have addressed the role of C-tail phosphorylation. One objective of this study was to examine the functional impact of the C-tail by examining its structural and biophysical characteristics and identifying novel interacting proteins. Understanding these parameters will help us understand why mammalian calnexin has such a highly conserved transmembrane domain and cytoplasmic tail.

Calnexin's Unique Cytoplasmic Tail

Calnexin's cytoplasmic tail is highly conserved between mammalian species (Figure 1.5).

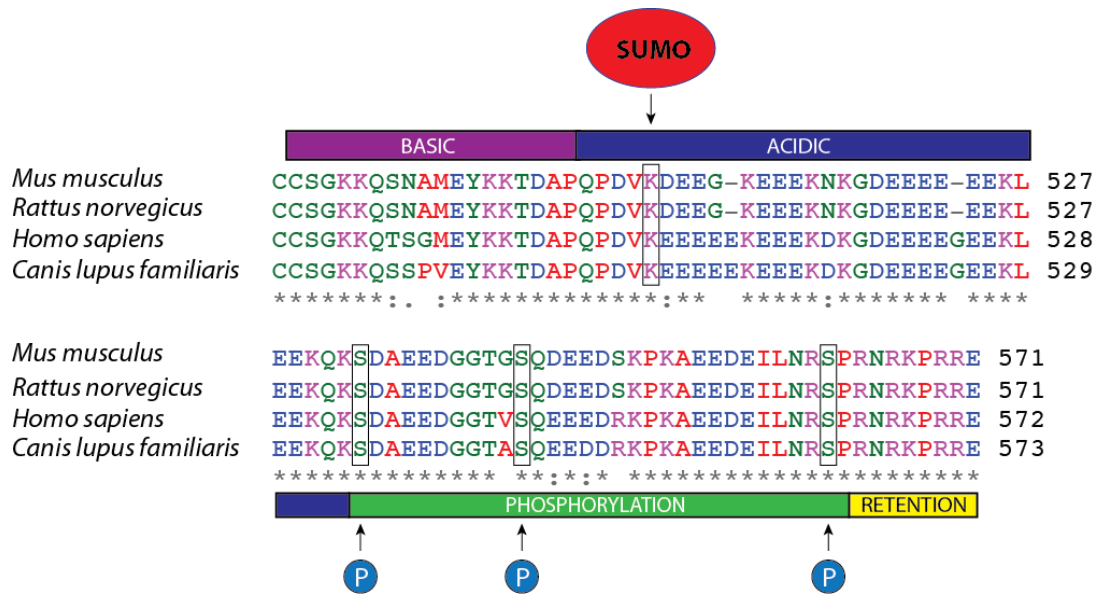


Figure 1.5. Amino acid sequence alignment of the calnexin C-tail in mammalian species.

The above sequence alignment depicts amino acids directly following the transmembrane domain of calnexin from several different mammalian species. * indicates sequence identity whereas : indicates conserved substitutions and . indicates semi-conserved substitutions. **RED**, Small (small + hydrophobic including aromatic - Y); **BLUE**, Acidic; **MAGENTA**, Basic; **GREEN**, Hydroxyl + Amine + Basic - Q. Sequence alignment was conducted with ClustalW2EBI. The calnexin C-tail is highly conserved between mouse, rat, dog and human species. This conservation includes modifiable amino acid residues such as the phosphorylation and SUMOylation (Chapter 4) sites as indicated above by P and SUMO, respectively. Also indicated are the four subdomains of the calnexin C-tail: basic, acidic, phosphorylation and retention.

Approximately 90 amino acids in length, the C-tail can be categorized into four subdomains: a juxtamembrane basic region (lysine rich), an acidic region (glutamic acid rich), a phosphorylation domain, and a putative ER retrieval sequence (Figure 1.5) [100]. The C-tail also contains two putative DXXD caspase cleavage sites. At least one cleavage event following apoptotic stimulus was recorded where over-expression of this cleavage product is found to partially inhibit apoptosis [101]. Thus, calnexin is cleaved at 548D by a DEVDase-like caspase in apoptotic cells. Either caspase 3 or caspase 7 could provide the candidate caspase as they both cleave calnexin at this site *in vitro* [101]. However, both caspase 3 and 7 are effector (executioner) caspases indicating calnexin cleavage takes place after the initiation of apoptosis. Thus, the physiological role and functional relevance of such a cleavage event remains to be investigated. The C-tail contains multiple phosphorylation sites [100, 102] and there is also some evidence that calnexin's cytoplasmic tail binds Ca^{2+} [103]. Studies of a series of early truncation calnexin mutants in *Drosophila* indicate that calnexin's cytoplasmic tail buffers cytosolic Ca^{2+} rise during phototransduction, helping to prevent Ca^{2+} toxicity and promote photoreceptor cell survival [104]. However, there are several calnexin homologs in *Drosophila*, and this function may not be conserved in mammalian species.

Phosphorylation of Calnexin

The cytoplasmic tail of human calnexin contains six potentially phosphorylatable serine residues [100]. Of these potential sites, Ser⁵³⁴ and

Ser⁵⁴⁴ were *in vivo* substrates for casein kinase II (CKII), and Ser⁵⁶³ was an *in vivo* substrate for the proline-directed kinase (PDK) ERK-1 (equivalent residues in canine are Ser⁵³⁵, Ser⁵⁴⁵ and Ser⁵⁶⁴) [100] (Fig. 1.5). Phosphorylation of the C-tail by ERK-1 was shown to enhance association of the cytoplasmic tail with the ribosome, specifically with ribosomal protein L4, a component of the 60S ribosome large subunit [105, 106]. Phosphorylation of Ser⁵⁶² of a rat calnexin construct expressed in *Xenopus* oocytes was demonstrated to regulate an interaction with SERCA2b and control Ca²⁺ oscillations [107]. Interestingly, while phosphorylation events take place in the cytosol, the molecular interaction between calnexin and the SERCA2b Ca²⁺ transporter requires the C-terminal tail of SERCA2b, which is positioned in the lumen [107], indicating more work is needed to understand the molecular mechanism. Recently, it has been demonstrated that ER stress leads to the calcineurin-dependent dephosphorylation of calnexin and subsequent release of SERCA2b inhibition [108]. Calcineurin is a Ca²⁺ and calmodulin dependent serine/threonine phosphatase composed of a catalytic subunit, calcineurin A (CN-A), and a regulatory subunit, calcineurin B (CN-B) [109, 110]. At basal Ca²⁺ levels, the phosphatase is relatively inactive and increases in intracellular Ca²⁺ activate CN-A through Ca²⁺/CaM binding and dissociation of its autoinhibitory domain [111]. Calcineurin expression levels are upregulated and the phosphatase was also shown to interact with PERK to promote its autophosphorylation and resulting downstream protein translation inhibition [108]. It was proposed that the phosphorylation and

dephosphorylation of Ser⁵⁶² regulates ER stores via SERCA2b in response to ER stress.

Phosphorylation of calnexin has also been proposed to control calnexin's distribution in the ER membrane. Fractionation techniques indicate calnexin is moderately enriched in MAM [112]. Nonphosphorylated calnexin associates with PACS-2, an interaction that sequesters calnexin preferentially to the MAM [22]. PACS-2 siRNA treatment causes a reduction of calnexin on the MAM and redistribution to RER membranes. Mutation of Ser⁵³⁴/Ser⁵⁴⁴ to aspartic acid as a phosphorylation mimic reduced the interaction with PACS-2 and resulted in some redistribution to MAM whereas mutation of Ser⁵³⁴/Ser⁵⁴⁴ to alanine had no effect on distribution [22]. Thus, CK2 phosphorylation at Ser⁵³⁴/Ser⁵⁴⁴ of calnexin disrupts its interaction with PACS-2, leading to its redistribution from MAM to RER.

Phosphorylation of the calnexin C-tail has also been postulated to impact its function as a quality control chaperone. A cell based assay was used where the pharmacological agent L-azetidine 2-carboxylic acid (Azc) was used to promote misfolding of a known calnexin substrate, glycoprotein α 1-antitrypsin (AAT), while still allowing its partial secretion [113]. Calnexin phosphorylation at Ser⁵⁶³ by ERK-1 was enhanced under these conditions leading to a prolonged association with AAT and degradation by the proteasome. Inhibition of calnexin Ser⁵⁶³ phosphorylation attenuated AAT degradation and enhanced its secretion, demonstrating phosphorylation of calnexin at Ser⁵⁶³ impacts the retention and degradation of a calnexin

substrate [113]. As ERK-1 activation leads to the recruitment of calnexin to membrane-bound ribosomes [105], it was postulated that calnexin phosphorylation might represent a rapid mechanism to modulate glycoprotein quality control at sites of ER translocons [113]. This suggests that the C-tail is a modifiable entity that can communicate cross-membrane, linking cytoplasmic and ER luminal events.

Other C-tail Post-translational Modifications

Several other post-translational modifications are known to modify the calnexin C-tail. The C-tail contains two juxtamembrane cysteine residues (C⁴⁸³C⁴⁸⁴), predicted as an S-palmitoylation site in a large scale profile of protein palmitoylation [114]. As discussed in Chapter 4, the C-tail binds components of the SUMOylation machinery and can be modified by SUMO *in vivo*.

SUMOylation

Modification by SUMO

SUMO (small ubiquitin-related modifier) is a reversible post-translational modification discovered just over a decade ago [115]. The mechanism of reversible SUMOylation is similar in ways to ubiquitination. SUMOylation is the formation of an isopeptide bond between the C-terminal Gly residue of SUMO and the ϵ -amino group of a Lys residue on the acceptor protein [116]. SUMOylation of a protein takes place in multiple steps (Figure 1.6). The immature SUMO protein precursor must be processed by ubiquitin-like

protein-specific proteases (Ulp) or sentrin-specific proteases (SENPs) to generate the mature SUMO protein with an exposed C-terminal diglycine motif. This motif is required for efficient adenylation by the SUMO-specific E1 activating enzyme heterodimer, SAE1/SAE2 [117]. A conserved Cys on the E1 enzyme forms an E1-SUMO thioester linkage that is then transferred from the E1 to the E2 conjugating enzyme UBC9 to form an E2-SUMO thioester. UBC9 can directly interact with substrates to transfer SUMO to acceptor Lys residues or this process can be facilitated by SUMO E3 ligases [118-120]. Although SUMO E3 ligases are not required and only a few have been identified, SUMO conjugation is almost always enhanced with E3 ligases [121]. E3 ligases can promote specificity by sequestering E2-SUMO and the substrate in a complex or they can stimulate the ability of UBC9 to transfer SUMO to the substrate protein [121]. The consensus acceptor site for SUMOylation is ΨKxE in which Ψ is a bulky aliphatic amino acid and x is any amino acid although extended SUMOylation motifs have also been identified [116]. In addition to the core consensus motif, additional flanking sequences have been proposed to extend the SUMO consensus motif. These include a phosphorylation-dependent SUMOylation motif (PDSM) and a negatively charged amino acid-dependent SUMOylation motif (NDSM). Phosphorylation-dependent SUMOylation is where the canonical SUMOylation site is followed by a phosphorylated Ser and a Pro residue ($\Psi KxE_{\text{pp}}SP$) [122]. The NDSM is composed of the core consensus motif followed by a cluster of acidic residues in the 10-amino-acid region immediately downstream. These acidic residues

are often found in a hotspot consisting of downstream amino acid residues 3-6 [123]. These extended motifs confer increased specificity for SUMO modification. SUMO-relevant but not SUMO modified motifs also exist. A SUMO interaction motif can be found in proteins that interact non-covalently with SUMOylated proteins. This SIM/SBM (SUMO-interaction/binding motif) is composed of a hydrophobic core flanked by acidic residues and in some cases Ser residues [124]. SUMOylation is a reversible modification, a process carried out by the SENPs which can also act as isopeptidases in addition to their endopeptidase activity in activating immature SUMOs [125].

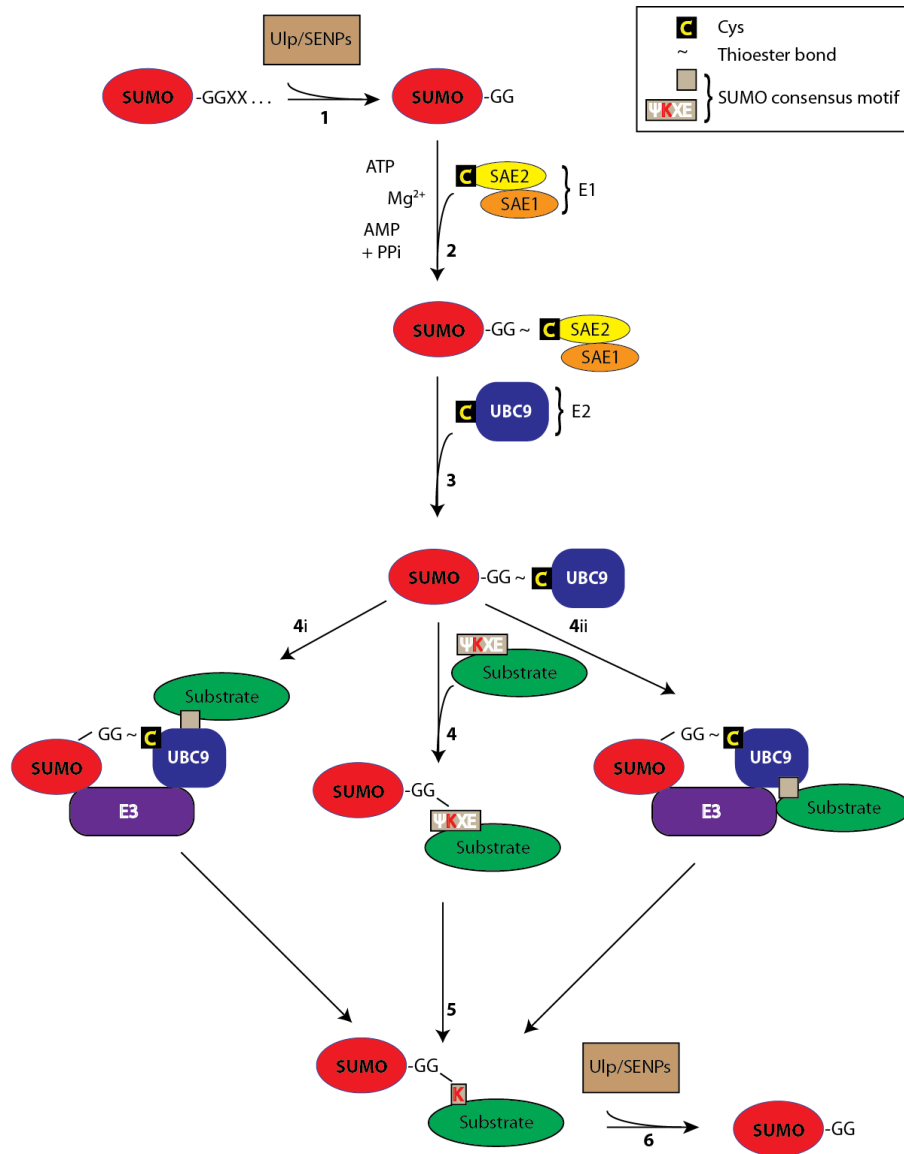


Figure 1.6. The SUMOylation pathway.

1) The immature SUMO precursor is processed by Ulp or SENP proteases to expose a carboxy-terminal Gly-Gly motif. 2) SUMO is adenylated by the SAE1/SAE2 E1 activating enzyme and transferred to the catalytic Cys residue of the SAE2 subunit. 3) SUMO is transferred to the Cys of the E2 conjugating enzyme, UBC9. 4) SUMO is transferred to a Lys residue in the SUMO consensus motif, ΨKxE. This can be facilitated directly through UBC9, **4i**) coordinated through an E3 ligase that does not directly contact the substrate or **4ii**) through substrate specificity imparted by the E3 enzyme where the E3 directly binds the substrate, SUMO and UBC9. 5) SUMO conjugation to the lysine residue can be reversed through the **6**) deconjugation by Ulp and SENP proteases.

There are four known SUMO paralogues in mammals, SUMO 1, 2, 3 and 4. SUMO 2 and 3 are 95% identical in amino acid sequence whereas SUMO-2 is 48% and SUMO-3 46% identical to SUMO-1 [126]. SUMO-4 has 86% amino acid homology to SUMO-2 and was discovered as a gene associated with type I diabetes mellitus susceptibility [127, 128]. Despite its similarity to SUMO-2, it appears to have some tissue specificity and mRNA expression was detectable in kidney, lymph and spleen but not significantly in liver, pancreas, testes or smooth muscle [127, 128]. It is somewhat controversial if SUMO-4 can be conjugated to substrates as it is thought that a unique proline residue prevents the hydrolyzation of SUMO-4 necessary for activation [129], although I κ B α and heat shock factor 2 (HSF2) have been reported as SUMO-4 substrates [127, 128] and SUMO-4 is thought to be conjugated under stress conditions [130]. SUMO-2 and -3 constitute the greatest percentage of total cellular protein SUMO modification. There is a large pool of free, non-conjugated SUMO-2/3 under basal conditions whereas most SUMO-1 appears to be conjugated to protein substrates [126]. While the functional implications of modification by SUMO-1 versus SUMO-2/3 are not understood, they appear to play distinct roles. SUMO-2/3 conjugation is activated after heat shock, whereas the pattern of SUMO-1 conjugation is not dramatically changed [126]. Additionally, the first SUMOylated substrate ever identified, RanGAP1, is known to be modified by SUMO-1 but very poorly modified by SUMO-2/3 [126]. Many substrates can undergo

modification by both SUMO-1 and SUMO 2/3 and in some cases SUMO-1 and SUMO 2/3 can form mixed chains [131]. The effect of SUMO-1 versus SUMO-2/3 conjugation likely depends on the target substrate and cellular localization and remains to be investigated.

Function of SUMOylation

SUMOylation has diverse functional implications and the impact of SUMO modification is related to the substrate modified, its cellular location, and the conditions under which it is regulated. Studies have shown significant changes in global SUMOylation patterns in response to stimuli such as heat shock, oxidative and ethanol stressors [126, 132]. Many SUMOylated proteins identified thus far are nuclear proteins and UBC9 activity and SUMOylation have been extensively studied in the nuclear compartment as a part of transcriptional control. However, targets for SUMOylation can be found in various locations throughout the cell [116]. Interestingly, in the last five years, examples of integral membrane proteins modified by SUMO have emerged [133, 134]. SUMO modification has been shown to inactivate the plasma membrane potassium leak channel K2P1 and regulate the endocytosis of the kainate receptor and subsequent synaptic transmission after SUMOylation of the GluR6 kainate receptor subunit [133, 134]. Other membrane protein targets include voltage-dependent K(+) (K_v) channels, glucose transporters and the group 3 metabotropic glutamate receptors [135-138]. SUMOylation has also been reported at mitochondrial membranes where dynamin related protein (DRP1), a protein that

coordinates membrane scission, is a substrate for SUMO-1 [139]. Additionally, although unidentified, SUMO-1 conjugates were observed in mitochondrial fractions potentially suggesting a role of SUMOylation in the regulation of mitochondrial protein turnover and/or function [140]. While the functional significance is not completely understood, SUMOylation at plasma and mitochondrial membranes would provide an additional level of post-translational regulation of protein localization, function or binding partners and might provide a method of communicating local events across a membrane partition.

Prior to the identification that calnexin is modified by SUMO (Chapter 4), only one ER protein was known to be SUMOylated. Protein tyrosine phosphatase 1B (PTP1B) is a protein of interest in metabolic studies as it negatively regulates growth-factor signaling by binding to and dephosphorylating receptor tyrosine kinases such as the insulin receptor [141]. Tyrosine phosphatase-1B localizes to the cytoplasmic face of the ER and nuclear envelope and is inactivated by SUMOylation [142]. Interestingly, changing the cellular localization of PTP1B changes its degree of SUMOylation [142]. The E3 ligase responsible for SUMOylation of DRP1 at mitochondrial membranes is mitochondrial-anchored SUMO E3 ligase (MAPL). Given the proximity of the two organelles, it has been postulated that MAPL might be involved in ER localized SUMO conjugation [143]. The significance of ER localized SUMOylation will be discussed further in Chapter 4.

Quality Control and Myelination

Myelin is a highly specialized entity unique to the nervous system. A defining feature of vertebrates, this evolutionary development reduced the energy required for neuronal communication and boosted the speed of impulse propagation to allow the timely and efficient operation of complex nervous systems [144]. Aberrant formation or maintenance of the myelin sheath results in a morphology collectively termed dysmyelination and contributes to a number of diseases including Multiple Sclerosis (MS), Charcot-Marie-Tooth (CMT), leukodystrophy, schizophrenia, Alzheimer's and Parkinson's disease. Myelin pathologies have been modeled in various murine models but complete molecular mechanisms of dysmyelination and therapeutic targets remain elusive. Recently, the importance of the ER and its resident molecules in myelination has been realized [145]. A site for myelin protein synthesis, specialized lipid synthesis, Ca²⁺ storage and protein folding quality control checks, the response of the ER to the unique demands of myelinating systems is critical in the maintenance of a healthy nervous system.

Myelin

Myelination is a membranous extension of embryological and morphologically distinct glial cells of the central and peripheral nervous system; an oligodendrocyte myelinates multiple axons and internodes in the former, whereas a Schwann cell is dedicated to the ensheathment of a single axon/internode in the latter. Myelin membranes have a unique composition

of lipids and proteins that maintain myelin structure and integrity (Figure 1.7). This integrity is critical for the timely and precise conduction of action potentials in axons with myelin increasing nerve conduction velocity up to 100-fold. Furthermore, myelinating glia are required for the long-term integrity and survival of axons [146]. A process initiated postnatally, myelinating glia are directed to axons with a diameter of 1 μM or greater [147]. In humans, myelin formation takes place during the second half of fetal life, peaking in the first year but continuing through to 20 years of age [148]. In mice, myelination is detectable at embryonic day 16.5 and peaks at postnatal day 18 [149]. During myelination, Schwann cells or oligodendrocytes wrap membranous spiral extensions around axons with a thickness correlating to axon diameter. Appropriate myelin thickness can be determined using a simple measurement known as the *g*-ratio, defined as a ratio of the inner axonal diameter to the total outer diameter (axon+myelin sheath). A *g*-ratio of 0.6 is expected in the peripheral nervous system (PNS) while a slightly higher *g*-ratio of 0.72-0.81 is appropriate in the central nervous system (CNS) [150, 151]. To initiate myelination, axon-derived signals relative to the axon size recruit and promote the differentiation of myelinating glia. In the PNS, myelination is initiated when a threshold level of axonal neuregulin-1 type III expression is reached and this expression is important for the subsequent regulation of myelin membrane growth [152].

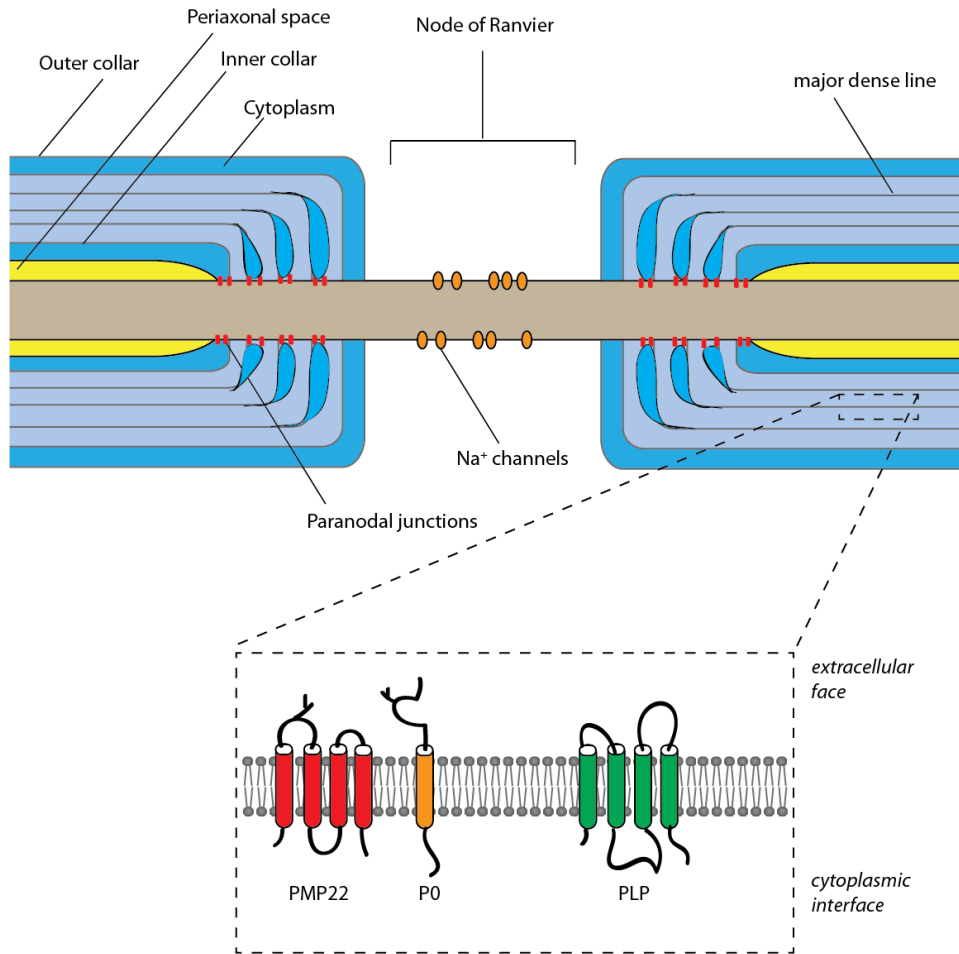


Figure 1.7. The compact myelin sheath.

Schwann cells and oligodendrocytes wrap membranous extensions around axons to form compact myelin sheaths. Each Schwann cell forms a distinct internode whereas oligodendrocytes myelinate multiple internodes. Voltage-gated Na⁺ channels are clustered at the Nodes of Ranvier, areas of unmyelinated axons between internodes. Paranodal junctions are found adjacent to the Nodes of Ranvier to provide a diffusion barrier. Compact myelin sheaths are maintained through adhesive myelin proteins expressed at the cell surface such as peripheral myelin protein 22 (PMP22) and myelin protein zero (P0) of the peripheral nervous system (PNS), and proteolipid protein (PLP) of the central nervous system (CNS).

Myelination in the CNS is more complex and appears to be regulated by a balance of positive and negative neuronal signals [153]. For example, expression of polysialylated-neural cell adhesion molecule (PSA-NCAM) has been shown to inhibit myelination on the neuronal cell surface [154] whereas expression of the L1 adhesion molecule on the neuronal cell surface is required for the initial stage of adhesion, after which it is down-regulated [153]. Regardless of how myelination is initiated, the appropriate timing of myelin formation is critical for nervous system development.

Myelin membranes are distinctive with cholesterol, phospholipids and glycosphingolipids accounting for 70% of the dry weight of the membrane. The unique lipid composition is enriched in galactosylceramide, sulfatide, ethanolamine, plasmalogen, and cholesterol with cholesterol comprising 25% of the total lipid content [155]. Cholesterol is not imported from the circulation but instead synthesized locally and is rate-limiting for myelin biogenesis [156, 157]. It has been reported that during active myelination in rats, the myelin-membrane surface area expands at an estimated rate of $5\text{--}50 \times 10^3 \mu\text{m}^2/\text{cell}/\text{day}$, a daily rate of more than 100-fold the surface area of the cell soma (i.e. plasma membrane) of approximately $0.3 \times 10^3 \mu\text{m}^2$ [158]. From an immature to a fully myelinated oligodendrocyte, this corresponds to an estimated 6,500-fold increase in membrane surface [159, 160]. Supply must meet demand and such an astounding rate of growth requires specialized cellular mechanisms. The large amounts of membrane and myelin specific proteins generated depend on vesicular trafficking for movement to

the plasma membrane. Generation of myelin depends on the exocytosis of myelin lipids and proteins from the biosynthetic pathway and an endosomal pool. Changes in the balance of exocytosis/endocytosis provide a mechanism of myelin generation where down-regulation of endocytosis contributes to membrane deposition [161].

The final architecture of a myelin sheath provides the structure to support fast, saltatory conduction down an axon in an insulated environment (Fig. 1.7). The sheaths provide an insulated and metabolically isolated environment for the axon that is interrupted by exposed axonal membranes known as nodes of Ranvier. Saltatory conduction takes place at the nodes of Ranvier where Na^+ channels are clustered in the axonal membrane between paranodal axoglial junctions that provide a diffusion barrier. Fast K^+ channels are concentrated in the adjacent juxtaparanodal region. Compact myelin forms a periodic structure around the axon with the innermost part of the sheath being the farthest extension of the myelinating glial cell. The axon and myelin sheath are separated by a periaxonal space, and the compact myelin is connected through gap junctions in the Schmidt-Lanterman incisures (SLIs) or local stacks of non-compact myelin. The periodic ultrastructure of myelin is maintained by homo and heterophilic interactions of specific myelin proteins expressed in glia cells that confer the structural stability for compact, organized myelin sheaths. Two such proteins, peripheral myelin protein 22 (PMP22) and myelin protein zero (P0), are components of compact myelin in the peripheral nervous system. Myelin protein zero (MPZ

or P0) is the most abundant protein in peripheral myelin, accounting for approximately 50% of the total protein content [162, 163]. A single-pass transmembrane protein, P0 has a glycosylated extracellular immunoglobulin-like domain stabilized by a disulfide domain [163, 164]. P0 undergoes homophilic interactions to act as an adhesion protein connecting adjacent myelin lamellae [165]. Both the extracellular and cytoplasmic domain of P0 are required for its adhesive function [166]. P0 also undergoes heterophilic interactions with PMP22 [167], a 22-kDa tetraspan transmembrane glycoprotein that constitutes 2-5% of the total myelin protein content [168].

While myelin is essential for physiologically relevant nerve conduction velocities and motor function, another very important function of myelination is its contribution to neuronal development and survival [169]. Secondary axon degeneration as a consequence of dysmyelination leads to the serious long-term disabilities seen in MS and CMT. Demyelination in the Trembler mouse (mutant PMP22) results in a decrease in neurofilament phosphorylation and reduces the rate of slow axonal transport [170]. Reduced axonal calibre was also observed as a consequence of the reduced neurofilament phosphorylation [170]. While myelination is important for axonal preservation, the presence of the glia, independent of myelination is also important. Myelinating glia regulate the microenvironment surrounding neurons, provide trophic support, and contribute to neuronal development independently of myelination [171, 172]. Neurons and myelinating glia have a symbiotic relationship and defects in either one will have detrimental

functional consequences on the other. Consequently, myelin disease could originate from problems with the neuron, and it has been proposed that in diseases like MS, aberrant expression of certain molecules on the neuronal surface could inhibit the remyelination process [173].

ER Protein Quality Control and Myelination

N-glycosylation of nascent proteins targets them to the calnexin/calreticulin cycle. A number of major myelin proteins are glycosylated including P0 and PMP22 of the PNS and the minor but highly immunogenic component of the CNS, myelin oligodendrocyte glycoprotein MOG [162, 174-177]. This makes lectin chaperones particularly important for myelin protein quality control (Figure 1.8). In its capacity as a lectin quality control chaperone, calnexin is likely involved in the folding of all glycosylated integral membrane myelin proteins.

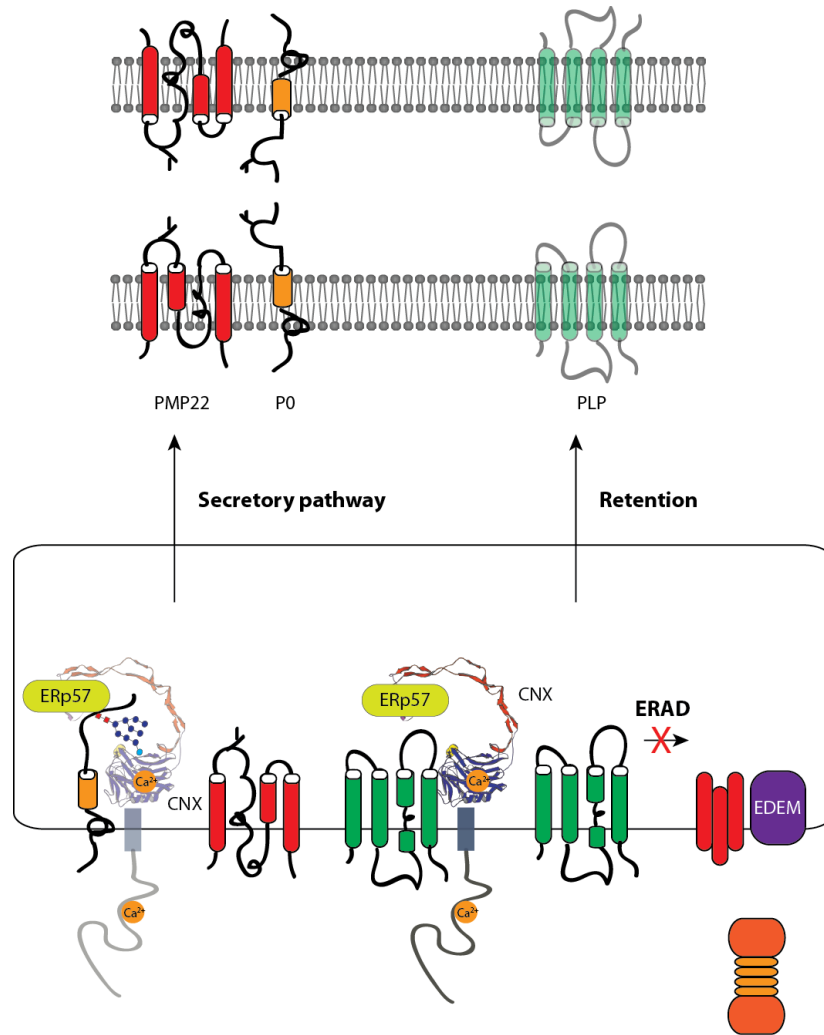


Figure 1.8. Quality control of myelin proteins.

Myelin proteins are often glycosylated and thus calnexin substrates. Problems with the quality control apparatus can lead to two independent outcomes: misfolded proteins either escape the quality control system and enter the secretory pathway or are successfully, although potentially more detrimentally, retained in the ER. Recently, misfolded peripheral myelin protein 22 (PMP22) and protein zero (P0) have been shown to traffic through the secretory pathway to the cell surface in the absence of calnexin. Mutant proteolipid protein (PLP) is retained in the ER, leading to loss of its expression at the plasma membrane. If ER-associated degradation (ERAD) is unable to cope with the misfolded protein load retained by quality control chaperones in the ER, it can lead to the induction of the Unfolded Protein Response (UPR). Both trafficking of misfolded proteins through the secretory pathway and retention of misfolded proteins in the ER results in problems with critical structural elements for compact myelin sheaths.

There are many animal models available to study different aspects and effects of dysmyelination [178] and several mouse models have led to the discovery of the genetic contributions underlying clinical disease. Notably, several of these dysmyelination mouse models are attributable to gene mutations that result in a loss of appropriate protein folding and trafficking quality control at the ER. One such example is the *trembler* (*Tr*) and *trembler-J* (*Tr-J*) mice. *Tr* and *Tr-J* mice carry natural autosomal dominant mutations in the gene encoding PMP22 [179] and led to the identification of a role for PMP22 in the clinical disease CMT [180]. CMT, one of the most commonly inherited neurological disorders with more than 30 different contributing genes, affects the peripheral nervous system. Clinically, the disease is categorized into 4 main types (CMT1-4) and these are classified into further subtypes depending on the causative gene (for a list see <http://www.molgen.ua.ac.be/CMTMutations/Home/IPN.cfm>). Since the identification of the *trembler* mice, PMP22 mutation and overexpression murine models have been used extensively to study various CMT subtypes. PMP22 duplication resembles CMT1 and mice overexpressing PMP22 demonstrate a slower rate of myelination restricted to small diameter axons with a resulting decreased myelin thickness (hypomyelination) [181]. Mice devoid of PMP22 have a delayed onset of myelination and develop abundant tomacula [182], a term derived from the Latin word *tomaculum* (meaning sausage) that is used to describe the bulbous expansions of redundant myelin. PMP22 deletion is reminiscent of hereditary neuropathy with liability

to pressure palsies (HNPP) [183, 184]. A number of PMP22 point mutants are retained in the ER and are never trafficked to the myelin membrane [185-187]. PMP22^{Tr} and PMP22^{Tr-J} mutants are known to have prolonged association with calnexin in the ER and it has been postulated that this prolonged retention of mutant PMP22 provides a mechanism for the resulting neuropathies [188]. Absence of PMP22 at the myelin membrane can result from lack of protein expression or a point mutation causing it to be retained in the ER. Either one leads to the loss of a critical myelin structural element (Figure 1.8).

Myelin P0 is the most abundant protein component of peripheral myelin and more than 90 different point mutations in the gene encoding P0 are known to contribute to inherited neuropathies including CMT and DSN. Similar to PMP22 mutant proteins, many P0 mutants are retained in the endoplasmic reticulum. Interestingly, curcumin, a dietary supplement, has been shown to stimulate the translocation of ER retained mutant P0 and subsequently reduce apoptosis induced by P0 mutant accumulation [189]. Thus, overcoming the ER retention of mutant P0 and PMP22 could be beneficial (Figure 1.8).

Pelizaeus-Merzbacher disease (PMD) is a dysmyelinating disease of the central nervous system. Reminiscent of CMT, PMD is caused by heterogeneous missense mutations, gene duplication or deletion of a myelin protein, proteolipid protein (PLP). Similarly to P0 in the PNS, PLP is the major protein component of the CNS. It was the similarities between PMD

and CMT1A (caused by a duplication of PMP22) that led to the identification of PLP duplications in PMD patients [190]. Correlations can be made between the type of mutation and the clinical phenotype with deletions resulting in mild disease, duplications in moderate PMD, and missense mutations leading to severe disease [191]. However, the clinical severity of PMD cannot be explained by the size of PLP duplication [192] and it has been proposed that modifier genes within the duplicated region or elsewhere in the genome may affect PLP expression and subsequent disease pathogenesis [191]. As well, the disease caused by missense mutations can range in phenotypic severity from mild PMD and late-onset spastic paraplegia type 2 (SPG2), characterized by hypomyelination [193, 194], to the severe congenital PMD, characterized by a severe deficit of myelin sheaths and widespread oligodendrocyte apoptosis [195, 196]. The pathogenic mechanism underlying PMD was thought to be related to the accumulation of misfolded PLP in the ER, leading to the activation of the UPR and oligodendrocyte apoptosis [197-199]. However, this did not address the range in phenotypic severity seen with various missense mutations. A recent study examined two different mutations within PLP, the A²⁴²V mutant associated with severe PMD and the G²⁴⁵A mutant associated with mild disease [200]. Both mutants were localized with calnexin in the ER, indicating ER retention. However, the G²⁴⁵A mutant associated with mild disease was more efficiently cleared from the ER for degradation than the severe-disease-associated A²⁴²V mutant. It was also observed that the A²⁴²V mutant formed oligomeric structures. The decreased

ERAD of the A^{242V} led to the induction of UPR, and reduced cell viability under high mutant expression conditions, whereas the mild phenotype G^{245A} mutant did not activate UPR. Similarly to PMP22 and P0 mutants, ER retention of PLP mutants appears to contribute to the resulting disease.

ER Stress in Demyelination

ER stress is thought to contribute to demyelinating pathologies. The ER is an essential site of secreted and transmembrane protein synthesis and folding and maintenance of ER homeostasis is critical for cellular function and survival. Glial cells require large amounts of lipids and proteins to form their myelinating processes and such a system would be particularly sensitive to any aberrations in the secretory organelle or its components that supplied the necessary building blocks for myelin. Recently, components and/or activation of UPR have been implicated in demyelination. It was proposed that the rate of which different proteolipid (PLP) mutants are cleared from the ER and the extent of UPR activation could explain the varying disease severity of the mutants where increased UPR correlates to increased severity [200]. In fact, ablation of CHOP (CCAAT/enhancer-binding protein (C/EBP) homologous protein), a downstream effector of UPR signaling, restores the motor function and reduces demyelination two-fold in POS^{63del} mice, a model of CMT1B [201].

Antibodies to MOG are elevated in MS patients and this is thought to be part of the autoimmune destruction of myelin [202-204]. Interestingly, when the molecular effects of antibody cross-linking of MOG on the surface of

oligodendrocytes were investigated, changes in stress response-related proteins were observed [205]. Anti-MOG antibodies led to the increased phosphorylation of EF-2, HSP74 and α -enolase, and subsequent activation of cellular stress pathways. This implicates that antibody recognition of MOG in autoimmune demyelinating diseases such as MS can activate an ER stress response.

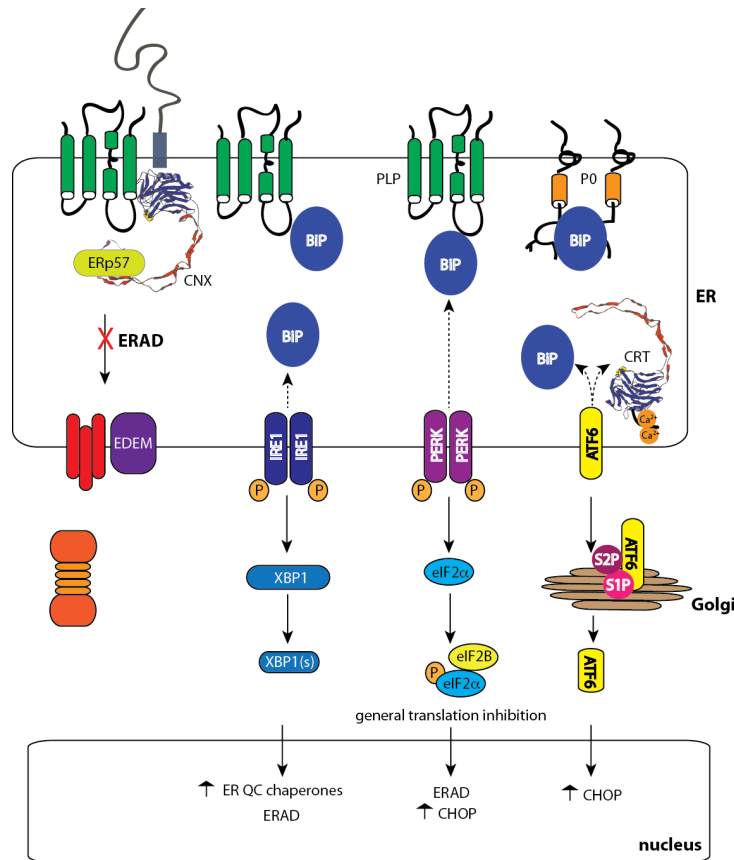


Figure 1.9. ER stress and misfolded myelin proteins.

Sustained protein unfolding in the ER, such as would be the case with myelin proteins proteolipid protein (PLP) or protein zero (P0) containing certain amino acid mutations, activates the Unfolded Protein Response. This is modulated through three endoplasmic proteins sensors, IRE1, PERK, and ATF6. BiP binds to all three proteins and it is titrated away by unfolded proteins in the ER lumen. Upon the dissociation of BiP, IRE1 dimerizes and auto-phosphorylates, activating its RNase domain. XBP-1 mRNA is cleaved with spliced XBP1 mRNA being an active transcription factor that induces the translation of ER quality chaperones and folding machinery to deal with the increased protein load. Upon BiP titration, PERK similarly dimerizes and auto-phosphorylates. PERK also phosphorylates eIF1 α , leading to the inhibition of general translation. Along with BiP, calreticulin also retains ATF6 in the ER, a retention mechanism that is overcome under ER stress conditions by underglycosylation of newly synthesized ATF6. Loss of BiP and CRT interaction allows ATF6 to translocate to the Golgi where it is cleaved by Site-1-protease (S1P) and Site-2-protease (S2P), releasing its cytosolic bZIP domain that translocates to the nucleus to activate transcription of proteins such as CHOP, a pro-apoptotic transcription factor.

The Role of ER Ca²⁺ Stores in Myelin

The ER is responsible for the storage of the majority of intracellular Ca²⁺ and this high Ca²⁺ concentration is required for protein folding and glycoprotein processing [7, 8]. The glutamatergic system of excitatory neurotransmission, where glutamate is the natural ligand for the ion-permeable channels α -amino-3-hydroxy-methyl-4-isoxazole propionic acid (AMPA), kainate and *N*-methyl-D-aspartate (NMDA) receptors, is critical for excitatory neurotransmission in the CNS and essential to plasticity and neuronal development. NMDA receptors are slow gating channels that are highly permeable to Na⁺ and Ca²⁺ and activation of NMDA receptors is known to induce Ca²⁺-induced Ca²⁺ release (CICR) from internal Ca²⁺ stores (i.e. ER) in hippocampal dendritic spines [206]. It was previously thought that AMPA and kainate receptors, but not NMDA receptors, were expressed in white matter glia [207]. Since then, several groups have demonstrated the presence of NMDAR in oligodendrocyte processes and the inner and outer loops of compact myelin where NMDAR is shown to mediate Ca²⁺ accumulation in myelin during chemical ischemia [208-210]. As previously discussed, resident chaperone molecules of the ER, such as calnexin, are critical for the quality control and assembly of transmembrane proteins, including plasma membrane receptors such as the NMDA and AMPA receptor. Calnexin has been shown to interact with the NR1 NMDA receptor subunit [211] and glycosylated AMPA receptors [212]. In this case, the contributions of the ER to healthy myelin sheaths is two-fold: first, quality control chaperones are

responsible for the appropriate folding, assembly and trafficking of the NMDAR subunits to the plasma membrane, second, the appropriate modulation of potentially damaging ER Ca^{2+} stores downstream of NMDAR activation is critical. Maintaining ER Ca^{2+} homeostasis through regulation of the plasma membrane receptors and the internal ER Ca^{2+} store is essential to prevent structural damage caused to myelin with Ca^{2+} accumulation.

Objectives

An objective of my thesis was to investigate the functional role of calnexin in a mouse model. We employed a loss-of-function approach to examine the impact of calnexin-deficiency in a mouse model. The major structural difference between calreticulin and calnexin is that calnexin has a transmembrane domain and cytoplasmic tail in addition to its N+P luminal domain. To determine the functional significance of the unique calnexin C-tail, we examined structural and biophysical characteristics of the C-tail. We also investigated novel protein-binding partners and post-translational modifications.

Hypothesis

My hypothesis was that abrogating calnexin protein expression in a mouse model would provide key information on the critical functional role of calnexin. As calnexin is ubiquitously expressed, a complete interruption of protein expression will indicate which system calnexin is most important for. As the major structural difference between calnexin and other ER quality control chaperones, such as calreticulin, is calnexin's unique transmembrane domain and cytoplasmic domain, I hypothesized that the C-tail of calnexin plays important structural and functional roles in the protein. Elucidating protein-binding partners will help define molecular complexes that interact with the C-tail and thus its function.

References

1. Cooper, G.M., *The Cell: A Molecular Approach*. 2nd ed. 2000, Sunderland MA: Sinauer Associates.
2. Shibata, Y., G.K. Voeltz, and T.A. Rapoport, *Rough sheets and smooth tubules*. *Cell*, 2006. **126**(3): p. 435-439.
3. Robinson, R., *Axonal signaling proteins take the ER highway*. *PLoS Biol.* **8**(10).
4. Fawcett, D.W., *The Cell*. 2nd ed ed. 1981, Philadelphia: Saunders.
5. Goldberg, M.W. and T.D. Allen, *Structural and functional organization of the nuclear envelope*. *Curr Opin Cell Biol*, 1995. **7**(3): p. 301-309.
6. Rizzuto, R., P. Pinton, W. Carrington, F.S. Fay, K.E. Fogarty, L.M. Lifshitz, R.A. Tuft, and T. Pozzan, *Close contacts with the endoplasmic reticulum as determinants of mitochondrial Ca²⁺ responses*. *Science*, 1998. **280**(5370): p. 1763-1766.
7. Lodish, H.F., N. Kong, and L. Wikstrom, *Calcium is required for folding of newly made subunits of the asialoglycoprotein receptor within the endoplasmic reticulum*. *J. Biol. Chem.*, 1992. **267**: p. 12753-12760.
8. Kuznetsov, G., M.A. Brostrom, and C.O. Brostrom, *Demonstration of a calcium requirement for secretory protein processing and export. Differential effects of calcium and dithiothreitol*. *J Biol Chem*, 1992. **267**(6): p. 3932-3939.
9. Berridge, M.J., M.D. Bootman, and H.L. Roderick, *Calcium signalling: dynamics, homeostasis and remodelling*. *Nature Rev. Mol. Cell Biol.*, 2003. **4**(7): p. 517-529.
10. Meldolesi, J. and T. Pozzan, *The endoplasmic reticulum Ca²⁺ store: a view from the lumen*. *Trends Biochem. Sci.*, 1998. **23**: p. 10-14.
11. Corbett, E.F. and M. Michalak, *Calcium, a signaling molecule in the endoplasmic reticulum?* *Trends Biochem. Sci.*, 2000. **25**(7): p. 307-311.
12. Demaurex, N. and M. Frieden, *Measurements of the free luminal ER Ca(2+) concentration with targeted "cameleon" fluorescent proteins*. *Cell Calcium*, 2003. **34**(2): p. 109-119.
13. Fliegel, L., K. Burns, K. Wlasichuk, and M. Michalak, *Peripheral membrane proteins of sarcoplasmic and endoplasmic reticulum. Comparison of carboxyl-terminal amino acid sequences*. *Biochem. Cell Biol.*, 1989. **67**: p. 696-702.
14. Nakamura, K., A. Zuppini, S. Arnaudeau, J. Lynch, I. Ahsan, R. Krause, S. Papp, H. De Smedt, J.B. Parys, W. Müller-Esterl, D.P. Lew, K.-H. Krause, N. Demaurex, M. Opas, and M. Michalak, *Functional specialization of calreticulin domains*. *J. Cell Biol.*, 2001. **154**: p. 961-972.
15. Baksh, S. and M. Michalak, *Expression of calreticulin in Escherichia coli and identification of its Ca²⁺ binding domains*. *J. Biol. Chem.*, 1991. **266**: p. 21458-21465.

16. Van, P.N., F. Peter, and H.-D. Soling, *Four intracisternal calcium-binding glycoproteins from rat liver microsomes with high affinity for calcium. No indication for calsequestrin-like proteins in inositol 1,4,5-trisphosphate-sensitive calcium sequestering rat liver vesicles.* J. Biol. Chem., 1989. **264**: p. 17494-17501.
17. Argon, Y. and B.B. Simen, *GRP94, an ER chaperone with protein and peptide binding properties.* Semin Cell Dev Biol, 1999. **10**(5): p. 495-505.
18. Macer, D.R.J. and G.E.L. Koch, *Identification of a set of calcium-binding proteins in reticuloplasm, the luminal content of the endoplasmic reticulum.* J. Cell Sci., 1988. **91**: p. 61-70.
19. Lievremont, J.P., R. Rizzuto, L. Hendershot, and J. Meldolesi, *BiP, a major chaperone protein of the endoplasmic reticulum lumen, plays a direct and important role in the storage of the rapidly exchanging pool of Ca²⁺.* J. Biol. Chem., 1997. **272**: p. 30873-33089.
20. Booth, C. and G.E.L. Koch, *Perturbation of cellular calcium induces secretion of luminal ER proteins.* Cell, 1989. **59**: p. 729-737.
21. de Brito, O.M. and L. Scorrano, *Mitofusin 2 tethers endoplasmic reticulum to mitochondria.* Nature, 2008. **456**(7222): p. 605-610.
22. Myhill, N., E.M. Lynes, J.A. Nanji, A.D. Blagoveshchenskaya, H. Fei, K. Carmine Simmen, T.J. Cooper, G. Thomas, and T. Simmen, *The subcellular distribution of calnexin is mediated by PACS-2.* Molecular Biol. Cell, 2008. **19**(7): p. 2777-2788.
23. Anelli, T. and R. Sitia, *Protein quality control in the early secretory pathway.* EMBO J, 2008. **27**(2): p. 315-327.
24. Walter, P. and G. Blobel, *Translocation of proteins across the endoplasmic reticulum. II. Signal recognition protein (SRP) mediates the selective binding to microsomal membranes of in-vitro-assembled polysomes synthesizing secretory protein.* J Cell Biol, 1981. **91**(2 Pt 1): p. 551-556.
25. Halic, M., M. Blau, T. Becker, T. Mielke, M.R. Pool, K. Wild, I. Sinning, and R. Beckmann, *Following the signal sequence from ribosomal tunnel exit to signal recognition particle.* Nature, 2006. **444**(7118): p. 507-511.
26. Hegde, R.S. and S.W. Kang, *The concept of translocational regulation.* J Cell Biol, 2008. **182**(2): p. 225-232.
27. von Heijne, G., *Signal sequences. The limits of variation.* J Mol Biol, 1985. **184**(1): p. 99-105.
28. Hegde, R.S. and H.D. Bernstein, *The surprising complexity of signal sequences.* Trends Biochem Sci, 2006. **31**(10): p. 563-571.
29. Schlenstedt, G., G.H. Gudmundsson, H.G. Boman, and R. Zimmermann, *A large presecretory protein translocates both cotranslationally, using signal recognition particle and ribosome, and post-translationally, without these ribonucleoparticles, when synthesized in the presence of mammalian microsomes.* J Biol Chem, 1990. **265**(23): p. 13960-13968.

30. Hamman, B.D., L.M. Hendershot, and A.E. Johnson, *BiP maintains the permeability barrier of the ER membrane by sealing the luminal end of the translocon pore before and early in translocation*. *Cell*, 1998. **92**(6): p. 747-758.
31. Haigh, N.G. and A.E. Johnson, *A new role for BiP: closing the aqueous translocon pore during protein integration into the ER membrane*. *J Cell Biol*, 2002. **156**(2): p. 261-270.
32. Meunier, L., Y.K. Usherwood, K.T. Chung, and L.M. Hendershot, *A subset of chaperones and folding enzymes form multiprotein complexes in endoplasmic reticulum to bind nascent proteins*. *Molecular Biol. Cell*, 2002. **13**(12): p. 4456-4469.
33. Aebi, M., R. Bernasconi, S. Clerc, and M. Molinari, *N-glycan structures: recognition and processing in the ER*. *Trends Biochem Sci*. **35**(2): p. 74-82.
34. Jager, M. and A. Pluckthun, *The rate-limiting steps for the folding of an antibody scFv fragment*. *FEBS Lett*, 1997. **418**(1-2): p. 106-110.
35. Feige, M.J., S. Groscurth, M. Marcinowski, Y. Shimizu, H. Kessler, L.M. Hendershot, and J. Buchner, *An unfolded CH1 domain controls the assembly and secretion of IgG antibodies*. *Mol Cell*, 2009. **34**(5): p. 569-579.
36. Schmid, F.X., *Prolyl isomerase: enzymatic catalysis of slow protein-folding reactions*. *Annu Rev Biophys Biomol Struct*, 1993. **22**: p. 123-142.
37. Helenius, J., D.T. Ng, C.L. Marolda, P. Walter, M.A. Valvano, and M. Aebi, *Translocation of lipid-linked oligosaccharides across the ER membrane requires Rft1 protein*. *Nature*, 2002. **415**(6870): p. 447-450.
38. Nilsson, I.M. and G. von Heijne, *Determination of the distance between the oligosaccharyltransferase active site and the endoplasmic reticulum membrane*. *J Biol Chem*, 1993. **268**(8): p. 5798-5801.
39. Williams, D.B., *Beyond lectins: the calnexin/calreticulin chaperone system of the endoplasmic reticulum*. *J Cell Sci*, 2006. **119**(Pt 4): p. 615-623.
40. Solda, T., C. Galli, R.J. Kaufman, and M. Molinari, *Substrate-specific requirements for UGT1-dependent release from calnexin*. *Mol Cell*, 2007. **27**(2): p. 238-249.
41. Caramelo, J.J., O.A. Castro, G. de Prat-Gay, and A.J. Parodi, *The endoplasmic reticulum glucosyltransferase recognizes nearly native glycoprotein folding intermediates*. *J Biol Chem*, 2004. **279**(44): p. 46280-46285.
42. Sousa, M.C., M.A. Ferrero-Garcia, and A.J. Parodi, *Recognition of the oligosaccharide and protein moieties of glycoproteins by the UDP-Glc:glycoprotein glucosyltransferase*. *Biochemistry*, 1992. **31**(1): p. 97-105.
43. Clerc, S., C. Hirsch, D.M. Oggier, P. Deprez, C. Jakob, T. Sommer, and M. Aebi, *Htm1 protein generates the N-glycan signal for glycoprotein*

- degradation in the endoplasmic reticulum.* J Cell Biol, 2009. **184**(1): p. 159-172.
44. Hosokawa, N., Y. Kamiya, D. Kamiya, K. Kato, and K. Nagata, *Human OS-9, a lectin required for glycoprotein endoplasmic reticulum-associated degradation, recognizes mannose-trimmed N-glycans.* J Biol Chem, 2009. **284**(25): p. 17061-17068.
 45. Liu, Y., P. Choudhury, C.M. Cabral, and R.N. Sifers, *Intracellular disposal of incompletely folded human alpha1-antitrypsin involves release from calnexin and post-translational trimming of asparagine-linked oligosaccharides.* J Biol Chem, 1997. **272**(12): p. 7946-7951.
 46. Ermonval, M., C. Kitzmuller, A.M. Mir, R. Cacan, and N.E. Ivessa, *N-glycan structure of a short-lived variant of ribophorin I expressed in the MadIA214 glycosylation-defective cell line reveals the role of a mannosidase that is not ER mannosidase I in the process of glycoprotein degradation.* Glycobiology, 2001. **11**(7): p. 565-576.
 47. Tokunaga, F., C. Brostrom, T. Koide, and P. Arvan, *Endoplasmic reticulum (ER)-associated degradation of misfolded N-linked glycoproteins is suppressed upon inhibition of ER mannosidase I.* J Biol Chem, 2000. **275**(52): p. 40757-40764.
 48. Wilson, C.M., M.R. Farmery, and N.J. Bulleid, *Pivotal role of calnexin and mannose trimming in regulating the endoplasmic reticulum-associated degradation of major histocompatibility complex class I heavy chain.* J Biol Chem, 2000. **275**(28): p. 21224-21232.
 49. Su, K., T. Stoller, J. Rocco, J. Zemsy, and R. Green, *Pre-Golgi degradation of yeast prepro-alpha-factor expressed in a mammalian cell. Influence of cell type-specific oligosaccharide processing on intracellular fate.* J Biol Chem, 1993. **268**(19): p. 14301-14309.
 50. Groisman, B., M. Shenkman, E. Ron, and G.Z. Lederkremer, *Mannose trimming is required for delivery of a glycoprotein from EDEM1 to XTP3-B and to late endoplasmic reticulum-associated degradation steps.* J Biol Chem. **286**(2): p. 1292-1300.
 51. Nakatsukasa, K. and J.L. Brodsky, *The recognition and retrotranslocation of misfolded proteins from the endoplasmic reticulum.* Traffic, 2008. **9**(6): p. 861-870.
 52. Johnson, A.E. and N.G. Haigh, *The ER translocon and retrotranslocation: is the shift into reverse manual or automatic?* Cell, 2000. **102**(6): p. 709-712.
 53. Rapoport, T.A., *Protein translocation across the eukaryotic endoplasmic reticulum and bacterial plasma membranes.* Nature, 2007. **450**(7170): p. 663-669.
 54. Schmitz, A., H. Herrgen, A. Winkeler, and V. Herzog, *Cholera toxin is exported from microsomes by the Sec61p complex.* J Cell Biol, 2000. **148**(6): p. 1203-1212.
 55. Schmitz, A., A. Schneider, M.P. Kummer, and V. Herzog, *Endoplasmic reticulum-localized amyloid beta-peptide is degraded in the cytosol by two distinct degradation pathways.* Traffic, 2004. **5**(2): p. 89-101.

56. Van den Berg, B., W.M. Clemons, Jr., I. Collinson, Y. Modis, E. Hartmann, S.C. Harrison, and T.A. Rapoport, *X-ray structure of a protein-conducting channel*. *Nature*, 2004. **427**(6969): p. 36-44.
57. Hebert, D.N., R. Bernasconi, and M. Molinari, *ERAD substrates: which way out?* *Semin Cell Dev Biol*. **21**(5): p. 526-532.
58. Benach, J. and J.F. Hunt, *Cell biology: shape-shifting protein channel*. *Nature*, 2004. **427**(6969): p. 24-26.
59. Knop, M., A. Finger, T. Braun, K. Hellmuth, and D.H. Wolf, *Der1, a novel protein specifically required for endoplasmic reticulum degradation in yeast*. *EMBO J*, 1996. **15**(4): p. 753-763.
60. Lilley, B.N. and H.L. Ploegh, *A membrane protein required for dislocation of misfolded proteins from the ER*. *Nature*, 2004. **429**(6994): p. 834-840.
61. Ye, Y., Y. Shibata, C. Yun, D. Ron, and T.A. Rapoport, *A membrane protein complex mediates retro-translocation from the ER lumen into the cytosol*. *Nature*, 2004. **429**(6994): p. 841-847.
62. Oda, Y., T. Okada, H. Yoshida, R.J. Kaufman, K. Nagata, and K. Mori, *Derlin-2 and Derlin-3 are regulated by the mammalian unfolded protein response and are required for ER-associated degradation*. *J Cell Biol*, 2006. **172**(3): p. 383-393.
63. Wahlman, J., G.N. DeMartino, W.R. Skach, N.J. Bulleid, J.L. Brodsky, and A.E. Johnson, *Real-time fluorescence detection of ERAD substrate retrotranslocation in a mammalian in vitro system*. *Cell*, 2007. **129**(5): p. 943-955.
64. Raasi, S. and D.H. Wolf, *Ubiquitin receptors and ERAD: a network of pathways to the proteasome*. *Semin Cell Dev Biol*, 2007. **18**(6): p. 780-791.
65. Rabinovich, E., A. Kerem, K.U. Frohlich, N. Diamant, and S. Bar-Nun, *AAA-ATPase p97/Cdc48p, a cytosolic chaperone required for endoplasmic reticulum-associated protein degradation*. *Mol Cell Biol*, 2002. **22**(2): p. 626-634.
66. Jarosch, E., C. Taxis, C. Volkwein, J. Bordallo, D. Finley, D.H. Wolf, and T. Sommer, *Protein dislocation from the ER requires polyubiquitination and the AAA-ATPase Cdc48*. *Nat Cell Biol*, 2002. **4**(2): p. 134-139.
67. Schubert, C., H. Richly, S. Rumpf, and A. Buchberger, *Shp1 and Ubx2 are adaptors of Cdc48 involved in ubiquitin-dependent protein degradation*. *EMBO Rep*, 2004. **5**(8): p. 818-824.
68. Schubert, C. and A. Buchberger, *Membrane-bound Ubx2 recruits Cdc48 to ubiquitin ligases and their substrates to ensure efficient ER-associated protein degradation*. *Nature Cell Biol*, 2005. **7**(10): p. 999-1006.
69. Biederer, T., C. Volkwein, and T. Sommer, *Role of Cue1p in ubiquitination and degradation at the ER surface*. *Science*, 1997. **278**(5344): p. 1806-1809.
70. Jentsch, S. and S. Rumpf, *Cdc48 (p97): a "molecular gearbox" in the ubiquitin pathway?* *Trends Biochem Sci*, 2007. **32**(1): p. 6-11.

71. Schroder, M. and R.J. Kaufman, *The Mammalian Unfolded Protein Response*. Annu. Rev. Biochem., 2005. **74**: p. 739-789.
72. Kim, R., M. Emi, K. Tanabe, and S. Murakami, *Role of the unfolded protein response in cell death*. Apoptosis, 2006. **11**(1): p. 5-13.
73. Blond-Elguindi, S., S.E. Cwirla, W.J. Dower, R.J. Lipshutz, S.R. Sprang, J.F. Sambrook, and M.J. Gething, *Affinity panning of a library of peptides displayed on bacteriophages reveals the binding specificity of BiP*. Cell, 1993. **75**(4): p. 717-728.
74. Chen, X., J. Shen, and R. Prywes, *The luminal domain of ATF6 senses endoplasmic reticulum (ER) stress and causes translocation of ATF6 from the ER to the Golgi*. J Biol Chem, 2002. **277**(15): p. 13045-13052.
75. Hong, M., S. Luo, P. Baumeister, J.M. Huang, R.K. Gogia, M. Li, and A.S. Lee, *Underglycosylation of ATF6 as a novel sensing mechanism for activation of the unfolded protein response*. J Biol Chem, 2004. **279**(12): p. 11354-11363.
76. Hong, M., M. Li, C. Mao, and A.S. Lee, *Endoplasmic reticulum stress triggers an acute proteasome-dependent degradation of ATF6*. J Cell Biochem, 2004. **92**(4): p. 723-732.
77. Bertolotti, A., Y. Zhang, L.M. Hendershot, H.P. Harding, and D. Ron, *Dynamic interaction of BiP and ER stress transducers in the unfolded-protein response*. Nature Cell Biol., 2000. **2**(6): p. 326-332.
78. Cox, J.S., C.E. Shamu, and P. Walter, *Transcriptional induction of genes encoding endoplasmic reticulum resident proteins requires a transmembrane protein kinase*. Cell, 1993. **73**: p. 1197-1206.
79. Mori, K., W. Ma, M.J. Gething, and J. Sambrook, *A transmembrane protein with a cdc2+/CDC28-related kinase activity is required for signaling from the ER to the nucleus*. Cell, 1993. **74**: p. 743-756.
80. Lee, K., W. Tirasophon, X. Shen, M. Michalak, R. Prywes, T. Okada, H. Yoshida, K. Mori, and R.J. Kaufman, *IRE1-mediated unconventional mRNA splicing and S2P-mediated ATF6 cleavage merge to regulate XBP1 in signaling the unfolded protein response*. Genes Dev., 2002. **16**: p. 452-466.
81. Yoshida, H., T. Matsui, A. Yamamoto, T. Okada, and K. Mori, *XBP1 mRNA is induced by ATF6 and spliced by IRE1 in response to ER stress to produce a highly active transcription factor*. Cell, 2001. **107**(7): p. 881-891.
82. Liu, C.Y., M. Schroder, and R.J. Kaufman, *Ligand-independent dimerization activates the stress response kinases IRE1 and PERK in the lumen of the endoplasmic reticulum*. J Biol Chem, 2000. **275**(32): p. 24881-24885.
83. Harding, H.P., Y. Zhang, and D. Ron, *Protein translation and folding are coupled by an endoplasmic-reticulum-resident kinase*. Nature, 1999. **397**(6716): p. 271-274.
84. Degen, E. and D.B. Williams, *Participation of a novel 88-kD protein in the biogenesis of murine class I histocompatibility molecules*. J Cell Biol, 1991. **112**(6): p. 1099-1115.

85. Wada, I., D. Rindress, P.H. Cameron, W.J. Ou, J.J. Doherty, 2nd, D. Louvard, A.W. Bell, D. Dignard, D.Y. Thomas, and J.J. Bergeron, *SSR alpha and associated calnexin are major calcium binding proteins of the endoplasmic reticulum membrane*. J Biol Chem, 1991. **266**(29): p. 19599-19610.
86. Ahluwalia, N., J.J. Bergeron, I. Wada, E. Degen, and D.B. Williams, *The p88 molecular chaperone is identical to the endoplasmic reticulum membrane protein, calnexin*. J Biol Chem, 1992. **267**(15): p. 10914-10918.
87. Ellgaard, L. and A. Helenius, *Quality control in the endoplasmic reticulum*. Nature Rev. Mol. Cell Biol., 2003. **4**(3): p. 181-191.
88. Chouquet, A., H. Paidassi, W.L. Ling, P. Frachet, G. Houen, G.J. Arlaud, and C. Gaboriaud, *X-ray structure of the human calreticulin globular domain reveals a peptide-binding area and suggests a multi-molecular mechanism*. PLoS One. **6**(3): p. e17886.
89. Brockmeier, A. and D.B. Williams, *Potent lectin-independent chaperone function of calnexin under conditions prevalent within the lumen of the endoplasmic reticulum*. Biochemistry, 2006. **45**(42): p. 12906-12916.
90. Brockmeier, A., U. Brockmeier, and D.B. Williams, *Distinct contributions of the lectin and arm domains of calnexin to its molecular chaperone function*. J Biol Chem, 2009. **284**(6): p. 3433-3444.
91. Schrag, J.D., J.J. Bergeron, Y. Li, S. Borisova, M. Hahn, D.Y. Thomas, and M. Cygler, *The Structure of calnexin, an ER chaperone involved in quality control of protein folding*. Mol Cell, 2001. **8**(3): p. 633-644.
92. Pollock, S., G. Kozlov, M.F. Pelletier, J.F. Trempe, G. Jansen, D. Sitnikov, J.J. Bergeron, K. Gehring, I. Ekiel, and D.Y. Thomas, *Specific interaction of ERp57 and calnexin determined by NMR spectroscopy and an ER two-hybrid system*. EMBO J, 2004. **23**(5): p. 1020-1029.
93. Ellgaard, L., R. Riek, T. Herrmann, P. Guntert, D. Braun, A. Helenius, and K. Wuthrich, *NMR structure of the calreticulin P-domain*. Proc. Natl. Acad. Sci. U.S.A., 2001. **98**(6): p. 3133-3138.
94. Michalak, M., J.M. Robert Parker, and M. Opas, *Ca²⁺ signaling and calcium binding chaperones of the endoplasmic reticulum*. Cell Calcium, 2002. **32**(5-6): p. 269-278.
95. Peterson, J.R., A. Ora, P.N. Van, and A. Helenius, *Transient, lectin-like association of calreticulin with folding intermediates of cellular and viral glycoproteins*. Mol Biol Cell, 1995. **6**(9): p. 1173-1184.
96. Danilczyk, U.G., M.F. Cohen-Doyle, and D.B. Williams, *Functional relationship between calreticulin, calnexin, and the endoplasmic reticulum luminal domain of calnexin*. J Biol Chem, 2000. **275**(17): p. 13089-13097.
97. Parlati, F., M. Dominguez, J.J. Bergeron, and D.Y. Thomas, *Saccharomyces cerevisiae CNE1 encodes an endoplasmic reticulum (ER) membrane protein with sequence similarity to calnexin and calreticulin and functions as a constituent of the ER quality control apparatus*. J Biol Chem, 1995. **270**(1): p. 244-253.

98. Parlati, F., D. Dignard, J.J. Bergeron, and D.Y. Thomas, *The calnexin homologue cnx1+ in Schizosaccharomyces pombe, is an essential gene which can be complemented by its soluble ER domain*. EMBO J, 1995. **14**(13): p. 3064-3072.
99. Elagoz, A., M. Callejo, J. Armstrong, and L.A. Rokeach, *Although calnexin is essential in S. pombe, its highly conserved central domain is dispensable for viability*. J. Cell Sci., 1999. **112**(Pt): p. 4449-4460.
100. Wong, H.N., M.A. Ward, A.W. Bell, E. Chevet, S. Bains, W.P. Blackstock, R. Solari, D.Y. Thomas, and J.J. Bergeron, *Conserved in vivo phosphorylation of calnexin at casein kinase II sites as well as a protein kinase C/proline-directed kinase site*. J Biol Chem, 1998. **273**(27): p. 17227-17235.
101. Takizawa, T., C. Tatematsu, K. Watanabe, K. Kato, and Y. Nakanishi, *Cleavage of calnexin caused by apoptotic stimuli: implication for the regulation of apoptosis*. J Biochem, 2004. **136**(3): p. 399-405.
102. Ou, W.J., D.Y. Thomas, A.W. Bell, and J.J. Bergeron, *Casein kinase II phosphorylation of signal sequence receptor alpha and the associated membrane chaperone calnexin*. J Biol Chem, 1992. **267**(33): p. 23789-23796.
103. Tjoelker, L.W., C.E. Seyfried, R.L. Eddy, Jr., M.G. Byers, T.B. Shows, J. Calderon, R.B. Schreiber, and P.W. Gray, *Human, mouse, and rat calnexin cDNA cloning: identification of potential calcium binding motifs and gene localization to human chromosome 5*. Biochemistry, 1994. **33**(11): p. 3229-3236.
104. Rosenbaum, E.E., R.C. Hardie, and N.J. Colley, *Calnexin is essential for rhodopsin maturation, Ca²⁺ regulation, and photoreceptor cell survival*. Neuron, 2006. **49**(2): p. 229-241.
105. Chevet, E., H.N. Wong, D. Gerber, C. Cochet, A. Fazel, P.H. Cameron, J.N. Gushue, D.Y. Thomas, and J.J. Bergeron, *Phosphorylation by CK2 and MAPK enhances calnexin association with ribosomes*. Embo J, 1999. **18**(13): p. 3655-3666.
106. Delom, F. and E. Chevet, *In vitro mapping of calnexin interaction with ribosomes*. Biochem Biophys Res Commun, 2006. **341**(1): p. 39-44.
107. Roderick, H.L., J.D. Lechleiter, and P. Camacho, *Cytosolic phosphorylation of calnexin controls intracellular Ca(2+) oscillations via an interaction with SERCA2b*. J Cell Biol, 2000. **149**(6): p. 1235-1248.
108. Bollo, M., R.M. Paredes, D. Holstein, N. Zheleznova, P. Camacho, and J.D. Lechleiter, *Calcineurin interacts with PERK and dephosphorylates calnexin to relieve ER stress in mammals and frogs*. PLoS One. **5**(8): p. e11925.
109. Sagoo, J.K., D.A. Fruman, S. Wesselborg, C.T. Walsh, and B.E. Bierer, *Competitive inhibition of calcineurin phosphatase activity by its autoinhibitory domain*. Biochem J, 1996. **320** (Pt 3): p. 879-884.
110. Rusnak, F. and P. Mertz, *Calcineurin: form and function*. Physiol. Rev., 2000. **80**(4): p. 1483-1521.

111. Perrino, B.A., L.Y. Ng, and T.R. Soderling, *Calcium regulation of calcineurin phosphatase activity by its B subunit and calmodulin. Role of the autoinhibitory domain*. J Biol Chem, 1995. **270**(12): p. 7012.
112. Hayashi, T. and T.P. Su, *Sigma-1 receptor chaperones at the ER-mitochondrion interface regulate Ca(2+) signaling and cell survival*. Cell, 2007. **131**(3): p. 596-610.
113. Cameron, P.H., E. Chevet, O. Pluquet, D.Y. Thomas, and J.J. Bergeron, *Calnexin phosphorylation attenuates the release of partially misfolded alpha1-antitrypsin to the secretory pathway*. J Biol Chem, 2009. **284**(50): p. 34570-34579.
114. Martin, B.R. and B.F. Cravatt, *Large-scale profiling of protein palmitoylation in mammalian cells*. Nature Methods, 2009. **6**(2): p. 135-138.
115. Matunis, M.J., E. Coutavas, and G. Blobel, *A novel ubiquitin-like modification modulates the partitioning of the Ran-GTPase-activating protein RanGAP1 between the cytosol and the nuclear pore complex*. J Cell Biol, 1996. **135**(6 Pt 1): p. 1457-1470.
116. Geiss-Friedlander, R. and F. Melchior, *Concepts in sumoylation: a decade on*. Nat Rev Mol Cell Biol, 2007. **8**(12): p. 947-956.
117. Desterro, J.M., M.S. Rodriguez, G.D. Kemp, and R.T. Hay, *Identification of the enzyme required for activation of the small ubiquitin-like protein SUMO-1*. J Biol Chem, 1999. **274**(15): p. 10618-10624.
118. Pichler, A., A. Gast, J.S. Seeler, A. Dejean, and F. Melchior, *The nucleoporin RanBP2 has SUMO1 E3 ligase activity*. Cell, 2002. **108**(1): p. 109-120.
119. Hochstrasser, M., *SP-RING for SUMO: new functions bloom for a ubiquitin-like protein*. Cell, 2001. **107**(1): p. 5-8.
120. Kagey, M.H., T.A. Melhuish, and D. Wotton, *The polycomb protein Pc2 is a SUMO E3*. Cell, 2003. **113**(1): p. 127-137.
121. Gareau, J.R. and C.D. Lima, *The SUMO pathway: emerging mechanisms that shape specificity, conjugation and recognition*. Nature Rev Mol Cell Biol. **11**(12): p. 861-871.
122. Hietakangas, V., J. Anckar, H.A. Blomster, M. Fujimoto, J.J. Palvimo, A. Nakai, and L. Sistonen, *PDSM, a motif for phosphorylation-dependent SUMO modification*. Proc Natl Acad Sci U S A, 2006. **103**(1): p. 45-50.
123. Yang, S.H., A. Galanis, J. Witty, and A.D. Sharrocks, *An extended consensus motif enhances the specificity of substrate modification by SUMO*. EMBO J, 2006. **25**(21): p. 5083-5093.
124. Song, J., L.K. Durrin, T.A. Wilkinson, T.G. Krontiris, and Y. Chen, *Identification of a SUMO-binding motif that recognizes SUMO-modified proteins*. Proc Natl Acad Sci U S A, 2004. **101**(40): p. 14373-14378.
125. Mukhopadhyay, D. and M. Dasso, *Modification in reverse: the SUMO proteases*. Trends Biochem Sci, 2007. **32**(6): p. 286-295.
126. Saitoh, H. and J. Hinchev, *Functional heterogeneity of small ubiquitin-related protein modifiers SUMO-1 versus SUMO-2/3*. J Biol Chem, 2000. **275**(9): p. 6252-6258.

127. Bohren, K.M., V. Nadkarni, J.H. Song, K.H. Gabbay, and D. Owerbach, *A M55V polymorphism in a novel SUMO gene (SUMO-4) differentially activates heat shock transcription factors and is associated with susceptibility to type I diabetes mellitus*. J Biol Chem, 2004. **279**(26): p. 27233-27238.
128. Guo, D., M. Li, Y. Zhang, P. Yang, S. Eckenrode, D. Hopkins, W. Zheng, S. Purohit, R.H. Podolsky, A. Muir, J. Wang, Z. Dong, T. Brusko, M. Atkinson, P. Pozzilli, A. Zeidler, L.J. Raffel, C.O. Jacob, Y. Park, M. Serrano-Rios, M.T. Larrad, Z. Zhang, H.J. Garchon, J.F. Bach, J.I. Rotter, J.X. She, and C.Y. Wang, *A functional variant of SUMO4, a new I kappa B alpha modifier, is associated with type 1 diabetes*. Nature Genet, 2004. **36**(8): p. 837-841.
129. Owerbach, D., E.M. McKay, E.T. Yeh, K.H. Gabbay, and K.M. Bohren, *A proline-90 residue unique to SUMO-4 prevents maturation and sumoylation*. Biochem Biophys Res Commun, 2005. **337**(2): p. 517-520.
130. Wei, W., P. Yang, J. Pang, S. Zhang, Y. Wang, M.H. Wang, Z. Dong, J.X. She, and C.Y. Wang, *A stress-dependent SUMO4 sumoylation of its substrate proteins*. Biochem Biophys Res Commun, 2008. **375**(3): p. 454-459.
131. Matic, I., M. van Hagen, J. Schimmel, B. Macek, S.C. Ogg, M.H. Tatham, R.T. Hay, A.I. Lamond, M. Mann, and A.C. Vertegaal, *In vivo identification of human small ubiquitin-like modifier polymerization sites by high accuracy mass spectrometry and an in vitro to in vivo strategy*. Mol Cell Proteomics, 2008. **7**(1): p. 132-144.
132. Zhou, W., J.J. Ryan, and H. Zhou, *Global analyses of sumoylated proteins in Saccharomyces cerevisiae. Induction of protein sumoylation by cellular stresses*. J Biol Chem, 2004. **279**(31): p. 32262-32268.
133. Rajan, S., L.D. Plant, M.L. Rabin, M.H. Butler, and S.A. Goldstein, *Sumoylation silences the plasma membrane leak K+ channel K2P1*. Cell, 2005. **121**(1): p. 37-47.
134. Martin, S., A. Nishimune, J.R. Mellor, and J.M. Henley, *SUMOylation regulates kainate-receptor-mediated synaptic transmission*. Nature, 2007. **447**(7142): p. 321-325.
135. Dai, X.Q., J. Kolic, P. Marchi, S. Sipione, and P.E. Macdonald, *SUMOylation regulates Kv2.1 and modulates pancreatic beta-cell excitability*. J Cell Sci, 2009. **122**(Pt 6): p. 775-779.
136. Benson, M.D., Q.J. Li, K. Kieckhafer, D. Dudek, M.R. Whorton, R.K. Sunahara, J.A. Iniguez-Lluhi, and J.R. Martens, *SUMO modification regulates inactivation of the voltage-gated potassium channel Kv1.5*. Proc Natl Acad Sci U S A, 2007. **104**(6): p. 1805-1810.
137. Lalioti, V.S., S. Vergarajauregui, D. Pulido, and I.V. Sandoval, *The insulin-sensitive glucose transporter, GLUT4, interacts physically with Daxx. Two proteins with capacity to bind Ubc9 and conjugated to SUMO1*. J Biol Chem, 2002. **277**(22): p. 19783-19791.

138. Tang, Z., O. El Far, H. Betz, and A. Scheschonka, *Pias1 interaction and sumoylation of metabotropic glutamate receptor 8*. J Biol Chem, 2005. **280**(46): p. 38153-38159.
139. Harder, Z., R. Zunino, and H. McBride, *Sumo1 conjugates mitochondrial substrates and participates in mitochondrial fission*. Curr Biol, 2004. **14**(4): p. 340-345.
140. Scorrano, L. and D. Liu, *The SUMO arena goes mitochondrial with MAPL*. EMBO Rep, 2009. **10**(7): p. 694-696.
141. Bourdeau, A., N. Dube, and M.L. Tremblay, *Cytoplasmic protein tyrosine phosphatases, regulation and function: the roles of PTP1B and TC-PTP*. Curr Opin Cell Biol, 2005. **17**(2): p. 203-209.
142. Dadke, S., S. Cotteret, S.C. Yip, Z.M. Jaffer, F. Haj, A. Ivanov, F. Rauscher, 3rd, K. Shuai, T. Ng, B.G. Neel, and J. Chernoff, *Regulation of protein tyrosine phosphatase 1B by sumoylation*. Nature Cell Biol, 2007. **9**(1): p. 80-85.
143. Braschi, E., R. Zunino, and H.M. McBride, *MAPL is a new mitochondrial SUMO E3 ligase that regulates mitochondrial fission*. EMBO Rep, 2009. **10**(7): p. 748-754.
144. Zalc, B. and D.R. Colman, *Origins of vertebrate success*. Science, 2000. **288**(5464): p. 271-272.
145. Kraus, A., J. Groenendyk, K. Bedard, T.A. Baldwin, K.H. Krause, M. Dubois-Dauphin, J. Dyck, E.E. Rosenbaum, L. Korngut, N.J. Colley, S. Gosgnach, D. Zochodne, K. Todd, L.B. Agellon, and M. Michalak, *Calnexin deficiency leads to dysmyelination*. J Biol Chem, 2010. **285**(24): p. 18928-18938.
146. Nave, K.A., *Myelination and the trophic support of long axons*. Nature Rev Neurosci. **11**(4): p. 275-283.
147. Peters, A., Palay S.L., Webster H deF, *The Fine Structure of the Nervous System*. 3rd ed. ed. 1991, New York: Oxford Univ. Press.
148. Pfefferbaum, A., D.H. Mathalon, E.V. Sullivan, J.M. Rawles, R.B. Zipursky, and K.O. Lim, *A quantitative magnetic resonance imaging study of changes in brain morphology from infancy to late adulthood*. Arch Neurol, 1994. **51**(9): p. 874-887.
149. McInnes, L.A. and T.L. Lauriat, *RNA metabolism and dysmyelination in schizophrenia*. Neurosci Biobehav Rev, 2006. **30**(4): p. 551-561.
150. Rushton, W.A., *A theory of the effects of fibre size in medullated nerve*. J Physiol, 1951. **115**(1): p. 101-122.
151. Chomiak, T. and B. Hu, *What is the optimal value of the g-ratio for myelinated fibers in the rat CNS? A theoretical approach*. PLoS One, 2009. **4**(11): p. e7754.
152. Taveggia, C., G. Zanazzi, A. Petrylak, H. Yano, J. Rosenbluth, S. Einheber, X. Xu, R.M. Esper, J.A. Loeb, P. Shrager, M.V. Chao, D.L. Falls, L. Role, and J.L. Salzer, *Neuregulin-1 type III determines the ensheathment fate of axons*. Neuron, 2005. **47**(5): p. 681-694.

153. Coman, I., G. Barbin, P. Charles, B. Zalc, and C. Lubetzki, *Axonal signals in central nervous system myelination, demyelination and remyelination*. J Neurol Sci, 2005. **233**(1-2): p. 67-71.
154. Charles, P., M.P. Hernandez, B. Stankoff, M.S. Aigrot, C. Colin, G. Rougon, B. Zalc, and C. Lubetzki, *Negative regulation of central nervous system myelination by polysialylated-neural cell adhesion molecule*. Proc Natl Acad Sci U S A, 2000. **97**(13): p. 7585-7590.
155. Simons, M. and J. Trotter, *Wrapping it up: the cell biology of myelination*. Curr Opin Neurobiol, 2007. **17**(5): p. 533-540.
156. Morell, P. and H. Jurevics, *Origin of cholesterol in myelin*. Neurochem Res, 1996. **21**(4): p. 463-470.
157. Saher, G., B. Brugger, C. Lappe-Siefke, W. Mobius, R. Tozawa, M.C. Wehr, F. Wieland, S. Ishibashi, and K.A. Nave, *High cholesterol level is essential for myelin membrane growth*. Nature Neurosci, 2005. **8**(4): p. 468-475.
158. Baron, W. and D. Hoekstra, *On the biogenesis of myelin membranes: sorting, trafficking and cell polarity*. FEBS Lett. **584**(9): p. 1760-1770.
159. Chrast, R., G. Saher, K.A. Nave, and M.H. Verheijen, *Lipid metabolism in myelinating glial cells: lessons from human inherited disorders and mouse models*. J Lipid Res. **52**(3): p. 419-434.
160. Webster, H.D., *The geometry of peripheral myelin sheaths during their formation and growth in rat sciatic nerves*. J Cell Biol, 1971. **48**(2): p. 348-367.
161. Kippert, A., K. Trajkovic, L. Rajendran, J. Ries, and M. Simons, *Rho regulates membrane transport in the endocytic pathway to control plasma membrane specialization in oligodendroglial cells*. J Neurosci, 2007. **27**(13): p. 3560-3570.
162. Ishaque, A., M.W. Roomi, I. Szymanska, S. Kowalski, and E.H. Eylar, *The PO glycoprotein of peripheral nerve myelin*. Can J Biochem, 1980. **58**(10): p. 913-921.
163. Lemke, G. and R. Axel, *Isolation and sequence of a cDNA encoding the major structural protein of peripheral myelin*. Cell, 1985. **40**(3): p. 501-508.
164. Lemke, G., E. Lamar, and J. Patterson, *Isolation and analysis of the gene encoding peripheral myelin protein zero*. Neuron, 1988. **1**(1): p. 73-83.
165. Filbin, M.T., F.S. Walsh, B.D. Trapp, J.A. Pizzey, and G.I. Tennekoon, *Role of myelin PO protein as a homophilic adhesion molecule*. Nature, 1990. **344**(6269): p. 871-872.
166. Wong, M.H. and M.T. Filbin, *The cytoplasmic domain of the myelin PO protein influences the adhesive interactions of its extracellular domain*. J Cell Biol, 1994. **126**(4): p. 1089-1097.
167. Hasse, B., F. Bosse, H. Hanenberg, and H.W. Muller, *Peripheral myelin protein 22 kDa and protein zero: domain specific trans-interactions*. Mol Cell Neurosci, 2004. **27**(4): p. 370-378.
168. Taylor, V., C. Zraggen, R. Naef, and U. Suter, *Membrane topology of peripheral myelin protein 22*. J Neurosci Res, 2000. **62**(1): p. 15-27.

169. Nave, K.A. and B.D. Trapp, *Axon-glia signaling and the glial support of axon function*. *Annu Rev Neurosci*, 2008. **31**: p. 535-561.
170. de Waegh, S.M., V.M. Lee, and S.T. Brady, *Local modulation of neurofilament phosphorylation, axonal caliber, and slow axonal transport by myelinating Schwann cells*. *Cell*, 1992. **68**(3): p. 451-463.
171. Sanchez, I., L. Hassinger, P.A. Paskevich, H.D. Shine, and R.A. Nixon, *Oligodendroglia regulate the regional expansion of axon caliber and local accumulation of neurofilaments during development independently of myelin formation*. *J Neurosci*, 1996. **16**(16): p. 5095-5105.
172. Barres, B.A., *The mystery and magic of glia: a perspective on their roles in health and disease*. *Neuron*, 2008. **60**(3): p. 430-440.
173. Charles, P., R. Reynolds, D. Seilhean, G. Rougon, M.S. Aigrot, A. Niezgod, B. Zalc, and C. Lubetzki, *Re-expression of PSA-NCAM by demyelinated axons: an inhibitor of remyelination in multiple sclerosis?* *Brain*, 2002. **125**(Pt 9): p. 1972-1979.
174. Snipes, G.J., U. Suter, A.A. Welcher, and E.M. Shooter, *Characterization of a novel peripheral nervous system myelin protein (PMP-22/SR13)*. *J Cell Biol*, 1992. **117**(1): p. 225-238.
175. Welcher, A.A., U. Suter, M. De Leon, G.J. Snipes, and E.M. Shooter, *A myelin protein is encoded by the homologue of a growth arrest-specific gene*. *Proc Natl Acad Sci U S A*, 1991. **88**(16): p. 7195-7199.
176. Amiguet, P., M.V. Gardinier, J.P. Zanetta, and J.M. Matthieu, *Purification and partial structural and functional characterization of mouse myelin/oligodendrocyte glycoprotein*. *J Neurochem*, 1992. **58**(5): p. 1676-1682.
177. Gardinier, M.V., P. Amiguet, C. Linington, and J.M. Matthieu, *Myelin/oligodendrocyte glycoprotein is a unique member of the immunoglobulin superfamily*. *J Neurosci Res*, 1992. **33**(1): p. 177-187.
178. Meyer Zu Horste, G. and K.A. Nave, *Animal models of inherited neuropathies*. *Curr Opin Neurol*, 2006. **19**(5): p. 464-473.
179. Suter, U., A.A. Welcher, T. Ozcelik, G.J. Snipes, B. Kosaras, U. Francke, S. Billings-Gagliardi, R.L. Sidman, and E.M. Shooter, *Trembler mouse carries a point mutation in a myelin gene*. *Nature*, 1992. **356**(6366): p. 241-244.
180. Patel, P.I., B.B. Roa, A.A. Welcher, R. Schoener-Scott, B.J. Trask, L. Pentao, G.J. Snipes, C.A. Garcia, U. Francke, E.M. Shooter, J.R. Lupski, and U. Suter, *The gene for the peripheral myelin protein PMP-22 is a candidate for Charcot-Marie-Tooth disease type 1A*. *Nat Genet*, 1992. **1**(3): p. 159-165.
181. Robaglia-Schlupp, A., J. Pizant, J.C. Norreel, E. Passage, D. Saberandjoneidi, J.L. Ansaldi, L. Vinay, D. Figarella-Branger, N. Levy, F. Clarac, P. Cau, J.F. Pellissier, and M. Fontes, *PMP22 overexpression causes dysmyelination in mice*. *Brain*, 2002. **125**(Pt 10): p. 2213-2221.

182. Adlkofer, K., R. Martini, A. Aguzzi, J. Zielasek, K.V. Toyka, and U. Suter, *Hypermyelination and demyelinating peripheral neuropathy in Pmp22-deficient mice*. Nat Genet, 1995. **11**(3): p. 274-280.
183. Lorenzetti, D., D. Pareyson, A. Sghirlanzoni, B.B. Roa, N.E. Abbas, M. Pandolfo, S. Di Donato, and J.R. Lupski, *A 1.5-Mb deletion in 17p11.2-p12 is frequently observed in Italian families with hereditary neuropathy with liability to pressure palsies*. Am J Hum Genet, 1995. **56**(1): p. 91-98.
184. Maycox, P.R., D. Ortuno, P. Burrola, R. Kuhn, P.L. Bieri, J.C. Arrezzo, and G. Lemke, *A transgenic mouse model for human hereditary neuropathy with liability to pressure palsies*. Mol Cell Neurosci, 1997. **8**(6): p. 405-416.
185. D'Urso, D., R. Prior, R. Greiner-Petter, A.A. Gabreels-Festen, and H.W. Muller, *Overloaded endoplasmic reticulum-Golgi compartments, a possible pathomechanism of peripheral neuropathies caused by mutations of the peripheral myelin protein PMP22*. J Neurosci, 1998. **18**(2): p. 731-740.
186. Naef, R. and U. Suter, *Impaired intracellular trafficking is a common disease mechanism of PMP22 point mutations in peripheral neuropathies*. Neurobiol Dis, 1999. **6**(1): p. 1-14.
187. Colby, J., R. Nicholson, K.M. Dickson, W. Orfali, R. Naef, U. Suter, and G.J. Snipes, *PMP22 carrying the trembler or trembler-J mutation is intracellularly retained in myelinating Schwann cells*. Neurobiol Dis, 2000. **7**(6 Pt B): p. 561-573.
188. Dickson, K.M., J.J. Bergeron, I. Shames, J. Colby, D.T. Nguyen, E. Chevet, D.Y. Thomas, and G.J. Snipes, *Association of calnexin with mutant peripheral myelin protein-22 ex vivo: a basis for "gain-of-function" ER diseases*. Proc Natl Acad Sci U S A, 2002. **99**(15): p. 9852-9857.
189. Khajavi, M., K. Inoue, W. Wiszniewski, T. Ohyama, G.J. Snipes, and J.R. Lupski, *Curcumin treatment abrogates endoplasmic reticulum retention and aggregation-induced apoptosis associated with neuropathy-causing myelin protein zero-truncating mutants*. Am J Hum Genet, 2005. **77**(5): p. 841-850.
190. Ellis, D. and S. Malcolm, *Proteolipid protein gene dosage effect in Pelizaeus-Merzbacher disease*. Nat Genet, 1994. **6**(4): p. 333-334.
191. Woodward, K.J., *The molecular and cellular defects underlying Pelizaeus-Merzbacher disease*. Expert Rev Mol Med, 2008. **10**: p. e14.
192. Woodward, K.J., M. Cundall, K. Sperle, E.A. Siermans, M. Ross, G. Howell, S.M. Gribble, D.C. Burford, N.P. Carter, D.L. Hobson, J.Y. Garbern, J. Kamholz, H. Heng, M.E. Hodes, S. Malcolm, and G.M. Hobson, *Heterogeneous duplications in patients with Pelizaeus-Merzbacher disease suggest a mechanism of coupled homologous and nonhomologous recombination*. Am J Hum Genet, 2005. **77**(6): p. 966-987.
193. Hodes, M.E., C.A. Blank, V.M. Pratt, J. Morales, J. Napier, and S.R. Dlouhy, *Nonsense mutation in exon 3 of the proteolipid protein gene*

- (PLP) in a family with an unusual form of Pelizaeus-Merzbacher disease. *Am J Med Genet*, 1997. **69**(2): p. 121-125.
194. Kobayashi, H., E.P. Hoffman, and H.G. Marks, *The rumpshaker mutation in spastic paraplegia*. *Nature Genet*, 1994. **7**(3): p. 351-352.
 195. Gencic, S., D. Abuelo, M. Ambler, and L.D. Hudson, *Pelizaeus-Merzbacher disease: an X-linked neurologic disorder of myelin metabolism with a novel mutation in the gene encoding proteolipid protein*. *Am J Hum Genet*, 1989. **45**(3): p. 435-442.
 196. Hudson, L.D., C. Puckett, J. Berndt, J. Chan, and S. Gencic, *Mutation of the proteolipid protein gene PLP in a human X chromosome-linked myelin disorder*. *Proc Natl Acad Sci U S A*, 1989. **86**(20): p. 8128-8131.
 197. Gow, A. and R.A. Lazzarini, *A cellular mechanism governing the severity of Pelizaeus-Merzbacher disease*. *Nature Genet*, 1996. **13**(4): p. 422-428.
 198. Gow, A., C.M. Southwood, and R.A. Lazzarini, *Disrupted proteolipid protein trafficking results in oligodendrocyte apoptosis in an animal model of Pelizaeus-Merzbacher disease*. *J Cell Biol*, 1998. **140**(4): p. 925-934.
 199. Southwood, C.M., J. Garbern, W. Jiang, and A. Gow, *The unfolded protein response modulates disease severity in Pelizaeus-Merzbacher disease*. *Neuron*, 2002. **36**(4): p. 585-596.
 200. Roboti, P., E. Swanton, and S. High, *Differences in endoplasmic-reticulum quality control determine the cellular response to disease-associated mutants of proteolipid protein*. *J Cell Sci*, 2009. **122**(Pt 21): p. 3942-3953.
 201. Pennuto, M., E. Tinelli, M. Malaguti, U. Del Carro, M. D'Antonio, D. Ron, A. Quattrini, M.L. Feltri, and L. Wrabetz, *Ablation of the UPR-mediator CHOP restores motor function and reduces demyelination in Charcot-Marie-Tooth 1B mice*. *Neuron*, 2008. **57**(3): p. 393-405.
 202. Reindl, M., C. Linington, U. Brehm, R. Egg, E. Dilitz, F. Deisenhammer, W. Poewe, and T. Berger, *Antibodies against the myelin oligodendrocyte glycoprotein and the myelin basic protein in multiple sclerosis and other neurological diseases: a comparative study*. *Brain*, 1999. **122** (Pt 11): p. 2047-2056.
 203. Iglesias, A., J. Bauer, T. Litzenburger, A. Schubart, and C. Linington, *T- and B-cell responses to myelin oligodendrocyte glycoprotein in experimental autoimmune encephalomyelitis and multiple sclerosis*. *Glia*, 2001. **36**(2): p. 220-234.
 204. von Budingen, H.C., N. Tanuma, P. Villoslada, J.C. Ouallet, S.L. Hauser, and C.P. Genain, *Immune responses against the myelin/oligodendrocyte glycoprotein in experimental autoimmune demyelination*. *J Clin Immunol*, 2001. **21**(3): p. 155-170.
 205. Marta, C.B., M.B. Montano, C.M. Taylor, A.L. Taylor, R. Bansal, and S.E. Pfeiffer, *Signaling cascades activated upon antibody cross-linking of myelin oligodendrocyte glycoprotein: potential implications for multiple sclerosis*. *J Biol Chem*, 2005. **280**(10): p. 8985-8993.

206. Emptage, N., T.V. Bliss, and A. Fine, *Single synaptic events evoke NMDA receptor-mediated release of calcium from internal stores in hippocampal dendritic spines*. *Neuron*, 1999. **22**(1): p. 115-124.
207. Matute, C., E. Alberdi, G. Ibarretxe, and M.V. Sanchez-Gomez, *Excitotoxicity in glial cells*. *Eur J Pharmacol*, 2002. **447**(2-3): p. 239-246.
208. Micu, I., Q. Jiang, E. Coderre, A. Ridsdale, L. Zhang, J. Woulfe, X. Yin, B.D. Trapp, J.E. McRory, R. Rehak, G.W. Zamponi, W. Wang, and P.K. Stys, *NMDA receptors mediate calcium accumulation in myelin during chemical ischaemia*. *Nature*, 2006. **439**(7079): p. 988-992.
209. Karadottir, R., P. Cavelier, L.H. Bergersen, and D. Attwell, *NMDA receptors are expressed in oligodendrocytes and activated in ischaemia*. *Nature*, 2005. **438**(7071): p. 1162-1166.
210. Salter, M.G. and R. Fern, *NMDA receptors are expressed in developing oligodendrocyte processes and mediate injury*. *Nature*, 2005. **438**(7071): p. 1167-1171.
211. Hughes, P.D., W.R. Wilson, and S.W. Leslie, *Effect of gestational ethanol exposure on the NMDA receptor complex in rat forebrain: from gene transcription to cell surface*. *Brain Res Dev Brain Res*, 2001. **129**(2): p. 135-145.
212. Rubio, M.E. and R.J. Wenthold, *Calnexin and the immunoglobulin binding protein (BiP) coimmunoprecipitate with AMPA receptors*. *J Neurochem*, 1999. **73**(3): p. 942-948.

Calnexin Deficiency in a Mouse Model

A version of this chapter has been previously published. Kraus, A., Groenendyk, J., Bedard, K., Baldwin, T.A., Krause, K-H., Dubois-Dauphin, M., Dyck, J., Rosenbaum, E.E., Korngut, L., Colley, N.J., Gosgnach, S., Zochodne, D., Todd, K., Agellon, L.B., and M. Michalak. *Calnexin Deficiency Leads to Dysmyelination*. J Biol Chem, 2010. 285 (24): p. 18928-18938.

Introduction

Calnexin is a ubiquitous ER resident transmembrane lectin chaperone responsible for the quality control of protein folding. It shares this role with the highly similar but soluble calreticulin. Calnexin deficiency is lethal in *S. pombe* but not in *S. cerevisiae* [1], *Dictyostelium* [2, 3] or in *C. elegans* [4, 5]. Loss of calnexin affects phagocytosis in *Dictyostelium* [2, 3] and promotes necrotic cell death in *C. elegans* [5]. Here, we investigate the effect of calnexin-deficiency in a mouse model. We generated calnexin-deficient mice with a fully disrupted gene and demonstrate that these mice have an aberrant neurological phenotype characterized by gait disturbance, a rolling walk and splaying of the hind limbs. The phenotype was linked to evidence of both central and peripheral dysmyelination. The peripheral abnormalities were prominent with a significant decrease in the nerve conduction velocity combined with wavy and decompacted myelin morphology indicating defective formation and compaction of myelin sheaths. This study reveals a surprisingly specific role for calnexin in myelin systems.

Materials and Methods

Generation of Calnexin-deficient Mice

Gene trapping with the trap vector pGT1TMpfs was used to generate the calnexin gene disrupted embryonic stem cells, designated KST286. The cell line KST286 was from the Gene Trap Resource at <http://baygenomics.ucsf.edu> (BayGenomics, University of San Francisco, San Francisco, California). The KST286ES cell line was generated from the 129P2 (formerly 129/Ola) embryonic stem cell line, the E14Tg2A.4 subclone. Parental cell lines (CGR8 and E14Tg2A) were established from delayed blastocysts. Embryonic stem cells were microinjected into 3.5-d-old C57BL/6J blastocysts to generate chimeric mice [6]. Chimeric males were analyzed for germline transmission by mating with C57BL/6J females, and the progeny was identified by PCR analysis, β -galactosidase staining, and Western blot analysis. All animal experimental procedures were approved by the Animal Welfare Program at the Research Ethics Office, University of Alberta and conformed to the guidelines set forth by the Canadian Council on Animal Care.

Genotype Analysis of Calnexin-deficient Mice

Genomic DNA was isolated from mouse tails using Trizol Reagent [6]. Inverse PCR technique was used to identify the gene trap insertion site in the calnexin gene. Briefly, genomic DNA was first digested with *Bfa*I restriction enzyme that cleaves at frequent intervals and digests the gene-trap vector

near the 3'-terminal end. The resulting DNA fragments were ligated under conditions that favor intramolecular circularization of single fragments. The nucleotide sequence located at the 3'-terminal end of the gene-trap vector was then selectively amplified using inverse DNA primers (INVF1, 5'-TCAAGGCGAGTTACATGATCCC-3'; INVR1, 5'-AAGCCATACCAAACGACGAGCG-3') derived from the nucleotide sequence of the gene-trap vector. The resulting PCR product was amplified a second time using nested DNA primers (F2, 5'-TCAAGGCGAGTTACATGATCCC-3'; R2, 5'-CGAGCGTGACACCACGATGC-3'), purified, and analyzed for nucleotide sequence. The PCR product obtained corresponded to the gene-trap vector and extension into the genomic sequence that resides immediately downstream. This allowed determination of the precise point of the vector integration in the calnexin gene. Once the integration site was identified, it was possible to design a protocol for genotyping wild-type, heterozygote and homozygote calnexin-deficient mice. DNA primers that flank the integration site allow detection of the wild-type allele [Primers F1 (exon 7) (5'-GGCCAGATGCAGATCTGAAGACC-3'), R3 (intron 7-8) (5'-CACACAGGGTATGGGGCTGTTTCAG-3')], whereas DNA primer F2 within the insertion vector sequence with primer R3 was used to detect the gene-trap allele insertion.

To determine that no alternative splicing around the interruption cassette took place, RNA was isolated from wild-type, heterozygote and calnexin-deficient brain tissue using Trizol reagent followed by RT-PCR with primers

designed to detect if there is splicing around the gene-trap insertion cassette; primers before the insertion (1F 5' GAAGGTGAGGGAGCCGCCAGTG 3', 7R – 5' GTAGTCCTCTCCACACTTATCTGG 3'), primers flanking the site of insertion (7F 5' CCAGATAAGTGTGGAGAGGACTAC 3', 8R 5' CACGTGAAGGGTTTACAGGAGGAG 3', and 7F, 12R 5' GACGCTCTTCAGCTGCCTCCAG 3'), primers within the insertion (InsR 5' CCTTCTCTGCCTTCCATCTCAACTC 3' with 7F) and primers following the insertion (12F 5' CTGGAGGCAGCTGAAGAGCGTC 3', 15R 5' GTCTCTAGGGCAACAGAACACTGC 3') as well as a GAPDH loading control (F 5' TTCACCACCATGGAGAAGGC 3', R 5' GGCATGGACTGTGGTCATGA 3').

***E. coli* Expression and Purification of Calnexin Domains**

cDNA encoding calnexin C-tail (amino acid residues 486-573) was synthesized by PCR-driven amplification of canine calnexin in a Bluescript plasmid DNA construct using the following primers: forward primer: 5'-CATGCCATGGCTGGAAAGAAACAGTCAAG-3' and reverse primer: 5'-GCTCTAGACACTCTCTTCGTGGCTTTC-3'. cDNA was cloned into pBAD His-tag vector using NcoI and XbaI restriction enzymes. cDNA encoding N+P-domain of calnexin (amino acid residues 1-461) was amplified by a PCR-driven reaction using the following primers: forward primer, 5'-CATGCCATGGATCATGAAGGACATGATGAT-3' and reverse primer 5'-GCTCTAGAGGGCGCTCCTCAGCTGCCTC-3'. cDNA was cloned into pBAD plasmid using NcoI and XbaI restriction sites. Proteins were expressed in Top 10 F' *E. coli* according to the pBAD expression system using 0.02% L-

arabinose induction for 4 hours. His-tagged protein purification was carried out on a Ni²⁺-nitriloacetic acid-agarose affinity column as previously described [7] (see Chapter Three “Materials and Methods”).

Western Blot Analysis

Two distinct polyclonal rabbit anti-calnexin antibodies were used: SPA-860 (Stressgen Biotechnologies) was raised against a synthetic peptide corresponding to the C-terminus of calnexin (amino acid residues 575-593) and SPA-865 (Stressgen Biotechnologies) was raised against a synthetic peptide near the amino-terminus. Antibodies were used at a 1:1000, and 1:500 dilution, respectively. Preparation of cell extracts, Western blot analysis and immunostaining of wild-type and calnexin-deficient cells were carried out as follows. Cells were lysed in RIPA buffer containing containing 50 mM Tris, pH, 7.0, 150 mM NaCl, 1 mM EGTA, 1 mM EDTA, 1% Triton X-100, 0.1% SDS, 0.5% sodium deoxycholate with a protease inhibitor cocktail (0.5 mM PMSF, 0.5 mM benzamidine, 0.05 µg/ml aproprotin, 0.025 µg/ml phosphormidone, 0.05 µg/ml TLCK, 0.05 µg/ml APMSF, 0.05 µg/ml E-64, 0.025 µg/ml leupeptin and 0.01 µg/ml pepstatin). Twenty µg of cell and brain tissue extracts and 200 ng of purified recombinant protein (C-tail and N+P-domain) was used for Western blot analysis of calnexin protein expression. Membranes were stripped with stripping buffer (1% SDS, 100 mM β-mercaptoethanol, 50 mM Tris-HCl, pH 6.8) and re-probed with anti-GAPDH antibodies (1:500, Abcam) for quantification.

Electrophysiology Measurements

Newborn, 1-day or 2-day-old mice (P0–P2) were used for the electrophysiological experiments [8]. The spinal cord was pinned ventral side up in a recording chamber and perfused with oxygenated Ringer's solution containing 111 mM NaCl, 3.08 mM KCl, 11 mM glucose, 25 mM NaHCO₃, 1.18 mM KH₂PO₄, 1.25 mM MgSO₄, 2.52 mM CaCl₂ at room temperature. Electroneurogram (ENG) recordings were made by placing bipolar suction electrodes on a combination of the second and fifth lumbar ventral roots (lL2–rL2 or lL2–lL5) [8]. The second lumbar ventral roots consist of primarily flexor motor axons and the L5 ventral roots consist of primarily extensor motor axons, therefore fictive locomotion involves alternation between lL2 and lL5 as well as alternation between lL2 and rL2. ENG signals were amplified, bandpass filtered (100 Hz–1 kHz), digitized, and collected using Axoscope software (Axon Instruments). Rhythmic fictive locomotor activity was induced by the addition of 5 μM 5-hydroxytryptamine (5-HT) and 10 μM N-methyl D-aspartic acid (NMDA) to the Ringer's solution [8].

Multifiber Motor and Sensory Conduction

Multifiber motor and sensory conduction studies were carried out in mice briefly anaesthetized with isoflurane, using protocols previously reported [9]. In brief, sciatic-tibial motor fibers were supramaximally stimulated at the sciatic notch and knee and a compound muscle action potentials (CMAP) was recorded (baseline-peak amplitude) from the motor endplate of tibial innervated dorsal interosseous foot muscles. Motor conduction velocity was

calculated for the notch to knee segment. For sensory conduction, digital hindpaw nerves were supramaximally stimulated and the sciatic-tibial SNAP (baseline-peak amplitude) recorded from the knee after averaging (5-10X). Stimulation and recording was carried out using E2 subdermal platinum electrodes (Grass/Astromed). All recordings were carried out with near nerve temperature maintained at $37.0 \pm 0.5^\circ\text{C}$.

Histological and Electron Microscopy Analyses

Mice were euthanized, the brains rapidly removed and flash frozen in 2-methyl butane on solid carbon dioxide [10]. Serial coronal sections of $20\ \mu\text{m}$ were obtained and sections thaw mounted on charged slides. To visualize neuronal cell bodies and astrocytes, immunoassays were performed using antibodies recognizing the neuron-specific marker mouse anti-neuronal nuclei (NeuN, Chemicon, 1:1,000) and glial fibrillary acidic protein (1:750, Dako), respectively. The fresh frozen sections were brought to room temperature, postfixed in buffered formalin and taken through graded ethanol washes. Sections were incubated in a humidifying chamber with 1% hydrogen peroxide to quench endogenous peroxidase enzyme activity, and were subsequently blocked with universal blocking serum (Dako) containing 0.2% Triton X-100. The sections were washed with phosphate buffered saline (PBS) and incubated with the primary antibodies for 1 hour at room temperature followed by the secondary antibody (rabbit anti-mouse, 1:200, Dako) for 30 min, then the sections were washed with PBS and incubated for 30 min with an avidin-biotin complex (1:100, Vector Laboratories), washed

three times and immunoreactivity was visualized with 3,3'-diaminobenzidine tetrahydrochloride. Sections were then rinsed, dehydrated in a series of ethanol washes and mounted with Permount.

To assess myelinated axons, Weil's stain for myelin was used. Fresh frozen sections were postfixated in buffered formalin, rinsed with water, and dehydrated. Sections were then incubated for 45 min at 55°C in Weil's staining solution containing 10% haematoxylin and 4% ferric ammonium sulphate solution preheated to 55°C. The sections were then washed with tap water and differentiated macroscopically with 4% ferric ammonium sulphate and microscopically with Weigert's differentiator (potassium ferricyanide with borax).

For electron microscopy analysis, mice were euthanized and their brains and spinal cord tissues removed. The following regions of the brain were dissected: rostral spinal cord, medulla, cerebellum, diencephalon, fornix, striatum, internal capsule, corpus callosum and motor cortex. Primary fixation was carried out at 4°C for 4 hours in a freshly prepared solution containing 2.5% glutaraldehyde and 2% paraformaldehyde in 100 mM cacodylate, pH 7.2 [11]. Spinal cord and sciatic nerve samples were obtained following fixation by perfusion or by euthanasia by cervical displacement, dissection, followed by fixation by immersion. Identical results were obtained for samples fixed by tissue perfusion or by fixation by immersion of the tissue in fixative. In both cases, the fixative used was 2.5% glutaraldehyde, 0.1 M sodium cacodylate, pH 7.0. Samples were processed for

electron microscopy and examined with a Hitachi Transmission Electron Microscope H-7000.

For morphological analysis of a comprehensive range of tissues, organs were obtained following euthanasia by cervical displacement and dissection. Samples were fixed in Zinc-Formal Fixx (Fisher Scientific) overnight, then processed and embedded in paraffin blocks after which 5 μm sections were cut and placed onto Histobond slides (Fisher Scientific). Sections were rehydrated to water and stained with Harris Hematoxylin and alcoholic eosin Y (Electon Microscopy Sciences) as per standard histology protocols, followed by mounting with Entellan media (Electron Microscopy Sciences).

Flow Cytometry

The thymus, lymph nodes and spleen were harvested from the mice following euthanasia. Single cell suspensions were generated and 2×10^6 cells were aliquoted into wells of a 96-well plate for antibody staining. All antibody incubations were carried out for thirty minutes on ice in a fluorescence-activated cell sorting (FACS) buffer (PBS containing 1% fetal calf serum and 0.02% sodium azide) and cells were washed twice with FACS buffer following antibody incubations. Cell events were collected with a BD FACS Canto II flow cytometer and analyzed with FlowJo software (Treestar).

Miscellaneous Procedures

Axon cultures (Campanot cultures) were set up and maintained as previously described [12]. Protein concentration was estimated using a BioRad DC Protein assay [13]. To determine the number of neurons, wild-type and *cnx*^{-/-} mice were anesthetized and fixed by sequential intracardiac perfusion of PBS and 4% paraformaldehyde in PBS. Brain and whole spinal cord were dissected out, post fixed in the same fixative overnight, processed for paraffin embedding and cut in 10 µm thick coronal sections. After paraffin removal, in xylol and graded alcohols, sections were counterstained with cresyl-violet. Spinal cord motoneurons exhibiting clear nucleus/nucleolus in layer IX were counted every 10 sections. Similarly, the number of brainstem facial motoneurons was counted every 3 sections.

Results

Calnexin-deficient Mice

Figure 2.1 summarizes the gene targeting strategy used to generate the calnexin gene knockout mice. The calnexin gene was disrupted by random gene trapping using a cassette containing β -galactosidase-neomycin genes [14]. Using specific primers F1, F2 and R3 (Fig. 2.1A), we determined the site of insertion to be preceding the first nucleotide of intron 7-8 (Fig. 2.1A). Sequencing confirmed the interruption cassette was inserted directly following exon 7. Primers F1 and R3 correspond to the calnexin gene, whereas primer F2 corresponds to a sequence within the β -galactosidase gene in the insertion cassette. We used these primers for PCR-driven amplification of genomic DNA to identify the genotype of the mice. As expected, analysis of DNA isolated from wild-type mice showed only a 316 base pair (bp) DNA product with F1/R3 primers (Fig. 2.1B) and no DNA product when F2/R3 primers were used (Fig. 2.1B). Analysis of genomic DNA from *cnx*^{-/-} mice showed amplification of a 941 bp DNA product with the use of F2/R3 primers and no DNA product with primers F1/R3, indicating that both alleles of the calnexin gene were interrupted by the insertion cassette (Fig. 2.1B). In contrast, PCR analysis of genomic DNA from *cnx*^{+/-} mice with F1/R3 and F2/R3 primers produced both 316 bp and 941 bp DNA fragments corresponding to the presence of both wild-type and calnexin gene interrupted alleles, respectively (Fig. 2.1B). To determine there was no

alternative splicing around the interruption cassette, primers were designed before (1F, 7R), flanking (7F, 8R, 12R) after (12F, 15R) and within (InsR paired with 7F) the interruption cassette (Fig. 2.1C). RNA was isolated from wild-type, heterozygote, and calnexin-deficient brain tissue and used for reverse transcription into cDNA and PCR using the above primers along with a GAPDH loading control (Fig. 2.1D). Exons 1-7 prior to the interruption cassette are transcribed with no detectable alternative splicing around the interruption cassette in calnexin-deficient brain tissue. Western blot analysis revealed that there was no detectable expression of calnexin protein when both alleles of the gene were interrupted (Fig. 2.1E, F). Identical results were obtained with a calnexin antibody specific for either the N-terminal ER luminal portion (Fig. 2.1E), or an antibody that recognizes the C-terminal cytoplasmic domain (Fig. 2.1F). We concluded that the expression of calnexin protein was fully disrupted.

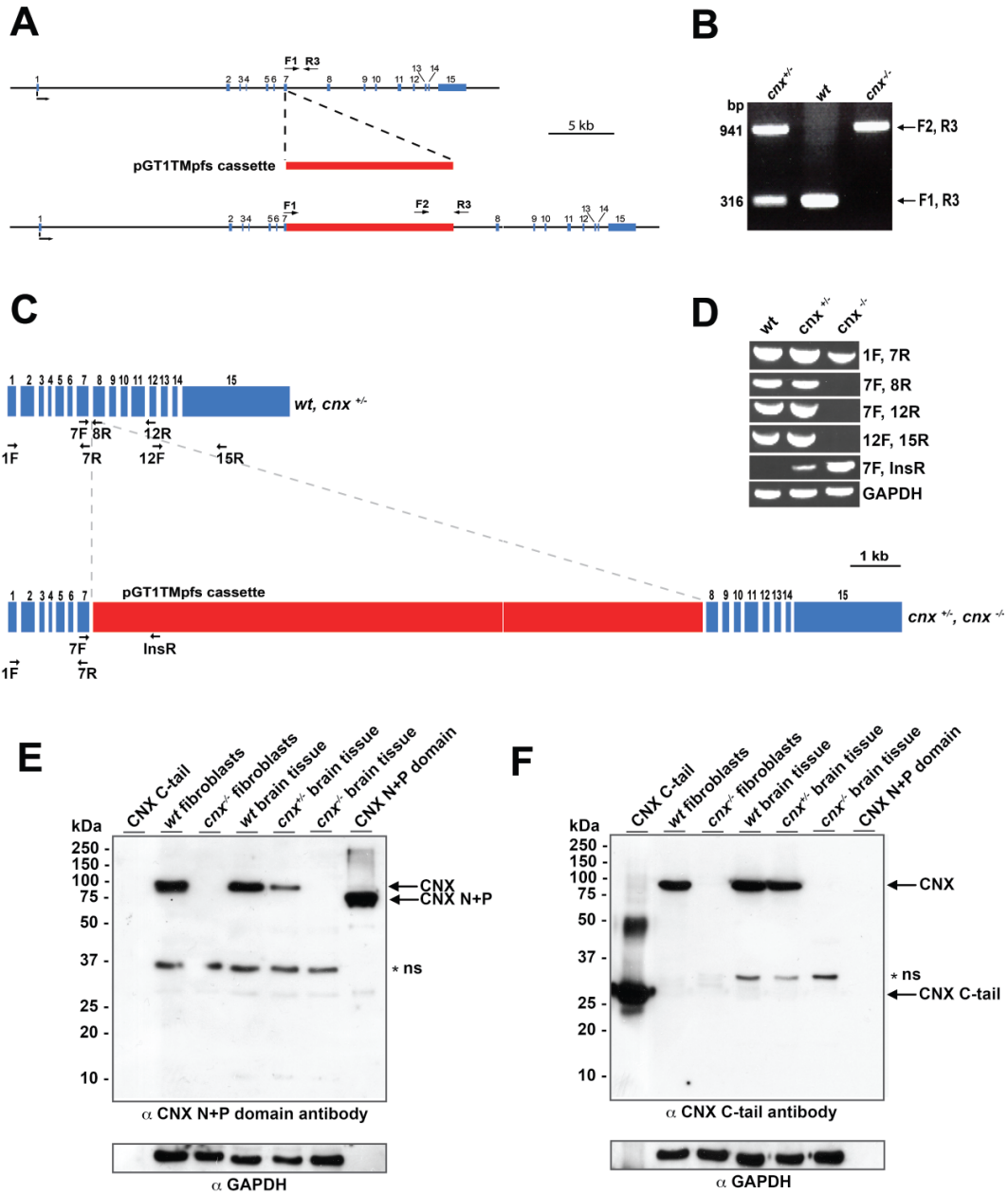


Figure 2.1. Generation of the calnexin-deficient mouse.

(A) Random gene trapping was used to generate the calnexin-deficient mice. An interruption cassette (pGT1TMpfs cassette, in *red*) containing β -galactosidase and neomycin genes was inserted into the calnexin gene. The *numbers* indicate the locations of calnexin gene exons (in *blue*). Forward (F1 and F2) and reverse (R3) primers are indicated with *arrows*. (B) PCR analysis of genomic DNA isolated from wild-type (*wt*), heterozygote (*cnx^{+/-}*), and homozygote (*cnx^{-/-}*) calnexin-deficient mice. Forward (F1 and F2) and reverse (R3) primers were used as indicated for A. A DNA product of 941 base pairs (bp) amplified with primers F2 and R3 identifies successful cassette insertion and interruption of the calnexin gene (*cnx^{-/-}*), whereas a DNA product of 316 bp amplified with primers F1 and R3 indicates the presence of the wild-type allele (*wt*). The presence of both 941 and 316-bp DNA products identifies heterozygotes. (C) schematic representation of calnexin mRNA. The location of the insertion cassette (in *red*) is shown. The location of specific primers used for RT-PCR analysis in D is indicated in the figure. (D) RT-PCR was carried out using wild-type (*wt*), heterozygote (*cnx^{+/-}*), and calnexin-deficient (*cnx^{-/-}*) RNA isolated from brain tissue. Pairs of specific DNA primers used for the analysis are indicated. (E) and (F) Western blot analysis of wild-type, heterozygote, and calnexin-deficient tissues and wild-type and calnexin-deficient fibroblasts with anti-calnexin antibodies. The location of molecular weight markers is indicated to the *left* of the gel. In (E), anti-N terminus (N+P domain) calnexin antibodies were used. In (F), the blot was probed with anti-C terminus calnexin antibodies. *N+P*, N+P domain of calnexin; *C-tail*, cytoplasmic C-terminal domain of calnexin. The *asterisk* and *ns* designate the nonspecific reactive protein band. *GAPDH*, glyceraldehyde-3-phosphate dehydrogenase. Chimeric mice were generated by Peter Dickie.

Calnexin-deficient Mice Display an Altered Phenotype Characterized by Gait Disturbance

Chimeric mice were crossed with wild-type mice to generate heterozygotes. The *cnx*^{+/-} mice had a normal phenotype, being viable and fertile. Intercrossing of *cnx*^{+/-} females and *cnx*^{+/-} males was carried out to generate homozygote calnexin-deficient mice. The majority of newborn calnexin-deficient mice were indistinguishable from wild-type and *cnx*^{+/-} littermates with respect to their size, weight and external appearance. Some were born slightly smaller and displayed difficulty righting themselves if turned on their backs. However, as early as day 11, calnexin-deficient animals failed to gain weight and a marked size difference became fully apparent approximately 14-16 days following birth between wild-type and calnexin-deficient mice (Fig. 2.2A). Figure 2.2A shows that between days 11 to 22 of life, calnexin-deficient mice failed to gain weight. Following this short period of time, weight gain resumed at a rate similar to the wild-type animals but this interruption in growth results in calnexin-deficient mice that remained smaller than their wild-type littermates.

The most obvious defect in calnexin-deficient mice was the demonstration of abnormalities manifested by a gait disturbance with instability, splaying of the hind limbs, ataxia, tremors, lower limb motor defects, and a rolling walk (Fig. 2.2B). Approximately 6 weeks after birth,

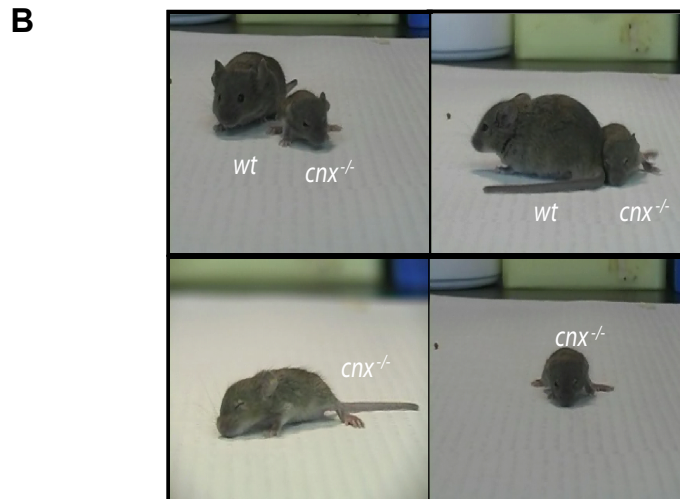
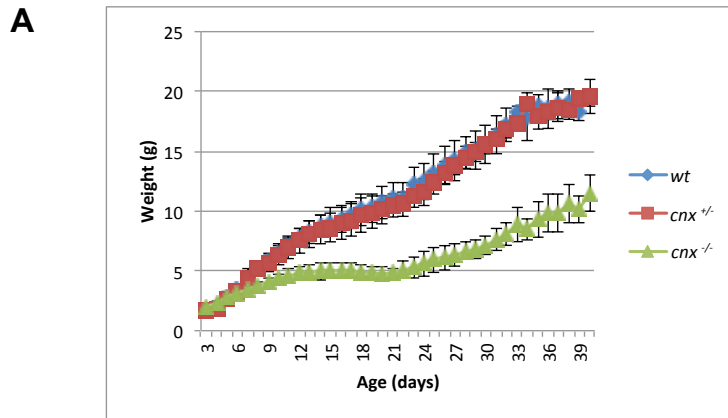


Figure 2.2. Calnexin-deficient mice are smaller than their wild-type littermates and demonstrate a neurological disorder.

(A) Calnexin-deficient mice are the same size and weight as their wild-type and heterozygote littermates at birth. A difference in weight gain is observable as early as day 11 and calnexin-deficient animals fail to gain weight between day 16-22 of life, leading to a marked size difference. After weaning, the animals gain weight at a similar rate to wild-type and heterozygote littermates. (B) Calnexin-deficient animals display a neurological phenotype characterized by gait disturbance, a rolling walk, and splaying of the hind limbs.

calnexin-deficient mice demonstrated the complete phenotype (Fig. 2.2B) with no further significant progression. Calnexin-deficient mice were fertile and their lifespan was comparable to wild-type animals.

Absence of Calnexin Results in Impaired Nerve Conduction Velocity

The neurological abnormalities observed in mice with no expression of calnexin may originate from either a defect in neuronal growth and function and/or problems with myelination processes. To assess neuronal status, we carried out morphological analysis of the brain tissue, counted motoneurons of the spinal cord and examined neuronal growth and function in the absence of calnexin. We did not observe any significant changes in the gross morphology of the brain in calnexin-deficient mice (Fig. 2.3A). Examination of the motoneuron distribution in the spinal cord indicated that while the spinal cord was shorter in the absence of calnexin (consistent with their smaller size), the motoneuron distribution was comparable to wild-type (Fig. 2.3B). Furthermore, a careful count of motoneurons in wild-type and calnexin-deficient mice revealed no difference in the number of motoneurons (Fig. 2.3B). Similarly, amplitudes of the compound muscle action potentials (CMAPs), indices of motor axon innervations, was not altered in *cnx*^{-/-} mice. Neuronal growth in *cnx*^{-/-} neurons was investigated by culturing sympathetic neurons in compartmentalized cultures [12]. We observed no difference in neuronal growth in the absence of calnexin (Fig. 2.3C).

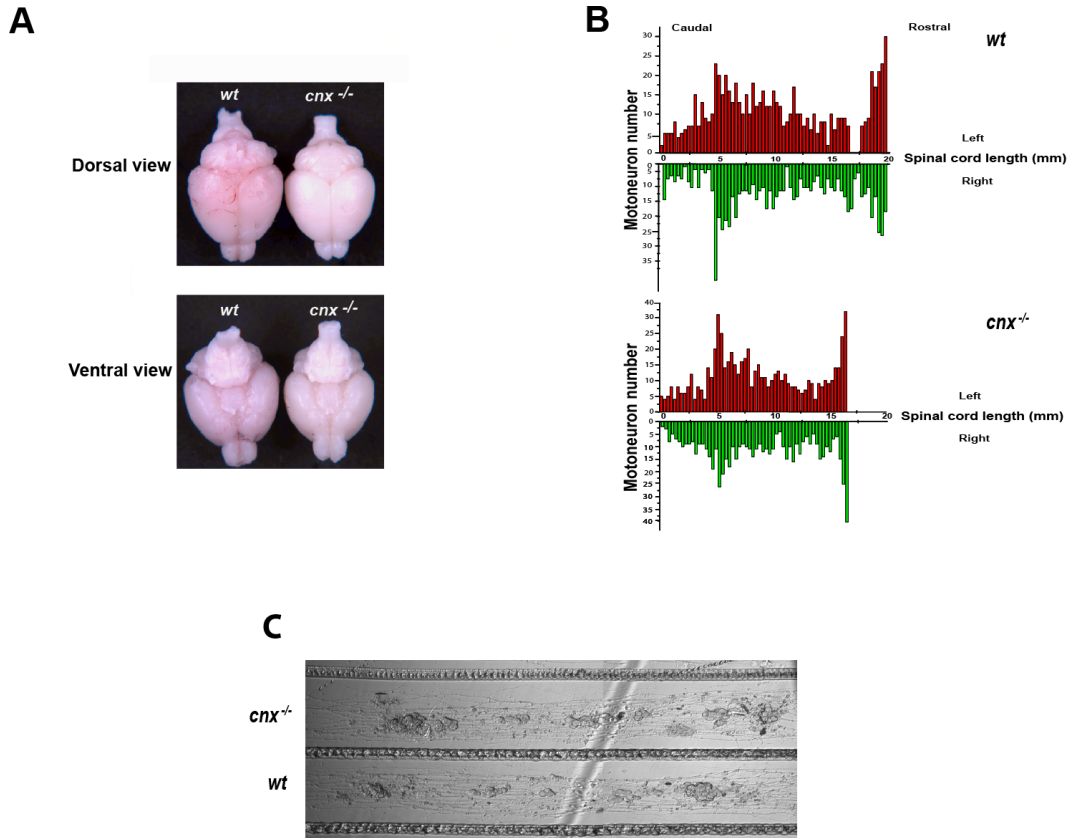


Figure 2.3. Calnexin in neuronal tissue.

(A) *cnx^{-/-}* and *wt* brains isolated from 21-day-old mice, viewed from the dorsal and ventral side. There were no morphological differences in the anatomical structure between *cnx^{-/-}* and *wt* brains. (B) Analysis of motor neuron number in wild-type (*wt*) and calnexin-deficient (*cnx^{-/-}*) mice. The spinal cord length is shorter in *cnx^{-/-}* mice but the spinal motoneuron distribution and number were not different from *wt* mice. In red, neurons counted on the left site of the spinal cord; in green, neurons counted on the right site of the spinal cord. (C) Sympathetic neurons from *cnx^{-/-}* and wild-type (*wt*) mice were grown in compartmentalized cultures (Campenot cultures) [15]. The absence of calnexin had no effect on axonal growth. Motor neuron number was determined by Michel Dubois-Dauphin and neurons cultured by Karen Bedard.

To assess neuron status in calnexin-deficient mice, we examined excitatory pharmacologically-induced lower limb walking movements in the isolated spinal cord. To evoke fictive locomotion (characterized by the oscillatory bursting of motor neurons in a step cycle period of 2-4 sec), we applied 5 μ M 5-hydroxytryptamine (5-HT, serotonin) and 10 μ M N-methyl D-aspartic acid (NMDA) (Fig. 4A) to isolated spinal cords [8] taken from wild-type and *cnx*^{-/-}. Electroneurograms were recorded from the second and fifth lumbar ventral root on the left side (i.e. IL2, IL5) and the second lumbar ventral root on the left and right side (i.e. IL2, rL2). Appropriate alternation between bursts was noted in wild-type and calnexin-deficient preparations (Fig. 2.4A), indicating that the fictive locomotor pattern is undisturbed in the *cnx*^{-/-} mouse.

Next, we tested for electrophysiological parameters of motor and sensory neurons in calnexin-deficient and wild-type mice. Figure 2.4B shows that motor nerve conduction velocities were significantly slowed in the absence of calnexin. There was a significant difference between wild-type and calnexin-deficient motor conduction velocities at values of 43.1 \pm 2.5 m/s and 31.0 \pm 3.2 m/s, respectively (p=0.01) (Fig. 2.4B). Wild-type and calnexin-deficient mouse CMAP amplitudes were preserved at 9.2 mV and 10.0 mV, respectively. Sensory nerve conduction velocities were also reduced in the *cnx*^{-/-} mice (Fig. 2.4C). The sensory nerve conduction velocity in wild-type mice was 46.1 m/s (Fig. 2.4C), with a significant decrease in sensory nerve

conduction velocity (38.2 m/s) in the absence of calnexin (Fig. 2.4C). The amplitude of the sensory nerve action potentials (SNAPs) in the wild-type mice was also comparable between the groups: 14.1 μ V in controls compared to a 10.9 μ V in the calnexin-deficient animals. The SNAP amplitude reflects the number of excitable myelinated axons that can be recruited by stimulation. Taken together, these results indicate that neuronal growth and neuron number were not altered in the absence of calnexin but there was a significant decrease in the nerve conduction velocity in *cnx*^{-/-} mice.

Dysmyelination in the Calnexin-deficient Mouse

Myelin surrounds axons and provides for rapid nerve conduction that is essential to nervous system function. Loss of myelin leads to reduced nerve conduction velocity, and therefore, we tested if myelination was affected in the absence of calnexin. First, we carried out electron microscopic analysis of spinal cord and sciatic nerve in calnexin-deficient mice to examine, at a higher resolution, if myelin formation was impaired in the absence of calnexin. Calnexin-deficient spinal cords have a thinner, wavy and decompacted myelin in the absence of calnexin (Fig. 2.5A-D) indicating that the absence of calnexin affects myelination of the spinal cord.

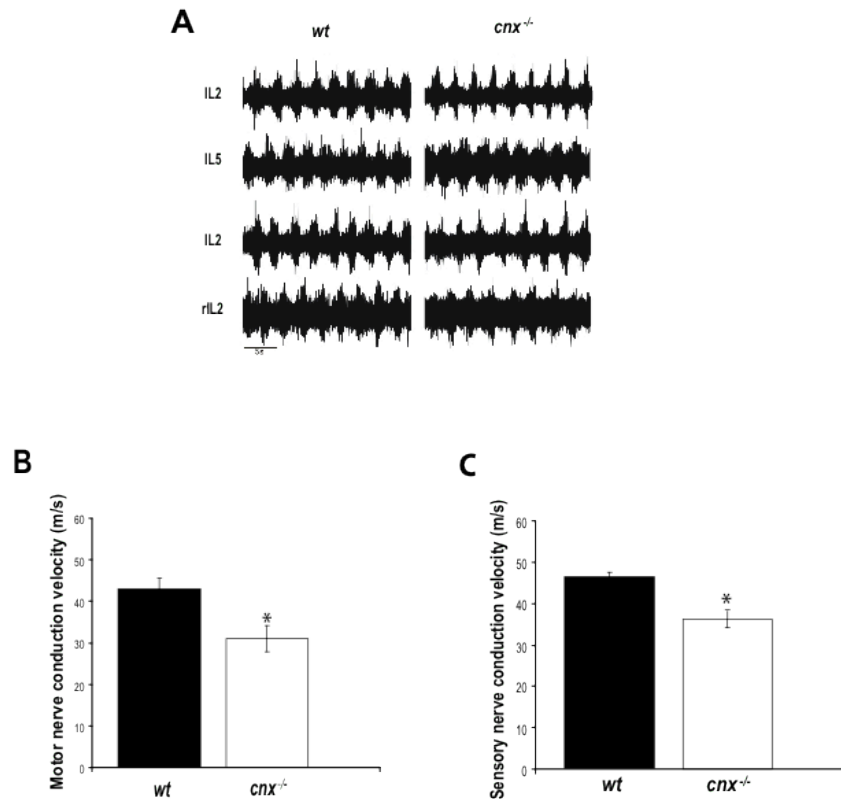


Figure 2.4. Neuronal function is not impaired but nerve conduction velocity is reduced in the absence of calnexin.

(A) The fictive locomotor pattern is undisturbed in the *cnx*^{-/-} mouse. Electroneurograms recorded from the second and fifth lumbar ventral root on the left side (i.e. IL2, IL5) and the second lumbar ventral root on the left and right side (i.e. IL2, rL2) of the spinal cord in the wild-type (*wt*, left traces) and *cnx*^{-/-} (right traces) mice. Fictive locomotion was evoked with 5 μ M serotonin (5-HT, 5-hydroxytryptamine) and 10 μ M N-methyl D-aspartic acid (NMDA). Note the appropriate alternation between bursts in both cases. **(B)** Motor nerve conductive analysis of wild-type (*wt*) and calnexin-deficient (*cnx*^{-/-}) mice. Motor nerve conduction velocity was significantly slower in the absence of calnexin. **(C)** Sensory nerve conductive analysis of wild-type (*wt*) and calnexin-deficient (*cnx*^{-/-}) mice. In the absence of calnexin, there was reduced sensory nerve conduction velocity. * indicates significant differences. Fictive locomotion was determined by Jason Dyck and Simon Gosgnach. Nerve conduction velocities were determined by Lawrence Korngut and Doug Zochodne.

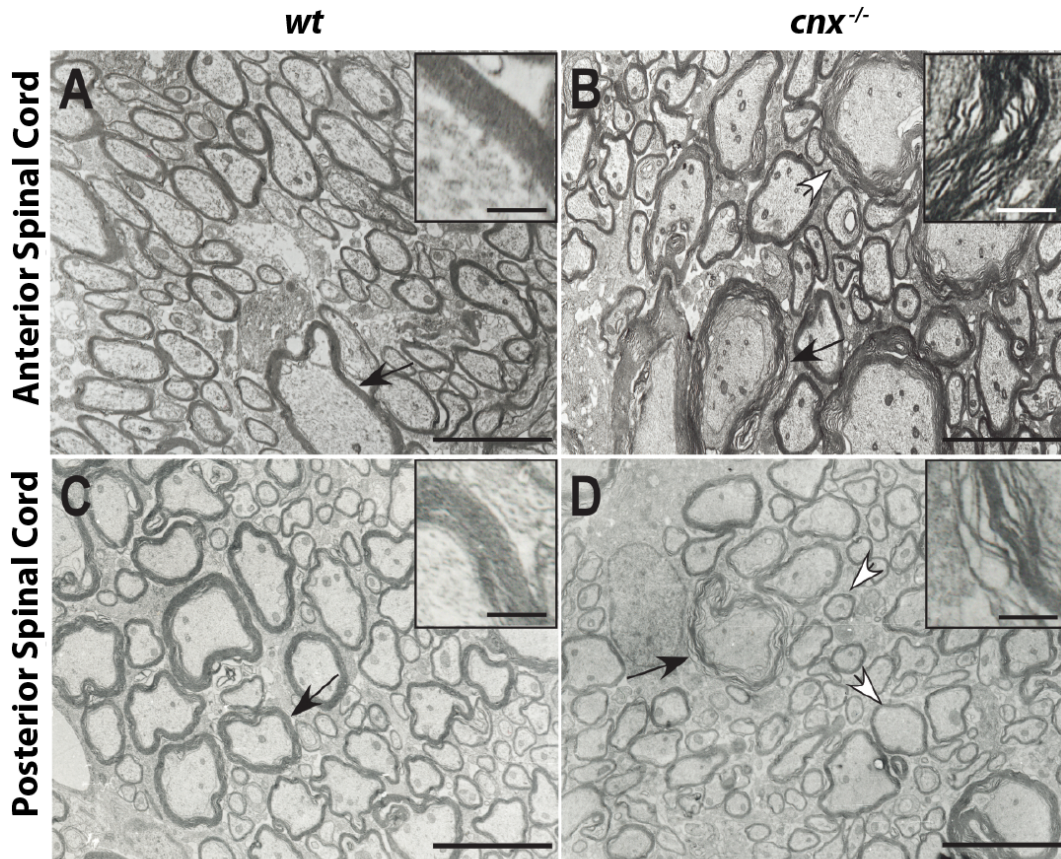


Figure 2.5. Dysmyelination in the spinal cord.

Electron micrographs demonstrate dysmyelination. Areas of wavy, decompacted myelin and hypomyelination appear in anterior (**A**, **B**) and posterior (**C**, **D**) regions of the spinal cord of *cnx*^{-/-} mice. The black arrows indicate areas of myelin shown magnified in the inserts. The open arrows indicate the areas of wavy myelination (**B**) or hypomyelination (**D**). Scale bar=5 μm; insert scale bar=500 nm.

A different kind of myelination defect was apparent in the sciatic nerve. Electron microscopic analysis of calnexin-deficient sciatic nerve revealed, in addition to wavy and decompacted myelin, a hypermyelination that appeared to invade the neuronal areas (Fig. 2.6). The findings resembled “G fibers” or tomaculae that are described in human hereditary neuropathy with sensitivity to pressure palsy (HNPP) or focally folded myelin described in CMT4B. To test if calnexin-deficiency resulted in a reduced amount of myelin in nervous tissue (hypomyelination), the *g*-ratio was calculated for calnexin-deficient and wild-type spinal cord and sciatic nerve. The *g*-ratio is defined as the ratio of the axonal diameter divided by the diameter of the axon plus the thickness of its myelin sheath. Calculation of the *g*-ratio revealed that calnexin-deficiency resulted in modest hypomyelination in the spinal cord and did not affect myelin sheath thickness in the sciatic nerve (*cnx*^{-/-} spinal cord *g*-ratio was 0.78±0.05 (n=40) compared to wild-type spinal cord at 0.71±0.05 (n=40); *cnx*^{-/-} sciatic nerve *g*-ratio was 0.73±0.09 (n=10) compared to wild-type sciatic nerve at 0.71±0.07 (n=10)). We concluded that in the absence of calnexin there was no significant reduction in myelin but defective formation and compaction of myelin sheaths. These findings indicate significant changes in the PNS of calnexin-deficient animals and may help explain the neuronal phenotype and decreased nerve conduction velocity in *cnx*^{-/-} mice.

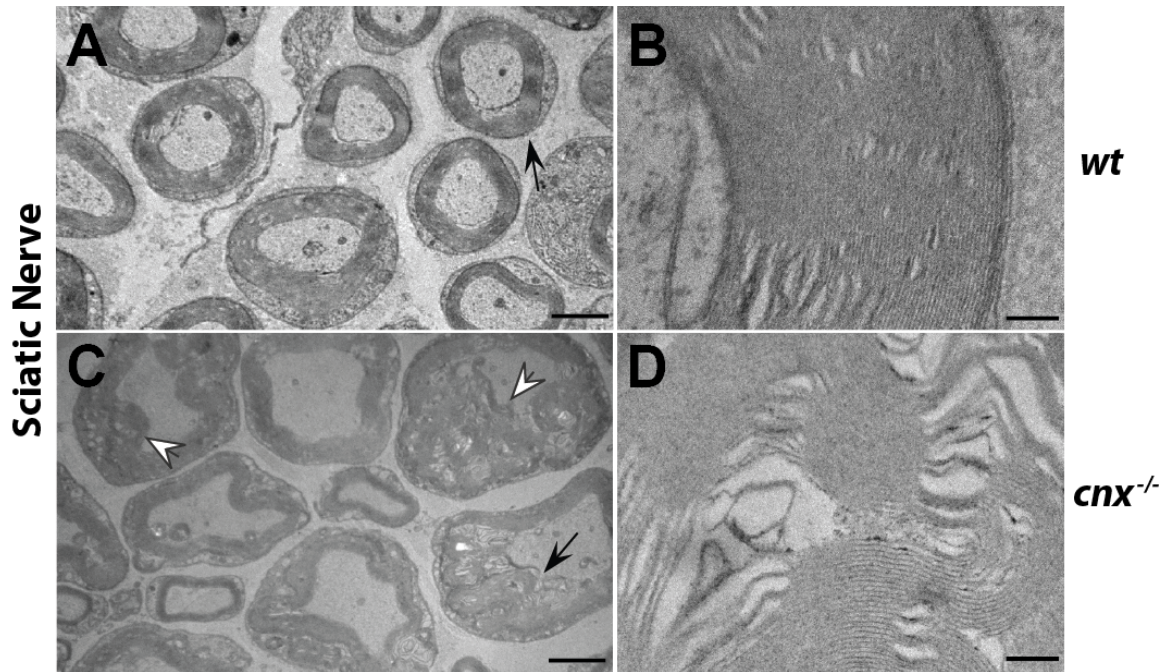


Figure 2.6. Dysmyelination in the sciatic nerve.

Myelin abnormalities in the peripheral nervous system included redundant myelin folds as well as decompact myelin sheaths. The black arrows indicate areas of myelin shown magnified in the inserts. The open arrows indicate areas of aberrant and redundant myelin folds. Scale bar=5 μm ; insert scale bar=500 nm.

We also carried out histological analysis of the brain tissue from wild-type and *cnx*^{-/-} animals to test the effect of calnexin deficiency on various regions of the CNS. In all brain regions examined, neuronal cell bodies, visualized using anti-neuronal specific nuclear protein (NeuN) antibodies, appeared normal and healthy in both the wild-type (Figure 2.7A) and calnexin-deficient (Fig. 2.7B) mice. However, large white matter tracts were variably affected. In calnexin-deficient animals the rostral corpus callosum was thinner and, particularly at the medial rise, displayed areas of patchy myelination or dysmyelination (Fig. 2.7C, D). However, the axons appeared to be spared. In the absence of calnexin the internal capsule (Fig. 2.7F) displayed less branching and was narrower than that observed in the wild-type (Fig. 2.7E), suggesting fewer myelinated fibers travelling between the periphery and cerebral cortex. Patchy areas of myelination were evident in the cerebral peduncle of the calnexin-deficient mouse (Fig. 2.7G, H). The cerebellar peduncles of the *cnx*^{-/-} mouse were also characterized by a patchy, loose myelination pattern (Fig. 2.7I, J). At low resolution, white matter tracts of the spinal cord did not show obvious dysmyelination, and cell bodies of the horns appeared normal and healthy. An increased number of glial fibrillary acid protein (GFAP)-positive astrocytic fibers were observed in the absence of calnexin (Fig. 2.7L) compared to the wild-type (Fig. 2.7K). The perpendicular organization of the glial fibers in the calnexin knockout mice were similar to that observed early in CNS development, suggesting that in the absence of calnexin, spinal cord development was altered.

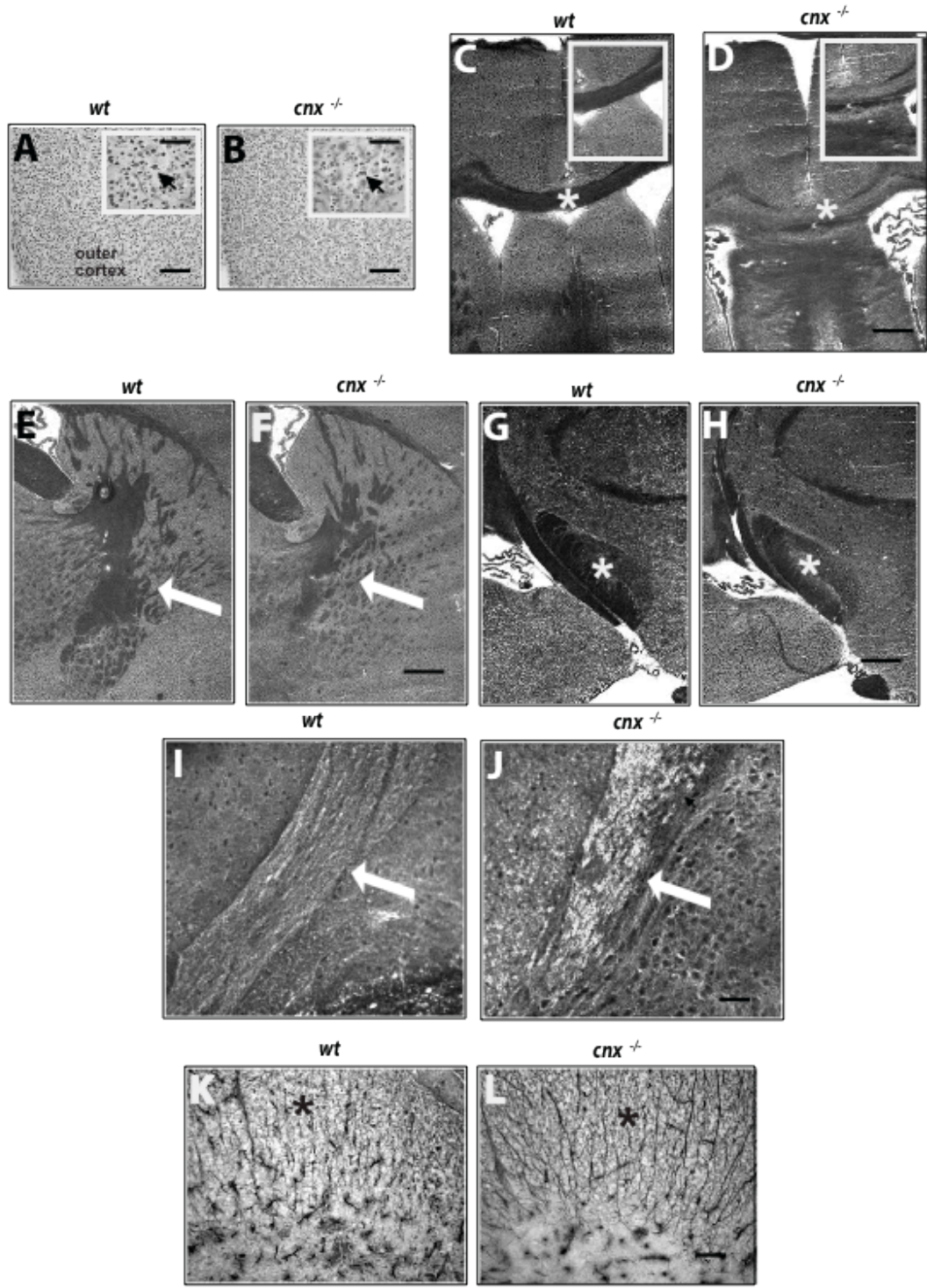


Figure 2.7. Dysmyelination in the brain of calnexin-deficient mice.

(A, B) Antibodies to neuronal specific nuclear protein (NeuN) were used to visualize neuronal cell bodies in all brain regions. Representative photomicrographs of the premotor cortex are shown in **(A)** (*wt*) and **(B)** (*cnx^{-/-}*). Normal cortical cytoarchitecture was observed and neurons appeared normal and healthy (arrows point to NeuN positive neurons). Scale bar=50 μm , insert scale bar=10 μm .

(C, D) Examination of large white matter tracts showed that the rostral corpus callosum was thinner and contained patchy areas of myelination in the absence of calnexin **(D)**. Asterisks in **(C)** and **(D)** identify rostral corpus callosum and areas magnified for inserts. Scale bar=50 μm , insert scale bar=20 μm .

(E, F) Compared to wild-type **(E)** the overall amount of myelin in the internal capsule (identified with arrows) was reduced in *cnx^{-/-}* mice **(F)** Scale bar=50 μm .

(G, H) The cerebral peduncle (identified with asterisks) in the *cnx^{-/-}* mouse **(H)** contained areas of patchy myelin compared to wild-type **(G)**. Scale bar in **(H)** = 50 μm .

(I, J) The cerebellar peduncles (identified with arrows) in the *cnx^{-/-}* mouse **(J)** showed a patchy, loose myelination pattern as compared to wild-type animals **(I)**. Scale bar=20 μm .

(K, L) In the white matter of the spinal cord, an increased number of glial fibrillary acid protein (GFAP)-positive astrocytic fibers (identified with asterisks) was observed in the absence of calnexin **(L)** compared to the wild-type **(K)**. Scale bar=10 μm .

Dissection and analysis were carried out with the help of Kathryn Todd.

Considering that calnexin is a ubiquitously expressed ER-associated protein, the specificity of the neurological phenotype and effect on myelination in *cnx*^{-/-} mice was surprising. We expected that calnexin deficiency may also affect other tissues and this may have been masked by the predominant neurological phenotype described above. However, we found no gross histological abnormalities in heart, lung, pancreas, spleen, femur, skeletal muscle, colon, liver, kidney or stomach in the absence of calnexin (Fig. 2.8).

Given the role that calnexin plays in the early events of MHC Class I protein folding [16] and the fact that calnexin is able to associate with cell surface CD3 complexes [17] and regulate T-cell receptor (TCR) assembly [18], we anticipated that the elimination of calnexin would lead to aberration of these processes. Unexpectedly, calnexin deficiency had no impact on the immune system (Fig. 2.9). The CD4/CD8 profiles of wild-type and *cnx*^{-/-} thymocytes were indistinguishable (Fig. 2.9A) and the number of thymocytes recovered from each strain was similar. We did not detect any differences in CD25/CD44 expression within the CD4⁻CD8⁻ double negative compartment or changes in the expression of MHC Class I in any thymocyte sub-population in *cnx*^{-/-} mice (Fig. 2.9C). The expression of TCR β on bulk thymocytes and CD69 on CD4⁺CD8⁺ double positive thymocytes was also identical (Fig. 2.9A) suggesting that positive selection occurred normally in the absence of calnexin. Maturation of CD8 single positive thymocytes as evaluated by CD24

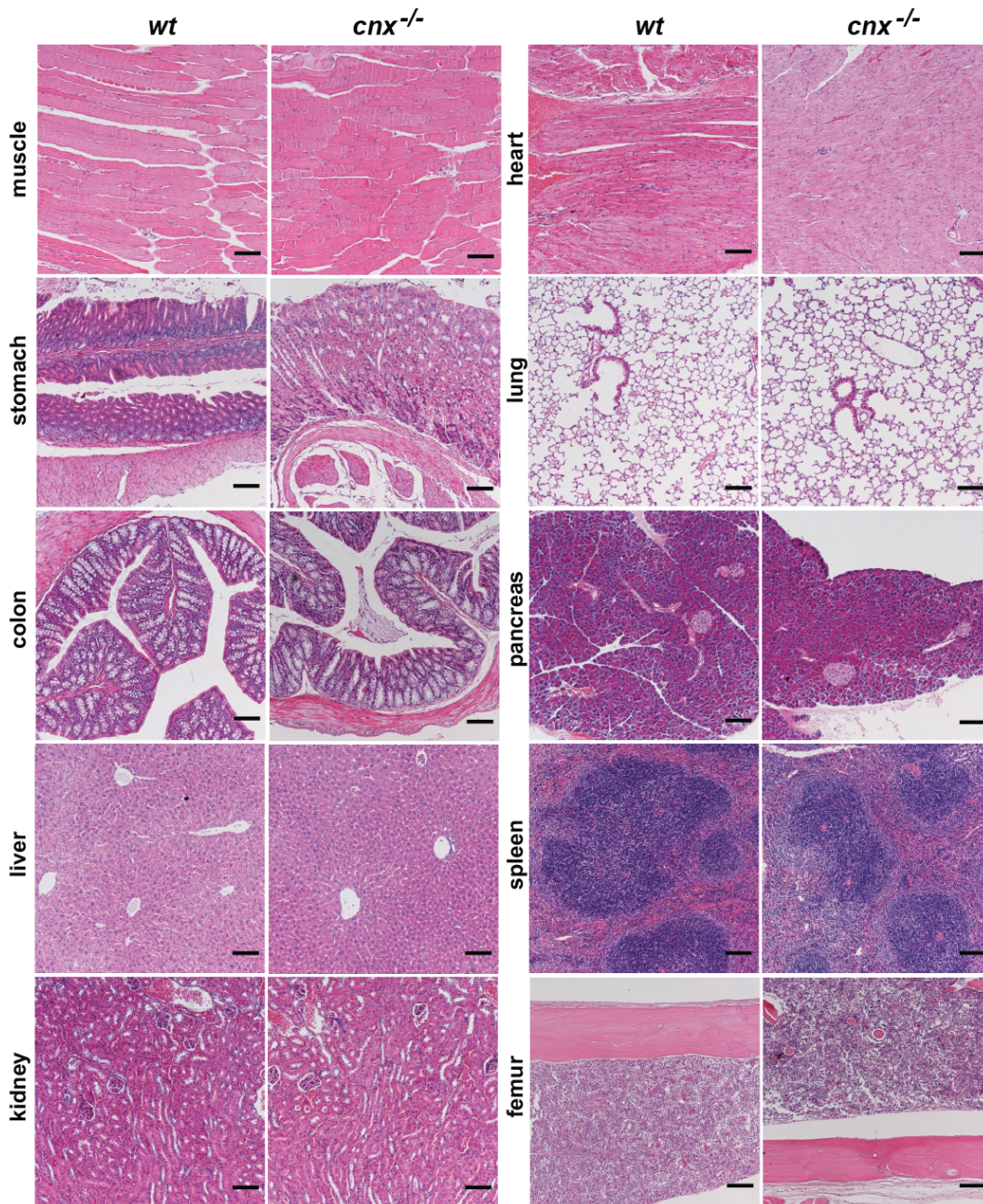


Figure 2.8. Histological analysis of calnexin-deficient tissues.

Histological analysis of wild-type (*wt*) and calnexin-deficient (*cnx^{-/-}*) tissues was carried out as described under “Material and Methods”. Tissues were stained with haematoxylin and eosin. No significant morphological changes were observed between wild-type and calnexin-deficient tissues. Scale bar=100 μ m.

down-regulation occurred normally in *cnx*^{-/-} mice. The splenic lymphocyte population also appeared grossly normal in *cnx*^{-/-} mice (Fig. 2.9B). We did notice a decrease in splenic cellularity in *cnx*^{-/-} mice; however, we attributed this to the reduced size and weight of *cnx*^{-/-} animals. The percentage of T cells in the spleen as well as the CD4/CD8 profile of the T cell population was unaffected by calnexin-deficiency (Fig. 2.9B). Again, no dramatic change in cell surface marker expression (CD44, CD62L, CD25, TCR β and MHC Class I) was observed in *cnx*^{-/-} T cells (not shown and Fig. 2.9B). Finally, we examined MHC Class I expression on dendritic cells from *cnx*^{-/-} mice and found no change when compared to the wild-type mice (Fig. 2.9D). Overall, the thymus and peripheral T cell populations appeared normal in *cnx*^{-/-} mice. These results demonstrate that the absence of calnexin had no significant impact on the immune system, indicating that this protein is not essential for the formation of the immune system in mice.

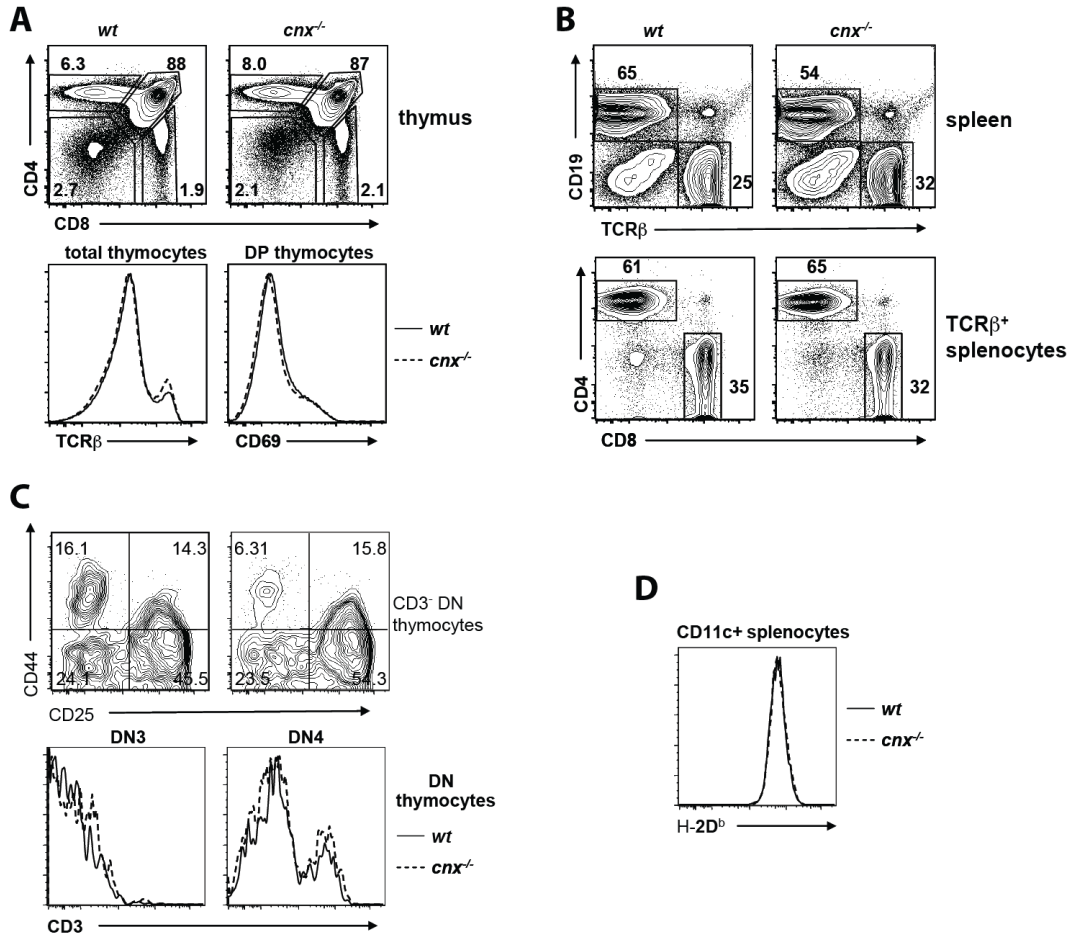


Figure 2.9. Calnexin Deficiency Does Not Affect the Immune System.

(A) Thymocytes from wild-type and *cnx*^{-/-} mice were probed with anti-CD4, anti-CD8, anti-CD69 and anti-TCR β antibodies. Cells were analyzed by flow cytometry. CD4/CD8 profile of bulk thymocytes (*top row*), TCR β expression on bulk thymocytes and CD69 expression on CD4+CD8+ thymocytes from wild-type (*wt*, *solid line*) or *cnx*^{-/-} (*broken line*) mice are shown (*bottom row*). (B) Splenocytes from wild-type and *cnx*^{-/-} mice were stained with anti-CD19, anti-TCR β , anti-CD4 and anti-CD8 antibodies followed by flow cytometry analysis. The CD19/TCR β profile of bulk splenocytes (*top row*) and the CD4/CD8 profile of TCR β ⁺ cells are depicted (*bottom row*). (C) Cells were probed with anti-CD25 and anti-CD44 followed by FACS analysis. There are neither detectable differences in CD25/CD44 expression within the CD4-CD8- double negative compartment nor changes in the expression of MHC Class I in any thymocyte sub-population in calnexin-deficient mice. (D) Analysis of H-2D^b expression in wild-type (*wt*) and calnexin-deficient (*cnx*^{-/-}) cells. There is no change in MHC Class I expression on dendritic cells from *cnx*^{-/-} mice when compared to the wild-type mice. FACS analysis was conducted by Troy Baldwin.

Expression Profile of Calnexin-deficient Spinal Cord

Spinal cords were obtained from 21-day calnexin-deficient mice and the tissue flash frozen, crushed, and used for RNA extraction using Trizol reagent. The RNA was assessed for quality and used for Affymetrix microarray analysis. Analysis of the results indicate that mRNA encoding select myelin proteins are more than two-fold down-regulated in the calnexin-deficient spinal cord including early growth response 2 (Egr2), peripheral myelin protein (PMP), periaxin and myelin P2 protein. Egr2, also known as Krox20, is a transcriptional factor that regulates the expression of myelin genes. PMP, periaxin and P2 protein are all myelin proteins that are expressed following myelin initiation. Periaxin is a structural element that connects myelin to the surrounding basal lamina and is downstream of Egr2 regulation. PMP22 is myelin structural element as previously discussed. P2 protein is located at the major dense line of myelin sheaths and thought to likely play a similar structural role in the PNS as myelin basic protein in the CNS and PNS. Additionally, it is thought that cholesterol, a major rate-limiting component of myelin, is a potential ligand for P2 [19]. Down-regulation of these myelin protein elements was confirmed using specific primers and RT-PCR. While the mechanism by which the absence of calnexin impacts on transcription is unknown, decreased expression of such myelin proteins could impact on myelin formation and maintenance and could contribute to the myelin abnormalities found in the calnexin-deficient mouse.

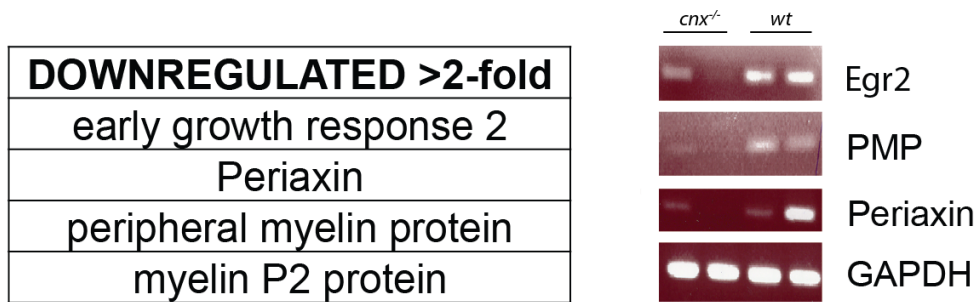


Figure 2.10. Decreased RNA expression levels of myelin proteins.

Affymetrix microarray analysis showed down-regulation of select myelin proteins. This was confirmed using RT-PCR with specific primers for Egr2, PMP22, and periaxin with GAPDH as a control. Duplicates of detectable transcripts from wild-type (*wt*) and calnexin-deficient (*cnx^{-/-}*) spinal cord are shown as indicated by *wt* and *cnx^{-/-}*. *Egr2*, early growth response 2, *PMP22*, peripheral myelin protein 22, *GAPDH*, glyceraldehyde-3-phosphate dehydrogenase.

Discussion

The important finding of this study is that calnexin, a ubiquitously expressed ER-associated molecular chaperone, has a specific and detrimental effect on myelin formation. We have shown that calnexin-deficiency results in a combined central and peripheral dysmyelinating syndrome. The findings have identified an important, previously undiscovered role for calnexin in myelination and myelin diseases. This is supported by the following observations: calnexin-deficient mice have disturbed motor function characterized by gait disturbance, lower limb dysfunction, and ataxia with myelin of the PNS and CNS being disorganized and decompacted in the absence of calnexin. This is consistent with the slower motor and sensory neuron conduction velocities observed in the *cnx*^{-/-} mice.

Despite its ubiquitous expression, calnexin-deficient mice are viable. In fact, calnexin-deficiency is only lethal in *S. pombe* but not in *S. cerevisiae* [1], *Dictyostelium* [2, 3] or in *C. elegans* [4, 5]. Previously Denzel *et al.* showed that partial deletion of the calnexin gene in the mouse results in a motor disorder associated with a loss of the large myelinated nerve fibers [20]. In contrast to our observations, these animals die early, with very few surviving to 3 months [20]. Calnexin-deficient mice generated in the present study do not have a reduced number of neurons, they are fertile and they have a normal lifespan. The discrepancy between this study and Denzel *et al.* [20] likely represents the difference between only partial deletion [21] and

disruption of the calnexin gene (this study). The truncated protein produced from a partial deletion could act in a dominant-negative fashion and contribute to the different phenotype observed by Denzel *et al.* In addition, the mice generated by Denzel *et al.* were created using 129/Sv stem cells and differences in the genetic background between the mice generated here (129/Ola stem cells) and those generated by Denzel *et al.* could contribute to the phenotype discrepancies. We have not observed any abnormalities in neuronal growth or fictive locomotor pattern in the absence of calnexin. Instead, we observed that calnexin deficiency in mice resulted in dysmyelination in both the central and peripheral nervous system. The existence of calnexin-deficient organisms indicates that calnexin's chaperone function is not required for viability. In the mouse, calnexin has a specific role in neurological systems and myelination.

Considering that calnexin is a ubiquitously expressed ER-associated protein, the specificity of the neurological phenotype and effect on myelination in *cnx*^{-/-} mice was surprising. We expected that calnexin deficiency may also affect other tissues and this may have been masked by the predominant neurological phenotype described above. However, we found no gross histological abnormalities in heart, lung, pancreas, spleen, femur, skeletal muscle, colon, liver, kidney and stomach in the absence of calnexin. Given the role that calnexin plays in the early events of MHC Class I protein folding [16] and the fact that calnexin is able to associate with cell surface CD3 complexes [17] and regulate T-cell receptor (TCR) assembly

[18], we also anticipated that the development of the immune system might be compromised in the absence of the protein. Unexpectedly, calnexin deficiency had no significant impact on the immune system, indicating that the protein is not essential during the formation of the immune system in mice. These findings further support our conclusions that calnexin plays a critical and specific role during myelination. The molecular chaperone function of calnexin is essential for proper formation of the myelin sheaths for which there are no compensatory mechanisms provided by other ER chaperones, including the homologous calreticulin. Yet, evidently, there must be compensatory redundancy through other mouse tissues in calnexin-deficient mice, including the immune system.

The interruption cassette used to generate the calnexin-deficient mice contained a β -galactosidase and neomycin coding region. Thus, calnexin gene expression could be assessed throughout development. As early as day 12.5, high calnexin expression is seen in neuronal tissue and cartilage [22]. High calnexin expression in neuronal tissue including the brain and spine regions continued through day 18.5 of embryonic development. At this embryonic stage, high calnexin expression was also detectable in the lung, cartilage, and liver with very low β -galactosidase activity in the heart and smooth muscle [22]. RT-PCR analysis also indicated high calnexin mRNA levels in neuronal tissue such as the brain through embryonic and post-natal development. Thus, the expression profile of calnexin through development supports its specific role in neurological systems.

Calnexin Deficiency Results in a Dysmyelinating Peripheral Neuropathy

The specificity of calnexin deficiency towards myelination is remarkable considering that calnexin is a ubiquitously expressed ER-associated molecular chaperone [23]. Neuropathies can arise from problems with the neuron or problems with the myelin sheath. We measured neuron number, growth and the function of motor neurons of the spinal cord in calnexin-deficient mice. CMAP amplitudes of the compound muscle action potentials, indices of motor axon innervations, were not altered in *cnx*^{-/-} mice and motoneurons of the spinal cord were similar in number and distribution. Sympathetic neuron cultures indicated comparable growth to wild-type animals. Fictive locomotion measurements, an indication of lower limb walking movements, were undisturbed in calnexin-deficient animals. Together, these measurements indicate that neuronal function is unimpaired.

Problems with the myelin sheath can result from mutations in myelin structural proteins. Mutations in the myelin proteins P0 and PMP22 are known to contribute to CMT pathologies. Missense point mutations in or over-expression of PMP22 lead to CMT-like peripheral neuropathies [24] that have features reminiscent of the phenotype of the *cnx*^{-/-} mouse. Similarly, abnormal myelin folding, or tomaculae, similar to those observed in the *cnx*^{-/-} mice, are a feature of HNPP (hereditary neuropathy with liability to pressure palsies), a disorder with a loss of PMP22 expression. PMP22-deficient mice have a delayed onset of myelination and develop abundant tomacula [25]. Mice deficient in P0 exhibit abnormal motor coordination, tremors and

severe hypomyelination [26]. Mice over-expressing P0 display delayed nerve development due to deregulation in the expression of other myelin genes and altered trafficking to the plasma membrane [27, 28]. Calnexin is the folding chaperone for PMP22 [29] and recently has also been identified to chaperone myelin oligodendrocyte glycoprotein (MOG) [30] and P0 [31]. In the absence of calnexin, P0 and PMP22 traffic to the plasma membrane but they are misfolded and non-functional as adhesive structural components of the myelin membrane [31]. While mechanisms of neuropathy associated with mutations of myelin proteins are not fully appreciated, disruption of normal axon-glia signaling is an integral part of the process. This work indicates that calnexin may also play an important role in the pathology of peripheral neuropathies and contribute to the diversity of these neurological disorders. Although calnexin is not a myelin protein, the protein is a critical regulator of myelin protein expression, folding and function. This study points at the emerging importance of the ER and ER associated proteins involved in the quality control of the secretory pathways as key upstream elements during the early stages of myelination, and as such, the ER and molecular chaperones such as calnexin may be contributors to a peripheral neuropathy such as CMT. Understanding the contribution of calnexin and ER-associated pathways in peripheral neuropathies may lay the groundwork for the design of therapeutic strategies to promote the function of myelinating glial cells.

References

1. Parlati, F., D. Dignard, J.J.M. Bergeron, and D.Y. Thomas, *The calnexin homologue cnx1+ in Schizosaccharomyces pombe, is an essential gene which can be complemented by its soluble ER domain*. EMBO J., 1995. **14**: p. 3064-3072.
2. Muller-Taubenberger, A., A.N. Lupas, H. Li, M. Ecke, E. Simmeth, and G. Gerisch, *Calreticulin and calnexin in the endoplasmic reticulum are important for phagocytosis*. EMBO J., 2001. **20**: p. 6772-6782.
3. Fajardo, M., M. Schleicher, A. Noegel, S. Bozzaro, S. Killinger, K. Heuner, J. Hacker, and M. Steinert, *Calnexin, calreticulin and cytoskeleton-associated proteins modulate uptake and growth of Legionella pneumophila in Dictyostelium discoideum*. Microbiology, 2004. **150**(Pt 9): p. 2825-2835.
4. Lee, W., K.R. Kim, G. Singaravelu, B.J. Park, D.H. Kim, J. Ahnn, and Y.J. Yoo, *Alternative chaperone machinery may compensate for calreticulin/calnexin deficiency in Caenorhabditis elegans*. Proteomics, 2006. **6**(4): p. 1329-1339.
5. Xu, K., N. Tavernarakis, and M. Driscoll, *Necrotic cell death in C. elegans requires the function of calreticulin and regulators of Ca²⁺ release from the endoplasmic reticulum*. Neuron, 2001. **31**: p. 957-971.
6. Mesaeli, N., K. Nakamura, E. Zvaritch, P. Dickie, E. Dziak, K.-H. Krause, M. Opas, D.H. MacLennan, and M. Michalak, *Calreticulin is essential for cardiac development*. J. Cell Biol., 1999. **144**: p. 857-868.
7. Martin, V., J. Groenendyk, S.S. Steiner, L. Guo, M. Dabrowska, J.M. Parker, W. Muller-Esterl, M. Opas, and M. Michalak, *Identification by mutational analysis of amino acid residues essential in the chaperone function of calreticulin*. J Biol Chem, 2006. **281**(4): p. 2338-2346.
8. Gosgnach, S., G.M. Lanuza, S.J. Butt, H. Saueressig, Y. Zhang, T. Velasquez, D. Riethmacher, E.M. Callaway, O. Kiehn, and M. Goulding, *V1 spinal neurons regulate the speed of vertebrate locomotor outputs*. Nature, 2006. **440**(7081): p. 215-219.
9. Toth, C., J.A. Martinez, W.Q. Liu, J. Diggle, G.F. Guo, N. Ramji, R. Mi, A. Hoke, and D.W. Zochodne, *Local erythropoietin signaling enhances regeneration in peripheral axons*. Neuroscience, 2008. **154**(2): p. 767-783.
10. Jantzie, L.L., P.Y. Cheung, and K.G. Todd, *Doxycycline reduces cleaved caspase-3 and microglial activation in an animal model of neonatal hypoxia-ischemia*. J Cereb Blood Flow Metab, 2005. **25**(3): p. 314-324.
11. Lozyk, M.D., S. Papp, X. Zhang, K. Nakamura, M. Michalak, and M. Opas, *Ultrastructural analysis of development of myocardium in calreticulin-deficient mice*. BMC Dev Biol, 2006. **6**: p. 54.

12. MacInnis, B.L. and R.B. Campenot, *Retrograde support of neuronal survival without retrograde transport of nerve growth factor*. *Science*, 2002. **295**(5559): p. 1536-1539.
13. Bradford, M.M., *A rapid and sensitive method for the quantitation of microgram quantities of protein utilizing the principle of protein-dye binding*. *Anal. Biochem.*, 1976. **72**: p. 248-254.
14. Leighton, P.A., K.J. Mitchell, L.V. Goodrich, X. Lu, K. Pinson, P. Scherz, W.C. Skarnes, and M. Tessier-Lavigne, *Defining brain wiring patterns and mechanisms through gene trapping in mice*. *Nature*, 2001. **410**(6825): p. 174-179.
15. Senger, D.L. and R.B. Campenot, *Rapid retrograde tyrosine phosphorylation of trkA and other proteins in rat sympathetic neurons in compartmented cultures*. *J. Cell Biol.*, 1997. **138**(2): p. 411-421.
16. Wearsch, P.A. and P. Cresswell, *The quality control of MHC class I peptide loading*. *Curr Opin Cell Biol*, 2008. **20**(6): p. 624-631.
17. Wiest, D.L., W.H. Burgess, D. McKean, K.P. Kearse, and A. Singer, *The molecular chaperone calnexin is expressed on the surface of immature thymocytes in association with clonotype-independent CD3 complexes*. *EMBO J.*, 1995. **14**: p. 3425-3433.
18. Bennett, M.J., J.E. Van Leeuwen, and K.P. Kearse, *Calnexin association is not sufficient to protect T cell receptor alpha proteins from rapid degradation in CD4+/CD8+ thymocytes*. *J. Biol. Chem.*, 1998. **273**: p. 23674-23680.
19. Majava, V., E. Polverini, A. Mazzini, R. Nanekar, W. Knoll, J. Peters, F. Natali, P. Baumgartel, I. Kursula, and P. Kursula, *Structural and functional characterization of human peripheral nervous system myelin protein P2*. *PLoS One*. **5**(4): p. e10300.
20. Denzel, A., M. Molinari, C. Trigueros, J.E. Martin, S. Velmurgan, S. Brown, G. Stamp, and M.J. Owen, *Early postnatal death and motor disorders in mice congenitally deficient in calnexin expression*. *Mol. Cell Biol.*, 2002. **22**(21): p. 7398-7404.
21. Kosmaoglou, M. and M.E. Cheetham, *Calnexin is not essential for mammalian rod opsin biogenesis*. *Mol Vis*, 2008. **14**: p. 2466-2474.
22. Coe, H., K. Bedard, J. Groenendyk, J. Jung, and M. Michalak, *Endoplasmic reticulum stress in the absence of calnexin*. *Cell Stress Chaperones*, 2008. **13**(4): p. 497-507.
23. Hebert, D.N. and M. Molinari, *In and out of the ER: protein folding, quality control, degradation, and related human diseases*. *Physiol. Rev.*, 2007. **87**(4): p. 1377-1408.
24. Fontanini, A., R. Chies, E.L. Snapp, M. Ferrarini, G.M. Fabrizi, and C. Brancolini, *Glycan-independent role of calnexin in the intracellular retention of Charcot-Marie-tooth 1A Gas3/PMP22 mutants*. *J Biol Chem*, 2005. **280**(3): p. 2378-2387.
25. Adlkofer, K., R. Martini, A. Aguzzi, J. Zielasek, K.V. Toyka, and U. Suter, *Hypermyelination and demyelinating peripheral neuropathy in Pmp22-deficient mice*. *Nat Genet*, 1995. **11**(3): p. 274-280.

26. Giese, K.P., R. Martini, G. Lemke, P. Soriano, and M. Schachner, *Mouse P0 gene disruption leads to hypomyelination, abnormal expression of recognition molecules, and degeneration of myelin and axons*. Cell, 1992. **71**(4): p. 565-576.
27. Wrabetz, L., M.L. Feltri, A. Quattrini, D. Imperiale, S. Previtali, M. D'Antonio, R. Martini, X. Yin, B.D. Trapp, L. Zhou, S.Y. Chiu, and A. Messing, *P(0) glycoprotein overexpression causes congenital hypomyelination of peripheral nerves*. J Cell Biol, 2000. **148**(5): p. 1021-1034.
28. Yin, X., G.J. Kidd, L. Wrabetz, M.L. Feltri, A. Messing, and B.D. Trapp, *Schwann cell myelination requires timely and precise targeting of P(0) protein*. J Cell Biol, 2000. **148**(5): p. 1009-1020.
29. Dickson, K.M., J.J. Bergeron, I. Shames, J. Colby, D.T. Nguyen, E. Chevet, D.Y. Thomas, and G.J. Snipes, *Association of calnexin with mutant peripheral myelin protein-22 ex vivo: a basis for "gain-of-function" ER diseases*. Proc Natl Acad Sci U S A, 2002. **99**(15): p. 9852-9857.
30. Jung, J. and M. Michalak, *Cell surface targeting of myelin oligodendrocyte glycoprotein (MOG) in the absence of endoplasmic reticulum molecular chaperones*. Biochim Biophys Acta, 2011. **1813**(5): p. 1105-1110.
31. Jung, J., H. Coe, and M. Michalak, *Specialization of endoplasmic reticulum chaperones for the folding and function of myelin glycoproteins P0 and PMP22*. Faseb J, 2011.

Structural Analysis of the Calnexin Cytoplasmic Tail

Introduction

Calnexin and calreticulin are highly similar molecular chaperones with one major difference being calreticulin is a luminal protein whereas calnexin has a transmembrane domain and cytoplasmic tail. The calnexin cytoplasmic tail provides a unique entity that allows calnexin to bridge two distinctive cellular environments, the ER lumen and the cytoplasm. While the structure of the calnexin N+P ER luminal domain has been solved [1], the structure of the C-tail has not been examined. Structural and biophysical information on the calnexin C-tail will provide clues as to the functional importance of the unique C-tail. To examine the biophysical and structural characteristics of the calnexin cytoplasmic tail, we employed analytical centrifugation, circular dichroism (CD), nuclear magnetic resonance (NMR), and biochemical techniques.

Materials and Methods

Expression and Purification of Recombinant Calnexin C-tail

cDNA encoding the C-tail of calnexin (amino acids 486-573) was generated by PCR-driven amplification of canine calnexin in a Bluescript plasmid. The following DNA primers were used: forward primer, 5'-CATGCCATGGCTGGAAAGAAACAGTCAAG -3', and reverse primer, 5'-GCTCTAGACACTCTCTTCGTGGCTTTC -3'. The cDNA product was cloned into the NcoI and XbaI sites of pBAD/gIII *E. coli* expression vector yielding a plasmid encoding the C-tail of calnexin and designated pBAD-Ctail. Top 10 *E. coli* transformed with calnexin native and mutant C-tail expression vectors were grown in TB medium containing 13.5 g bacto-tryptone, 26.5 g yeast, 60 mM glycerol per liter deionized water with 286.2 μ M ampicillin. Cultures were grown to the midlog phase followed by induction of recombinant protein expression with 0.02% L-arabinose induction for 4 hours. Cells were spun down at 6,000 xg for 15 min and the pellet re-suspended in lysis buffer containing 600 mM NaCl, 50 mM Tris, pH 8.0, 10% Glycerol, 0.1% Triton X-100 and lysed with a French Press set at 1000 p.s.i., followed by centrifugation at 12,000 xg for 10 min. His-tagged proteins were purified on a Ni²⁺-nitriloacetic acid-agarose affinity column. Lysates were mixed with Ni²⁺-nitriloacetic acid-agarose beads equilibrated in column buffer containing 600 mM NaCl, 50mM Tris, pH 8.0, 20 mM Imidazole and washed with wash buffer containing 50 mM Tris, 20 mM Imidazole pH 8.0, then eluted from the

beads with elution buffer containing 250 mM Imidazole, 50 mM Tris pH 8.0. Recombinant proteins were concentrated by a centrifugal filter (Biomax 30K NMWL membrane; Millipore), and proteins were dissolved in a buffer containing 10 mM Tris, pH 7.0, and 1 mM EDTA. For purification of ^{15}N labeled C-tail for NMR spectroscopy, the following modifications to the above protocol were made. *E. coli* culture (2 L) was spun at 6000 x g and the pellet re-suspended in 1 L minimal media containing 100 mM NaH_2PO_4 , 35 mM K_2HPO_4 pH 7.3 with 10 ml 1M MgSO_4 , 1.8 ml 1 mM FeSO_4 and incubated for 30 min. One gram of ^{15}N NH_4Cl dissolved in 4 ml of ddH₂O was added with induction of protein expression. Following purification on the Ni^{2+} -nitriloacetic acid-agarose affinity column as described above, samples were further purified on FPLC, followed by 10-50K MWCO size exclusion filters. Purified protein was solubilized in 10 mM ammonium bicarbonate. Recombinant human UBC9 encoded by the pET28b vector was expressed in BL21 *E. coli* cells and purified [2]. Protein concentrations were estimated using near UV absorbance (280 nm).

Sedimentation Equilibrium

Sedimentation equilibrium experiments were conducted at 22°C using a Beckman XL-I analytical ultracentrifuge using absorbance optics, as described by Laue and Stafford [3]. Aliquots (110 μl) of the sample solution were loaded into six sector CFE sample cells, allowing three concentrations to be tested simultaneously. Runs were performed at a minimum of three

different speeds and each speed was maintained until there was no significant difference in $r^2/2$ versus absorbance scans taken 2 h apart to ensure that equilibrium was achieved. Sedimentation equilibrium data were evaluated using the NONLIN program, which employs a nonlinear least squares curve-fitting algorithm [4]. The program allows for analysis of both single and multiple data files and can be fit to models containing up to four associating species, depending upon which parameters are permitted to vary during the fitting routine. The partial specific volume of the protein, the solvent density were estimated using the Sednterp program [5].

Circular Dichroism Spectroscopy

Spectra were recorded in a Jasco J720 spectropolarimeter in cells with a 0.05 cm pathlength. The measurements were collected at 25°C. The protein concentration was calculated by quantitative amino acid analysis for each independent protein preparation and protein in buffer containing 10 mM Tris pH 7.0, 1 mM EDTA was diluted with ddH₂O to the final concentration of 300 µg/mL. Data were converted to mean residue ellipticity using a mean residue weight of 116 calculated based on a predicted molecular weight of 13,158 of 113 amino acids for the canine C-tail His-myc construct.

Ruthenium Red

One or 10 µg purified protein samples were run on a 10% SDS-PAGE gel and transferred to a nitrocellulose membrane. The membranes were rinsed several times in rinse buffer containing 10 mM Tris-HCl pH 7.5 and then

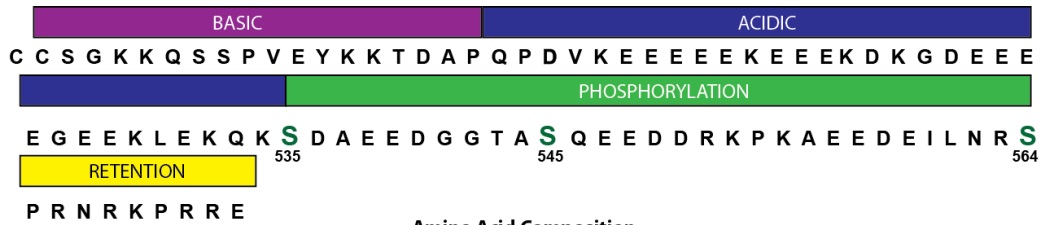
incubated with 100 mL Ruthenium Red (Sigma) stain containing 0.025 mg/mL (w/v) Ruthenium Red for 1 hour at room temperature. The blots were destained in rinse buffer.

NMR spectroscopy

The [¹⁵N] labelled C-tail and UBC9 samples were flash frozen with liquid nitrogen, lyophilised, and dissolved in the standard NMR buffer containing 100 mM KCl and 10 mM imidazole. Deuterated DSS (4,4-dimethyl-4-silapentane-1-sulfonic acid) was added for referencing. A 1D ¹H and 2D ¹H-¹⁵N HSQC NMR spectra was obtained for the C-tail alone. Unlabelled recombinant UBC9 (1.2 mg) was added to the C-tail and 2 µl of 1 M HCl was added to adjust the pH to 6.79 according to the chemical shift of the imidazole protons. A 1D ¹H and 2D ¹H-¹⁵N HSQC NMR spectra were acquired. Three µl of 1 M CaCl₂ was added to the NMR sample, to ensure that Ca²⁺ is not a requirement for binding. A 1D ¹H and 2D ¹H-¹⁵N HSQC NMR spectra were acquired. (NB. no EDTA was present in the sample at any time)

Results

The C-tail is a highly unusual sequence with a significant number of acidic residues and a correspondingly low theoretical isoelectric point of 4.57. The C-tail can be divided into 4 functional domains based on its amino acid sequence; a juxtamembrane basic region (lysine rich), an acidic region (glutamic acid rich), a phosphorylation domain, and a putative ER retrieval sequence [6]. Glutamic acid is the most frequent amino acid of the C-tail, making up 27% of the total amino acid composition. Aspartic acid makes up 10% whereas the basic amino acids arginine and lysine make up 6.7% and 15.6%, respectively. Two juxtamembrane cysteines are thought to be palmitoylated. Additionally, phosphorylation of Ser⁵³⁴, Ser⁵⁴⁴ and Ser⁵⁶³ has been shown to play a role in calnexin's chaperone function, C-tail/protein interactions and calnexin localization [7-9]. Calnexin can be cleaved under apoptotic conditions at a DEED caspase cleavage site at amino acid residue D⁵⁴⁸ and the overexpression of this cleavage product is found to partially inhibit apoptosis [10]. Interestingly, this cleavage site is conserved in mouse and rat calnexin C-tail, but not in dog and human (EEDD instead).



Amino Acid Composition		
Ala (A)	4	4.4%
Arg (R)	6	6.7%
Asn (N)	2	2.2%
Asp (D)	9	10.0%
Cys (C)	2	2.2%
Gln (Q)	4	4.4%
Glu (E)	24	26.7%
Gly (G)	5	5.6%
His (H)	0	0.0%
Ile (I)	1	1.1%
Leu (L)	2	2.2%
Lys (K)	14	15.6%
Met (M)	0	0.0%
Phe (F)	0	0.0%
Pro (P)	6	6.7%
Ser (S)	6	6.7%
Thr (T)	2	2.2%
Trp (W)	0	0.0%
Tyr (Y)	1	1.1%
Val (V)	2	2.2%

Figure 3.1. The calnexin C-tail is composed of multi-functional regions.

The canine C-tail is depicted above. The C-tail can be organized into 4 functional domains based on its amino acid sequence; a basic region (purple), an acidic region (blue), a phosphorylation domain (green), and a retention signal (yellow) (figure adapted from [6]). The phosphorylatable serines, Ser⁵³⁵, Ser⁵⁴⁵ and Ser⁵⁶⁴, are indicated in green. The table shows the amino acid composition of the C-tail in percentages of the entire C-tail sequence. The most frequently occurring amino acid is glutamic acid at 26.7% of total. Lysine and aspartic acid are the second and third most frequently occurring amino acids at 15.6% and 10.0%, respectively. Acidic residues (Asp and Glu) are shown in blue, basic residues (Lys and Arg) are shown in purple and Ser residue composition in green.

Calnexin C-tail Associates as a Homo-dimer

Canine calnexin C-tail was expressed and purified using the pBAD expression system and Ni²⁺ affinity chromatography. The purity of the C-tail samples was assessed using SDS-PAGE and Coomassie blue staining. When increasing amounts of C-tail were separated on a SDS-PAGE gel, two independent species were visible (Fig. 3.2). Calnexin C-tail has a predicted molecular weight of 13, 158 but the mobility on an SDS-PAGE gel is approximately 30-kDa. The second species visible on a gel had an apparent molecular weight of approximately 60-kDa. To confirm the identity of these species, western blotting with an antibody specific to the last 18 amino acids of the calnexin C-tail and mass spectrometry identification were used. Both the 30-kDa and 60-kDa species were recognized by the calnexin antibody and mass spectrometry confirmed that the identity of both species was calnexin C-tail. This implicates that purified calnexin C-tail can associate as a dimeric species, even in the presence of SDS.

We used analytical centrifugation to assess the nature of the C-tail homo-oligomeric association and to determine the predominant C-tail species (Figure 3.3). Sedimentation equilibrium is an analytical ultracentrifugation technique that can measure molecular mass and establish the monomeric/oligomeric state of the protein in solution. The centrifugal force produces a concentration gradient that at equilibrium is dependent only on the molecular mass and is independent of the shape of the molecule. Sedimentation-equilibrium data were obtained using a Beckman XL-I

analytical ultracentrifuge equipped with absorbance optics, monitoring the absorbance at 280 nm. The runs were carried out at speeds ranging from 2.4×10^4 rpm to 2.8×10^4 rpm and with loading protein concentrations in the range of 3.8 to 1.9 mg/ml. The combined data from 9 data sets were analyzed using the nonlinear least squares curve-fitting program, NONLIN. The data obtained for the calnexin cytoplasmic tail was best fit to a monomer-dimer model with a global molecular average of 19,595 Da, higher than the sequence molecular weight of 13, 158, and a calculated association constant (K_a) value of $1.853 \times 10^5 \text{M}^{-1}$. The molecular average indicates the predominant species of the C-tail is a dimer. The analytical centrifugation was conducted in buffer without Ca^{2+} and thus does not tell us the oligomeric structure of the C-tail in the presence of Ca^{2+} .

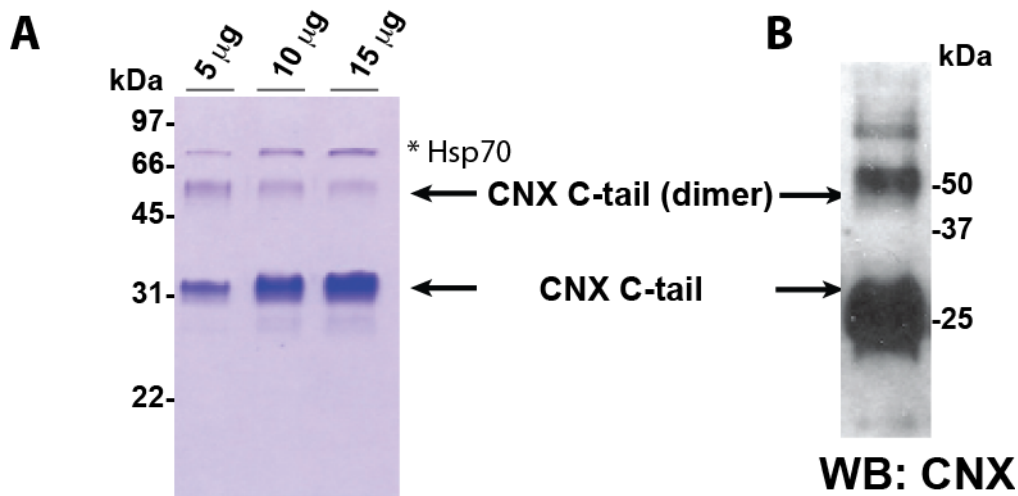


Figure 3.2. The purified calnexin C-tail migrates as two species according to molecular weight.

(A) Increasing amounts of purified calnexin C-tail (as indicated) were separated on an SDS-PAGE gel and stained with Coomassie to visualize the proteins. Two distinct species were visible, one at approximately 30-kDa and the other at 60-kDa, and both were identified as calnexin by mass spectrometry analysis. The upper protein band was identified as Hsp70, a contaminant in all protein purification preparations. (B) Western blot analysis using a anti-calnexin antibodies specific to the C-tail of calnexin recognized two independent molecular weight species, one at 30-kDa and one at 60-kDa, consistent with the Coomassie blue staining. Purified calnexin C-tail appears to self-associate, even in the presence of SDS.

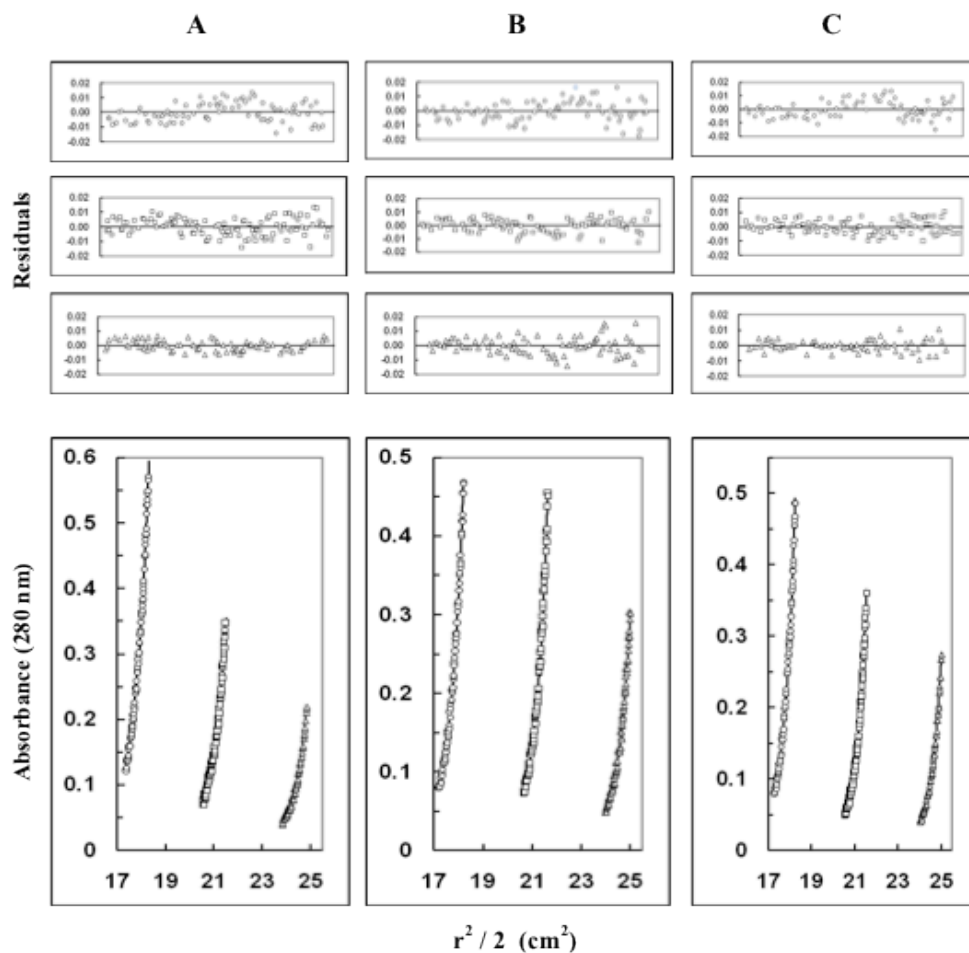


Figure 3.3. Sedimentation-equilibrium analysis of the calnexin cytoplasmic tail (CNXC).

CNXC was dissolved in 50 mM Tris (pH 7.0), 100 mM sodium chloride and centrifuged at 24000 (A), 26000 (B) and 28000 (C) rpm at 4°C. The protein concentration was 3.8 mg/mL (circles), 2.5 mg/mL (squares), or 1.9 mg/mL (triangles). The lower graphs illustrate plots of $r^2/2$ versus absorbance. The symbols represent measured data points, and solid lines represent best-fit curves to a monomer-dimer model. The upper graphs illustrate the residuals from the fitting. The random, nonsystematic distribution of the residuals indicates a good fit of the data to the models. Sedimentation equilibrium was carried out by Emmanuel Guigard and Cyril Kay.

Circular Dichroism Analysis of the C-tail

While the structure of the calnexin N+P ER luminal domain has been solved [1], the structural properties of the cytoplasmic domain have not been investigated. Purified C-tail protein was used for analysis by circular dichroism (CD) to determine its secondary structure. Due to the acidic nature of the C-tail, the protein concentration could not be accurately obtained using colorimetric protein assays. Instead, the concentration was determined using amino acid analysis and a concentration of 300 $\mu\text{g}/\text{mL}$ protein was used for each CD run. The CD spectra were obtained at 25°C and the mean residue ellipticity was evaluated between the wavelengths 190-250 nm. Different structural elements in a protein have characteristic CD spectra [11]. α -helical proteins have negative bands at 222 nm and 208 nm and a positive band at 193 nm. Proteins containing antiparallel β -pleated sheets have negative bands at 218 nm and positive bands at 195 nm. Disordered proteins have very low ellipticity at 210 nm and negative bands near 195 nm. Thus, the CD spectra of purified calnexin C-tail indicate it is a random coil in solution. It has been postulated that the C-tail can act as a Ca^{2+} oscillation sensor and Ca^{2+} binding could impact calnexin's known inhibitory association with SERCA [12]. Further, while there are no known Ca^{2+} binding domains (i.e. EF-hand) within the C-tail, its acidic sequence would support electrostatic interactions with Ca^{2+} . To investigate Ca^{2+} binding to the C-tail, CD spectra were obtained in the presence of 0.1 mM EGTA to sequester any Ca^{2+} from

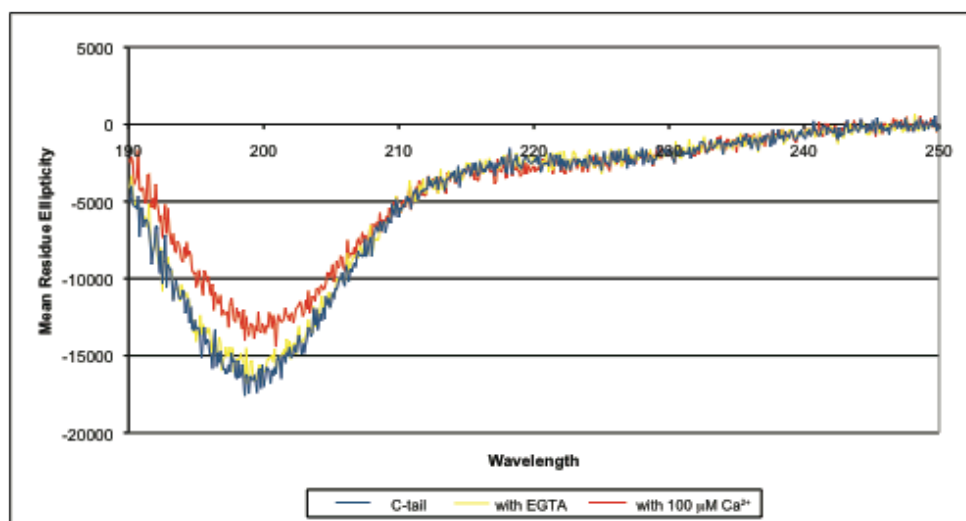


Figure 3.4. Circular dichroism analysis of the C-tail.

CD analysis of the purified C-tail indicates it is a random coil. The structure is unchanged in the presence of EGTA. In the presence of 100 μM Ca^{2+} , there is an increase in the mean residue ellipticity at 200 nm, indicating that Ca^{2+} binds and has some impact on C-tail structure in solution.

solution, and then in the presence of 100 μM excess Ca^{2+} . Ca^{2+} has some effect on the spectra of the C-tail and induces a shift corresponding to an increase in mean residue ellipticity at 200 nm. This indicates that Ca^{2+} does bind the C-tail and impacts on its structure.

Ruthenium Red Indicates the C-tail can Bind Ca^{2+}

We used Ruthenium Red stain to assess the ability of the C-tail to bind Ca^{2+} . Ruthenium Red is a polycationic stain that can be used to assess the Ca^{2+} -binding propensity of proteins [13]. It is known to bind to the Ca^{2+} -binding site of several Ca^{2+} sequestering proteins such as calmodulin and calsequestrin and this binding can be blocked by incubation with Ca^{2+} [13, 14]. Ruthenium Red inhibits Ca^{2+} -dependent processes including inhibition of Ca^{2+} -induced Ca^{2+} release from skeletal and cardiac muscle fibres and tissue-derived sarcoplasmic reticulum vesicles and can be used as a tool for analysis of Ca^{2+} -binding [15, 16]. We used a range of different purified proteins, some known to bind Ca^{2+} and some that don't bind Ca^{2+} for comparison. The luminal domain of Stim 1 (Stim 1A), calreticulin and the luminal domain of calnexin (CNX N+P) all bind Ca^{2+} as expected. Neither the RIKEN MGC32324 protein or ERp57 bind Ca^{2+} , providing a negative control. A cytoplasmic portion of Stim (Stim 1C) binds some Ca^{2+} . The calnexin C-tail binds modest amounts of Ca^{2+} , less than known Ca^{2+} -buffering protein calreticulin and the luminal domain of Stim (Stim1A), a Ca^{2+} sensor. It also appears to bind less Ca^{2+} than the luminal domain of calnexin. This is in

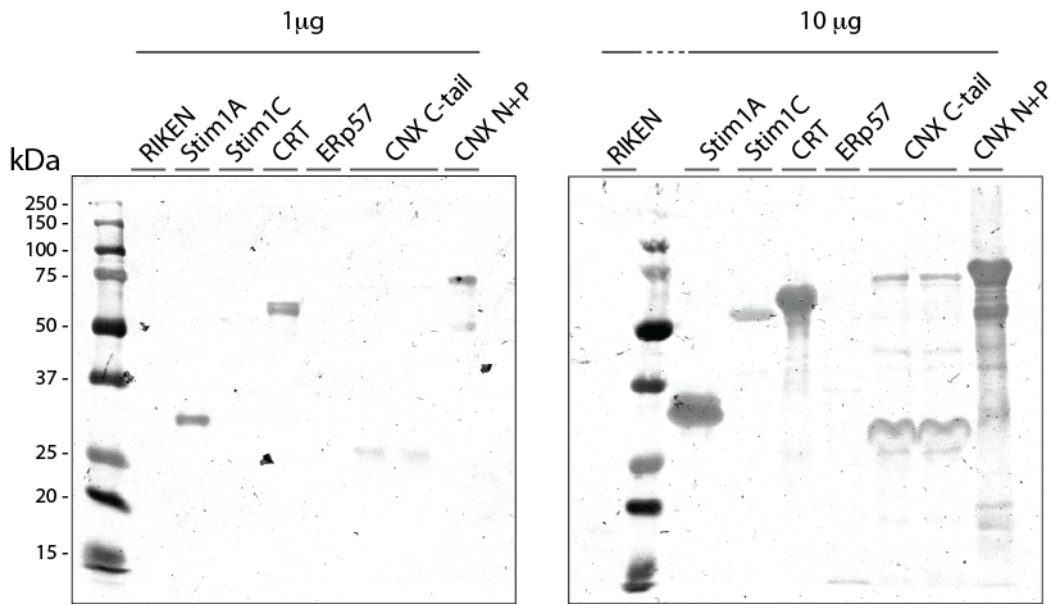


Figure 3.5. Ruthenium Red stain indicates the C-tail can bind Ca^{2+} .

One or 10 μg of select purified proteins were run on an SDS-PAGE gel, transferred to a nitrocellulose membrane and stained with Ruthenium Red. Positive staining indicates the propensity to bind Ca^{2+} . The RIKEN MGC32324 protein and ERp57 do not bind Ca^{2+} and provide a negative control. Stim1A (ER luminal domain), CRT, and the luminal domain of CNX bind Ca^{2+} as previously reported. The C-tail binds less Ca^{2+} than CRT, Stim1A or CNX N+P but more Ca^{2+} than ERp57 and the RIKEN protein. CRT, calreticulin, CNX, calnexin, Stim 1A, ER luminal domain of Stim, Stim 1C, cytoplasmic portion of Stim, RIKEN MGC32324, unknown protein that binds CNX C-tail.

agreement with earlier studies on Ca^{2+} binding to the C-tail using *E. coli* expressed GST fusion calnexin fragments. [17].

NMR Spectroscopy of the C-tail in Apo and Ca^{2+} -bound States

We used NMR spectroscopy techniques to confirm the structure and Ca^{2+} binding characteristics of the calnexin C-tail. NMR spectroscopy of the ^{15}N calnexin C-tail indicates an absence of nascent structure. A 1D ^1H NMR spectrum was acquired for unlabelled C-tail in the apo and Ca^{2+} saturated states. The low chemical shift dispersion observed for both the amide and aliphatic regions, combined with the few number of NOE cross-peaks observable supports that the C-tail is mostly unfolded. Comparison of these spectra indicates that while the aliphatic region is unchanged with Ca^{2+} saturation, there are small changes in the aromatic region of the 1D ^1H NMR spectra between the apo and Ca^{2+} saturated C-tail. A 2D ^1H - ^{15}N HSQC NMR spectra of the C-tail of calnexin in the apo and Ca^{2+} saturated state was obtained (Figure 3.6). Small chemical shifts were visible with addition of 6mM Ca^{2+} indicating that the C-tail can bind Ca^{2+} . This is consistent with the CD analysis and Ruthenium Red stain.

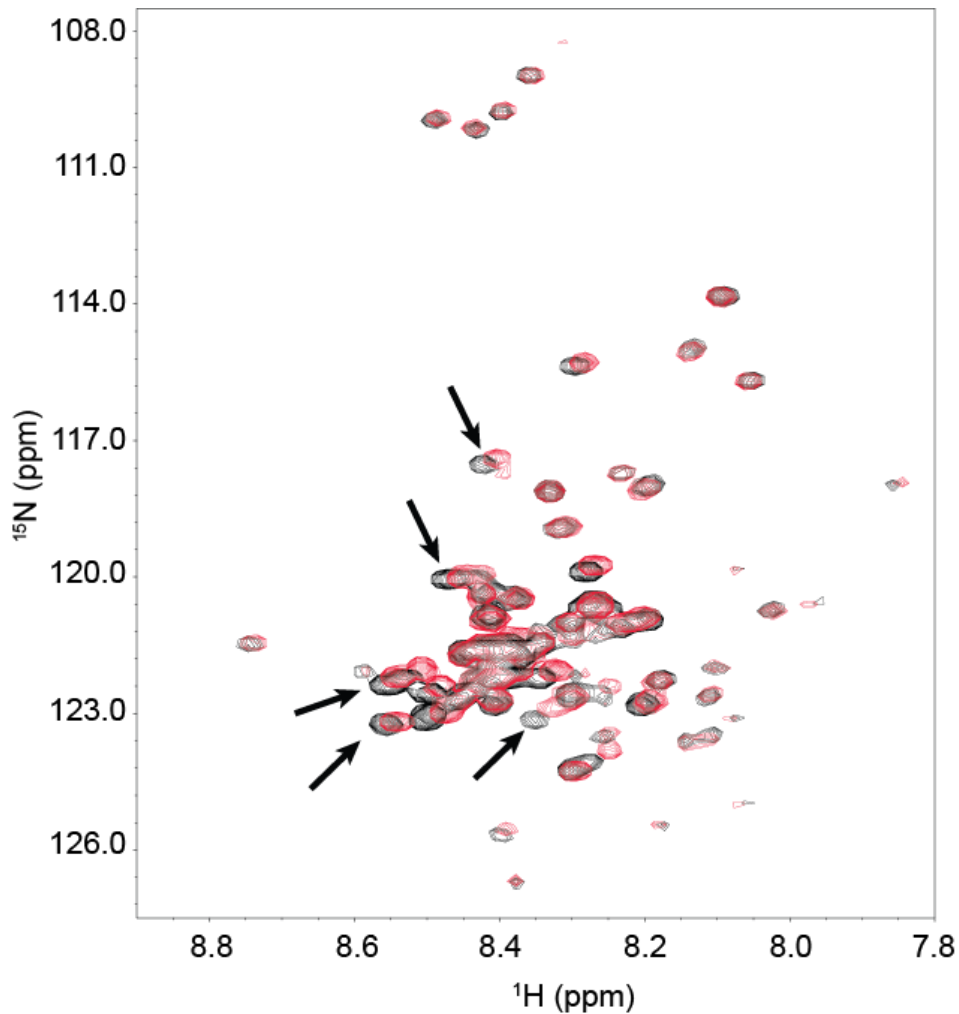


Figure 3.6. NMR spectroscopy of ^{15}N C-tail indicates Ca^{2+} binding

2D ^1H - ^{15}N HSQC NMR spectra of the C-tail of calnexin in the **apo** (black) and **Ca^{2+}** (red) states. Small chemical shift changes were observed after addition of 6 mM CaCl_2 . The C-tail lacks nascent structure and the small chemical shifts with the addition of Ca^{2+} suggest Ca^{2+} binding. NMR spectroscopy was conducted by Olivier Julien and Brian Sykes.

Discussion

This work identifies the C-tail lacks nascent structure as assessed by CD and NMR spectroscopy. It can homo-dimerize as indicated by SDS-PAGE and sedimentation equilibrium analysis. Further, Ruthenium Red stain, CD analysis and NMR spectroscopy demonstrate the C-tail binds Ca^{2+} .

When purified calnexin C-tail is run on an SDS-PAGE gel, two different molecular weight species were visible with Coomassie stain. Both of these species were identified by mass spectrometry as calnexin and this was supported by Western blot data with a calnexin C-tail antibody. Analytical centrifugation confirmed that the purified C-tail associated in a dimer-monomer equilibrium. A limitation of the biophysical studies carried out here is they were conducted with the soluble cytoplasmic calnexin domain that could display different properties when it is membrane-anchored. For example, the acidic and basic regions of a soluble C-tail (Figure 3.1) could electrostatically interact in reverse orientation end to end with another monomer to form the soluble C-tail dimer. Membrane-anchored C-tail might instead form a loop where the acidic region loops back on the juxtamembrane basic region of a monomeric calnexin. While the relevance of C-tail dimerization *in vitro* remains to be tested *in vivo*, C-tail self-association could have intriguing implications for calnexin *in vivo*. Self-association of the calnexin C-tail could result in the nucleation of interacting proteins and their relevant activity. C-tail-C-tail interactions could help one calnexin recruit another to the ribosomal docking sites and the translocon to aid with protein

folding. Conversely, self-association of the C-tail could block sites for interaction with other proteins. Further studies will reveal if C-tail self-association has a functional role *in vivo* and if this association is impacted by post-translational modification of the C-tail.

Both CD and NMR spectroscopy indicate purified C-tail lacks intrinsic structure. This might be expected from the highly acidic amino acid composition as extensive folding of such a highly charged entity would be electrostatically unfavourable. Lack of intrinsic structure of the C-tail has interesting implications for protein-protein interactions and post-translational modifications. An unstructured C-tail would provide a molecular plasticity that could be modified depending on the protein binding partners and type of post-translational modification. Unstructured protein regions will have a lower entropy cost of binding due to a greater number of accessible conformations achievable to locate and bind specific residues [18]. Flexible protein tails are often seen in DNA binding proteins and bind to the DNA by a mechanism known as “fly-casting”. The fly-casting mechanism involves the unfolded protein binding weakly to the substrate from a distance, followed by folding as the protein approaches the binding site [18]. While we do not know if the C-tail attains any structure when bound to other proteins, its lack of nascent structure in solution identifies it as a dynamic and malleable entity that would have a great capacity to participate in protein-protein interactions.

Considering the highly acidic nature of the tail, it is not surprising that it binds cationic Ca^{2+} . The tail does not appear to attain definitive structure in the Ca^{2+} -saturated state and instead Ca^{2+} -binding induces small chemical shifts in the C-tail as assessed by NMR spectroscopy. Ca^{2+} binding to the C-tail was originally postulated in a series of biochemical experiments with recombinant calnexin fragments [17]. Since then, it has been postulated that the C-tail acts as a sensor for cytosolic Ca^{2+} oscillations [12]. The phosphorylation state of the calnexin C-tail is regulated through calcineurin in a Ca^{2+} -dependent manner in order to regulate the interaction of calnexin with SERCA [19]. Ca^{2+} binding to the C-tail could modulate protein-protein interactions with the apo and Ca^{2+} bound states having different substrate specificities. Cytosolic Ca^{2+} and Ca^{2+} -binding to the C-tail could have direct effects on protein-protein interactions through electrostatic effects, or indirectly, such as when we consider SERCA and the Ca^{2+} -dependent phosphorylation status of the C-tail. Together, these studies provide insights into the biophysical properties of the C-tail that could have important implications for calnexin function.

References

1. Schrag, J.D., J.J. Bergeron, Y. Li, S. Borisova, M. Hahn, D.Y. Thomas, and M. Cygler, *The Structure of calnexin, an ER chaperone involved in quality control of protein folding*. Mol Cell, 2001. **8**(3): p. 633-644.
2. Yunus, A.A. and C.D. Lima, *Purification and activity assays for Ubc9, the ubiquitin-conjugating enzyme for the small ubiquitin-like modifier SUMO*. Methods Enzymol, 2005. **398**: p. 74-87.
3. Laue, T.M. and W.F. Stafford, 3rd, *Modern applications of analytical ultracentrifugation*. Annu Rev Biophys Biomol Struct, 1999. **28**: p. 75-100.
4. Johnson, M.L., J.J. Correia, D.A. Yphantis, and H.R. Halvorson, *Analysis of data from the analytical ultracentrifuge by nonlinear least-squares techniques*. Biophys J, 1981. **36**(3): p. 575-588.
5. Laue, T.M., Shah, B.D., Ridgeway, T.M. and Pelletier, S.L., *Computer-aided interpretation of sedimentation data for proteins*, in *Analytical Ultracentrifugation in Biochemistry and Polymer Science*, A.J.R. S.E. Harding, J.C. Horton, Editor. 1992, Royal Society of Chemistry: Cambridge, UK. p. pp. 90-125.
6. Chevet, E., J. Smirle, P.H. Cameron, D.Y. Thomas, and J.J. Bergeron, *Calnexin phosphorylation: Linking cytoplasmic signalling to endoplasmic reticulum lumenal functions*. Semin Cell Dev Biol.
7. Cameron, P.H., E. Chevet, O. Pluquet, D.Y. Thomas, and J.J. Bergeron, *Calnexin phosphorylation attenuates the release of partially misfolded alpha1-antitrypsin to the secretory pathway*. J Biol Chem, 2009. **284**(50): p. 34570-34579.
8. Chevet, E., H.N. Wong, D. Gerber, C. Cochet, A. Fazel, P.H. Cameron, J.N. Gushue, D.Y. Thomas, and J.J. Bergeron, *Phosphorylation by CK2 and MAPK enhances calnexin association with ribosomes*. EMBO J, 1999. **18**(13): p. 3655-3666.
9. Myhill, N., E.M. Lynes, J.A. Nanji, A.D. Blagoveshchenskaya, H. Fei, K. Carmine Simmen, T.J. Cooper, G. Thomas, and T. Simmen, *The subcellular distribution of calnexin is mediated by PACS-2*. Molecular Biol. Cell, 2008. **19**(7): p. 2777-2788.
10. Takizawa, T., C. Tatematsu, K. Watanabe, K. Kato, and Y. Nakanishi, *Cleavage of calnexin caused by apoptotic stimuli: implication for the regulation of apoptosis*. J Biochem, 2004. **136**(3): p. 399-405.
11. Greenfield, N.J., *Using circular dichroism spectra to estimate protein secondary structure*. Nat Protoc, 2006. **1**(6): p. 2876-2890.
12. Roderick, H.L., J.D. Lechleiter, and P. Camacho, *Cytosolic phosphorylation of calnexin controls intracellular Ca(2+) oscillations via an interaction with SERCA2b*. J Cell Biol, 2000. **149**(6): p. 1235-1248.

13. Charuk, J.H., C.A. Pirraglia, and R.A.F. Reithmeier, *Interaction of ruthenium red with Ca²⁺-binding proteins*. Anal. Biochem., 1990. **188**: p. 123-131.
14. Sasaki, T., M. Naka, F. Nakamura, and T. Tanaka, *Ruthenium red inhibits the binding of calcium to calmodulin required for enzyme activation*. J Biol Chem, 1992. **267**(30): p. 21518-21523.
15. Chamberlain, B.K., P. Volpe, and S. Fleischer, *Inhibition of calcium-induced calcium release from purified cardiac sarcoplasmic reticulum vesicles*. J Biol Chem, 1984. **259**(12): p. 7547-7553.
16. Volpe, P., G. Salviati, and A. Chu, *Calcium-gated calcium channels in sarcoplasmic reticulum of rabbit skinned skeletal muscle fibers*. J Gen Physiol, 1986. **87**(2): p. 289-303.
17. Tjoelker, L.W., C.E. Seyfried, R.L. Eddy, Jr., M.G. Byers, T.B. Shows, J. Calderon, and P.W. Gray, *Human, mouse, and rat calnexin cDNA cloning: identification of potential calcium binding motifs and gene localization to human chromosome 5*. Biochemistry, 1994. **33**: p. 3229-3236.
18. Shoemaker, B.A., J.J. Portman, and P.G. Wolynes, *Speeding molecular recognition by using the folding funnel: the fly-casting mechanism*. Proc Natl Acad Sci U S A, 2000. **97**(16): p. 8868-8873.
19. Bollo, M., R.M. Paredes, D. Holstein, N. Zheleznova, P. Camacho, and J.D. Lechleiter, *Calcineurin interacts with PERK and dephosphorylates calnexin to relieve ER stress in mammals and frogs*. PLoS One. 5(8): p. e11925.

CHAPTER FOUR

Calnexin forms Complexes with Components of the SUMOylation Machinery and is SUMOylated *in vivo*

Introduction

Calnexin and calreticulin share a functionally and structurally similar N+P-domain in the lumen of the ER, responsible for binding nascent polypeptides. However, calreticulin is a luminal protein whereas calnexin is a type I transmembrane protein that spans the ER membrane and cytoplasmic compartments with approximately 15% of the protein residing in the cytoplasm. The cytoplasmic tail (C-tail) of calnexin is a highly acidic, highly conserved entity in mammalian species (85% amino acid identity with 40% conservation of the non-identical amino acid residues in dog, mouse, rat and human calnexin). The functional role of the calnexin C-tail has only been addressed in a limited number of studies. One study proposed that the transmembrane domain and C-tail of calnexin may play a role in substrate folding [1]. Additionally, the transmembrane domain and C-tail have an effect on specificity for folding substrates, determined when a soluble calnexin molecule lacking the transmembrane domain and cytoplasmic tail failed to interact with the folding substrates lymphocyte tyrosine kinase (Ltk), IgM heavy chains and MHC I heavy chain protein [2]. The C-tail is also known to be modified by distinct post-translational modifications and to participate in protein-protein interactions including an interaction with select ribosomal proteins [3]. The C-tail has been postulated to affect Ca^{2+} oscillations through phosphorylation-dependent interactions with SERCA [4] and phosphorylation of the C-tail has also been shown to affect protein interactions such as the interaction with ribosomal proteins as well as the

secretion of a known calnexin substrate [3-5]. Many of the studies on the calnexin C-tail are recent and very little was known about the functional contributions of the C-tail at the beginning of my thesis work. The C-tail contains two juxtamembrane cysteines, predicted as an S-palmitoylation site in a large scale profile of protein palmitoylation [6]. As well, the C-tail contains a DXXD caspase target site that is cleaved following apoptotic stimuli [7]. Together, these post-translational modifications highlight the cytoplasmic tail as a modifiable signaling entity that impacts on calnexin function.

SUMOylation is a post-translational modification that ultimately alters protein-protein interactions, protein activity, stability or localization. The SUMOylation machinery consists of the heterodimer SAE1/SAE2 E1 activating enzyme and the SUMO-conjugating enzyme, the E2 ligase UBC9 [8]. In contrast to the over 600 known ubiquitin E3 ligases [9], only a limited number of SUMO E3 ligases have been identified. For SUMO modification of proteins a di-glycine motif must be exposed allowing the conjugation of SUMO to lysine residues within the consensus motif ψ KxE (where ψ is a large hydrophobic residue) [10, 11]. SUMO conjugation has diverse consequences depending on the target substrate and cellular location of modification as well as the conditions under which SUMOylation takes place [12].

Here we examined protein partners of the calnexin C-tail by using yeast-2-hybrid system with the C-tail as bait. We identified several C-tail

interacting proteins including UBC9, the SUMOylation E2 ligase. Using several biochemical, cell biological and biophysical techniques we showed that UBC9 interacts with C-tail of calnexin. Importantly, the calnexin cytoplasmic domain can be SUMOylated *in vitro* and *in vivo* in mammalian systems. To our knowledge, this is the first report of a SUMO modified ER resident chaperone. Via interaction with the calnexin C-tail, UBC9 might be sequestered at the ER membrane and it might assist in SUMOylation of intracellular substrates. This study investigates the nature of the C-tail/UBC9 interaction and UBC9's association with ER membranes.

Material and Methods

Yeast-2-Hybrid

The mouse brain Matchmaker cDNA library in pACT2 (Clontech, 638841) was transformed into yeast strain AH109. The library was screened for interacting proteins with the C-terminal cytoplasmic region of calnexin (C-tail) corresponding to the last 88 amino acids (C⁴⁸⁴-E⁵⁷¹) (Fig. 1A). cDNA encoding the C-tail of calnexin was obtained by PCR amplification of a mouse calnexin template cDNA using the following primers: the 5' forward primer 5'-GGA ATT CCA TAT GTG TTC TGG AAA GAA AC-3' and the 3' reverse primer 5'-AAG GTT CTG CAG TCA CTC TCT TCG TGG CT-3'. The PCR product was cloned in frame with the GAL4 DNA-binding domain at *NdeI* and *PstI* restriction sites to generate the clone pGBKT7-CNX-C. Screening of the mouse library was carried out as recommended by the manufacturer (Clontech). The C-tail (C⁴⁸⁶-E⁵⁷³) from a canine calnexin template was also used as bait to screen a human leukemia (Jurkat T cell) Matchmaker cDNA library (Clontech). Plasmid DNA from positive clones was isolated and used as a template for amplification of the insert in the library vector by the AD (activating domain) sequencing primer and the T7 yeast-2-hybrid sequencing primer.

Expression and Purification of Recombinant Calnexin Domains, UBC9 and *in vitro* SUMOylation

cDNA encoding the C-tail of calnexin (amino acids 486-573) was generated by PCR-driven amplification of a canine calnexin in a Bluescript plasmid DNA construct. The following DNA primers were used: forward primer, 5'- CAT GCC ATG GCT GGA AAG AAA CAG TCAAG -3', and reverse primer, 5'- GCT CTA GAC ACT CTC TTC GTG GCT TTC -3'. The cDNA product was cloned into the NcoI and XbaI sites of pBAD/gIII *E. coli* expression vector yielding a plasmid encoding the C-tail of calnexin and designated pBAD-Ctail. C-tail. Top 10 F' *E. coli* transformed with calnexin native and mutant C-tail expression vectors were grown in TB medium containing 13.5 g bacto-tryptone, 26.5 g yeast, 60 mM glycerol per liter deionized water with 286.2 μ M ampicillin. Cultures were grown to the midlog phase followed by induction of recombinant protein expression with 0.02% L-arabinose induction for 4 hours. Cells were spun down at 6,000 xg for 15 min and the pellet re-suspended in lysis buffer containing 600 mM NaCl, 50 mM Tris, pH 8.0, 10% Glycerol, 0.1% Triton X-100 and lysed with a French Press set at 1000 p.s.i., followed by centrifugation at 12,000 x g for 10 min. His-tagged proteins were purified on a Ni²⁺-nitriloacetic acid-agarose affinity column. Lysates were mixed with Ni²⁺-nitriloacetic acid-agarose beads equilibrated in column buffer containing 600 mM NaCl, 50 mM Tris, pH 8.0, 20 mM Imidazole and washed with wash buffer containing 50 mM Tris, 20mM Imidazole pH 8.0, then eluted from the beads with elution buffer containing 250 mM Imidazole, 50 mM Tris pH 8.0.

Recombinant proteins were concentrated by a centrifugal filter (Biomax 30K NMWL membrane; Millipore), and proteins were dissolved in a buffer containing 10 mM Tris, pH 7.0, and 1 mM EDTA. For purification of ^{15}N labeled C-tail for NMR spectroscopy, the following modifications to the above protocol were made. *E. coli* culture (2 L) was spun at 6000 $\times g$ and the pellet re-suspended in 1 L minimal media containing 100 mM NaH_2PO_4 , 35 mM K_2HPO_4 pH 7.3 with 10 ml 1M MgSO_4 , 1.8 ml 1 mM FeSO_4 and incubated for 30 min. One gram of ^{15}N NH_4Cl dissolved in 4 ml of dd H_2O was added with induction of protein expression. Samples were further purified on FPLC, followed by 10-50K MWCO size exclusion filters. Purified protein was solubilized in 10 mM ammonium bicarbonate. Recombinant human UBC9 encoded by the pET28b vector was expressed in BL21 *E. coli* cells and purified [13]. Protein concentrations were estimated using near UV absorbance (280 nm).

Plasmids and Mutagenesis

GFP-SUMO-1 expression vector was a kind gift from Gianni Del Sal, Consortium for Biotechnology National Laboratory, Trieste, Italy. Human UBC9 expression plasmid was a kind gift from Christopher D. Lima, Sloan-Kettering Institute, New York, NY [13]. cDNA encoding canine calnexin C-tail (amino acid residues 486-573) (see above) was used with QuikChange Site-Directed Mutagenesis (Stratagene) to mutate lysine 506 to an alanine residue (primers; 5'-CCT CAG CCA GAT GTG GCG GAG GAG GAA GAA GAA AAG G-3' and 5'- CCT TTT CTT CTT CCT CCT CCG CCA CAT CTG GCT GAG G-3').

Mutations were confirmed with DNA sequencing. Purified C-tail protein and the C-tail SUMOylation mutant were used with an *in vitro* sumoylation kit (Vaxron) as per the manufacturer's protocol.

NMR Spectroscopy

The [¹⁵N] labelled C-tail and UBC9 samples were flash frozen with liquid nitrogen, lyophilised, and dissolved in the standard NMR buffer containing 100 mM KCl and 10 mM imidazole. Deuterated DSS (4,4-dimethyl-4-silapentane-1-sulfonic acid) was added for referencing. A 1D ¹H and 2D ¹H-¹⁵N HSQC NMR spectra was obtained for the C-tail alone. Unlabelled recombinant UBC9 (1.2 mg) was added to the C-tail and 2 µl of 1 M HCl was added to adjust the pH to 6.79 according to the chemical shift of the imidazole protons. A 1D ¹H and 2D ¹H-¹⁵N HSQC NMR spectra were acquired. Three µl of 1 M CaCl₂ was added to the NMR sample, to ensure that Ca²⁺ is not a requirement for binding. A 1D ¹H and 2D ¹H-¹⁵N HSQC NMR spectra were acquired. (NB. no EDTA was present in the sample at any time)

Cell Lines, Cell Culture, Transfection and RNAi

Mouse fibroblasts were derived from day 7 wild-type and calnexin-deficient mice and were immortalized as described previously [14]. *Sumo-1*^{-/-} mouse embryonic fibroblasts (MEFs) were a kind gift from Olli A. Jänne, University of Helsinki, Finland [15]. Cells were maintained in Dulbecco's Modified Eagle's Medium (Sigma) supplemented with 10% fetal bovine serum (Sigma) and 1% penicillin/streptomycin (Gibco) at 37°C with 5% CO₂. The Neon

Transfection System (Invitrogen) was used for electroporation of cells as per the manufacturer's protocol with the following settings: *wt* and *cnx*^{-/-} mouse fibroblasts were electroporated with a pulse voltage of 1500v, a pulse width of 20 ms and a pulse number of 1, HeLa cells were electroporated with a pulse voltage of 1005v, a pulse width of 35 ms and a pulse number of 2 and NIH 3T3 cells were electroporated with a pulse voltage of 1200V, a pulse width of 20, and a pulse number of 3. For RNAi experiments UBC9 sense and antisense strands were derived from a NIH 3T3 cDNA library and cloned into XhoI and HindIII sites of pcDNA 3.1 vector using the following primers (XhoI 5'-ATG CCT CGA GAT GTC GGG GAT C-3'; HindIII 5'-ATG CAA GCC TTT ATG AGG GGG C-3'). The plasmids encoding UBC9 sense and anti-sense were transfected into NIH 3T3 cells using the Neon electroporation system (Invitrogen) as per the manufacturer's protocol.

Isolation of Microsomal Membranes

Microsomes were isolated from HeLa cells grown to 80-90% confluency. A protease inhibitor cocktail (0.5 mM PMSF, 0.5 mM benzamidine, 0.05 µg/ml aproprotin, 0.025 µg/ml phosphormidone, 0.05 µg/ml TLCK, 0.05 µg/ml APMSF, 0.05 µg/ml E-64, 0.025 µg/ml leupeptin and 0.01 µg/ml pepstatin) [16]) and de-sumoylation inhibitor cocktail [800 µM N-ethyl maleimide (NEM) and 200 µM iodoacetamide (IAA)] were included in all buffers. Cells were harvested, spun at 1000 xg for 3 min at 4°C, re-suspended in 20 ml PBS followed by transfer to low ionic strength (LIS) Buffer containing 10 mM

Tris-HCl, pH 7.5, 0.5 mM MgCl₂ for 10 min. Cells were homogenized with a Dounce homogenizer in a buffer containing 0.5 M Sucrose, 10 mM Tris-HCl, pH 7.5, 40 μM CaCl₂, 300 mM KCl, 6.3 mM β-mercaptoethanol. The solution was spun at 8000 xg, the supernatant layered onto 1/5 volume of 2.5 M KCl, mixed and centrifuged at 120,000 xg for 1 hour at 4°C. The pellet containing the microsomal fraction was washed and re-suspended in a buffer containing 5 mM Tris-HCl, pH 7.5, 20 μM CaCl₂, and 150 mM KCl.

Immunoprecipitation and Western Blot Analysis

Mouse fibroblast or HeLa cells, at 80% confluency, were lysed in a buffer containing 10 mM Tris, pH 8.0, 150 mM NaCl, 1% NP40, 1 mM EDTA pH 8.0, 10% glycerol, with the protease/deSUMOylation inhibitor cocktail or in RIPA buffer containing 50 mM Tris, pH, 7.0, 150 mM NaCl, 1 mM EGTA, 1 mM EDTA, 1% Triton X-100, 0.1% SDS, 0.5% sodium deoxycholate with the protease/deSUMOylation inhibitor cocktail. After 30 min incubation on ice, the lysed cells were spun at 15,000 xg for 15 min. at 4°C. The supernatant was pre-cleared with Protein A or a 50% Protein A/Protein G (for anti-GFP antibodies) bead slurry for 1 hour at 4°C with rotation after which the primary antibodies were added to the supernatant for overnight incubation at 4°C with rotation. Protein A or a 50% Protein A/Protein G bead slurry was added for 4-5 hours at 4°C with rotation. The beads were spun down, washed 5 times with lysis buffer, and re-suspended in SDS-PAGE sample buffer containing 10% glycerol, 1% β-mercaptoethanol, 2% SDS, 0.065 M Tris, pH

6.8, 0.01 w/v bromophenol blue for analysis. Proteins were separated on 6% - 10% acrylamide SDS-PAGE gels and transferred onto nitrocellulose for subsequent Western blotting. Two polyclonal rabbit anti-calnexin antibodies were used: SPA-860 (Enzo Life Sciences) raised against a synthetic peptide corresponding to the C-terminus of calnexin (amino acid residues 575–593) and SPA-865 (Enzo Life Sciences) raised against a synthetic peptide near the N terminus. Antibodies were used at 1:1000 and 1:500 dilutions, respectively. Other antibodies used included anti-UBC9 (Abgent), 1:200 dilution, anti-SUMO-1 (Sigma), 1:200 dilution, anti-GFP (Abcam), 1:10,000 dilution, and anti-GAPDH (Abcam), 1:1000 dilution. Any re-probed immunoblots were first stripped with a stripping buffer containing 1% SDS, 100 mM β -mercaptoethanol, and 50 mM Tris-HCl, pH 6.8, and washed several times with PBS before incubation with a primary antibody.

Cellular Fractionation

Fractionation protocols were carried out using the Opti-prep (Sigma) system. Wild-type or *cnx*^{-/-} mouse fibroblasts were washed twice with PBS, then re-suspended in homogenization buffer containing 10 mM HEPES, pH 7.4, 250 mM sucrose, 1 mM EDTA, 1 mM EGTA with the protease inhibitor cocktail. Cells were lysed *via* 25 passes through an 18 micron clearance ball bearing homogenizer (Isobiotec), and then centrifuged at 800 x g for 10 minutes at 4°C to remove nuclei and cellular debris. The homogenate supernatant was layered onto an eight-step gradient of 25%, 22%, 19%, 16%, 13%, 10%, 7%, and 4% (% iodoxanol) dilutions of Opti-prep in homogenization buffer. The

gradient was centrifuged in a Beckman Sw50.1 rotor for 3 hours at 4°C at 150,000 xg. Twelve fractions were harvested from the top of the gradient, followed by acetone precipitation of proteins. Acetone precipitated protein fractions were washed in 100% EtOH, re-suspended in SDS-PAGE sample buffer followed by SDS-PAGE and Western blot analysis.

Miscellaneous

Unless otherwise stated, protein concentration was estimated using a BioRad DC Protein assay [17].

Results

Components of the SUMOylation Machinery Interact with the Calnexin C-tail

The major structural difference between the quality control chaperones calreticulin and calnexin is the presence of calnexin's transmembrane domain and cytoplasmic tail (C-tail) (Figure 4.1). To date, only limited studies have addressed the function of the calnexin C-tail. To gain insight into function of calnexin cytoplasmic domain (C-tail) we used yeast-2-hybrid techniques to identify proteins that interact with the C-tail domain of calnexin. Screening a mouse brain cDNA library with the 88 amino acid *mus musculus* calnexin C-tail (C⁴⁸⁴-E⁵⁷¹) as bait identified 9 positive clones. One of these clones encoded UBC9, an E2 SUMOylation ligase. A second independent yeast-2-hybrid screen of a human T cell leukemia (JURKAT) library with calnexin C-tail (C⁴⁸⁶-E⁵⁷³) as bait identified 10 putative clones, including UBC9. To confirm the UBC9/C-tail interaction identified from the yeast-2-hybrid screens and to investigate if endogenous UBC9 interacts with calnexin *in vivo*, we used immunoprecipitation techniques. Wild-type and calnexin-deficient (negative control) cells were used for immunoprecipitation with anti-calnexin antibodies followed by Western blot analysis with anti-calnexin and anti-UBC9 antibodies (Figure 4.2). As expected, calnexin could be efficiently immunoprecipitated from wild-type cells but not from calnexin-deficient cells (Figure 4.2). Most importantly, Western blotting techniques with antibodies against both calnexin and UBC9

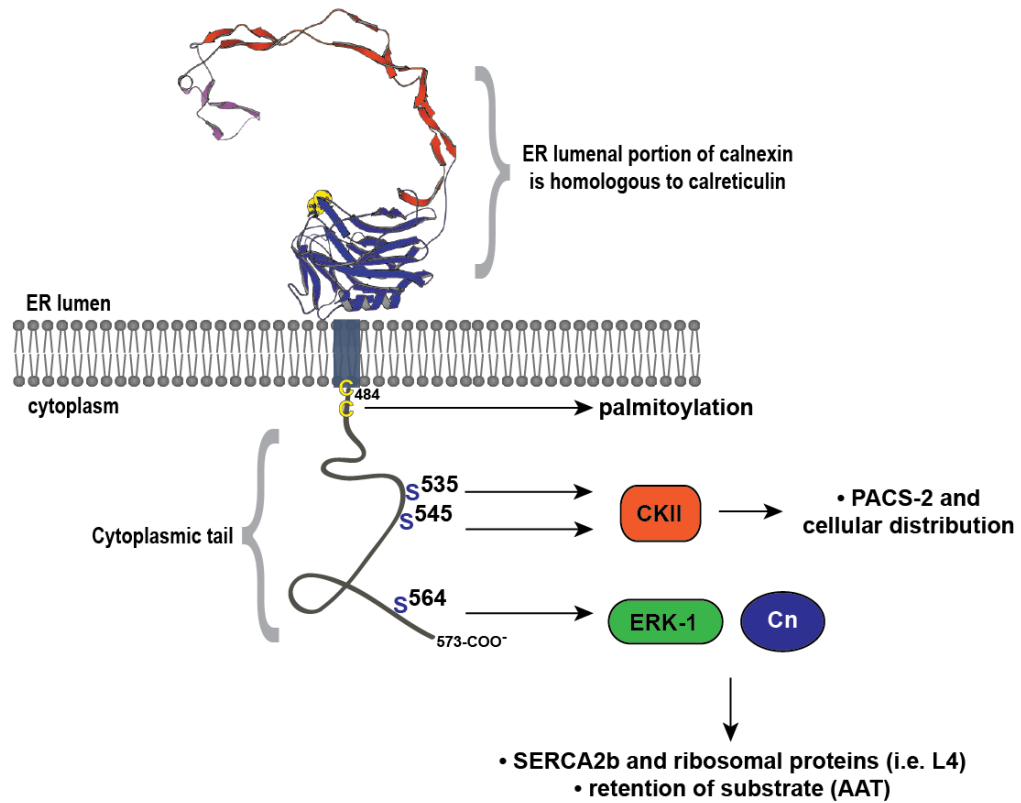


Figure 4.1. The calnexin cytoplasmic tail.

Calnexin can be divided into functionally and structurally distinct domains: the N+P luminal domain, the transmembrane domain, and the cytoplasmic domain. The amino acid sequence of mammalian calnexin, including the C-tail is highly conserved. Depicted in the figure is the amino acid sequence of canine calnexin. The cytoplasmic domain is the site of several post-translational modifications including palmitoylation and phosphorylation. The juxtamembrane cysteine residues (depicted as yellow C's) are palmitoylated. Serine residues 535 and 545 (S⁵³⁵ and S⁵⁴⁵) are phosphorylated by casein kinase II (CKII) and phosphorylation of these residues blocks interaction with phosphorin acidic cluster sorting protein 2 (PACS-2), an interaction that sequesters calnexin preferentially to mitochondrial associated membranes. Serine residue 564 (S⁵⁶⁴) is phosphorylated by extracellular regulated kinase-1 (ERK-1) and dephosphorylated by calcineurin (Cn). Phosphorylation of this residue prolongs association with misfolded glycoprotein α 1 antitrypsin (AAT). Phosphorylation of S⁵⁶⁴ also enhances the association of the C-tail with the ribosome (and ribosomal protein L4) and promotes an inhibitory interaction with SERCA2b that is released upon de-phosphorylation by Cn.

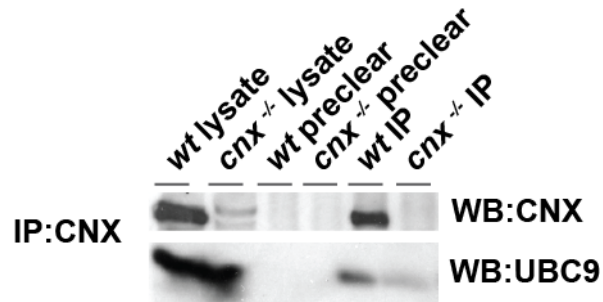


Figure 4.2. UBC9 co-immunoprecipitates with calnexin.

Wild-type (*wt*) and calnexin-deficient (*cnx*^{-/-}) (control) mouse fibroblast lysates were used for immunoprecipitation (*IP*) with anti-calnexin antibodies followed by Western blot (*WB*) analysis with anti-calnexin (*CNX*) or anti-UBC9 antibodies. Western blot (*WB*) analysis indicates that UBC9 can be co-immunoprecipitated with calnexin in wild-type cells. A representative Western blot of 3 independent experiments is shown. The initial interaction of UBC9 with the *CNX* C-tail was identified by yeast-2-hybrid analysis with the C-tail as bait and was carried out by Hao-Dong Li and Robert Evans.

revealed that calnexin co-immunoprecipitated with UBC9 in wild-type fibroblasts (Figure 4.2). We concluded that calnexin and UBC9 form complexes *in vivo* in cell culture.

UBC9 is known to distribute in the nucleus, nuclear envelope and cytoplasm [18]. We used confocal microscopy to examine the co-distribution of UBC9 and calnexin in wild-type fibroblasts. UBC9 (Figure 4.3A) and calnexin (Figure 4.3B) immunostaining can be found in the nuclear envelope and some colocalization is visible at the ER (Figure 4.3C). This was quantified and UBC9 and calnexin have an average thresholded Pearson's colocalization coefficient of 0.558 ± 0.060 . This indicates some but not complete colocalization, consistent with UBC9 localization in the nucleus and throughout the cytoplasm. Based on the yeast-2-hybrid screening of two independent libraries, the co-immunoprecipitation of calnexin and UBC9 (Figure 4.2) and the co-localization data (Figure 4.3), we concluded that the C-tail and UBC9 form complexes.

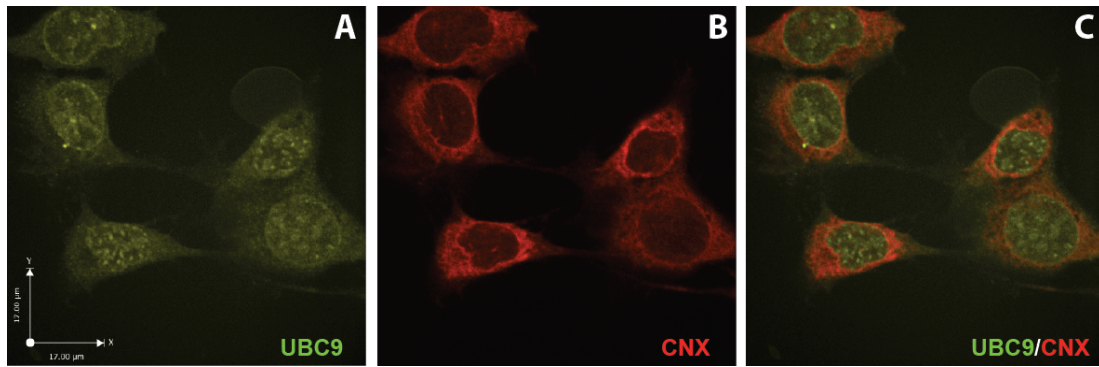


Figure 4.3. The cellular distribution of UBC9.

Confocal microscopy of mouse fibroblasts with immunostaining for UBC9 and calnexin (CNX) indicates colocalization of UBC9 and CNX. UBC9 is distributed throughout the cell and can be found in the nucleus and cytoplasm, with strong localization at the nuclear envelope (A). Mouse anti-UBC9 antibodies were used at a 1:100 dilution with rabbit anti-mouse Alexa 488 secondary antibodies. Anti-rabbit calnexin antibodies specific to the C-tail of calnexin were used at a 1:100 dilution with a mouse anti-rabbit Texas Red secondary antibodies (B). Colocalization between UBC9 and CNX is indicated in (C).

UBC9 Expression in the Absence of Calnexin

Next we investigated if the absence of calnexin had any impact on the expression of UBC9. Proteins and RNA were isolated from tissues from calnexin-deficient [19] and wild-type mice followed by semi-quantitative RT-PCR (Figure 4.4A) and Western blot (Figure 4.4B) analyses. RT-PCR indicated that UBC9 expression is modestly elevated in brain, liver, and kidney calnexin-deficient tissues. However, Western blot analysis with anti-UBC9 antibodies shows that the level of UBC9 protein was unchanged in a comprehensive range of calnexin-deficient tissues including kidney, brain, heart, liver and skeletal muscle (Figure 4.4B). The mouse UBC9 expression profile is consistent with analysis of UBC9 protein expression in rat tissues which demonstrated high UBC9 expression in spleen and lung, moderate expression in kidney and liver, and low expression in brain with virtually no expression in heart and skeletal muscle [20].

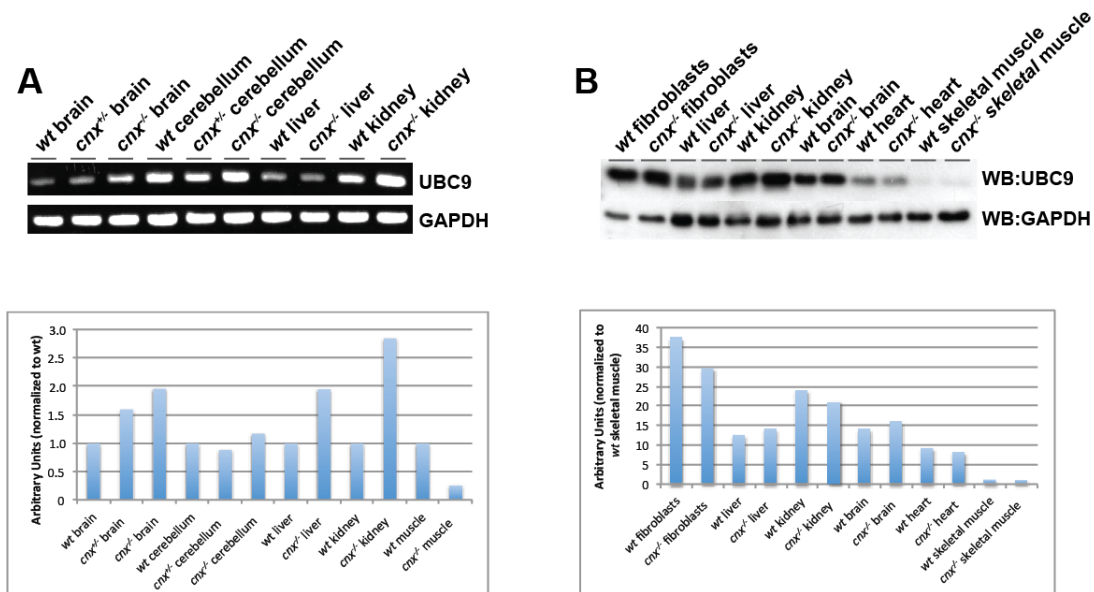


Figure 4.4. UBC9 expression levels in the calnexin-deficient mouse are similar to wild-type.

(A) Semi-quantitative RT-PCR indicates that UBC9 mRNA levels are up-regulated in calnexin-deficient (*cnx*^{-/-}) brain, liver and kidney tissues compared to wild-type (*wt*) tissue levels. Quantitation of expression levels was conducted using ImageJ software. UBC9 expression was normalized to GAPDH. UBC9 expression in calnexin-deficient tissues is shown as a fold-change of wild-type expression (set to 1). (B) Western blot analyses of a comprehensive range of wild-type (*wt*) and calnexin-deficient tissues (*cnx*^{-/-}) indicate that UBC9 protein expression in the absence of calnexin is similar to wild-type. Quantitation was conducted using ImageJ software and UBC9 levels were normalized to a GAPDH loading control and then to wild-type skeletal muscle (set to 1). Representative of 2 independent experiments.

To examine if there were any effects of UBC9 depletion on the expression of calnexin we used RNAi techniques to down-regulate the level of UBC9 protein in NIH 3T3 cells. Using this technique we consistently obtained up to 60-70% reduction of the level of endogenous UBC9 in NIH 3T3 cells. Figure 4.5A shows that UBC9 depletion in NIH 3T3 cells had no effect on the expression of calnexin but it led to the loss of SUMO-1 expression. Analysis of *sumo-1*^{-/-} fibroblasts showed that the absence of SUMO had no effect on the expression of calnexin (Figure 4.5B).

Next we tested if calnexin interaction with UBC9 may impact on global SUMOylation patterns. Wild-type and calnexin-deficient fibroblasts were harvested directly into SDS-PAGE sample buffer containing the de-SUMOylation inhibitor N-ethyl maleimide, heated and loaded on an SDS-PAGE gel for Western blot analysis. Figure 4.6A shows that the SUMO-1 global SUMOylation pattern was unchanged in the absence of calnexin. Figure 4.6B shows the banding pattern of global SUMO-2/3 modification was unchanged. We concluded that the absence of calnexin did not affect either the expression of UBC9 or the SUMOylation pattern and that reduced expression of UBC9 or SUMO-1 did not affect expression of calnexin.

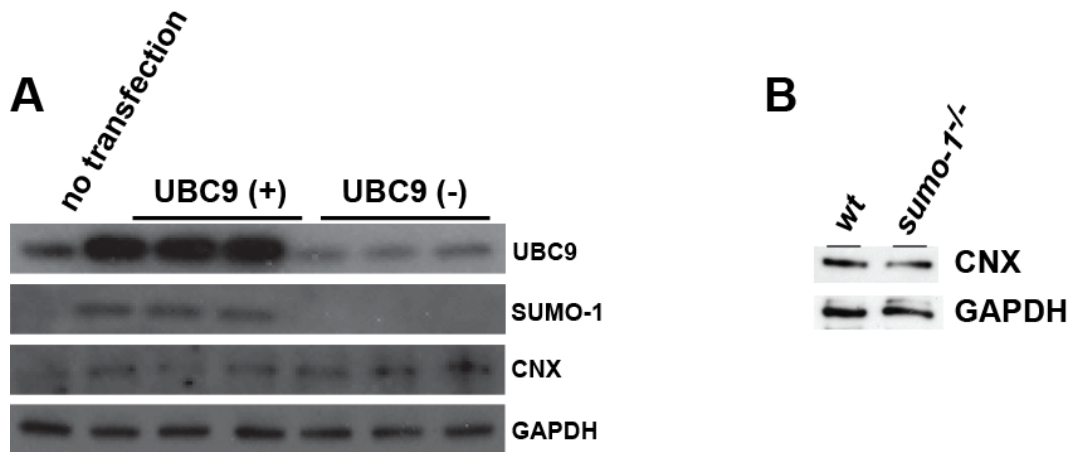


Figure 4.5. Depletion of components of the SUMOylation machinery has no impact on calnexin expression levels.

(A) RNAi-driven down-regulation of UBC9 was carried out in NIH 3T3 cells as described under “Material and Methods”. Up to 60-70% reduction of UBC9 protein was achieved. Neither the sense (+) nor sense + anti-sense (-) (up-regulation or down-regulation) of UBC9 expression had any effect on expression of calnexin. SUMO-1 expression was up-regulated with the over-expression of UBC9, and the expression GAPDH was unchanged with the up-regulation or down-regulation of UBC9. Blots are representative of 3 independent experiments. *CNX*, calnexin, *GAPDH*, glyceraldehyde-3-phosphate dehydrogenase. UBC9 RNAi experiments were carried out by Dukgyu Lee. (B) Expression of calnexin was examined by Western blot analysis in SUMO-1-deficient (*sumo-1^{-/-}*) cells using anti-calnexin (*CNX*) and GAPDH antibodies. The expression of calnexin was unchanged in the absence of SUMO-1. *CNX*, calnexin; *GAPDH*, glyceraldehyde-3-phosphate dehydrogenase.

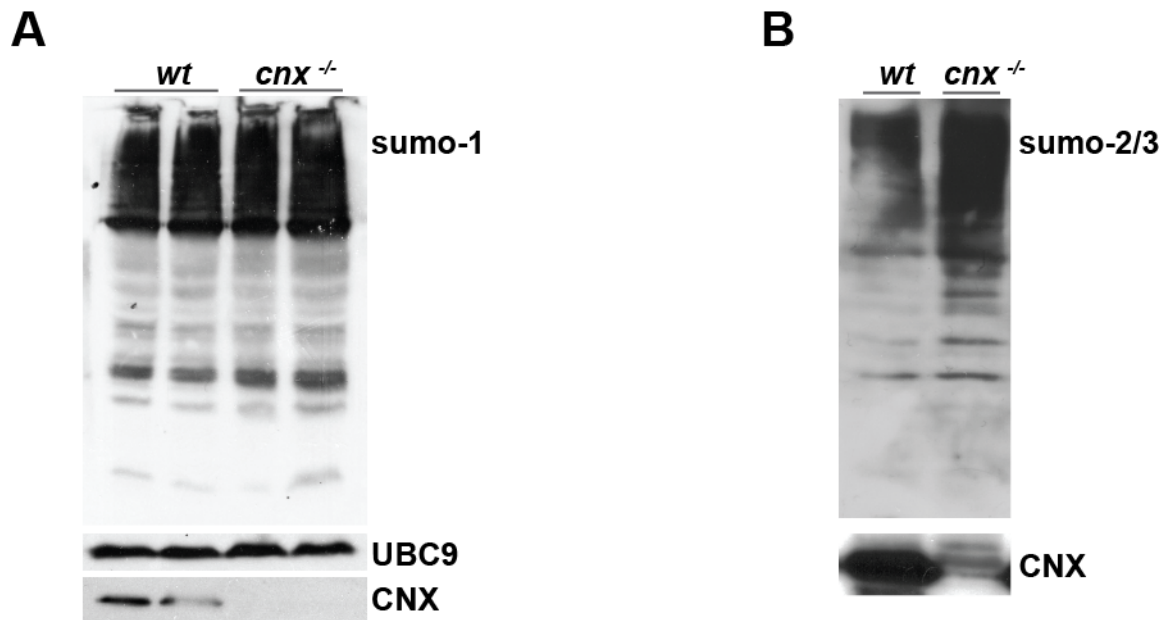


Figure 4.6. The global SUMOylation pattern is unchanged in the absence of calnexin.

Western blot analysis of the pattern of SUMO-1 modification in wild-type and calnexin-deficient fibroblasts. Cell lysates were analyzed using Western blot techniques for (A) SUMO-1 conjugates, UBC9 and CNX expression and (B) SUMO-2/3 conjugates using antibodies specific to SUMO-1, SUMO-2/3, UBC9 or the C-terminus of calnexin. *CNX*, calnexin.

The Calnexin C-tail Binds UBC9 in a Ca²⁺-Independent Manner

To date only the structure of the luminal domain of calnexin has been solved [21] and there is no structural information about the calnexin C-tail. To understand the nature of the C-tail/UBC9 interaction we employed various techniques to examine the structural and biophysical properties of the C-tail alone and with UBC9. We have determined with NMR spectroscopy that the calnexin C-tail lacks nascent structure and only small chemical shifts are observable in the presence of excess Ca²⁺ (Chapter 3). To examine the nature of the C-tail/UBC9 interaction, we applied NMR spectroscopy to obtain 2D ¹H-¹⁵N HSQC spectra of unlabelled UBC9 binding to ¹⁵N labelled C-tail. In the absence of Ca²⁺, an HSQC of ¹⁵N calnexin C-tail shows changes in approximately ten to twelve resonances of the C-tail with strong chemical shift broadening or disappearance with the addition of UBC9. This suggests that these residues are in slow conformational exchange, created by the binding of UBC9 to calnexin. Several cross-peaks remained unaffected with the addition of UBC9, which is not surprising considering the size of the C-tail of calnexin. Because most of the unperturbed resonances seem to be coming from the resonances with the highest intensities, this suggests that the N- and C-termini of calnexin most likely remain labile, even in the bound form. 6 mM Ca²⁺ was added to the NMR sample and both a ¹H and 2D ¹H-¹⁵N HSQC NMR spectra were acquired to investigate the Ca²⁺ requirement for UBC9 binding. Negligible changes were observed, indicating that Ca²⁺ saturation is not required for UBC9 interaction with the C-tail.

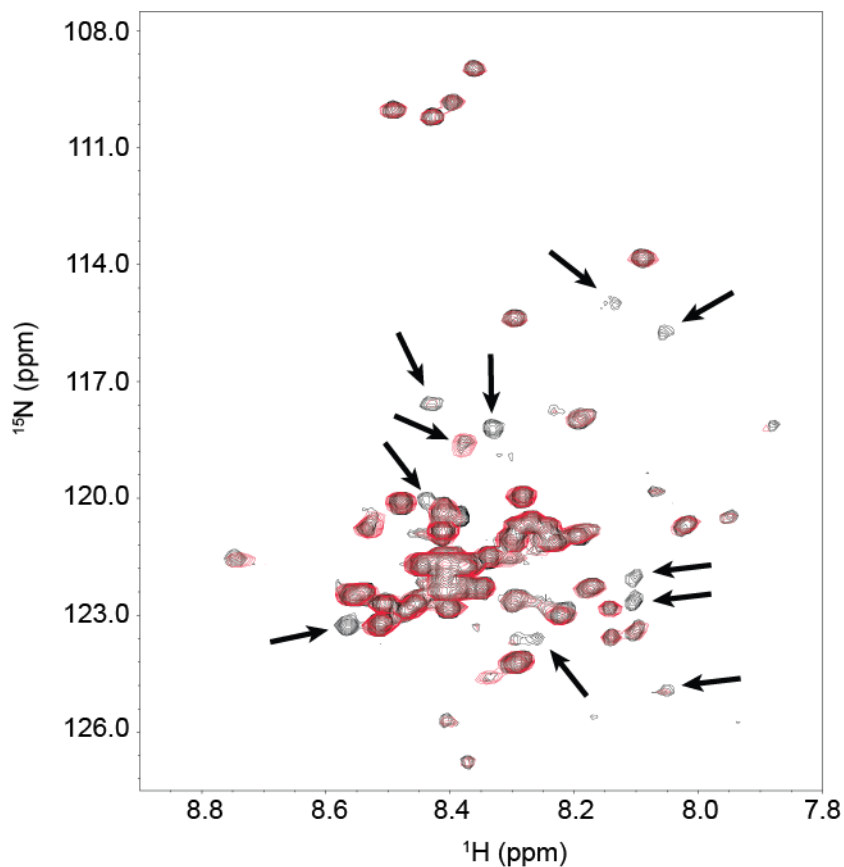


Figure 4.7. A 2D ^1H - ^{15}N HSQC NMR spectra of the C-tail of calnexin before (black) and after the addition of UBC9 (red).

Important line broadening is observed after addition of 1.2 mg of UBC9. Approximately ten to twelve resonances in calnexin showed strong chemical shift broadening or disappeared with the addition of UBC9. This suggests that these residues are in slow conformational exchange, created by the binding of UBC9 to calnexin. Protein purification was conducted with the technical support of Monika Dabrowska and NMR spectroscopy was carried out by Brian Sykes and Olivier Julien.

Association of UBC9 with the ER Membrane

UBC9 plays an important role in SUMOylation in the nuclear and cytoplasmic compartments of the cell [22]. The discovery of UBC9 binding to ER-associated calnexin C-tail indicates that the protein might be sequestered in the vicinity of the ER membrane allowing its action on ER proximal cytoplasmic substrates. Therefore, we investigated what proportion of UBC9 can be found at the ER membrane and if calnexin has an impact on its localization. To investigate this, we used cellular fractionation on Opti-prep gradients to compare UBC9 localization in wild-type and calnexin-deficient fibroblasts (Figure 4.8). GAPDH was used as a marker to cytoplasmic compartment (fractions 2-4) and the location of Ribophorin I indicated the location of rough ER fractions (fractions 5-11). UBC9 is distributed throughout all the fractions but has a bimodal distribution with the majority found in fractions 1-3 (low density, cytoplasmic compartment) and a second peak of distribution in fractions 7 and 8 (Figure 4.8A). Calnexin is distributed through fractions 5-12 with the peak of distribution in fractions 6-8. Thus, UBC9 and calnexin co-distribute and both proteins show peaks of distribution in fractions 7-8 with approximately 15% of total UBC9 residing in these fractions. Interestingly, in the absence of calnexin UBC9 becomes more evenly distributed across the fractions, including the heavy fractions, and the bimodal appearance is less distinct (Figure 4.8B). Thus, a portion of UBC9 was associated with the ER membrane and co-distributes with calnexin.

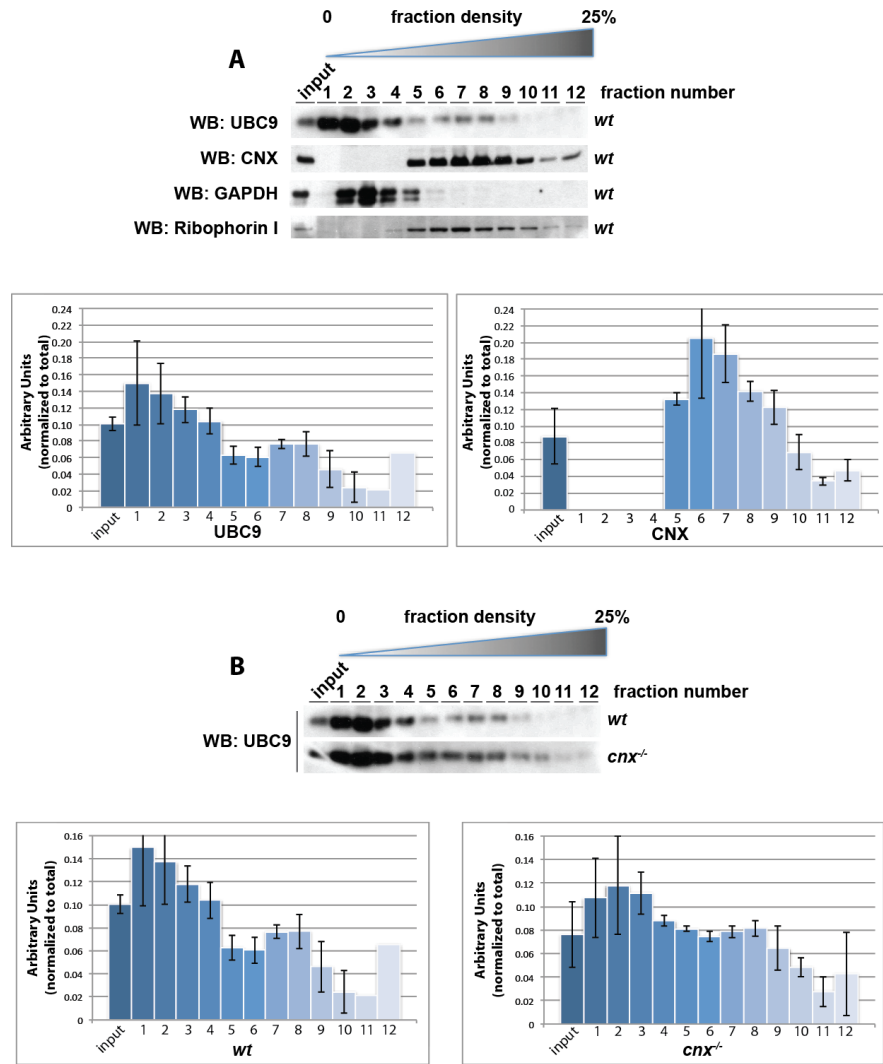


Figure 4.8. UBC9 has a bimodal cellular distribution.

(A). Cellular subfractionation was carried out on Opti-prep gradients (0-25% iodoxanol) followed by Western blot analysis with anti-UBC-9, anti-calnexin, anti-GAPDH and anti-ribophorin I antibodies. GAPDH and ribophorin I were used as a reference for cytosolic and rough ER fractions, respectively. Calnexin and UBC9 can be found in the same fractions indicating co-distribution in the cell, particularly in fractions 7 and 8. (B). UBC9 cellular distribution was examined in the presence and absence of calnexin. UBC9 distribution in wild-type cells has a bimodal distribution with peaks of UBC9 expression identified in fractions 1 and 7-8. In the absence of calnexin, UBC9 appears to more evenly distribute throughout the cellular fractions. Blots are representative of two independent experiments. *WB*, Western blot; *CNX*, calnexin; *GAPDH*, glyceraldehyde-3-phosphate dehydrogenase. Fractionation gradient samples used for Western blot analysis were obtained from Daniel Prins.

Next we isolated microsomal fractions (enriched in ER) from HeLa cells expressing recombinant UBC9 followed by Western blot analysis of purified membrane with anti-UBC9 antibodies. Figure 4.9A shows that the UBC9 was present in calnexin containing, ER-enriched microsomal fractions indicating that UBC9 was associated with isolated ER membranes. To examine if the associated UBC9 could be titrated away from the ER membranes with the calnexin C-tail, we incubated isolated microsomal vesicles with purified C-tail for two hours at 4°C (Figure 4.9B). Figure 4.9B and C show that UBC9 remains associated with the microsomes despite increasing concentrations of purified calnexin C-tail. However, the C-tail itself associates with the ER membranes (Figure 4.9C). This is in agreement with equilibrium sedimentation centrifugation experiments and indicates that the calnexin C-tail can homo-dimerize. It is likely that purified calnexin C-tail bound to endogenous calnexin, and consequently some UBC9 remained associated with the ER membranes. Alternatively, the purified C-tail might not be able to effectively compete with membrane-anchored endogenous C-tail for UBC9 association.

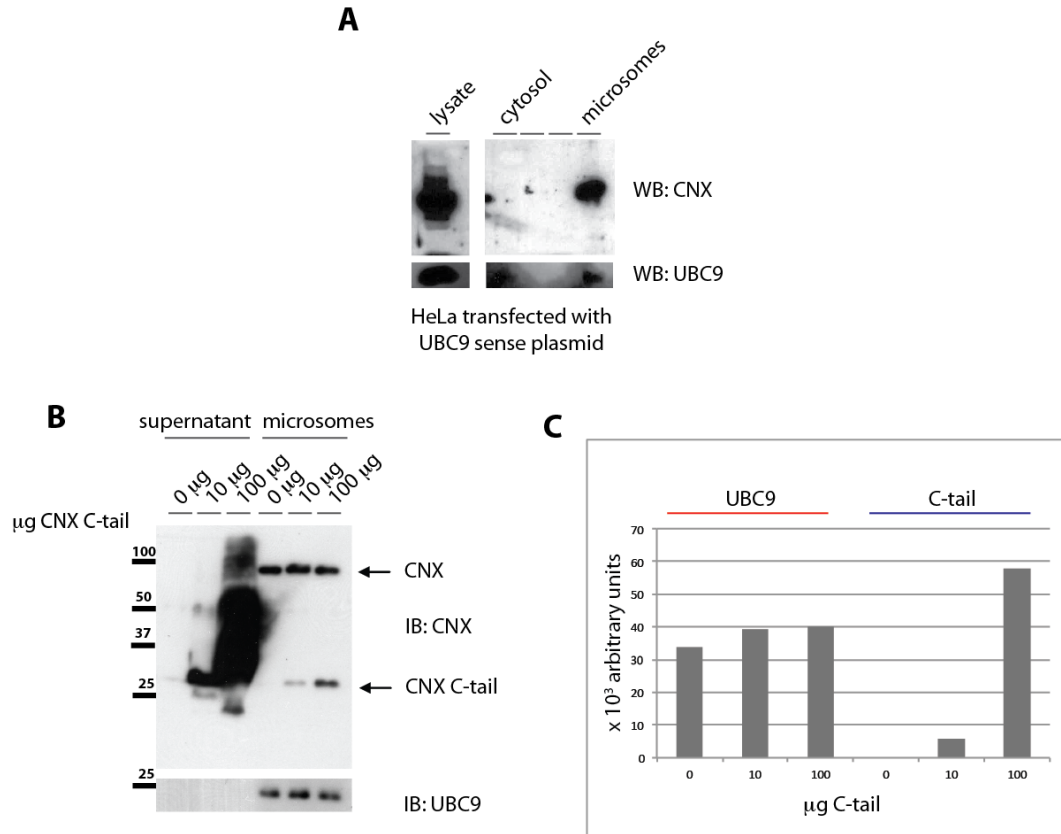


Figure 4.9. UBC9 associates with ER membranes.

(A). HeLa cells were transfected with the UBC9 sense plasmid and used for ER microsome isolation, followed by Western blot analysis of purified ER microsomes with anti-UBC9 antibodies. *WB*, Western blot. (B). Western blot analysis of microsomal fractions with anti-calnexin and anti-UBC9 antibodies. Microsomal membranes were incubated with purified calnexin C-tail for two hours at 4°C prior to SDS-PAGE and Western blot analysis. UBC9 remains associated with the microsomes but the C-tail itself appears to associate with the microsomes with an increasing concentration of calnexin C-tail. (C). Quantitation of the Western blot in B. Representative of three independent experiments. *WB*, Western blot.

The Calnexin C-tail is SUMOylated *in vitro*

SUMO conjugation modifies a lysine residue typically within the core consensus motif ψ KxE where ψ is a bulky hydrophobic residue [23]. In addition to the core consensus motif, additional flanking amino acid sequences have been proposed to extend the SUMO consensus motif [24, 25]. These include the phosphorylation-dependent SUMOylation motif (PDSM) of ψ KxE_{xx}SP [24] and the negatively charged amino acid-dependent SUMOylation motif (NDSM)[25]. A global search of NDSM containing proteins in the SWISSPROT database identified that the highly acidic calnexin C-tail contains a NDSM (residues 505-518), VK⁵⁰⁶EEEEEEKEEEKDK, a motif previously used successfully in determining *in vivo* SUMO substrates (Figure 4.10A) [25]. To examine if this site can be SUMOylated, we used an *in vitro* SUMOylation system with purified canine calnexin C-tail (Figure 4.10B) and a K⁵⁰⁶A C-tail mutant (Figure 4.10C). Figure 4.10B shows that in the presence of SUMO-1 there was a shift of the C-tail mobility of approximately 12-kDa as detected with an anti-calnexin antibody, a size shift consistent with the addition of SUMO-1. Mutation of K⁵⁰⁶ to an alanine abrogated *in vitro* SUMOylation of the C-tail indicating that the predicted NDSM motif in the calnexin C-tail was the site of SUMO addition (Figure 4.10C). Thus, we concluded that the calnexin C-tail can be SUMOylated *in vitro* at K⁵⁰⁶ within the predicted SUMOylation NDSM consensus site.

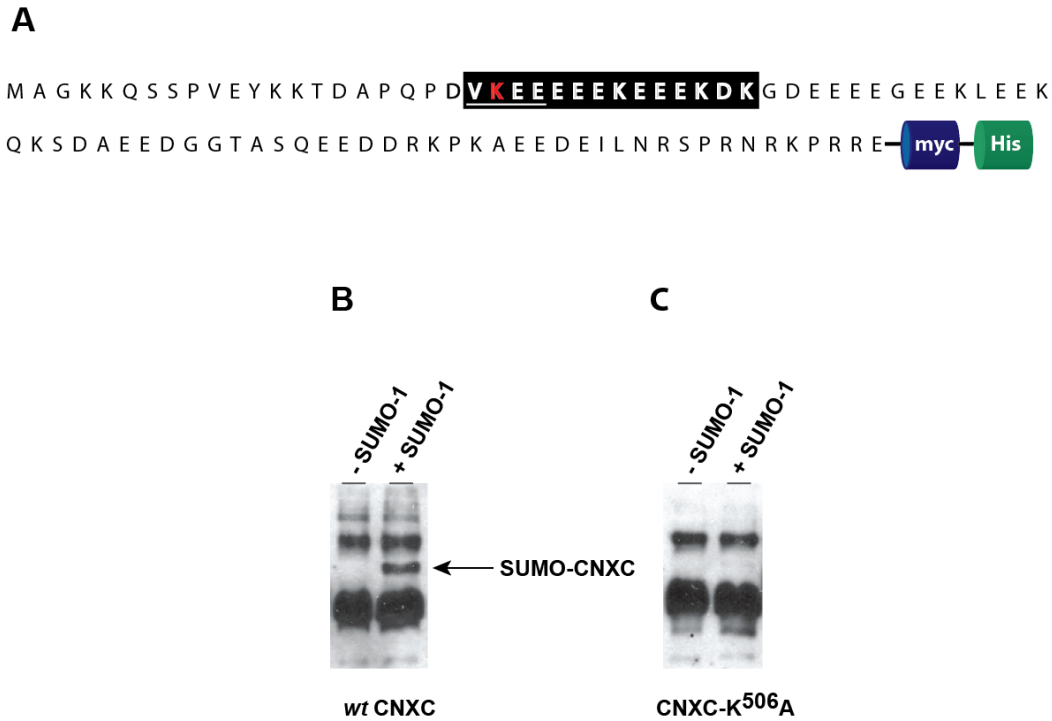


Figure 4.10. Calnexin is SUMOylated *in vitro* at K⁵⁰⁶.

(A) A schematic representation of the calnexin C-tail amino acid sequence. The proposed negatively charged amino acid-dependent SUMOylation motif (NDSM) is highlighted in black with the core consensus motif underlined in white. The location of the myc and His tag are indicated. (B) *In vitro* SUMOylation of the calnexin C-tail. Purified calnexin C-tail was SUMOylated as described under “Material and Methods”. SUMOylated C-tail was identified by Western blot analysis with anti-calnexin antibodies. The location of SUMO-calnexin C-tail is indicated by the arrow (SUMO-CNXC). CNXC, calnexin C-tail. (C) K⁵⁰⁶A C-tail mutant is not SUMOylated *in vitro*. *In vitro* SUMOylation was carried out as described under “Material and Methods”. Western blots depicted in (B) and (C) were from the same immunoblot. CNXC, calnexin C-tail.

Calnexin is SUMOylated *in vivo*

While a calnexin SUMO site has been predicted and was modified *in vitro* (Figure 4.10) it is important to examine if the protein can be SUMOylated *in vivo*. The SUMO enigma is a well-documented phenomenon where only a small portion of the total substrate is detectably SUMOylated at any given time even when functional evidence indicates complete SUMOylation [26]. To increase the probability of detecting SUMOylated calnexin (and the corresponding molecular shift) *in vivo*, we tested isolated ER microsomes for the presence of SUMOylated endogenous calnexin. SUMO-1 immunostaining of purified ER microsomes revealed a SUMO-1 high molecular weight species of the same molecular weight as calnexin (Figure 4.11A, *arrow*). To confirm the SUMOylated protein band in the microsomal fraction is calnexin, HeLA cells were transfected with an expression vector encoding GFP-SUMO-1 followed by the isolation of ER enriched microsomes and immunoprecipitation followed by Western blot analyses. Immunoprecipitation from solubilized microsomes with goat anti-GFP antibodies, and immunoblotting with rabbit anti-GFP antibodies indicates that a GFP-SUMO-1 modified protein at approximately 100-kDa can be specifically immunoprecipitated with anti-GFP antibodies (Figure 4.11B). Western blot analysis of the same sample with anti-calnexin antibodies revealed that calnexin (detectable at approximately 100-kDa) was co-immunoprecipitated with GFP-SUMO-1 from ER membranes (Figure 4.11B). We concluded that calnexin is SUMOylated *in vivo*.

RanBPM and the C-tail

The mouse brain Matchmaker cDNA library screen also identified that the C-tail interacts with RanBPM, a postulated SUMO E3 ligase [27, 28]. E3 SUMO ligases have only been identified for certain SUMOylated substrates and are not required in all cases. RanBPM had areas of co-localization with calnexin as determined by confocal microscopy with a thresholded Pearson's coefficient of 0.504 ± 0.037 indicating that it may be a specific E3 for calnexin SUMOylation (Figure 4.12). This indicates that E3 specificity (RanBPM) may be required for calnexin SUMOylation.

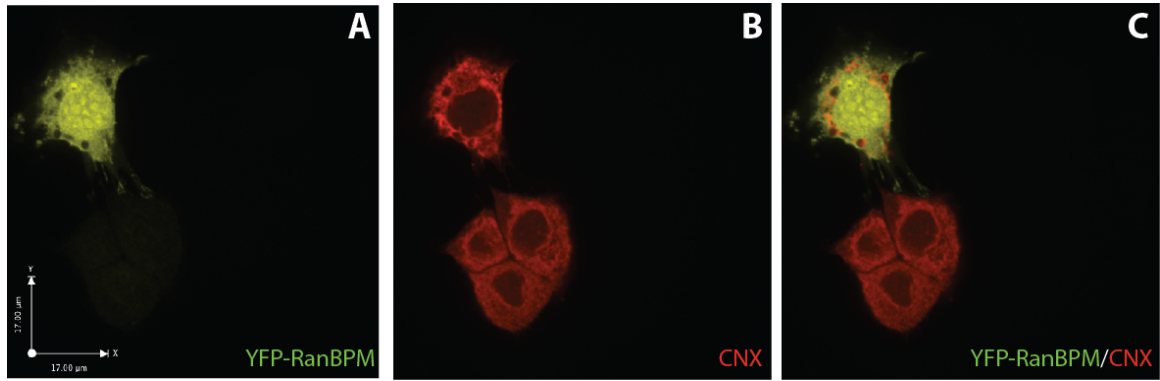


Figure 4.12. Cellular distribution of RanBPM.

Confocal microscopy of (A) YFP tagged RanBPM and (B) immunostaining for calnexin with Texas Red secondary antibodies indicate that RanBPM is distributed throughout the cell, including the nucleus, and has some degree of (C) colocalization with calnexin at the ER compartment.

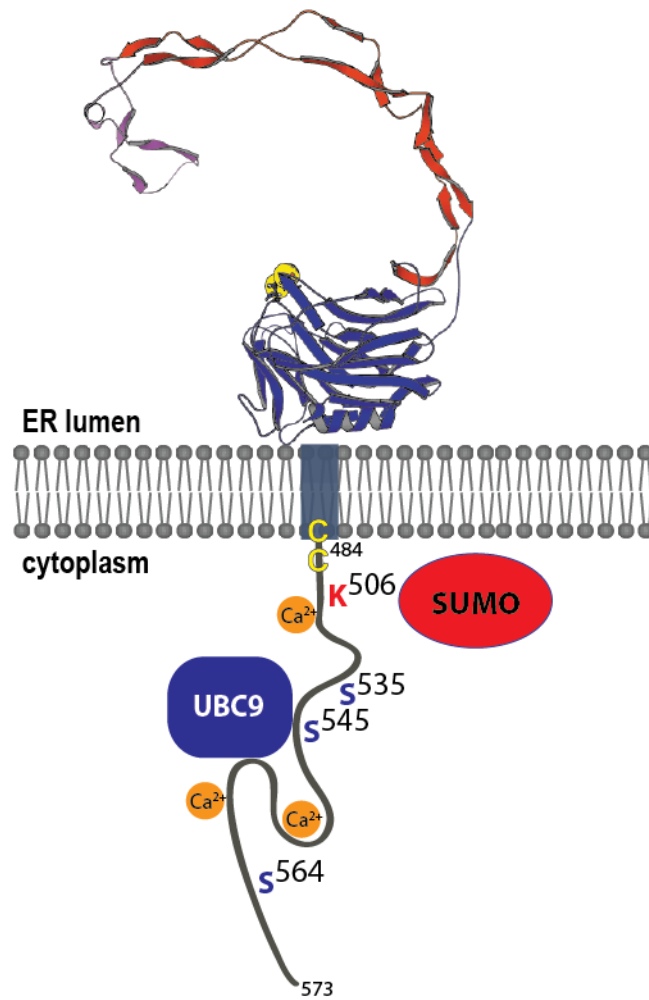


Figure 4.13. The C-tail binds UBC9 and can be SUMOylated.

The C-tail binds UBC9 in a manner that leaves its N and C-terminus labile, indicating it binds somewhere in between. UBC9 binding is Ca^{2+} -dependent and leads to the SUMOylation of the calnexin C-tail at Lys⁵⁰⁶. The phosphorylatable Ser residues are indicated in blue, the palmitoylated juxtamembrane cysteines in yellow and Lys⁵⁰⁶ in red.

Discussion

Calnexin is an integral membrane ER associated chaperone with a C-terminal cytoplasmic tail domain almost 90 amino acids in length. The majority of previous studies have focused on calnexin's ER luminal chaperone domain. Here we show that the C-terminal domain of calnexin may form complexes with cytoplasmic proteins and impact on cellular functions independent of its role as a chaperone. In this study we demonstrate that the calnexin cytoplasmic tail binds UBC9, a SUMO E2 ligase and it is SUMOylated within a negatively charged amino acid-dependent SUMOylation motif at K⁵⁰⁶. The C-tail domain of calnexin binds UBC9 in a Ca²⁺-independent manner as determined with NMR spectroscopy. To our knowledge, this is the first report of an integral ER membrane molecular chaperone that can be modified by SUMO.

UBC9 and the Calnexin C-tail

We used yeast-2-hybrid techniques to identify potential cytoplasmic proteins interacting with the C-terminal cytoplasmic tail of calnexin. The initial screen identified several potential partners of the unique cytoplasmic domain of calnexin. Two independent yeast-2-hybrid screens of brain and Jurkat libraries identified UBC9 as a C-tail interacting partner. UBC9 associates with ER membranes and likely plays a role in SUMOylation of other ER associated and cytoplasmic substrates. A recent study reported that UBC9 was present in the ER luminal compartment based on studies including microscopy analysis where UBC9 was found to co-localize with calnexin [29].

We postulate that UBC9 resides on the cytosolic side of the ER membrane and associates with the calnexin C-tail.

The ER is the major storage site for cellular Ca^{2+} and the C-tail has been shown to regulate SERCA and Ca^{2+} -reuptake. Thus, Ca^{2+} could impact on UBC9 interaction with the C-tail. The structure and biophysical nature of the C-tail, Ca^{2+} -binding to the C-tail and the impact this has on protein-protein interactions have never been investigated. Phosphorylation of the calnexin C-tail is involved in ER Ca^{2+} homeostasis and is regulated by cytosolic Ca^{2+} through dephosphorylation by calcineurin [30]. Cytosolic Ca^{2+} could also impact on UBC9 binding and subsequent SUMOylation of the C-tail. We used NMR spectroscopy to examine UBC9/C-tail binding in the presence of Ca^{2+} . The calnexin C-tail lacks nascent structure and binds Ca^{2+} (Chapter 3). However, UBC9 binding to the C-tail appears to be Ca^{2+} independent as the UBC9/[^{15}N] C-tail 2D ^1H - ^{15}N HSQC spectra is unchanged in the presence of excess Ca^{2+} .

UBC9 activity and SUMOylation have been extensively studied in the nuclear compartment as a part of transcriptional control. However, in the last five years, examples of integral membrane proteins modified by SUMO have emerged [31, 32]. SUMO modification has been shown to inactivate the plasma membrane potassium leak channel K2P1 and regulate the endocytosis of the kainate receptor and subsequent synaptic transmission after SUMOylation of the GluR6 kainate receptor subunit [31, 32]. Other membrane protein targets include voltage-dependent K^+ (Kv) channels,

glucose transporters and the group 3 metabotropic glutamate receptors [33-36]. Here we show that the C-tail of calnexin, an ER chaperone, is SUMOylated within a NDSM consensus motif at K⁵⁰⁶ by SUMO-1. SUMO modification at the ER membrane is a novel finding as the majority of studied SUMO substrates reside in the nucleus or more recently, at the plasma membrane. Calnexin is the first ER molecular chaperone shown to be SUMOylated. There has only been one previous report of an ER localized protein being SUMOylated, the protein tyrosine phosphatase PTP1B [37]. There are four known SUMO paralogues in mammals, SUMO 1, 2, 3 and 4. SUMO 2 and 3 are 95% identical whereas SUMO-2 is 48% and SUMO-3 46% identical to SUMO-1 [38]. There are databases available from large-scale mass spectrometry screens of SUMOylated proteins [39, 40] and two independent databases also identified calnexin as a SUMOylated substrate. In the first study, an investigation of the cross-talk between the ubiquitin/proteasome system and SUMO-2/3 modification led to the identification of calnexin as a SUMO-2 substrate [39]. In the second study, an investigation of the effect heat shock had on SUMO modifications also identified calnexin as a SUMO-2 substrate [40]. While the literature reported modification by SUMO-2, our *in vitro* SUMOylation analysis indicated that the C-tail could be modified by SUMO-1 and *in vivo* SUMOylation was detectable with a SUMO-1 antibody. While the significance between SUMO-1 and SUMO 2/3 modification is not understood, it is known that many substrates undergo modification by both SUMO-1 and SUMO 2/3 and in some cases

SUMO-1 and SUMO 2/3 can form mixed chains [41]. It is possible that calnexin is modifiable by different SUMO moieties.

Functional Implications of Calnexin SUMOylation

The implications of SUMOylation of a molecular chaperone are difficult to determine due to the lack of a definitive activity assay. Calnexin is the molecular chaperone for virtually every glycosylated transmembrane protein translated through the ER. Other post-translational modifications have a wide variety of effects on calnexin function. Phosphorylation of Ser⁵⁶³ the C-tail regulates an inhibitory interaction with SERCA2b where elevated cytosolic Ca²⁺ concentrations and ER stress lead to the dephosphorylation of calnexin by calcineurin and removal of its inhibitory effect on SERCA2b [4, 30]. Phosphorylation also recruits calnexin to the translocons bound by ribosomes, disrupt its interaction with the cytosolically associated PACS-2 protein resulting in its re-distribution from peripheral to juxtannuclear ER, and leads to prolonged retention of a known substrate, AAT, under misfolding conditions [1]. SUMOylation of the C-tail could be related to any one of the above or provide a novel C-tail function. One of the large scale screens that identified calnexin conjugated to SUMO was with heat shock conditions, indicating SUMO modification on calnexin could be related to ER stress signalling [40]. However, calnexin SUMO conjugation was also detected in a screen to determine the effect of proteasome inhibition on SUMO conjugation, indicating that SUMO is conjugated under both basal and ER stress conditions. Detectable calnexin SUMO levels were unchanged when

the proteasome was inhibited with MG132 indicating SUMOylation of calnexin is likely not related to ER associated degradation (ERAD) [39]. Considering the unique and non-redundant nature of the calnexin C-tail, SUMOylation of the C-tail could impact on calnexin's specificity for myelin systems [42, 43]. While the function of calnexin SUMOylation remains to be investigated, this study provides a novel modification of the unique calnexin C-tail that has important implications for regulation of a ubiquitous ER molecular chaperone.

References

1. Chevet, E., J. Smirle, P.H. Cameron, D.Y. Thomas, and J.J. Bergeron, *Calnexin phosphorylation: Linking cytoplasmic signalling to endoplasmic reticulum lumenal functions*. Semin Cell Dev Biol.
2. Ho, S.C., S. Rajagopalan, S. Chaudhuri, C.C. Shieh, M.B. Brenner, and S. Pillai, *Membrane anchoring of calnexin facilitates its interaction with its targets*. Mol Immunol, 1999. **36**(1): p. 1-12.
3. Chevet, E., H.N. Wong, D. Gerber, C. Cochet, A. Fazel, P.H. Cameron, J.N. Gushue, D.Y. Thomas, and J.J. Bergeron, *Phosphorylation by CK2 and MAPK enhances calnexin association with ribosomes*. EMBO J, 1999. **18**(13): p. 3655-3666.
4. Roderick, H.L., J.D. Lechleiter, and P. Camacho, *Cytosolic phosphorylation of calnexin controls intracellular Ca(2+) oscillations via an interaction with SERCA2b*. J Cell Biol, 2000. **149**(6): p. 1235-1248.
5. Cameron, P.H., E. Chevet, O. Pluquet, D.Y. Thomas, and J.J. Bergeron, *Calnexin phosphorylation attenuates the release of partially misfolded alpha1-antitrypsin to the secretory pathway*. J Biol Chem, 2009. **284**(50): p. 34570-34579.
6. Martin, B.R. and B.F. Cravatt, *Large-scale profiling of protein palmitoylation in mammalian cells*. Nat Methods, 2009. **6**(2): p. 135-138.
7. Takizawa, T., C. Tatematsu, K. Watanabe, K. Kato, and Y. Nakanishi, *Cleavage of calnexin caused by apoptotic stimuli: implication for the regulation of apoptosis*. J Biochem, 2004. **136**(3): p. 399-405.
8. Gareau, J.R. and C.D. Lima, *The SUMO pathway: emerging mechanisms that shape specificity, conjugation and recognition*. Nat Rev Mol Cell Biol. **11**(12): p. 861-871.
9. Deshaies, R.J. and C.A. Joazeiro, *RING domain E3 ubiquitin ligases*. Annu Rev Biochem, 2009. **78**: p. 399-434.
10. Desterro, J.M., M.S. Rodriguez, and R.T. Hay, *SUMO-1 modification of IkkappaBalpha inhibits NF-kappaB activation*. Mol Cell, 1998. **2**(2): p. 233-239.
11. Rodriguez, M.S., C. Dargemont, and R.T. Hay, *SUMO-1 conjugation in vivo requires both a consensus modification motif and nuclear targeting*. J Biol Chem, 2001. **276**(16): p. 12654-12659.
12. Geiss-Friedlander, R. and F. Melchior, *Concepts in sumoylation: a decade on*. Nat Rev Mol Cell Biol, 2007. **8**(12): p. 947-956.
13. Yunus, A.A. and C.D. Lima, *Purification and activity assays for Ubc9, the ubiquitin-conjugating enzyme for the small ubiquitin-like modifier SUMO*. Methods Enzymol, 2005. **398**: p. 74-87.
14. Nakamura, K., E. Bossy-Wetzels, K. Burns, M. Fadel, M. Lozyk, I.S. Goping, M. Opas, R.C. Bleackley, D.R. Green, and M. Michalak, *Changes*

- in endoplasmic reticulum luminal environment affect cell sensitivity to apoptosis.* J. Cell Biol., 2000. **150**: p. 731-740.
15. Zhang, F.P., L. Mikkonen, J. Toppari, J.J. Palvimo, I. Thesleff, and O.A. Janne, *Sumo-1 function is dispensable in normal mouse development.* Mol Cell Biol, 2008. **28**(17): p. 5381-5390.
 16. Milner, R.E., S. Baksh, C. Shemanko, M.R. Carpenter, L. Smillie, J.E. Vance, M. Opas, and M. Michalak, *Calreticulin, and not calsequestrin, is the major calcium binding protein of smooth muscle sarcoplasmic reticulum and liver endoplasmic reticulum.* J. Biol. Chem., 1991. **266**: p. 7155-7165.
 17. Bradford, M.M., *A rapid and sensitive method for the quantitation of microgram quantities of protein utilizing the principle of protein-dye binding.* Anal. Biochem., 1976. **72**: p. 248-254.
 18. Lee, G.W., F. Melchior, M.J. Matunis, R. Mahajan, Q. Tian, and P. Anderson, *Modification of Ran GTPase-activating protein by the small ubiquitin-related modifier SUMO-1 requires Ubc9, an E2-type ubiquitin-conjugating enzyme homologue.* J Biol Chem, 1998. **273**(11): p. 6503-6507.
 19. Kraus, A., J. Groenendyk, K. Bedard, T.A. Baldwin, K.H. Krause, M. Dubois-Dauphin, J. Dyck, E.E. Rosenbaum, L. Korngut, N.J. Colley, S. Gosgnach, D. Zochodne, K. Todd, L.B. Agellon, and M. Michalak, *Calnexin deficiency leads to dysmyelination.* J Biol Chem.
 20. Golebiowski, F., A. Szulc, M. Sakowicz, A. Szutowicz, and T. Pawelczyk, *Expression level of Ubc9 protein in rat tissues.* Acta Biochim Pol, 2003. **50**(4): p. 1065-1073.
 21. Schrag, J.D., J.J. Bergeron, Y. Li, S. Borisova, M. Hahn, D.Y. Thomas, and M. Cygler, *The Structure of calnexin, an ER chaperone involved in quality control of protein folding.* Mol Cell, 2001. **8**(3): p. 633-644.
 22. Pichler, A. and F. Melchior, *Ubiquitin-related modifier SUMO1 and nucleocytoplasmic transport.* Traffic, 2002. **3**(6): p. 381-387.
 23. Melchior, F., *SUMO--nonclassical ubiquitin.* Annu Rev Cell Dev Biol, 2000. **16**: p. 591-626.
 24. Hietakangas, V., J. Anckar, H.A. Blomster, M. Fujimoto, J.J. Palvimo, A. Nakai, and L. Sistonen, *PDSM, a motif for phosphorylation-dependent SUMO modification.* Proc Natl Acad Sci U S A, 2006. **103**(1): p. 45-50.
 25. Yang, S.H., A. Galanis, J. Witty, and A.D. Sharrocks, *An extended consensus motif enhances the specificity of substrate modification by SUMO.* EMBO J, 2006. **25**(21): p. 5083-5093.
 26. Hay, R.T., *SUMO: a history of modification.* Mol Cell, 2005. **18**(1): p. 1-12.
 27. Kabil, O., Y. Zhou, and R. Banerjee, *Human cystathionine beta-synthase is a target for sumoylation.* Biochemistry, 2006. **45**(45): p. 13528-13536.
 28. Chang, L.K., S.T. Liu, C.W. Kuo, W.H. Wang, J.Y. Chuang, E. Bianchi, and Y.R. Hong, *Enhancement of transactivation activity of Rta of Epstein-Barr virus by RanBPM.* J Mol Biol, 2008. **379**(2): p. 231-242.

29. Zhang, Y.Q. and K.D. Sarge, *Sumoylation of amyloid precursor protein negatively regulates Abeta aggregate levels*. Biochem Biophys Res Commun, 2008. **374**(4): p. 673-678.
30. Bollo, M., R.M. Paredes, D. Holstein, N. Zheleznova, P. Camacho, and J.D. Lechleiter, *Calcineurin interacts with PERK and dephosphorylates calnexin to relieve ER stress in mammals and frogs*. PLoS One. **5**(8): p. e11925.
31. Rajan, S., L.D. Plant, M.L. Rabin, M.H. Butler, and S.A. Goldstein, *Sumoylation silences the plasma membrane leak K⁺ channel K2P1*. Cell, 2005. **121**(1): p. 37-47.
32. Martin, S., A. Nishimune, J.R. Mellor, and J.M. Henley, *SUMOylation regulates kainate-receptor-mediated synaptic transmission*. Nature, 2007. **447**(7142): p. 321-325.
33. Dai, X.Q., J. Kolic, P. Marchi, S. Sipione, and P.E. Macdonald, *SUMOylation regulates Kv2.1 and modulates pancreatic beta-cell excitability*. J Cell Sci, 2009. **122**(Pt 6): p. 775-779.
34. Benson, M.D., Q.J. Li, K. Kieckhafer, D. Dudek, M.R. Whorton, R.K. Sunahara, J.A. Iniguez-Lluhi, and J.R. Martens, *SUMO modification regulates inactivation of the voltage-gated potassium channel Kv1.5*. Proc Natl Acad Sci U S A, 2007. **104**(6): p. 1805-1810.
35. Lalioti, V.S., S. Vergarajauregui, D. Pulido, and I.V. Sandoval, *The insulin-sensitive glucose transporter, GLUT4, interacts physically with Daxx. Two proteins with capacity to bind Ubc9 and conjugated to SUMO1*. J Biol Chem, 2002. **277**(22): p. 19783-19791.
36. Tang, Z., O. El Far, H. Betz, and A. Scheschonka, *Pias1 interaction and sumoylation of metabotropic glutamate receptor 8*. J Biol Chem, 2005. **280**(46): p. 38153-38159.
37. Dadke, S., S. Cotteret, S.C. Yip, Z.M. Jaffer, F. Haj, A. Ivanov, F. Rauscher, 3rd, K. Shuai, T. Ng, B.G. Neel, and J. Chernoff, *Regulation of protein tyrosine phosphatase 1B by sumoylation*. Nat Cell Biol, 2007. **9**(1): p. 80-85.
38. Saitoh, H. and J. Hinchey, *Functional heterogeneity of small ubiquitin-related protein modifiers SUMO-1 versus SUMO-2/3*. J Biol Chem, 2000. **275**(9): p. 6252-6258.
39. Schimmel, J., K.M. Larsen, I. Matic, M. van Hagen, J. Cox, M. Mann, J.S. Andersen, and A.C. Vertegaal, *The ubiquitin-proteasome system is a key component of the SUMO-2/3 cycle*. Mol Cell Proteomics, 2008. **7**(11): p. 2107-2122.
40. Golebiowski, F., I. Matic, M.H. Tatham, C. Cole, Y. Yin, A. Nakamura, J. Cox, G.J. Barton, M. Mann, and R.T. Hay, *System-wide changes to SUMO modifications in response to heat shock*. Sci Signal, 2009. **2**(72): p. ra24.
41. Matic, I., M. van Hagen, J. Schimmel, B. Macek, S.C. Ogg, M.H. Tatham, R.T. Hay, A.I. Lamond, M. Mann, and A.C. Vertegaal, *In vivo identification of human small ubiquitin-like modifier polymerization sites by high accuracy mass spectrometry and an in vitro to in vivo strategy*. Mol Cell Proteomics, 2008. **7**(1): p. 132-144.

42. Kraus, A., J. Groenendyk, K. Bedard, T.A. Baldwin, K.H. Krause, M. Dubois-Dauphin, J. Dyck, E.E. Rosenbaum, L. Korngut, N.J. Colley, S. Gosgnach, D. Zochodne, K. Todd, L.B. Agellon, and M. Michalak, *Calnexin deficiency leads to dysmyelination*. J Biol Chem, 2010. **285**(24): p. 18928-18938.
43. Jung, J. and M. Michalak, *Cell surface targeting of myelin oligodendrocyte glycoprotein (MOG) in the absence of endoplasmic reticulum molecular chaperones*. Biochim Biophys Acta, 2011. **1813**(5): p. 1105-1110.

CHAPTER FIVE

Discussion and Future Directions

Calnexin is a ubiquitously expressed endoplasmic reticulum (ER) chaperone responsible for the proper folding and assembly of nascent glycosylated polypeptides translated through the ER. Calnexin shares this role with the highly similar lectin chaperone, calreticulin. These two molecules share a highly homologous ER luminal N+P domain responsible for binding the carbohydrate on glycosylated proteins. However, calreticulin resides only in the lumen of the ER whereas calnexin is a Type I transmembrane protein and differs from calreticulin with the addition of a transmembrane domain and an approximately 90 amino acid residue cytoplasmic tail. Despite the similarity of these two chaperones, it has been determined that some glycoprotein folding substrates are shared but specific substrates exclusively associate with either calnexin or calreticulin [1-3]. One objective of this study was to contribute to our understanding of the role of calnexin in a mouse model by using a loss-of-function approach. Additionally, we hypothesized that examining protein-binding partners of the unique C-tail of calnexin would provide us with clues about its essential functions. This study indicates that calnexin plays a specific and non-redundant role in myelin systems. Myelination in the central and peripheral nervous system is impaired with a corresponding reduction in nerve conduction velocities in the absence of calnexin. Thus, calnexin provides a novel contributor to myelin and myelin pathologies. As the unique C-tail and transmembrane domain defines calnexin from many other ER chaperones, including calreticulin, we carried out biophysical and structural studies as well as

analysis of novel protein binding partners to define the role of this region. Understanding the function of the calnexin's transmembrane domain and C-tail could provide insights into its specific role in myelination. We show that the unique calnexin C-tail binds UBC9 and can be SUMOylated *in vivo*. This study of the role of calnexin and its unique domains provide novel insight into the specificity and pathways of a critical protein folding quality control chaperone.

Calnexin plays a critical and non-redundant role in neuronal systems

We generated calnexin-deficient mice to examine the impact of the loss of a ubiquitous protein folding quality control chaperone. Interruption of the calnexin gene with gene-trapping techniques resulted in total loss of calnexin protein expression. Calnexin-deficient mice demonstrate a neurological phenotype with a rolling walk, gait disturbance and splaying of the hind limbs [4]. The neurological phenotype was attributable to central and peripheral myelin defects as assessed by electron microscopy and nerve conduction velocity measurements. Neuronal growth, number and function were not impaired. No major other abnormalities were noted in a comprehensive range of tissues as assessed with histological and morphological analysis. This indicates calnexin plays a critical role in myelin systems and contributes to the formation and/or maintenance of myelin sheaths. It is surprising that we don't require the ubiquitously expressed calnexin for viability and its function in most tissues is redundant. Further,

that it specifically impacts myelin systems provides a new avenue to investigate myelin processes and pathology.

Calnexin and Myelination

The myelin sheath is a unique entity composed of large quantities of specific lipids and specialized proteins. Misfolded and absent myelin proteins are known to contribute to myelin pathology in many diseases such as Charcot-Marie-Tooth. Many myelin proteins are glycosylated membrane proteins and thus would be typical calnexin folding substrates. Calnexin is known to interact with myelin structural glycoproteins PMP22 [5] and P0 and in the absence of calnexin, PMP22 and P0 are misfolded and dysfunctional as adhesive structural proteins [6]. Calnexin is also known to interact with myelin oligodendrocyte glycoprotein (MOG), a highly immunogenic myelin protein found in the central nervous system [7]. Thus, calnexin is a known obligate chaperone for glycosylated myelin proteins. Calnexin may also be important for membrane myelin protein quality control as a transmembrane protein itself. Proteolipid protein (PLP), the major membrane protein of the central nervous system, interacts with calnexin in a glycan-independent manner where calnexin specifically binds the fourth transmembrane segment of PLP. This indicates calnexin provides the quality control checkpoint for both glycosylated and non-glycosylated myelin proteins and the absence of calnexin likely results in the expression of misfolded and non-functional myelin proteins that cannot form compact myelin sheaths.

Determining Folding Substrate Specificity: Calnexin versus Calreticulin

Why does calreticulin not compensate as a folding chaperone for myelin proteins? Considering the similarity between calreticulin and calnexin, one might expect calreticulin to compensate as a folding chaperone for calnexin, and it seems to do so in most tissues in the absence of calnexin. One possible explanation for this lack of compensatory redundancy in myelin systems is calnexin's transmembrane domain and unique cytoplasmic tail. Membrane anchoring of calnexin restricts its spatial proximity and may encourage a preferential interaction with transmembrane myelin proteins. In fact, when calreticulin is membrane-anchored with calnexin's transmembrane domain, its substrate specificity is more similar to calnexin's [2]. Being membrane bound appears to help determine calnexin's substrate specificity as calnexin without its transmembrane domain and cytoplasmic tail has substrate specificity similar to calreticulin. However, the requirement of calnexin's transmembrane domain specifically or any transmembrane segment may depend on the particular folding substrate. Replacement of calnexin's transmembrane domain with the transmembrane segment from the adenovirus E3/19K glycoprotein resulted in binding to a similar set of glycoproteins [2]. Further, membrane proximity of calnexin, whether conferred through its own membrane domain or a foreign transmembrane segment, is important for interaction with lymphocyte tyrosine kinase, membrane IgM and human MHC class I heavy chain [8]. These substrates appear to only require the membrane proximity of calnexin and not its

transmembrane domain specifically. Yet, the transmembrane domain and/or cytoplasmic tail of calnexin could directly mediate an interaction with myelin proteins. Calnexin is the molecular chaperone for PLP albeit in a glycan independent manner [9]. Calnexin interacts with the fourth transmembrane domain of PLP and a glycan-independent quality control mechanism was proposed where calnexin binds misfolded or unassembled transmembrane domains [9]. A role for the calnexin C-tail in substrate interaction was indicated in a recent study where phosphorylation of the calnexin tail impacts the retention and degradation of folding substrate glycoprotein AAT [10]. Thus, the transmembrane domain and C-tail play a role in chaperone-mediated quality control and post-translational modification of the C-tail modulates cross-membrane communication. Thus, considering the chaperone activity of calreticulin and calnexin is not interchangeable for myelin proteins, the transmembrane domain and C-tail of calnexin are likely very important for myelin protein quality control. A lack of compensatory redundancy also highlights functional differences between these two key quality control chaperones.

Calnexin as the Prototype Chaperone

Previous mouse models of ER chaperone-deficiency almost exclusively result in embryonic lethality. Calreticulin-deficient mice are embryonic lethal before day 18 due to a defect in ventricular wall formation in the heart [11]. This embryonic lethality is reversible with cardiac-specific expression of active calcineurin [12] as it circumvents calreticulin-dependent

maintenance of ER Ca^{2+} stores. This highlights the importance of Ca^{2+} dependent pathways downstream of calreticulin in cardiac development and demonstrates the most critical role of calreticulin is not as a molecular chaperone but as a major Ca^{2+} binding molecule. Targeted disruption of the 78-kDa glucose-regulated protein GRP78 (also known as immunoglobulin binding protein BiP), a stress-inducible ER chaperone of the heat shock protein 70 (HSP70) family, results in lethality at the peri-implantation stage due to a general proliferation defect and increased apoptosis of the inner cell mass of the blastocysts [13]. Early embryonic lethality is also seen in glucose-regulated protein 94, a stress-inducible ER chaperone of the HSP90 family [14]. GRP94 is not a chaperone required for global protein folding and it has a limited number of known folding substrates. Lethality is seen at embryonic day 6.5 due to a defect in gastrulation and mesoderm induction [14]. That disruption of ubiquitously expressed calnexin does not result in the embryonic lethality so commonly associated with chaperone-deficiency supports its specific role in myelin systems, as myelination is initiated postnatally. As such, calnexin may provide an ideal prototype for a molecular chaperone. Calnexin-deficiency in mice indicates that its most critical function is as an upstream regulator of myelin protein quality control and subsequent formation and maintenance of compact myelin sheaths.

As calnexin provides an upstream regulator of myelin protein folding and quality control, it is possible that problems with calnexin could contribute to myelin-related neuropathies in humans. As calnexin is not

required for viability, calnexin gene polymorphisms are plausible in the human population. Considering a hallmark of myelin disease is its heterogeneity, calnexin gene polymorphisms could contribute to the diversity of disease presentation. Investigation of calnexin gene polymorphisms in patients with myelin disease will indicate if there is a genetic basis for calnexin in human diseases such as Charcot-Marie-Tooth or even in neuropathies with unknown molecular mechanisms. Additionally, as a regulator of myelin protein folding and subsequent function, modulation of calnexin function provides an upstream therapeutic target to improve myelin disease pathology.

Calnexin gene polymorphisms could result in two foreseeable outcomes: premature release of unfolded/misfolded myelin proteins from the quality control system, resulting in the trafficking and cell surface expression of misfolded myelin proteins or accumulation of myelin proteins in the ER as a result of aberrant retention. The severity of myelin disease can be related to the degree of intracellular retention of the misfolded myelin protein causing the disease. Thus modulating calnexin's chaperone activity and promoting either retention or release of folding substrates could lessen the pathology severity. Overcoming retention of misfolded myelin proteins has been shown to have some beneficial impact. Curcumin, a dietary supplement found in turmeric, has been shown to stimulate the translocation of ER retained mutant myelin P0 and subsequently reduce apoptosis induced by P0 mutant accumulation [15]. However, one must consider the dichotomy

of retention versus release of mutant proteins: overcoming myelin protein retention could alleviate the severity of disease but the insertion of misfolded myelin proteins at the surface membrane could lead to a very detrimental demyelinating inflammatory immune response. Experimental autoimmune encephalomyelitis (EAE) is a mouse model used to study autoantibody mediated demyelination reminiscent of Multiple Sclerosis and is induced with injection of myelin protein MOG or MOG₃₅₋₅₅ peptide. Further studies in animal models are required to examine the benefits of overcoming ER retention of mutant proteins in the context of an immune system. Another consideration is how do we target a ubiquitous chaperone involved in the folding of any proximal glycosylated substrate without inadvertent detrimental consequences? The modifiable C-tail of calnexin could provide a good target as blocking or enhancing specific modification would directly impact calnexin, and thus its substrates.

The Unique Calnexin C-tail

The calnexin C-tail is a highly conserved, unique domain that allows the molecular chaperone to bridge two distinctive cellular compartments, the ER lumen and the cytoplasm. The ER luminal domain of calnexin is classically considered the “chaperone” segment of calnexin and has been more extensively studied than the cytoplasmic domain of the molecule. To define the function of the C-tail, our approach in this study was to examine the structural and biophysical characteristics of the C-tail as well as its protein-binding partners.

Structural and Biophysical Characteristics

The structure and biophysical characteristics of the calnexin cytoplasmic domain have not been previously determined. Our structural characterization of the C-tail reveals that the cytoplasmic domain is a random coil and lacks nascent structure. In addition, it binds Ca^{2+} and can self-associate, forming homo-dimers. An unstructured cytoplasmic tail provides a very flexible template for protein-protein interactions and post-translational modifications as it theoretically can adopt any conformation for modification or protein binding. It remains to be investigated if C-tail structure is conferred when it interacts with other proteins or is post-translationally modified. Dimerization of the C-tail needs to be confirmed *in vivo* as self-association might only be seen with non-anchored segments such as the expressed protein construct. However, calnexin self-association could have interesting implications as it may provide an additional mechanism of regulation. For example, self-association could nucleate calnexin to areas of active protein folding. Alternatively, calnexin binding to itself could block other protein interactions. This self-association could additionally be regulated by post-translational modification of the tail. While we can only extrapolate the *in vivo* function of the observed calnexin C-tail dimerization, structural analysis of the C-tail indicates it provides an ideal substrate for regulation by post-translational modification and protein-binding partners.

Protein-binding Partners

We used yeast-two-hybrid techniques with the C-tail as bait to screen for novel interacting proteins. Nine different interacting proteins were identified including UBC9, an E2 SUMOylation ligase. Additional proteins identified included RanBP9, an unknown RIKEN clone, SGIP1, and a Na⁺/K⁺-ATPase. This study identifies a novel *in vivo* interaction of UBC9 with the calnexin C-tail. Additionally, the C-tail can be modified by SUMO at Lys⁵⁰⁶. Interaction with UBC9 and SUMOylation of the C-tail could have a number of functional consequences. Interaction with the calnexin C-tail brings UBC9 into proximity of ER membranes where it could SUMOylate ER localized substrates. Calnexin interacts with EDEM, a component of ER-associated degradation, through its transmembrane domain in order to transfer terminally misfolded glycoproteins [16] which would bring calnexin, UBC9, EDEM, and the retrotranslocon into close proximity. Ubiquitination of substrates is a necessary step in targeting to the 26S proteasome for degradation. SUMO modifies lysine residues of its substrate and this modification can block ubiquitination of the same lysine. For example, the cytoplasmic inhibitor of NF- κ B, I κ B α , can be SUMOylated at Lys²¹ which is the same lysine for ubiquitin modification. SUMO-1- modified I κ B α cannot be ubiquitinated and is resistant to proteasome-mediated degradation [17]. As ubiquitination is a critical part of proteasomal targeting, one could speculate that UBC9 interaction with the calnexin C-tail could bring it into proximity of the ERAD machinery where it might compete with ubiquitin ligases for

modification of substrate lysines in order block or delay degradation. However, while SUMOylation has previously been considered antagonist to ubiquitination, it has recently been discovered that SUMOylation itself acts as a signal to mediate ubiquitin-dependent degradation by the proteasome [18]. Several groups independently identified a new subgroup of RING finger ubiquitin ligases containing multiple SUMO-interacting motifs (SIMs). Called SUMO-targeted ubiquitin ligases (STUbls), they recognize SUMO as a signal for ubiquitination of the substrate [19-22]. The extent of SUMOylation of particular substrates has been proposed as quality control mechanism. A mutant version of Mot1, a regulator of TATA-binding protein (TBP), demonstrates increased SUMOylation and subsequent degradation [23]. Whether it blocks or enhances ubiquitination of misfolded substrates, SUMOylation mediated by UBC9 bound to the calnexin C-tail could impact on ER-associated degradation pathways. The spatial proximity provided by UBC9 binding to the calnexin C-tail might also permit modification of other ER resident transmembrane proteins and not just ERAD substrates. However, calnexin C-tail SUMOylation was detected *in vivo* and it is possible that UBC9 binding to the C-tail functions only to SUMOylate the C-tail. SUMOylation of the C-tail could regulate calnexin's interaction with other proteins or folding substrates, similar to the differential effects of calnexin phosphorylation. It is worth noting that modifying the C-tail with SUMO is the covalent addition of a protein modification that is approximately the same amino acid number and molecular weight as the entire C-tail. Such a large addition might be

expected to significantly impact on C-tail protein interactions and potentially the flexibility identified in our structural analyses of unmodified C-tail. Determining the cellular conditions under which calnexin SUMOylation is enhanced will provide a direction to investigate the function of calnexin SUMO-modification.

The yeast-two-hybrid screen also revealed an interaction of the C-tail with RanBPM, a nucleo-cytoplasmic shuttling protein that has been postulated to be an E3 SUMO ligase. We observed some degree of co-localization between RanBPM and calnexin and preliminary immunoprecipitation experiments indicate that RanBPM and calnexin do interact. This implicates that RanBPM may provide additional E3 specificity for calnexin SUMOylation.

Another protein identified in the yeast-2-hybrid screen as a C-tail interacting protein is Src homology 3-domain growth factor receptor-bound 2-like (Endophilin) interacting protein 1 (SGIP1) [24]. SGIP1 was first identified as a neuronal protein involved in the regulation of energy balance and has since been implicated to play a role in clathrin-mediated endocytosis [25, 26]. Cerebellar granule cells were isolated from wild-type and calnexin-deficient mice and used to assess transferrin uptake, a measure of clathrin-dependent endocytosis [24]. Calnexin-deficiency leads to increased endocytotic activity in cultured fibroblast and neuronal cells and a corresponding increase in synaptic vesicles is visible in the hypothalamus. Expression of full-length calnexin or the C-tail alone reduces the increased

transferrin uptake in calnexin-deficient cells. Thus, the C-tail is a potent inhibitor of clathrin-dependent endocytosis in neuronal cells [24].

The Multi-faceted Molecular Chaperone

Together, this study has identified calnexin as a novel candidate in myelin formation and maintenance. Additionally, the calnexin C-tail is a malleable template that interacts with a number of proteins including UBC9 and here we identify SUMOylation as an additional C-tail post-translational modification. Most importantly, this study implicates calnexin in several new pathways and opens up new avenues for investigation that will impact on our understanding of cellular quality control and could lead to new therapeutic approaches to myelin disease.

References

1. Molinari, M., K.K. Eriksson, V. Calanca, C. Galli, P. Cresswell, M. Michalak, and A. Helenius, *Contrasting functions of calreticulin and calnexin in glycoprotein folding and ER quality control*. Mol. Cell, 2004. **13**(1): p. 125-135.
2. Danilczyk, U.G., M.F. Cohen-Doyle, and D.B. Williams, *Functional relationship between calreticulin, calnexin, and the endoplasmic reticulum luminal domain of calnexin*. J. Biol. Chem., 2000. **275**: p. 13089-13097.
3. Pipe, S.W., J.A. Morris, J. Shah, and R.J. Kaufman, *Differential interaction of coagulation factor VIII and factor V with protein chaperones calnexin and calreticulin*. J. Biol. Chem., 1998. **273**: p. 8537-8544.
4. Kraus, A., J. Groenendyk, K. Bedard, T.A. Baldwin, K.H. Krause, M. Dubois-Dauphin, J. Dyck, E.E. Rosenbaum, L. Korngut, N.J. Colley, S. Gosgnach, D. Zochodne, K. Todd, L.B. Agellon, and M. Michalak, *Calnexin deficiency leads to dysmyelination*. J Biol Chem, 2010. **285**(24): p. 18928-18938.
5. Dickson, K.M., J.J. Bergeron, I. Shames, J. Colby, D.T. Nguyen, E. Chevet, D.Y. Thomas, and G.J. Snipes, *Association of calnexin with mutant peripheral myelin protein-22 ex vivo: a basis for "gain-of-function" ER diseases*. Proc Natl Acad Sci U S A, 2002. **99**(15): p. 9852-9857.
6. Jung, J., H. Coe, and M. Michalak, *Specialization of endoplasmic reticulum chaperones for the folding and function of myelin glycoproteins P0 and PMP22*. Faseb J, 2011.
7. Jung, J. and M. Michalak, *Cell surface targeting of myelin oligodendrocyte glycoprotein (MOG) in the absence of endoplasmic reticulum molecular chaperones*. Biochim Biophys Acta, 2011. **1813**(5): p. 1105-1110.
8. Ho, S.C., S. Rajagopalan, S. Chaudhuri, C.C. Shieh, M.B. Brenner, and S. Pillai, *Membrane anchoring of calnexin facilitates its interaction with its targets*. Mol Immunol, 1999. **36**(1): p. 1-12.
9. Swanton, E., S. High, and P. Woodman, *Role of calnexin in the glycan-independent quality control of proteolipid protein*. EMBO J, 2003. **22**(12): p. 2948-2958.
10. Cameron, P.H., E. Chevet, O. Pluquet, D.Y. Thomas, and J.J. Bergeron, *Calnexin phosphorylation attenuates the release of partially misfolded alpha1-antitrypsin to the secretory pathway*. J Biol Chem, 2009. **284**(50): p. 34570-34579.
11. Mesaeli, N., K. Nakamura, E. Zvaritch, P. Dickie, E. Dziak, K.-H. Krause, M. Opas, D.H. MacLennan, and M. Michalak, *Calreticulin is essential for cardiac development*. J. Cell Biol., 1999. **144**: p. 857-868.

12. Guo, L., K. Nakamura, J. Lynch, M. Opas, E.N. Olson, L.B. Agellon, and M. Michalak, *Cardiac-specific expression of calcineurin reverses embryonic lethality in calreticulin-deficient mouse*. J. Biol. Chem., 2002. **277**(52): p. 50776-50779.
13. Luo, S., C. Mao, B. Lee, and A.S. Lee, *GRP78/BiP is required for cell proliferation and protecting the inner cell mass from apoptosis during early mouse embryonic development*. Mol Cell Biol, 2006. **26**(15): p. 5688-5697.
14. Wanderling, S., B.B. Simen, O. Ostrovsky, N.T. Ahmed, S.M. Vogen, T. Gidalevitz, and Y. Argon, *GRP94 is essential for mesoderm induction and muscle development because it regulates insulin-like growth factor secretion*. Molecular Biol. Cell, 2007. **18**(10): p. 3764-3775.
15. Khajavi, M., K. Inoue, W. Wiszniewski, T. Ohyama, G.J. Snipes, and J.R. Lupski, *Curcumin treatment abrogates endoplasmic reticulum retention and aggregation-induced apoptosis associated with neuropathy-causing myelin protein zero-truncating mutants*. Am J Hum Genet, 2005. **77**(5): p. 841-850.
16. Oda, Y., N. Hosokawa, I. Wada, and K. Nagata, *EDEM as an acceptor of terminally misfolded glycoproteins released from calnexin*. Science, 2003. **299**(5611): p. 1394-1397.
17. Desterro, J.M., M.S. Rodriguez, and R.T. Hay, *SUMO-1 modification of IkkappaBalpha inhibits NF-kappaB activation*. Mol Cell, 1998. **2**(2): p. 233-239.
18. Uzunova, K., K. Gottsche, M. Miteva, S.R. Weisshaar, C. Glanemann, M. Schnellhardt, M. Niessen, H. Scheel, K. Hofmann, E.S. Johnson, G.J. Praefcke, and R.J. Dohmen, *Ubiquitin-dependent proteolytic control of SUMO conjugates*. J Biol Chem, 2007. **282**(47): p. 34167-34175.
19. Xie, Y., O. Kerscher, M.B. Kroetz, H.F. McConchie, P. Sung, and M. Hochstrasser, *The yeast Hex3.Slx8 heterodimer is a ubiquitin ligase stimulated by substrate sumoylation*. J Biol Chem, 2007. **282**(47): p. 34176-34184.
20. Mullen, J.R. and S.J. Brill, *Activation of the Slx5-Slx8 ubiquitin ligase by poly-small ubiquitin-like modifier conjugates*. J Biol Chem, 2008. **283**(29): p. 19912-19921.
21. Prudden, J., S. Pebernard, G. Raffa, D.A. Slavin, J.J. Perry, J.A. Tainer, C.H. McGowan, and M.N. Boddy, *SUMO-targeted ubiquitin ligases in genome stability*. EMBO J, 2007. **26**(18): p. 4089-4101.
22. Sun, H., J.D. Levenson, and T. Hunter, *Conserved function of RNF4 family proteins in eukaryotes: targeting a ubiquitin ligase to SUMOylated proteins*. EMBO J, 2007. **26**(18): p. 4102-4112.
23. Wang, Z. and G. Prelich, *Quality control of a transcriptional regulator by SUMO-targeted degradation*. Mol Cell Biol, 2009. **29**(7): p. 1694-1706.
24. Li, H.D., W.X. Liu, and M. Michalak, *Enhanced clathrin-dependent endocytosis in the absence of calnexin*. PLoS One, 2011. **6**(7): p. e21678.

25. Trevaskis, J., K. Walder, V. Foletta, L. Kerr-Bayles, J. McMillan, A. Cooper, S. Lee, K. Bolton, M. Prior, R. Fahey, K. Whitecross, G.J. Morton, M.W. Schwartz, and G.R. Collier, *Src homology 3-domain growth factor receptor-bound 2-like (endophilin) interacting protein 1, a novel neuronal protein that regulates energy balance*. *Endocrinology*, 2005. **146**(9): p. 3757-3764.
26. Uezu, A., A. Horiuchi, K. Kanda, N. Kikuchi, K. Umeda, K. Tsujita, S. Suetsugu, N. Araki, H. Yamamoto, T. Takenawa, and H. Nakanishi, *SGIP1alpha is an endocytic protein that directly interacts with phospholipids and Eps15*. *J Biol Chem*, 2007. **282**(36): p. 26481-26489.

**Expression of Full-length and Truncated Calnexin on the
Calnexin-deficient Mouse Background**

To investigate the impact of expressing calnexin and calnexin without its cytoplasmic domain on the calnexin-deficient background, we generated two transgenic mouse lines. These lines were designated *cnx*^{-/-} CNX (full-length calnexin) and *cnx*^{-/-} CNXAC (calnexin N+P+transmembrane domain), respectively. To generate the mice, we used an expression vector designed for ubiquitous expression of genes driven by the ROSA26 promoter. Using this system we generated transgenic mice expressing full-length calnexin and CNXAC (without the cytoplasmic tail) on a CD1 wild-type mouse background (Figure AI.1). Prior to the generation of the transgenic mice, the expression vectors encoding full-length calnexin and CNXAC domain were transfected into wild-type and *cnx*^{-/-} fibroblasts to examine expression of calnexin and calnexin domains. Intracellular localization of full-length calnexin or CNXAC was determined using confocal microscopy with specific calnexin antibodies to the C-terminus for the full-length construct or to the N-terminus for the truncated calnexin construct. Figure AI.2 shows ER localization with Concanavalin A staining and that both the full-length and truncated calnexin construct were properly localized to an ER-like structure. Following the confirmation of construct protein expression and localization, the transgenic mice were generated by pronuclear microinjection of the constructs and the oocytes transferred to pseudopregnant mice. Transgene expression was determined using PCR with two sets of primers: one set amplified a region extending from an N-terminal portion of the vector into the N-terminus of the calnexin encoding construct, the second set amplified a region at the C-

terminus of calnexin into the C-terminal portion of the vector (Figure AI.3, pink arrows). Primer amplification of a region including a portion of the expression vector outside the calnexin coding region was designed to differentiate calnexin transgene expression from endogenous calnexin. Mice were bred by first crossing CD1 wild-type expressing the transgene with wild-type C57BL/6 strain to generate a genetic background similar to the calnexin-deficient mice. The mice were then bred onto a calnexin-deficient background by crossing wild-type CD1/C57BL6 with the transgene with calnexin-deficient animals. Heterozygote progeny with the transgene were bred to calnexin-deficient animals again to give progeny with the transgene on a calnexin-deficient background (Figure AI.4).

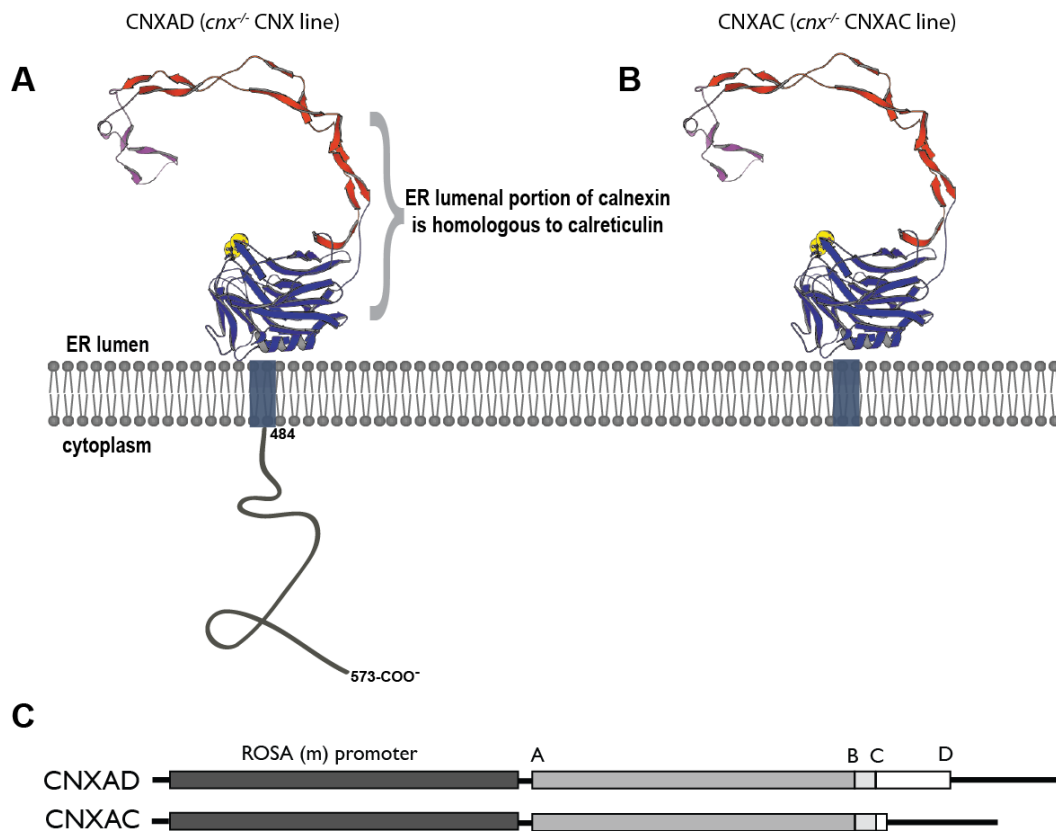


Figure AI.1. Schematic representation of the calnexin constructs used for transgenic mouse generation.

Two independent transgenic mouse lines were generated: **(A)** full-length CNX (A-D) and **(B)** truncated calnexin (CNX A-C) expressing the ER luminal (N+P) plus transmembrane domain without the cytoplasmic tail. **(C)** depicts a linear representation of the constructs with A-B indicating the luminal (N+P) domain, B-C the transmembrane domain and C-D the cytoplasmic tail.

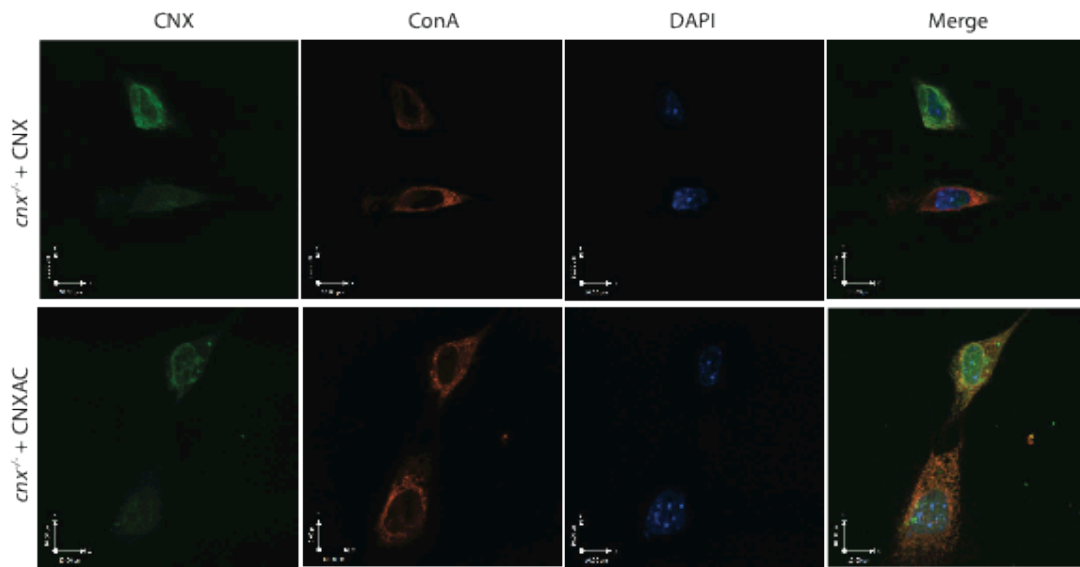


Figure A1.2. The full-length and truncated calnexin proteins both localize to an ER-like structure.

Calnexin-deficient fibroblasts were transfected with the constructs used for the generation of transgenic mice encoding full-length and truncated calnexin (CNXAC) proteins. The fibroblasts were fixed and immunostained with anti-calnexin antibodies to the C-terminus for the full-length calnexin or the luminal domain of the truncated calnexin protein with Alexa 488 secondary antibodies. Concanavalin A (Texas Red) and DAPI were used to stain the ER-like compartment and nucleus, respectively. The full-length and truncated calnexin constructs both localize to an ER-like structure.

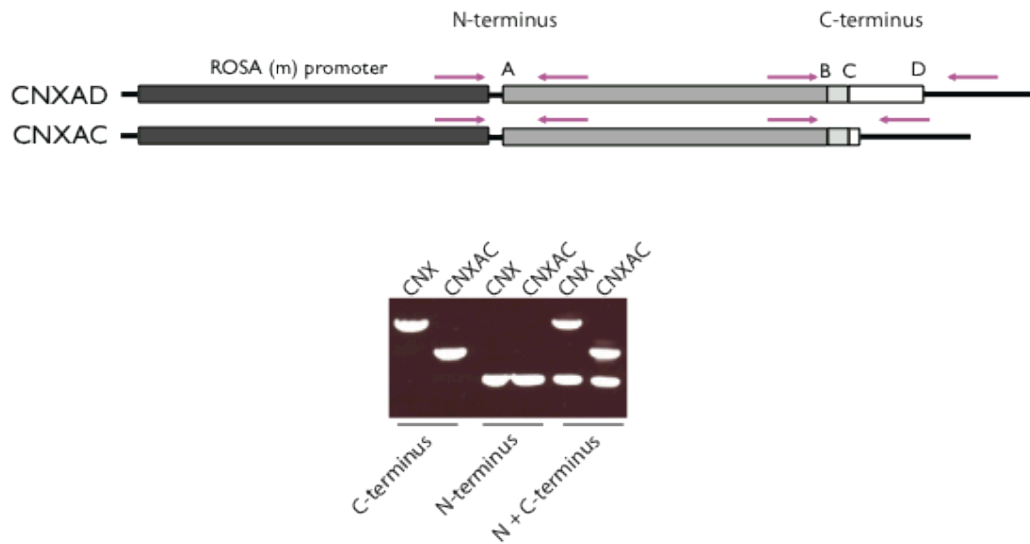


Figure AI.3. Genotyping strategy for the transgenic mouse lines.

To detect the presence of the transgene and differentiate it from endogenous calnexin, DNA primers were designed within the vector ROSA promoter and the N-terminus of calnexin at one end, and the vector and the C-terminus of calnexin at the other (purple arrows indicate approximate primer recognition sequence at both the N and C terminal ends of calnexin, extending into the vector sequence). The product of the C-terminal primers was larger for the full-length calnexin, allowing further differentiation between the presence of the full-length or truncated calnexin. This genotyping was used in conjunction with the calnexin-deficient genotyping described in Figure AI.1 to determine both transgene expression and a calnexin-deficient background.

RT-PCR analysis of a comprehensive range of tissues in both transgenic lines indicated that the transgene is expressed on an RNA level (Figure AI.5). Western-blot of tissue lysates using a calnexin antibody that recognizes the last 18 amino acids of the cytoplasmic portion of calnexin indicates ubiquitous expression of the *cnx*^{-/-} CNX construct at comparable levels to the protein expression of wild-type animals (Figure AI.7). Protein expression levels of the *cnx*^{-/-} CNXAC line were more difficult to determine as the calnexin antibody that recognizes the N-terminal domain of calnexin has a lower apparent titre (Figure AI.6). The truncated protein also has an unknown mobility on SDS-PAGE, although based on the mobility of purified calnexin N+P domain (without the transmembrane domain) it can be postulated to migrate at 70-kDa (Figure AI.8, CNX N+P lane). To overcome these difficulties, we used age-matched calnexin-deficient tissue lysates to compare non-specific banding patterns with our *cnx*^{-/-} CNXAC transgenic mice. There is detectable protein (marked by an asterisk) recognized by the calnexin N-terminal antibody that is not present in calnexin-deficient tissue lysates that is of the expected size for truncated calnexin. Thus, we concluded that there is expression of the CNXAC construct in a comprehensive range of tissues on the RNA level and in select tissues at the protein level.

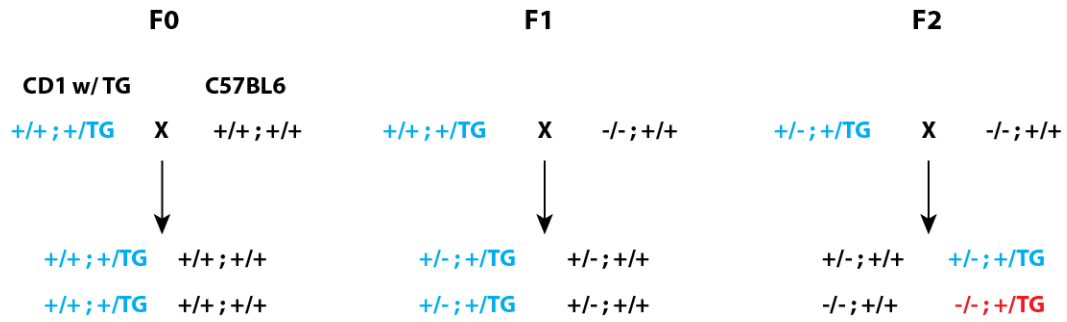


Figure AI.4. Breeding Strategy to Generate the Trangene on the Calnexin-deficient background.

CD1 mice expressing the transgene were crossed to C57BL6 to generate a similar mixed background to the calnexin-deficient mice (F0). Progeny expressing the transgene (blue) were then bred to calnexin-deficient animals (F1). Heterozygotes ($cnx^{+/-}$) with the transgene (blue) were bred to calnexin-deficient animals (F2) to generate calnexin-deficient animals with the transgene (red). Tg, transgene.

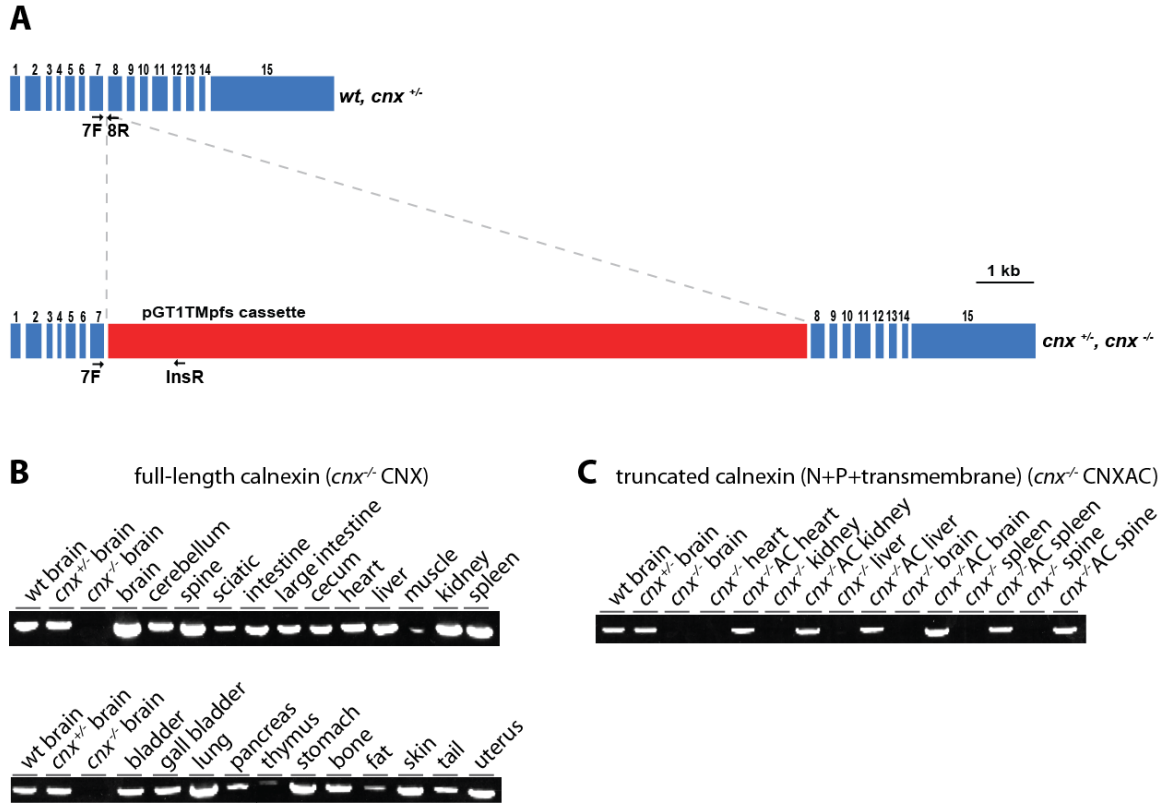


Figure AI.5. RNA expression of the transgene in a comprehensive range of tissues.

mRNA expression was determined using specific DNA primers to exon 7 and 8 as disruption of the calnexin gene in calnexin-deficient animals proceeds intron 7-8 (A). Thus, amplification indicates expression of the full-length calnexin (CNX) (B) or truncated calnexin (CNXAC) (C) transgene in all tissues assessed indicating comprehensive expression of the transgene for both constructs.

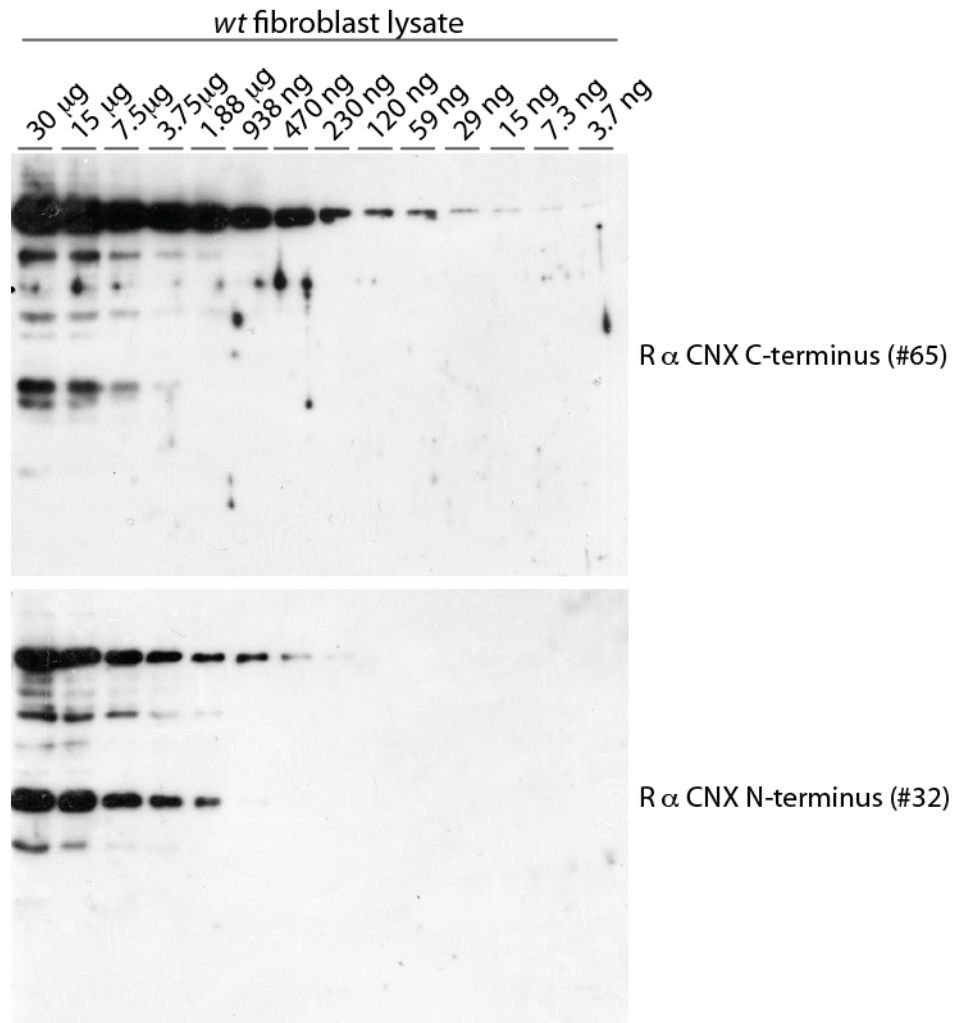


Figure AI.6. Reactivity of calnexin antibodies.

A titration of two calnexin antibodies, one recognizing the C-terminus (#65) and the other the luminal domain (#32) of calnexin. The C-terminal antibody is able to detect calnexin at 3 ng total protein. The N-terminal antibody has a lower titre and recognizes calnexin above 500 ng total protein.

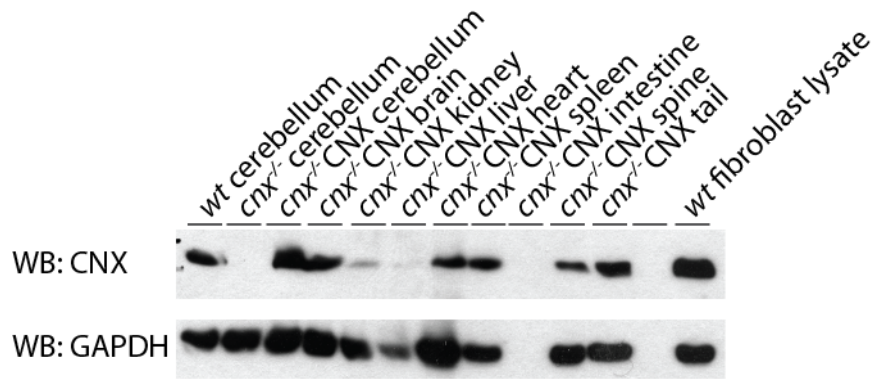


Figure AI.7. Full-length calnexin is expressed in a comprehensive range of tissues.

The full-length calnexin transgene was detected in a comprehensive range of tissues analyzed by Western blotting techniques with an antibodies raised against the last 18 amino acids of the calnexin C-terminus. Calnexin expression in wild-type cerebellum was analyzed for comparison. GAPDH was used as a loading control. Thirty μg of protein was loaded per lane. Full-length calnexin is expressed at a comparable level to calnexin in wild-type tissue. *CNX*, calnexin, *GAPDH*, glyceraldehyde-3-phosphate dehydrogenase.

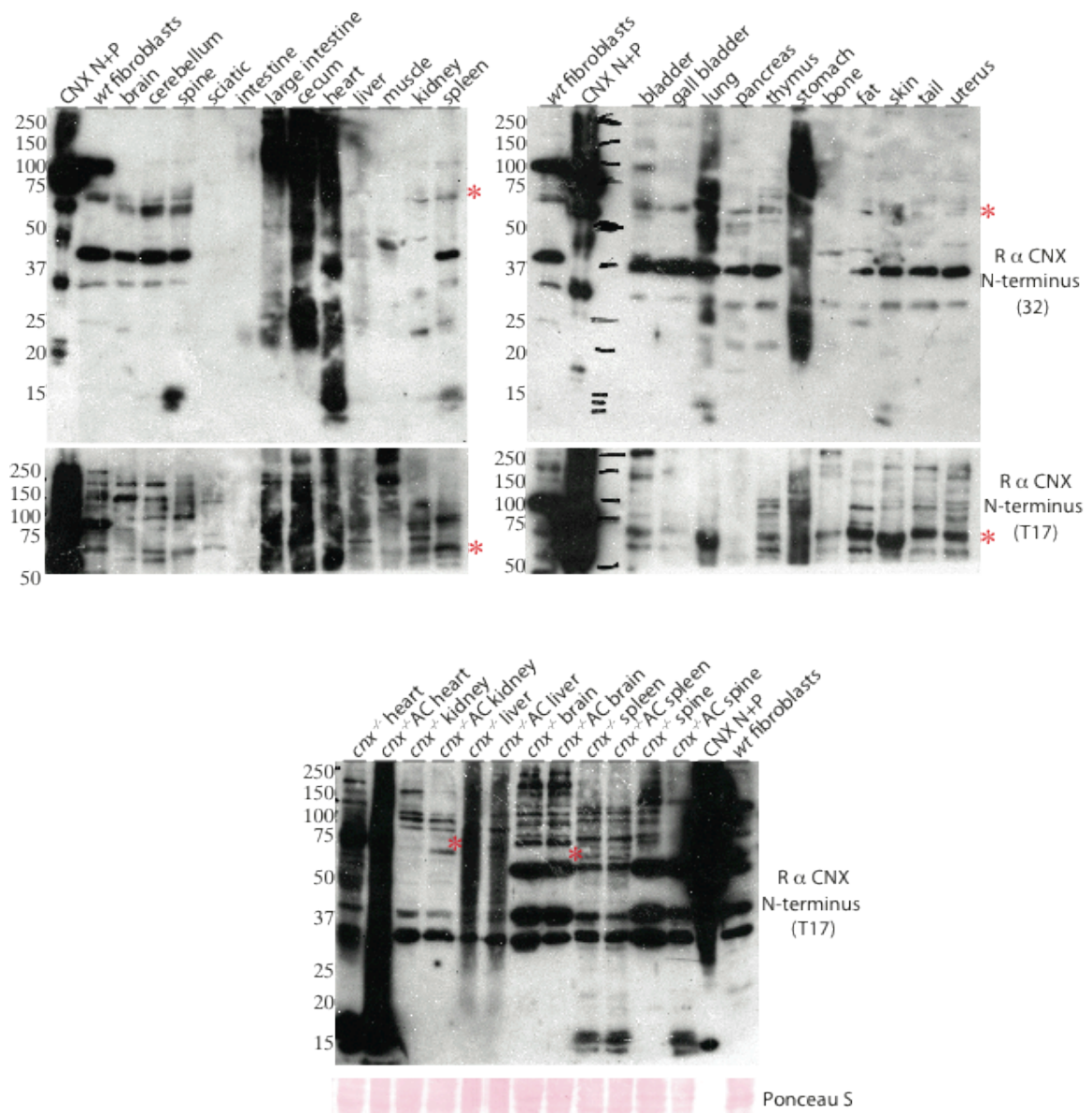


Figure A1.8. Truncated calnexin expression in mouse tissue.

Two independent antibodies raised against the N-terminus of calnexin were used to detect protein expression of the truncated calnexin transgene without the C-tail, antibody 32 and T17 (see “Materials and Methods” for information regarding these antibodies). A protein species at approximately 70-kDa, comparable to purified N+P CNX, was visible in *cnx*^{-/-} CNXAC transgenic mice that is not visible in calnexin-deficient mouse tissue of the same age (lower panel). The truncated calnexin protein is denoted with red asterisks. It is expressed in a range of tissues including kidney, brain, lung, cerebellum, spine and spleen.

The *cnx*^{-/-} CNX and *cnx*^{-/-} CNXAC neonates were undistinguishable from their wild-type littermates. Between day 11 to day 21, calnexin-deficient mice fail to gain weight, resulting in calnexin-deficient mice being 30-50% smaller than their wild-type and heterozygote littermates. Both the full-length (*cnx*^{-/-} CNX) and truncated calnexin transgenic mice (*cnx*^{-/-} CNXAC) continue to gain weight during this period with mice that end up being 10-20% smaller than their wild-type or heterozygote littermates, a discrepancy possibly accounted for by lower calnexin transgene expression levels than wild-type. The *cnx*^{-/-} CNX and *cnx*^{-/-} CNXAC mice do not display the gait disturbance and splaying of the hind limbs characteristic of the calnexin-deficient animals. The morphology of the myelin sheaths and electrophysiological properties are currently under investigation to examine the impact of full-length and truncated calnexin expression on the calnexin-deficient background. Expression of calnexin without its cytoplasmic tail on the calnexin-deficient background will provide us with a mouse model in which to separate the function of the luminal domain of calnexin from its C-tail.

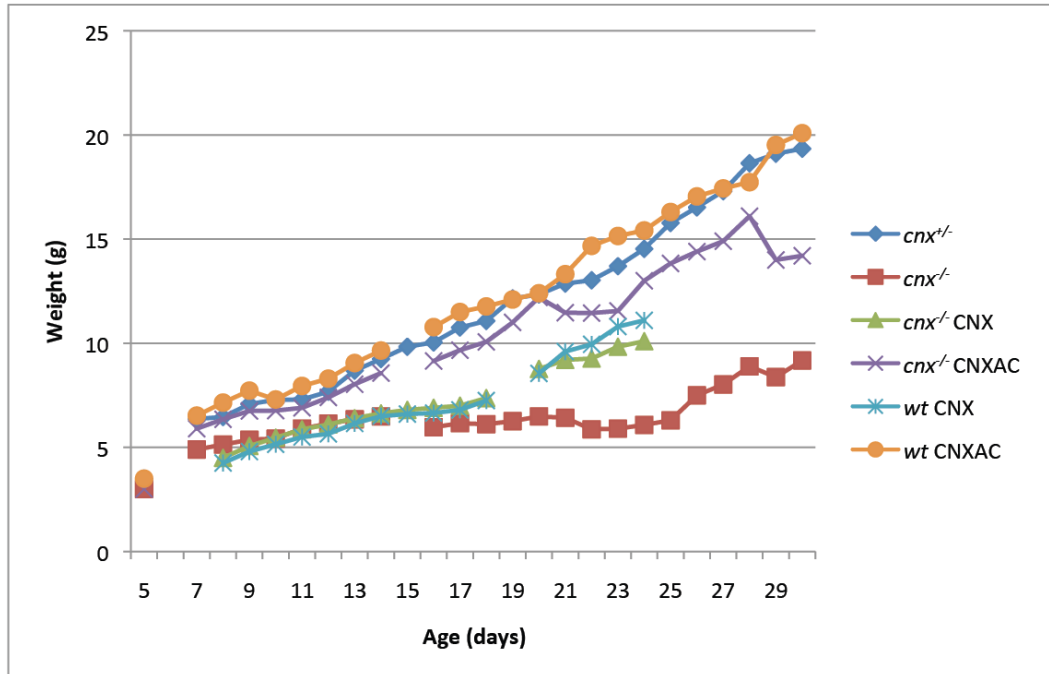


Figure AI.9. Transgenic mouse expressing full-length and truncated calnexin on a calnexin-deficient background gain weight similarly to wild-type animals.

Heterozygote (*cnx*^{+/-}), calnexin-deficient (*cnx*^{-/-}), full-length calnexin transgenic mice (*cnx*^{-/-} CNX), truncated calnexin mice (*cnx*^{-/-} CNXAC) and wild-type mice with either the full-length calnexin transgene (*wt* CNX) or truncated calnexin transgene (*wt* CNXAC) were weighed daily. Calnexin-deficient mice demonstrate a failure to gain weight between day 11 and 22 of age. However, the *cnx*^{-/-} CNX and *cnx*^{-/-} CNXAC transgenic mice lines gain weight steadily throughout this period. *cnx*^{-/-} CNX mice gain weight at a rate similarly to wild-type mice with the calnexin transgene and *cnx*^{-/-} CNXAC mice gain weight at a rate similarly to wild-type mice with the truncated calnexin transgene. The difference in weight gain between the heterozygote and wild-type lines reflects different litters. Thus, *cnx*^{-/-} CNX and *cnx*^{-/-} CNXAC mice gain weight at a rate similar to wild-type animals.

Calnexin and Metabolism

Calnexin-deficiency in mice results in adult animals that are 30-50% smaller than their wild-type littermates. We monitored the weight gain of calnexin-deficient neonates through to early adulthood and observed that between day 11 and 21 of life, calnexin-deficient mice failed to gain weight. Weight gain comparable to the wild-type animals resumed following this approximately 10-day interruption. However, it ultimately results in animals that remained 30-50% smaller than their wild-type and heterozygote littermates. We also observed that calnexin-deficient animals appeared lean with little or no body fat. Thus, we hypothesized that calnexin-deficiency impacts on metabolism in mice.

To assess the observable differences in fat tissue we quantified fat versus lean mass using magnetic resonance imaging (MRI) to obtain quantitative measurements of fat and lean tissue of calnexin-deficient and wild-type mice. When we normalized total fat to the total weight of the mouse, it was observed that calnexin-deficient mice had approximately 50% of the total fat per gram of body weight compared to the wild-type animals (Figure AII.1). Thus, calnexin-deficiency in mice results in smaller, leaner animals.

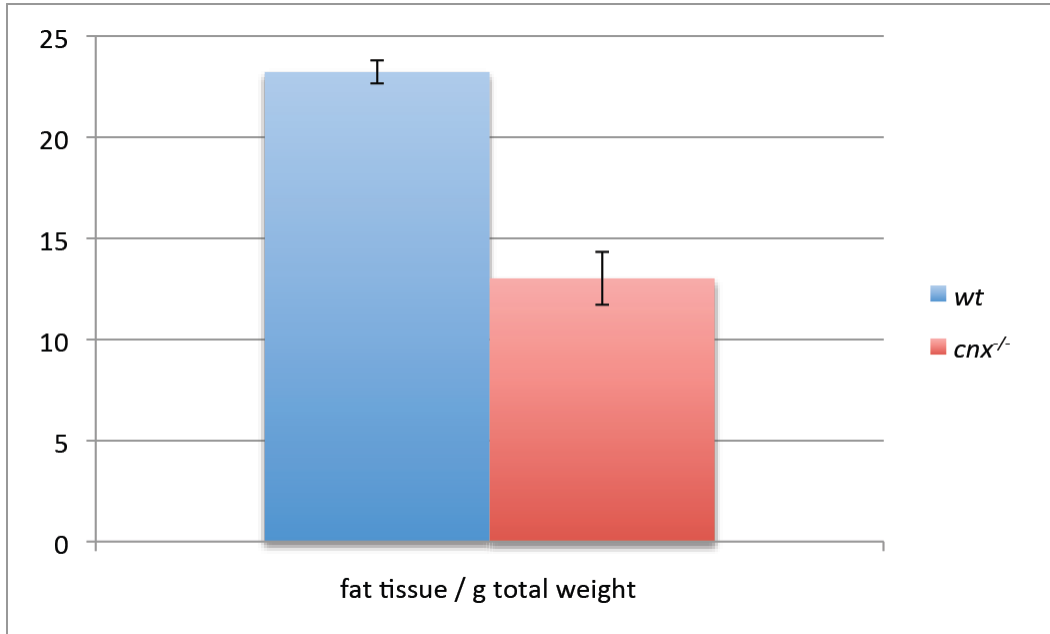


Figure AII.1. Calnexin-deficient mice have less fat than their wild-type counterparts.

MRI analysis of calnexin-deficient and wild-type mice at 12 weeks of age demonstrates that calnexin-deficient animals have a 50% reduction in total fat per g of body weight. Similar observations were made in animals at 3 weeks of age. *wt*, 23.23 ± SE 0.57 (n=2); *cnx^{-/-}*, 13.02 ± SE 1.3 (n=3). *wt*, wild-type, *cnx^{-/-}*, calnexin-deficient, *SE*, standard error.

Recently, malonyl-CoA has received attention in metabolic studies as an important regulator of energy control [1]. The hypothalamus plays a central role in mediating energy intake versus energy expenditure with increased hypothalamic malonyl-CoA signalling an energy surplus resulting in decreased food intake and increased energy expenditure [1]. Conversely, a decrease in hypothalamic malonyl-CoA signals an energy deficit leading to increased appetite and decreased energy expenditure. Considering the central role of malonyl-CoA levels in determining energy balance, we measured hypothalamic levels of malonyl-CoA in calnexin-deficient animals. Levels of malonyl-CoA are elevated in calnexin-deficient mice, which would signal an energy surplus and such a signaling state could contribute to the lean phenotype of the calnexin-deficient animals. The mechanism that leads to increased malonyl-CoA in the *cnx*^{-/-} mouse is still under investigation.

The contribution of calnexin to metabolism in the mouse is currently under investigation. The lean phenotype of the mice could be related to a dysregulation of neuronal satiety signals, such as the elevated malonyl-CoA that would cause the mice to consume less food for their energy output. Their difference in size and reduction of fat tissues could also reflect a molecular mechanism where calnexin directly impacts on fat synthesis and deposition. It will be important to examine the differences in biochemical states of the calnexin-deficient mice during day 11-21 of life where they fail to gain weight and compare it to adult mice that gain weight at a rate similar to wild-type animals.

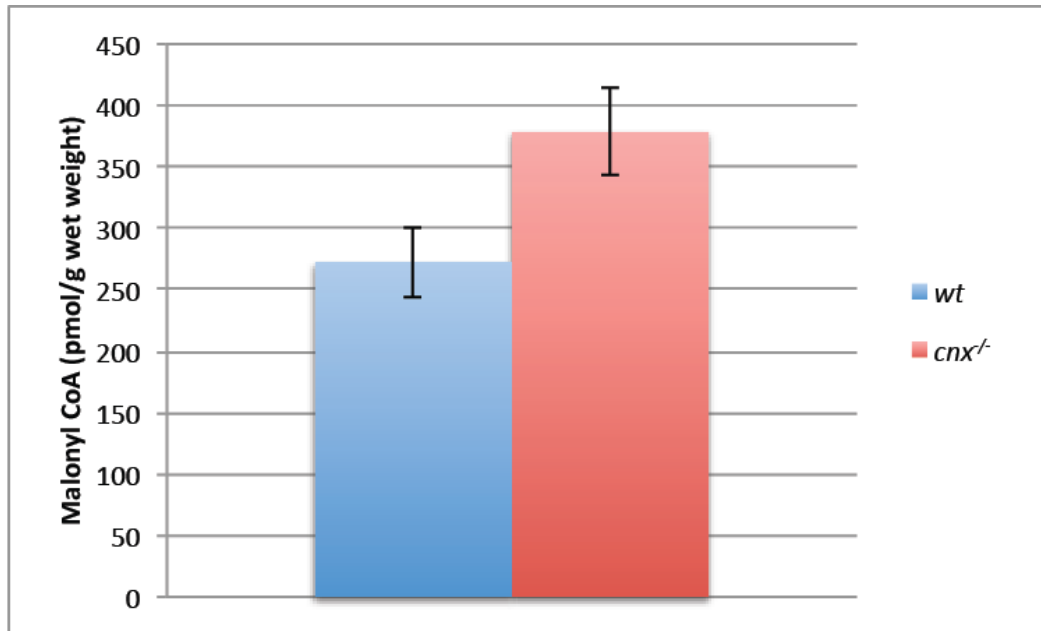


Figure AII.2. Hypothalamic malonyl-CoA levels are elevated in calnexin-deficient mice.

Hypothalami were obtained from wild-type and calnexin-deficient animals and used with a specific HPLC protocol designed for detection of CoA levels. Briefly, brains were removed from mice and flash frozen in isopentane. The hypothalamus was obtained by dissection from the frozen tissue. The tissue was crushed and used for CoA analysis by HPLC. *wt*, 280.3 +/- SE 29.5 (n=21), *cnx^{-/-}*, 380.3 +/- 32.6 (n=16) p<0.05 with one outlier removed from *wt*. *wt*, wild-type, *cnx^{-/-}*, calnexin-deficient.

If the lean phenotype of calnexin reflects problems with lipid or cholesterol biosynthesis it could have implications for the neuropathy of calnexin-deficient mice. Myelin is a lipid and cholesterol rich entity. Cholesterol, a major component of myelin, is not imported from the circulation but instead synthesized locally and is rate-limiting for myelin biogenesis [2, 3]. The rate-limiting effect of cholesterol was determined when a conditional mouse mutant was generated using Cre-mediated targeting of the squalene synthase (SQS) gene in oligodendrocytes and Schwann cells. SQS catalyzes the first step of the cholesterol synthetic pathway specific to the formation of sterols [4]. The mutant mice lagged behind the controls in weight gain and developed motor function deficits at two weeks of age characterized by ataxia, initiation tremor and impaired control of hindlimb movements. This was attributed to severe dysmyelination in the form of hypo-myelinated axons in the CNS and PNS. Interestingly, there was a stringent preservation of the cholesterol to lipid stoichiometry in the mutant myelin despite the abrogated ability of the myelinating glia to synthesize cholesterol. This suggested horizontal cholesterol transfer, potentially from neighbouring wild-type cells such as astrocytes and demonstrated cholesterol is an essential rate-limiting factor in myelin biogenesis. It is important to note that critical components of cholesterol biosynthesis are located at ER membranes, including the rate limiting step, HMG-CoA reductase (HMGR), an integral ER membrane protein. Many myelin proteins are known to partition into cholesterol-rich membrane rafts in myelin

membranes and it was postulated that an interaction with cholesterol could be part of the ER quality control system [5]. Consistent with this hypothesis, it was observed that the major peripheral myelin protein P0 requires cholesterol for its trafficking from the ER [5]. Trafficking was dependent on a functional cholesterol recognition/interaction amino acid consensus (CRAC) motif in P0 (amino acid residues 142-151). Expression of myelin protein genes was also dependent on high intracellular cholesterol levels as mRNA levels of MAG, MBP P0 and PMP22 were significantly reduced in sciatic nerves from SQS mutant animals [5]. Thus, calnexin may also play an important role in metabolism and problems with lipid synthesis pathways in the calnexin-deficient mouse might contribute to its aberrant myelination.

References

1. Lopaschuk, G.D., J.R. Ussher, and J.S. Jaswal, *Targeting intermediary metabolism in the hypothalamus as a mechanism to regulate appetite*. Pharmacol Rev, 2010. **62**(2): p. 237-264.
2. Morell, P. and H. Jurevics, *Origin of cholesterol in myelin*. Neurochem Res, 1996. **21**(4): p. 463-470.
3. Saher, G., B. Brugger, C. Lappe-Siefke, W. Mobius, R. Tozawa, M.C. Wehr, F. Wieland, S. Ishibashi, and K.A. Nave, *High cholesterol level is essential for myelin membrane growth*. Nat Neurosci, 2005. **8**(4): p. 468-475.
4. Bradfute, D.L., C.J. Silva, and R.D. Simoni, *Squalene synthase-deficient mutant of Chinese hamster ovary cells*. J Biol Chem, 1992. **267**(26): p. 18308-18314.
5. Saher, G., S. Quintes, W. Mobius, M.C. Wehr, E.M. Kramer-Albers, B. Brugger, and K.A. Nave, *Cholesterol regulates the endoplasmic reticulum exit of the major membrane protein P0 required for peripheral myelin compaction*. J Neurosci, 2009. **29**(19): p. 6094-6104.

Appendix III

PTP1B and Calnexin

To date, only one other ER protein, protein tyrosine phosphatase 1B (PTP1B), is known to be SUMOylated. PTP1B is translated in the cytoplasm and post-translationally targeted to ER membranes through a targeting motif at its C-terminus where it localizes to the cytoplasmic face of the ER and nuclear envelope. PTP1B deficiency in mice leads to increased sensitivity to insulin, decreased adiposity, and resistance to high-fat diet-induced obesity [1, 2]. These findings highlighted PTP1B as a molecule of interest for studies in metabolic regulation. Tyrosine phosphatase 1B negatively regulates growth factor signaling by binding to and dephosphorylating receptor tyrosine kinases such as the insulin receptor [3]. PTP1B can be modified by SUMO-1 at multiple lysine residues and SUMOylation reduces its catalytic activity [4]. SUMOylation of PTP1B is significantly reduced when its ER localization is abolished [4]. In addition to calnexin being the second ER protein identified as modifiable by SUMO, calnexin-deficient mice share some phenotypic characteristics with PTP1B deficient mice, including reduced adiposity as discussed earlier. Further, PTP1B has recently been implicated in the control of endocytic down-regulation of receptor tyrosine kinases and is reminiscent of enhanced clathrin-dependent endocytosis observed in the absence of calnexin. These molecular similarities led us to hypothesize that PTP1B and calnexin may coincide within molecular complexes at the ER. Preliminary evidence indicates that calnexin and PTP1B interact. Immunoprecipitation with PTP1B specific antibodies indicate that PTP1B immunoprecipitation from wild-type fibroblasts pulls down calnexin (Figure

AIII.1). As PTP1B is targeted to the ER membrane through a C-terminal targeting motif, the interaction of calnexin with PTP1B is likely mediated through calnexin's transmembrane or C-tail domain and may present an additional C-tail interacting protein. Considering PTP1B and calnexin are the only known ER proteins to be SUMOylated and they interact, it is plausible that SUMOylation of PTP1B might happen in a calnexin-dependent manner. Investigation into the PTP1B and calnexin interaction could help us understand the lean phenotype or increased endocytosis of the calnexin-deficient mouse.

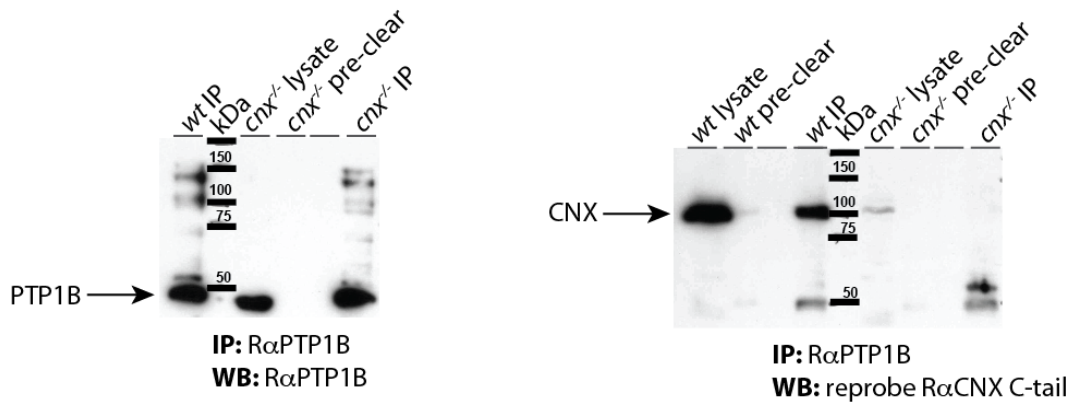


Figure AIII.1. Calnexin and PTP1B form complexes.

Immunoprecipitation of protein tyrosine phosphatase 1B (PTP1B) with antibodies to PTP1B from wild-type and calnexin-deficient fibroblasts and western blot analysis with PTP1B antibodies demonstrates successful immunoprecipitation of PTP1B (arrow). The higher molecular weight banding pattern observed is consistent with SUMO-modification of PTP1B. Re-probing the western blot with calnexin antibodies reveal a specific interaction of PTP1B and calnexin in wild-type but not calnexin-deficient fibroblasts. *PTP1B*, protein tyrosine phosphatase 1B. *CNX*, calnexin. *IP*, immunoprecipitation. *WB*, Western blot.

References

1. Klamann, L.D., O. Boss, O.D. Peroni, J.K. Kim, J.L. Martino, J.M. Zabolotny, N. Moghal, M. Lubkin, Y.B. Kim, A.H. Sharpe, A. Stricker-Krongrad, G.I. Shulman, B.G. Neel, and B.B. Kahn, *Increased energy expenditure, decreased adiposity, and tissue-specific insulin sensitivity in protein-tyrosine phosphatase 1B-deficient mice*. Mol Cell Biol, 2000. **20**(15): p. 5479-5489.
2. Elchebly, M., P. Payette, E. Michaliszyn, W. Cromlish, S. Collins, A.L. Loy, D. Normandin, A. Cheng, J. Himms-Hagen, C.C. Chan, C. Ramachandran, M.J. Gresser, M.L. Tremblay, and B.P. Kennedy, *Increased insulin sensitivity and obesity resistance in mice lacking the protein tyrosine phosphatase-1B gene*. Science, 1999. **283**(5407): p. 1544-1548.
3. Bourdeau, A., N. Dube, and M.L. Tremblay, *Cytoplasmic protein tyrosine phosphatases, regulation and function: the roles of PTP1B and TC-PTP*. Curr Opin Cell Biol, 2005. **17**(2): p. 203-209.
4. Dadke, S., S. Cotteret, S.C. Yip, Z.M. Jaffer, F. Haj, A. Ivanov, F. Rauscher, 3rd, K. Shuai, T. Ng, B.G. Neel, and J. Chernoff, *Regulation of protein tyrosine phosphatase 1B by sumoylation*. Nat Cell Biol, 2007. **9**(1): p. 80-85.